IAEA-TECDOC-970

Studies on fuels with low fission gas release

*Proceedings of a Technical Committee meeting
held in Moscow, 1–4 October 1996*

INTERNATIONAL ATOMIC ENERGY AGENCY

The originating Section of this publication in the IAEA was:

Nuclear Fuel Cycle and Materials Section
International Atomic Energy Agency
Wagramerstrasse 5
P.O. Box 100
A-1400 Vienna, Austria

STUDIES ON FUELS WITH LOW FISSION GAS RELEASE
IAEA, VIENNA, 1997
IAEA-TECDOC-970
ISSN 1011–4289

FOREWORD

For more than a decade, the IAEA has organized various specialists meetings to discuss advances in nuclear fuel technology for non-water cooled reactors. In order to review progress in research and development of fuels with low fission gas release for light water reactors, fast reactors and research reactors, an IAEA Technical Committee meeting was organized in October 1996. At the invitation of the Government of the Russian Federation, the meeting was held in Moscow. Experts from seven Member States and one international organization participated. The objective of the meeting was to exchange topical information on such fuels, to evaluate their advantages and drawbacks, and to explore their commercial utilization. The present volume contains the full text of the sixteen papers presented at the meeting.

The information compiled in these proceedings should be useful for engineers, scientists and managers from nuclear fuel development organizations, fuel fabrication plants, utilities and regulatory bodies who are involved in the analysis of fuel behaviour under normal and accident conditions.

The IAEA wishes to thank all the participants for their contributions to this publication. The IAEA officer responsible for the organization of the meeting and the compilation of this publication was V. Onoufriev of the Nuclear Fuel Cycle and Materials Section, Division of Nuclear Power and the Fuel Cycle.

EDITORIAL NOTE

CONTENTS

SUMMARY

BACKGROUND AND INTRODUCTION

At the invitation of the Government of the Russian Federation, following a proposal of the Standing Advisory Group on Advanced Fuel Technology and Performance, the IAEA convened a Technical Committee meeting on Research of Fuel Aimed at Low Fission Gas Release (Cermet, Cercer, Carbide, Nitride, Carbide-Nitride Fuels) from 1 to 4 October 1996 in Moscow, Russian Federation, to review progress made in R&D activities on fuels with low fission gas release for light water reactors (LWRs), fast reactors (FRs) and research reactors (RRs) during the past decade. Evaluation of advantages and drawbacks of these fuels in comparison with the presently used fuels, e.g. UO_2 and MOX fuels in LWRs and FRs and, as a consequence, in the perspective of their commercial utilization, was also a major purpose of the meeting.

The meeting was attended by 24 participants from seven countries (Argentina, France, Germany, India, Japan, the Republic of Korea and the Russian Federation), one international organization (the European Commission Joint Research Centre for Transuranium Elements) and a number of observers from the Russian Federation. A total of 16 papers was presented.

The meeting showed that R&D activities on advanced fuels, especially cermet fuels for LWRs, and RRs and nitride fuels for FRs, are being carried out by the Member States with nuclear power programmes. These fuels could be required for commercial use sooner or later depending on nuclear power development scenarios. The deliberations of the individual technical sessions and related panels are summarized below.

SESSION 1 - FUELS FOR WATER REACTORS

Chairmen: Ph. Dehaudt, France
A.V. Vatulin, Russian Federation

Summary

This session included the results of scientific, experimental and technological research of fuels and fuel rods, research on fuel irradiation behaviour and modelling of fission gas release (FGR). Six papers were presented covering the experience of Argentina, France and the Russian Federation in the area of development and research on cermet and cercer fuels for LWRs.

Most of the reports show composite fuels as dispersed fissile materials in metallic or ceramic matrix. This allows improvement of thermal conductivity and reduction of temperature in fuel. Typical matrixes which were proposed have a thermal conductivity better then UO_2 or $(U, Pu)O_2$. In addition, these composite fuels include the concept of double barrier (matrix+cladding) limiting and controlling fission gas release.

The results on irradiation behaviour and FGR from cermet (metal matrix) and cercer (ceramic matrix) were presented. It was stated that cermet behaviour was better than that of cercer. The level of fission gas release from cercer fuels and their thermal behaviour are similar to those of UO_2. The most perspective dispersed fuels are UO_2, $(U,Pu)O_2$ and uranium silicides in the Al or Zr matrix. The use of dispersed fuel on a base of high density uranium alloys may also be considered.

Modelling of the FGR and generation confirmed the possibility of reducing FGR by grain size increase in an oxide fuel (UO_2, etc.). In addition, fuels with lower densities have a tendency to lower FGR, but the value of the effect is relatively small.

Conclusions and Future Work

In order to limit FGR at the lowest level possible, fuel development exhibited in this TCM may be beneficial.

Composite fuel with a metal matrix could be called "cold fuel". For this reason, it limits FGR in normal conditions. In addition, its morphology (dispersed fissile materials in a metal matrix) provides good behaviour in case of power transients favouring the reduction of burst release and in case of cladding failure.

However, the introduction of a new fuel concept is in opposition to the present trend of no changes. It could be explained by 30 years of experience of commercial oxide fuel fabrication and utilization, its good performance under current burnups of up to ~60 MW·d/kg HM and satisfactory economics. However, the progressive introduction of cermet fuels in water reactors can be expected if their advantages are confirmed in order to provide:

–   Burnup increases up to ~100 MW·d/kg HM using Pu fraction instead of high U-235 enrichment;

–   Improved flexibility for every operation, particularly in the case of core control and power manoeuvring;

–   Enhanced safety margins in case of LOCA and RIA.

To be prepared for this the following activities should be performed in the near future:

–   Development of cermet fuel manufacturing with the cost equal or lower than for standard fuel;

–   Evaluation of the behaviour of cermet and cercer fuels and their components (fissile and matrix) at high burnups in normal operating conditions with regard to thermal conductivity degradation if any, fission gas release, cladding oxidation, core reactivity control, power manoeuvring and Xe poisoning;

–   Examination of the nature of fissile components in order to avoid high enrichment, to evaluate neuronic aspects of core control, storage and reprocessing aspects;

–   Experimental verification and creation of the data base on cermet fuels from irradiation in test and power reactors and PIE;

–   Extension of modelling of cermet fuels with regard to their thermal behaviour and FGR.

8

SESSION 2 - FUELS FOR RESEARCH REACTORS

Chairmen: A.K. Sengupta, India
               Yu.A. Stetsky, Russian Federation

Summary

The second session (three papers) was devoted to high density fuels for research reactors. The main theme of development of high density fuel with low FGR for research reactors is to use low enriched uranium (LEU :U-235 content is less than 20-25%) as the fissile material in some inert matrix and to obtain a high density of the fuel in the element core to achieve the advanced characteristics of research reactors.

The results of development of high density fuel in the scope of a Russian programme of converting research reactors utilizing LEU fuel were presented. The technological aspects of its development and investigation of the properties and irradiation behaviour of different U bearing fuels e.g. U_3Si, U_6Fe, U-Zr-Nb, U-Mo and other fuels are now in progress.

Very positive and encouraging results have been obtained with the development of new technology for production of high density fuel granules by centrifugal atomization (KAERI, Republic of Korea). Fuels based on the use of granules of U_3Si, U_3Si_2 and U-Mo have better properties than those fabricated by conventional comminution. Centrifugal atomization also helps in increasing the "uranium loading".

The method of estimation of thermal conductivity of the rolled fuel elements with dispersed U_3Si_2 (36 wt% U_3Si_2) fuel in Al matrix as well as some technological aspects were presented with regard to Al plate type fuel elements (India).

Conclusions and Future Work

It is beneficial to develop new types of dispersion fuel, as they are the most satisfactory and safe because of retention of fission gas products with the possibility to use the LEU fuel and increase parameters of research reactors.

The technology of high density fuel granules fabricated by centrifugal atomization is of practical interest.

SESSION 3 - FUELS FOR FAST REACTORS

Chairmen: Yu.K. Bibilashvili, Russian Federation
               M. Coquerelle, European Commission

Summary

The interest of the seven papers presented in Session 3 was focused on the use of mixed fuels as fuel driven in a fast reactor either as a breeder or a burner.

The in pile performance of Pu bearing fuels was presented by representatives of the European Commission and by JAERI (Japan). The first study based on irradiation tests in fast flux reactors at high rate (900–1300 W/cm) on fuels with composition ranging from MC to MN indicated a lower FGR for nitride. PIE showed that the release is determined by the fuel

restructuring, in particular by the interconnected porosity; the release of Xe and Kr processes to diffusion paths mainly by atomic diffusion. The Japanese irradiations carried out on mixed carbide and nitride fuels at low temperature confirm the low FGR of these fuels at low temperature and anticipate a mechanism controlled by open porosity; this point confirms the former conclusion.

The Russian scientists presented irradiation results on Pu bearing fuels mixed in an inert matrix excluding any breeding possibility. This allows an effective and economic elimination of weapons grade Pu. The selected fuels were PuC (55.5%), ZrC (45.5%) and PuO_2-MgO. The first fuel was irradiated at 400–450 W/cm up to 8 ~/0 burnup and showed a fuel swelling lower than 1% and a FGR never exceeding 2%. These results are a successful and effective demonstration of the proposed target.

The second fuel proposal is at the fabrication stage from experience acquired by preliminary studies carried out on uranium oxide mixture UO_2 (15 vol.%)-MgO (85 vol.%). Irradiations are planned in the BR-10 reactor (Obninsk) in the near future.

The thermal and mechanical properties of mixed carbide and nitride fuels were determined in India.

Finally, within the framework of a development of a safer FBR (BREST-300 project), the inherent properties of mixed nitride (ρ, λ and good irradiation stability) make this fuel a potential candidate for a safer FBR.

Conclusions and Future Work

Important FBR programmes are still being developed in the Russian Federation, Japan, India and France. A new potential strategy for this reactor type is their use for elimination of weapons grade Pu .There is a relatively extensive programme in this field.

Mixed carbide and mixed oxide dissolved or dispersed in an inert matrix, ZrC and MgO respectively, could be potential candidates. In particular, the carbide fuel has been irradiated up to 8% and analysed. The feasibility of the oxide as a cercer has to be demonstrated by irradiation tests. The nitride option could be envisaged; theoretically its high density, good thermal conductivity behaviour at high burnup and the possibility of using the Purex process make this fuel another potential candidate. These new technological approaches have to compete with the possible use of MOX fuels irradiated in thermal power reactors. The new concepts can be used for eliminating civilian Pu as well; this possibility has to be kept in mind and has to be demonstrated by irradiation tests.

In the back end of the nuclear fuel cycle, with the use of nitride or cercer fuels in FRs, the combination of electrochemistry techniques with the Purex process reported by Russian specialists has been evaluated as a very promising one.

10

PANEL DISCUSSIONS

Chairmen: H. Weidinger, Germany
Yu.K. Bibilashvili, Russian Federation

Summary of the panel discussion on Session 1: Fuels for water reactors

The present situation for UO$_2$/MOX fuels counts more than 30 years of commercial experience with high reliability; economically LWR fuel is in competition with other fuels (both fissile and fossile). The UO$_2$/MOX fuel fabrication industry is well established and serious constraints to basic changes in fuel origin can be expected.

From a technical point of view current batch average burnups of UO$_2$ fuel are ≤50 MW·d/kg HM, and an increase of batch average burnup up to ~60 MW·d/kg HM is expected soon with a simultaneous increase of power density and heat flux. With regard to fuel (fuel rod), FGR is no design limit as yet. However, rim effect could be a barrier for future burnup increase, and therefore remedies are now in development.

Development trends include increased manoeuvrability (load follow), improved fuel utilization, use of burnable absorber fuels and extension of the use of MOX fuel.

The chances of introducing cold fuel into commercial LWR operation are:

–   In a burnup range of ≥100 MW·d/kg HM, and if cladding material corrosion calls for decreased surface temperature;

–   When increased safety margins (e.g. LOCA or RIA) can be demonstrated;

–   As fuel for inherently safe reactors.

The following questions should be answered in order to evaluate the above mentioned chances:

–   Are candidate fuel materials or targets for them visible (conductivity, enrichment, etc.)?
–   Commercial experience with fabrication cost?
–   Experience with the fuel cycle cost?
–   Experience with the back end of the nuclear fuel cycle?
–   Experience with behaviour under power ramping and power cycling conditions?
–   Proven solutions for fuel rod claddings, with regard to chemical interaction with fuel, PCI and operation of defective fuel (secondary degradation)?

However, future development should focus on promising cermet candidates which have found international acceptance at least among participants of the meeting.

Summary of the panel discussion on Session 2: Fuels for research reactors

There is an international need for high density fuel with decreased enrichment in order to:

–   decrease the cost of R&D of reactor cores and auxiliary (safety) equipment;
–   decrease the risk of proliferation.

The emphasis of development is currently on silicide fuel.

A major problem to be solved is fuel swelling. Therefore efforts should be made to increase irradiation resistance.

Summary of the panel discussion on Session 3: Fuels for fast reactors

Mixed carbide, nitride, cermet, cercer (MgO-matrix) and metallic U- and Pu- alloys were discussed to some extent as alternatives to MOX fuels.

It was generally accepted that the major impact on the future development comes from two sides:

-   The economy of fast reactor cores has to be significantly improved;
-   Fast reactor fuel technology has to include the use of weapons grade Pu.

It was agreed that:

-   Major technical and economic improvements can be expected from nitride type fuel.

-   Reprocessing on the basis of electrochemical refinement is a technically and economically promising alternative to Purex-type reprocessing;

-   Fast reactor fuel cycle with nitride fuel and electrochemical reprocessing has a good economic chance in comparison with the existing oxide fuel cycle.

FUELS FOR WATER REACTORS

(Session 1)

Chairmen
Ph. DEHAUDT
France

A.V. VATULIN
Russian Federation

DEVELOPMENT OF CERMET FUEL AND CERMET FUEL BASED ELEMENTS FOR WWER TYPE REACTORS

A.V. VATULIN, Yu.A. STETSKY,
V.B. SUPRUN, G.I. KHOTYASHOV
All Russian Scientific and Research Institute of
    Inorganic Materials,
Moscow, Russian Federation

Abstract

Presented are the results of research on development of cermet fuel based on UO_2-Zr, UO_2-Al, U_3Si-Zr and U_3Si-Al compositions.
Design and schematic technology of manufacturing of a cermet fuel element for WWER reactors.
Results of out-of-pile investigations of fuel compositions and of calculational justification of fuel elements serviceability for operation in the active zone of VVER-440 reactor are presented

1. Introduction

One of promising directions of improvement of power reactors is development of a fuel element with cermet fuel in which, due to high thermal conductivity of fuel composition and to low thermal resistivity between fuel and shell, fuel element temperature is essentially lower than that in a fuel element with traditional oxide fuel.

Our Institute, in cooperation with other Russian enterprises, is developing a fuel element with cermet fuel for usage in WWER-type reactors.

Creation of a cermet fuel element would make it possible to improve safety of active cores of WWER-type reactors in emergency situations and to provide for possibility of their operation in manoeuvre modes.

A well-known advantage of dispersed-type cermet fuel is its ability to retain within itself gaseous fission products at significant levels of accumulation.

We consider promising those cermet compositions based on zirconium or aluminium with fuel in the form of uranium dioxide or silicide possessing good thermal and radiational stability.

Original microstructures of fuel compositions UO_2-Zr, UO_2-Al, U_3Si-Zr and U_3Si-Al are presented in Fig 1.

Behaviour of fuel compositions at heating was investigated at long-term (up to 500 hours) high temperature annealings (up to 1000°C) in isothermal and cyclic modes (up to 200 cycles). These researches have made it possible to establish absence of intensive interaction of composition fuel component with matrix material up to 800°C for UO_2-Zr and U_3Si-Zr compositions and up to 550°C for UO_2-Al and U_3Si-Al compositions (Fig. 2).

Increasing of annealing temperature of zirconium-based fuel compositions up to 1000°C and that of aluminium-based ones up to 600°C brings about an insignificant increase of volume related to the process of interaction of fuel component with matrix material which is accompanied by mutual diffusion leading to mass transport with porosity production. Using as matrix materials zirconium or aluminium possessing low cross-section of neutron capture, high thermal conductivity and high corrosion resistivity in combination with high uranium-content fuel in the form of uranium dioxide or silicide enabled us to develop the design of a cermet fuel element and technology of its manufacturing providing for reduction of a fuel element temperature 1.5 to 2 times compared to a standard fuel element based on oxide fuel

2. Fuel Element Design

A fuel element is a core of cermet fuel compositions housed in a shell tube of a zirconium alloy (Fig 3) The core has an additional cladding of matrix material

Tight fit is provided between the fuel element shell and the core Faces are sealed by zirconium plugs by means of electron-beam welding

Microstructure of Fuel Compositions

UO$_2$-Zr Composition
x 200/x 1000
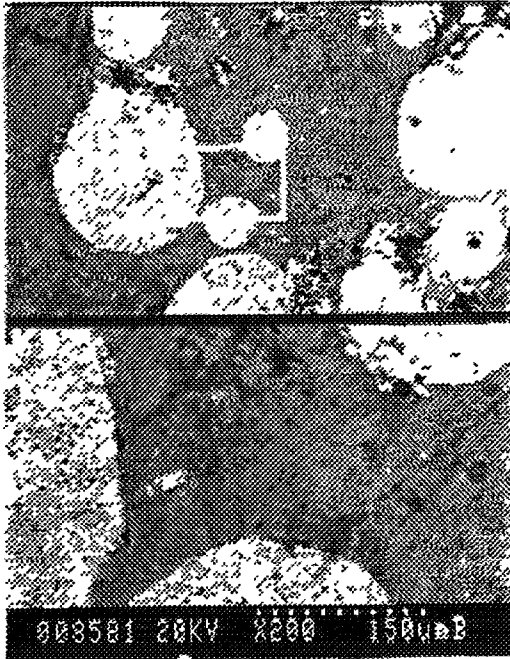
UO$_2$-Al Composition
x 2000
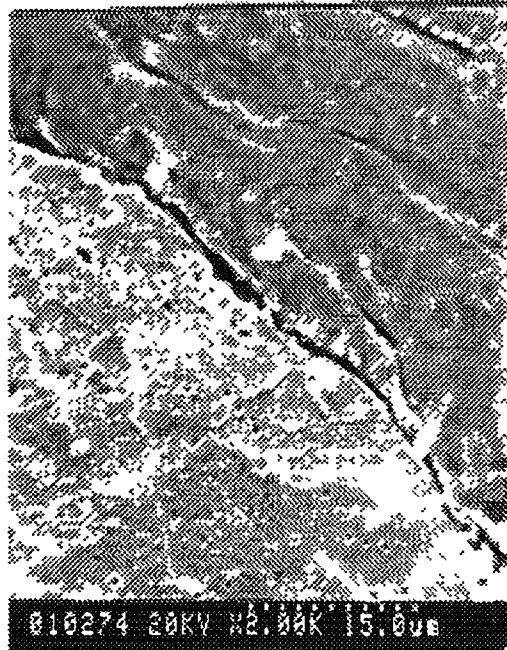
U$_3$Si-Zr Composition
x 700

U$_3$Si -Al Composition
x 2000
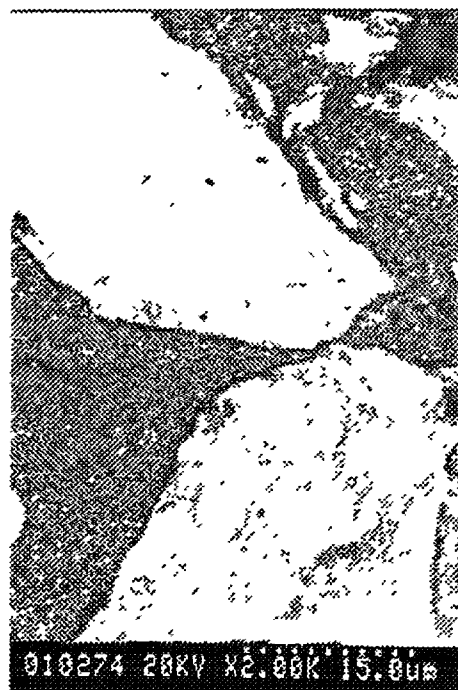
Fig.1

Influence of Annealing Temperature on Volume Changes of Compositions
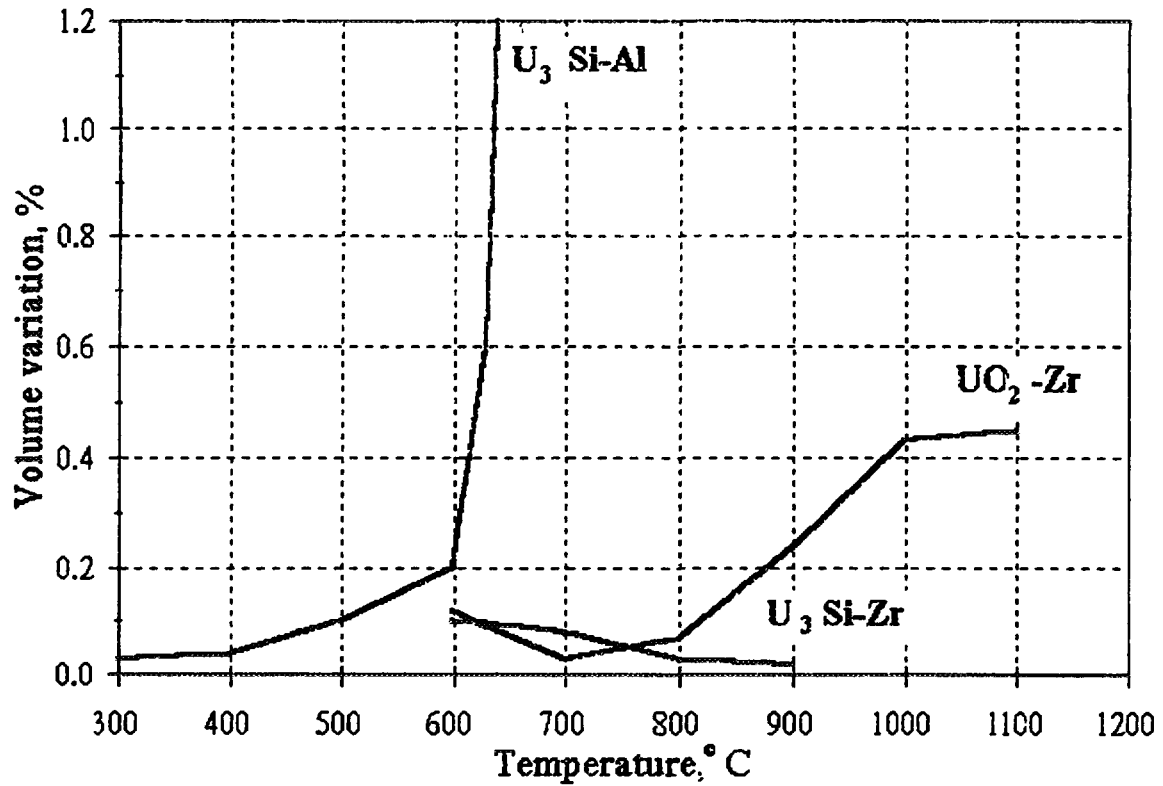
Fig. 2

Design of a Fuel Element for VVER-440
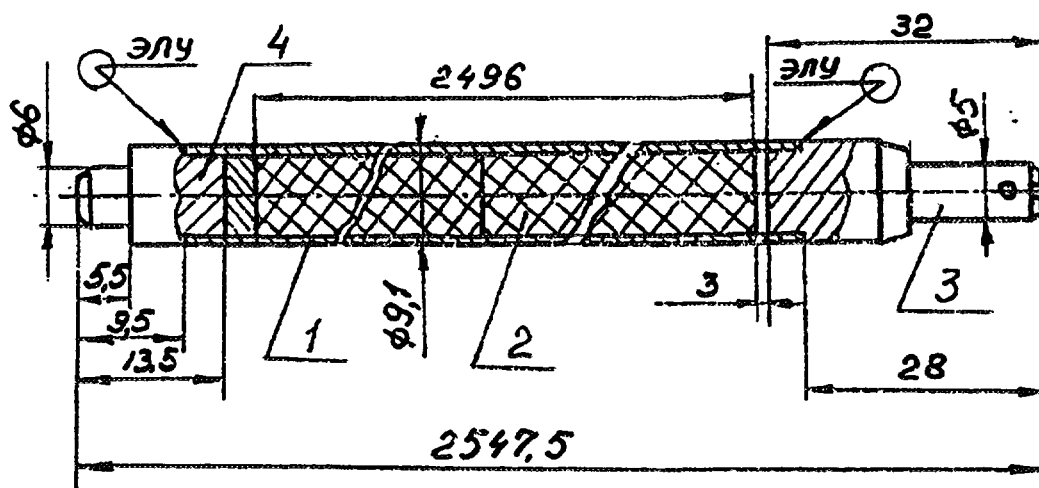
1 - fuel element shell; 2 - core in cladding; 3, 4 - plugs

Fig.3

The basic features of a cermet fuel element for WWER-440 with UO$_2$-Zr and UO -Al are pr6sented in Table 1.

We have developed technologies of manufacturing of cennet fuel elements with UO$_2$-Zr and UO$_2$-Al compositions. The basis of the technology are traditional methods of powder metallurgy and extrusion moulding (Fig. 4).

Technological process of fuel element manufacturing can be schematically divided into the following basic stages:

- preparation of fuel composition;

- manufacturing of core blanks

- assembling of a fuel element and welding of face components;

- control operations.

The developed technology has been tested in production conditions at fuel elements manufacturing factories where experimental cermet fuel elements were manufactured with UO$_2$Zr and UO$_2$-Al compositions for WWER-type reactors designed for resource tests in MIR reactor loops.

Both calculations and experiments confirm serviceability of fuel elements with cermet fuel in Russian WWER-type reactors.

3. Results of Thermal Calculations for Fuel Elements in the Active Core of WWER-440 Reactor

Calculations of thermal state of cermet fuel elements with UO$_2$-Al and UO$_2$-Zr have been carried out for operational conditions of the most thermally loaded fuel assemblies of the active core of WWER-440 reactor. The following reference data were used for calculations.

3.1. Operational Conditions in WWER-440

1. Fuel assembly - hexahedral, with the inner "spanner" dimension 144 mm.

2. Number of fuel elements - 126 plus one central technological tube.

3. Standard heat-transport medium pressure - 12.6 MPa.

Table 1. Basic Features of a Cermet Fuel Element for VVER-440

with UO$_2$-Zr and UO$_2$-Al Compositions

No	Parameter	Value
1	Mass of uranium in a fuel element, g	515
2	Fuel enrichment in uranium-235, per cent	4.4; 6.5
3	Volume content of uranium dioxide, per cent	up to 55
4	Thickness of zirconium or aluminium core cladding, mm	0.12 - 0.15
5	Grain size of fuel particles, um	50 - 200
6	Total core porosity, per cent	7 - 8
7	Inhomogeneity of fuel distribution in height, Coef	< 1.1

18

TECHNOLOGICAL FLOWCHART OF FUEL ELEMENTS MANUFACTURING ON UO_2-Zr COMPOSITION

| UO_2 Grains | — | Plasticizer | — | Zr powder |

Preparation of the blend

Cold moulding and degassing of blanks

Calibration and degassing of blanks

Calibration moulding, extrusion and degassing of blanks

Trimming of blanks, clarification control, marking

Degassing of core billets

Manufacturing of blanks of shell barrels and plugs from E-110 allow

Manufacturing of copper barrels

Degreassing and clarification of barrel blanks

Degassing of barrel blanks

Assembling of fuel blanks, sealing of metal/ceramic cores into zirconium barrels, marking

Degreasing of assemblies and their sealing into copper barrels, marking

Moulding of smooth rods in false shell

Ready-made shell out of alloys E-110, 635

Cutting of rods to size and chemical processing

Assembling of fuel elements

Joint rolling

X-ray examination, marking of boundaries of the active layer

Sealing plugs out of zirconium alloys

Machining of a fuel element to size

Sealing — Control — FINISHED PRODUCTS

Fig. 4

19

4   Average heat-transport medium temperature:

*   on entering the active zone - 265 to 270°C;
*   on quitting the active zone - 292 to 302 C.

5.   Heat-transport medium rate of flow through the fuel assembly - 100 to 130 m³/hour.

6.   Maximum temperature of heat-transport medium on quitting the cell with maximum load - 325°C.

7.   Linear thermal load of the most loaded fuel element (over the campaign) taking into account mechanical coefficients:

*   maximum - 325 W/cm;
*   minimum - 167 W/cm;
*   average - 211 W/cm.

8   Height distribution of thermal load: sinusoidal, K_z = 1.36.

3.2.   Thermal Constants

1.   Thermal conductivity of external zirconium shell of a fuel element - 20.8 W/m°C.

2.   Thermal conductivity of Zr cladding - 20.8 W/m°C, of Al one - 220 W/m°C.

3   Thermal conductivity of fuel compositions UO_2-Zr - 9 W/m°C, UO_2-Al - 66 W/m°C.

4.   Thermal resistivity of diffusion contact fuel/cladding R_T=O.

5   Thermal resistivity of contact of external shell and cladding: R_T= 50 C m²/MW in the first half of the campaign (1 st to 3 rd years of operation), R_T=O in the end of the campaign (4th year of operation).

Results of calculation are presented in Fig. 5.

Maximum temperature is located in the center of a fuel element and for maximum thermal load value 325 W/cm constitutes 713°C for UO_2-Zr composition and 490°C for UO2-Al composition. Taking into account inhomogeneity of fuel distribution in a fuel element KT = 1. I maximum temperature would constitute 755 and 505°C, respectively. In compliance with WWER-440 reactor operation schedule this value of temperature could be achieved by the beginning of the second year of operation and would be maintained within approximately 90 effective days which constitute not more than 7 per cent of the total active zone operation time.

By the end of the campaign (R_T=O) maximum temperature levels within a fuel element could be reduced due to increase of thermal conductivity of mechanical contact of the core with the shell up to 650°C for UO_2-Zr composition and 425 C for UO -Al composition (if inhomogeneity of fuel distribution is taken into account, these figures would be 685 and 435°C, respectively)

4.   Results of Calculations of Stressed-Deformed State (SDS) of Fuel Elements

Calculation of SDS of a fuel element with the shell set down on the core has been carried out according to flow theory taking into account ductility and creep; calculation of swelling of porous core - according to the model of spherical gaseous pores within the framework of flow theory. Hard-fragment oxide swelling was calculated basing of maximum assessment:

$$\Delta V/V = 0.12 \text{ m}$$

where m being accumulation of fission products 'n the core volume unit.

Total core porosity determined by the technology constitutes 7 to 8 per cent. Two types of porosity distribution over the core have been considered:

1)   there exists porosity of the order of 3.5 per cent between UO_2 grains and the matrix (most favourable case);

2)   porosity between UO_2 grains and the matrix is absent and is distributed uniformly (worst case).

Results of calculations for fuel element section with the most unfavourable SDS, located at the mark 1200 to 1400 mm from the bottom of the active part are presented in Table 2.

Results of calculations demonstrate that maximum shell deformation would not exceed 1 per cent which corresponds to the level of maximum deformations appearing in the shells of standard fuel elements of WWER-440 by the end of operation. Maximum change of a fuel element diameter would constitute 0.092 mm which is significantly less than the limiting value of 0.2 mm set forth in fuel element technical specification.

It should be noted as well that at all fuel element operation modes, including transient ones, tough core/shell fit is provided for due to permanently acting compressing radial stresses at the interface. This fact testifies to the conclusion that such a fuel element, in the aspect of the pattern of loading and deformation, actually does not differ from a fuel element with metallurgical shell/core adhesion possessing high reliability at transient mode operation.

Results of Thermal Calculations of a Cermet Fuel Element:

Fuel element with UO_2-Zr fuel composition   Fuel element with UO_2+Al fuel composition

Height distribution of characteristic temperatures in the beginning of the campaign

Height of fuel assembly, mm   Height of fuel assembly, mm
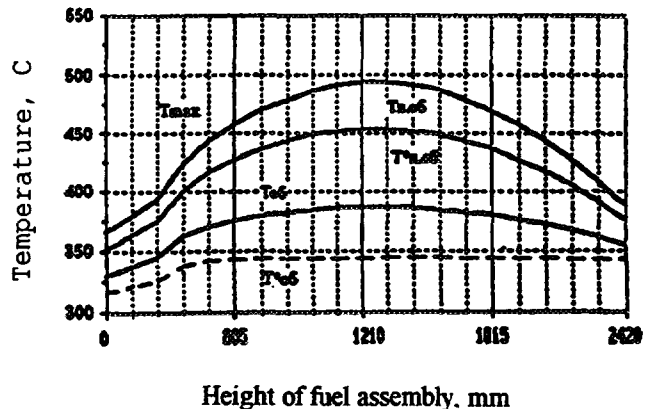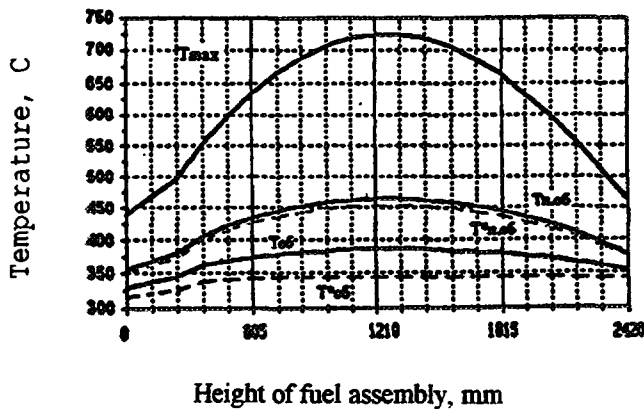
Height distribution of characteristic temperatures in the end of the campaign

Height of fuel assembly, mm   Height of fuel assembly, mm
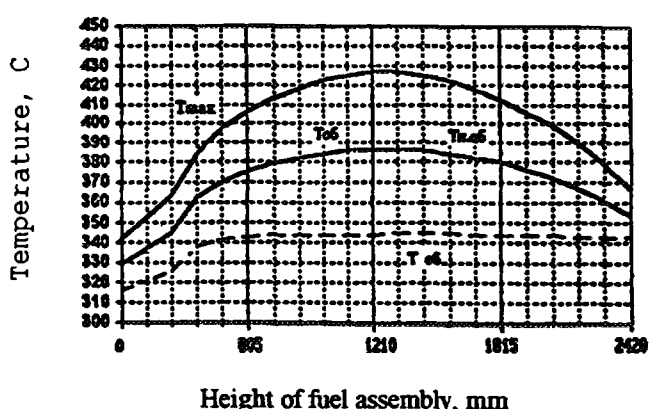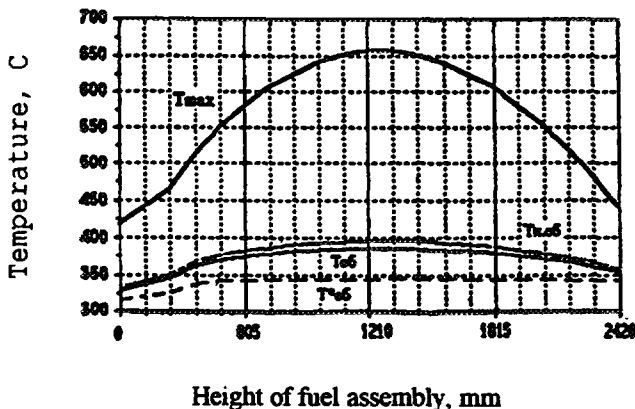
Fig.5

Table 2. Results of Calculations of SDS of Fuel Element Section with Depletion Depth 62 MW.day/kg U (0.55 g of fragments/cu.cm)

SDS Feature	Existence of Pores between UO2 and Matrix	
	Yes	No
Maximum tangential stress of the shell, t, Mpa	54 (83)	113 (170)
Minimum radial pressure at the boundary shell/core (tension), MPa	25 (20)	37 (28)
Maximum shell deformation, t, per cent	0.49	1.01
Maximum variation of fuel element diameter, mm	0.045	0.092
Axial elongation of a fuel element, per cent	0.01	0.02

Note: Maximum possible stresses taking into account influence of the most hard transient modes are in parentheses.

Besides, maximum stresses in the fuel element shell over all operation time of the latter would be less than E- II0 alloy yield point, hence fuel element shell deformations at various transient operation modes (including start-up and shutdown of the reactor) would occur in the domain of elastic deformations.

5.   Conclusion

Henceforth, using of cermet fuel elements in WWER reactors eliminates actually all constraints restrictions on the number of transient modes and on the rates of reactor power variation characteristic for standard pellet fuel elements. Our existing positive experience of operation of similar fuel elements in other devices having much more hard operation modes than WWER-440 testifies to the same.

COMPOSITE FUEL BEHAVIOUR UNDER AND AFTER IRRADIATION

Ph. DEHAUDT, A. MOCELLIN, G. EMINET, L. CAILLOT, G. DELETTE
Département de thermohydraulique et de physique,
Service d'études du comportement des combustibles,
Commissariat à l'énergie atomique,
Grenoble

M. BAUER, I. VIALLARD
Département d'études des combustibles,
Service plutonium et uranium,
Commissariat à l'énergie atomique,
Saint-Paul-lez-Durance

France

XA9745718

Abstract

Two kinds of composite fuels have been irradiated in the SILOE reactor. They are made of UO_2 particles dispersed in a molybdenum metallic (CERMET) or a $MgAl_2O_4$ ceramic (CERCER) matrix.

The irradiation conditions have allowed to reach a 50000 MWd/t U burn-up in these composite fuels after a hundred equivalent full power days long irradiation. The irradiation is controlled by a continuous measure of the pellets centre line temperature. It allows to have information about the TANOX rods thermal behaviour and the fuels thermal conductivities in comparing the centre line temperature versus linear power curves among themselves. Our results show that the CERMET centre line temperature is much lower than the CERCER and UO_2 ones : 520°C against 980°C at a 300W/cm linear power.

After pin puncturing tests the rods are dismantled to recover each fuel pellet. In the CERCER case, the cladding peeling off has revealed that the fuel came into contact with the cladding and that some of the pellets were linked together. Optical microscopy observations show a changing of the $MgAl_2O_4$ matrix state around the UO_2 particles at the pellets periphery. This transformation may have caused a swelling and would be at the origin of the pellet-cladding and the pellet-pellet interactions. No specific damage is seen after irradiation. The CERMET pellets are not cracked and remain as they were before irradiation. The CERCER crack network is slightly different from that observed in UO_2.

Kr retention was evaluated by annealing tests under vacuum at 1580°C or 1700°C for 30 minutes. The CERMET fission gas release is lower than the CERCER one. Inter- and intragranular fission gas bubbles are observed in the UO_2 particles after heat treatments. The CERCER pellet periphery has also cracked and the matrix has transformed again around UO_2 particles to present a granular and porous aspect

1. INTRODUCTION

In fuel rod manufacture, the use of composite materials is still a highly innovative, even futuristic concept. Basic research is being conducted on this subject and consideration is being given to ways of identifying all potential and promising uses of the concept. For end fuel cycle applications in particular, the introduction of actinides in an inert ceramic matrix could be envisaged with a view to their incineration in a cooled water or fast flux reactor In all cases, the behaviour of a composite containing small accumulations of fissile matter (uranium and/or plutonium) is not sufficiently detailed and numerous studies will be needed to check the concept.

This article presents the results of a research programme on two specific composite fuels, designed as study materials. They differ by their inert matrices, one being a metal (CERMET), molybdenum, and the other a ceramic (CERCER), MgAl2O4 spinel. The UO2 fuel is in the form of

dispersed granules in the matrix. Data are provided on the behaviour of these irradiated fuels and suggested answers and considerations are given on the two main benefits expected, namely, enhanced thermal conductivity and reduction in fission gas release at high burnups. The analysis and interpretation of the post-irradiation examinations has not yet been completed and, consequently, no final conclusions can be drawn at this stage. Further studies in the programme will be aimed at gaining a better understanding of the mechanical and thermal properties of the various phases taken separately and of the composite as a whole. Plutonium is the fissile element considered for composite fuels in order to avoid high enrichments which would be required in the uranium case.

2. CHARACTERISTICS OF COMPOSITE FUELS BEFORE IRRADIATION

The two fuels will be designated by:

- CERMET for the one with molybdenum matrix,
- CERCER for the one with $MgAl_2O_4$ matrix.

Both composites contain 36% by volume of essentially ellipsoid UO_2 particles, of 100 to 150 μm size (Fig. 1a and 1b). The aim is to obtain as homogeneous a distribution of particles as possible but a few clusters will inevitably remain. The matrix coats the particles with an inter-particular distance greater than 5 μm, stopping distance of fission products emitted by ejection and recoil. The uranium is enriched with 19.6 wt.% of ^{235}U in order to obtain a content of around 1.7 x 10^{21} atoms of ^{235}U per cm^3 of composite which is compatible with irradiation conditions. The density, open porosity, redensification, pellet geometry and grain size of the sintered products are listed in Table I.

Note that there is a significant proportion of open porosity (2.5%) in the CERMET after sintering. This porosity is, for the most part, found in the molybdenum matrix which redensifies during the thermal stability test. This inconvenience is eliminated when the sintering time is made longer. Microstructural observations show that the UO_2/Mo interface is of high quality (Fig. 1c) and can be considered to be perfect for the thermal calculations. In the CERCER, the UO_2 particles are cracked although there is no reason why the UO_2/MgAl$_2$O$_4$ link should be incriminated. The cylindrical surface of the pellets is ground to allow them to be assembled with a reduced cladding gap. There are then surface irregularities between Mo and UO_2 for the CERMET and traces of pitting for the CERCER. The 100 mm long fissile columns are made up of 10 full pellets at the bottom and 10 annular pellets at the top to allow a thermocouple to be positioned to measure the centre line temperature continuously during irradiation.

Tab. I : Characteristics of the studied composite fuels before irradiation

	CERMET		CERCER
	full pellets	annular pellets	all pellets
Geometrical density (g/cm³)	9.80	9.84	5.98
% of theoretical density	93.4	93.8	96
Open porosity (vol. %)	2.5	1.9	≤ 2.1
Redensification (%)	1.54		0.58
External diameter (mm)	4.917	4.916	4.917
Internal diameter (mm)		1.3	1.3
Height (mm)	5.086	5.067	5.008
Mean grain size (µm)	5 to 15		≈ 5

Fig. 1a :
General aspect

200 µm

Fig. 1b :
Morphology of UO$_2$ particles

50 µm

Fig. 1c :
UO$_2$/Mo interface

10 µm
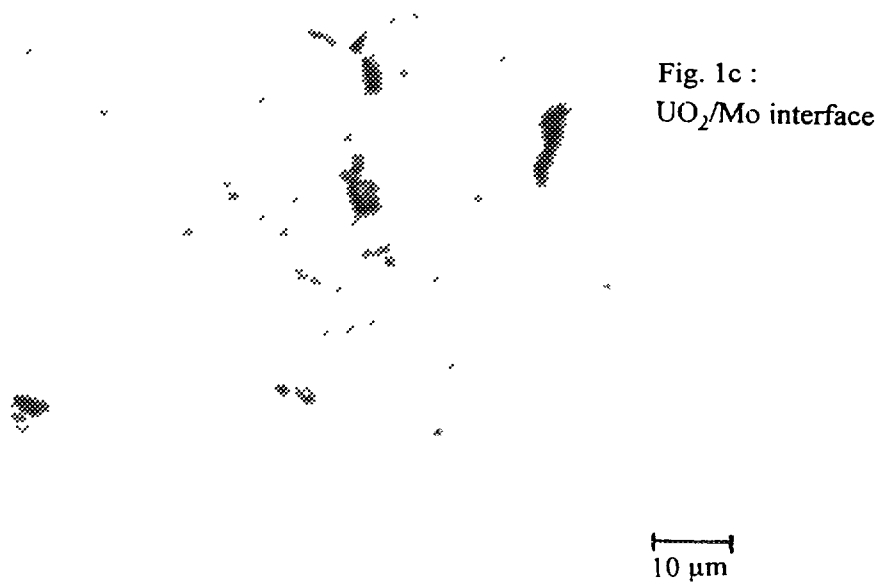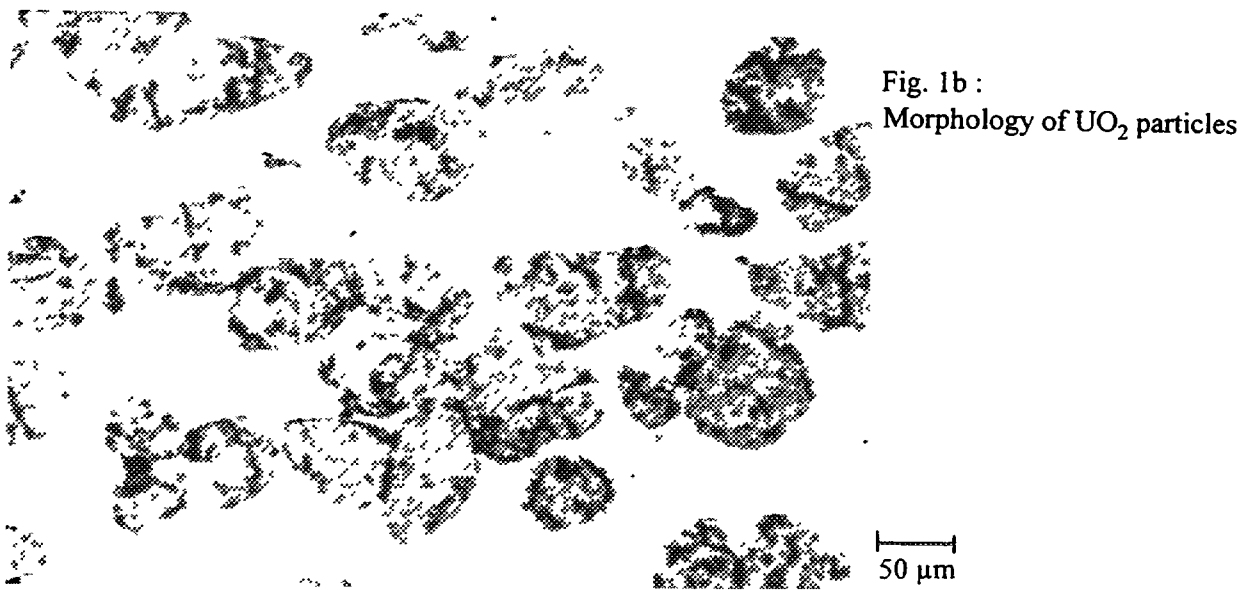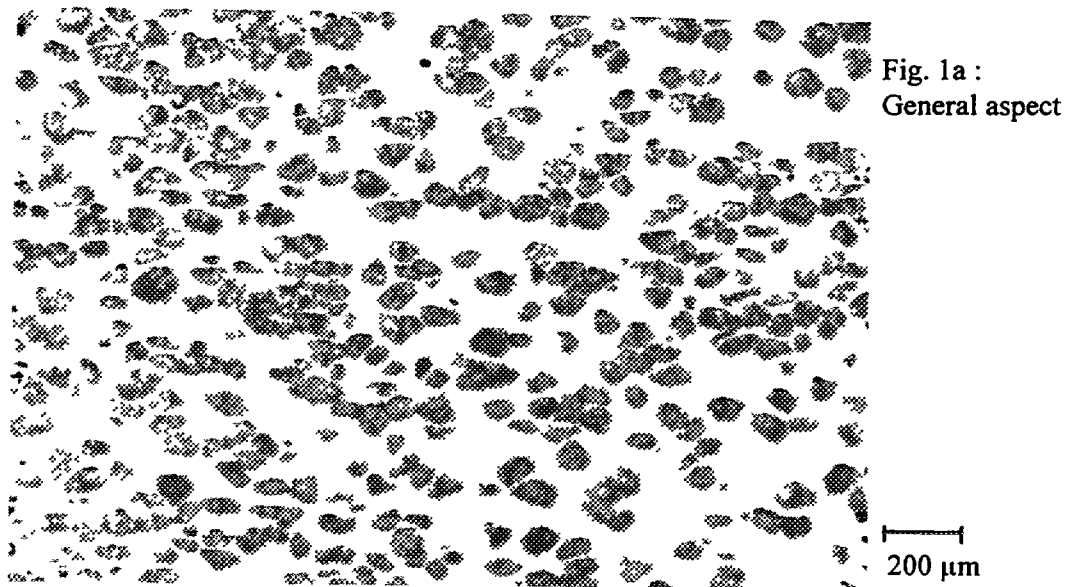
Fig. 1 : Microstructure of the CERMET fuel before irradiation

3 IRRADIATION IN THE TANOX DEVICE

Analytical irradiation is performed in the TANOX device in the SILOE experimental reactor in Grenoble A more detailed description of the TANOX device and its position with respect to the SILOE pile is given elsewhere [1]. Thanks to the original design of the device, significant burnups can be attained with short irradiation times. By using composite fuel, the effect is exacerbated and local burnups in the UO_2 particles increase rapidly. For example, for CERMET (fuel rod T2-2), with an irradiation level of 104.5 EFPD (Equivalent Full Power Days), a burnup of 55400 MWd/t U was achieved, while for CERCER (fuel rod T2-3), with an irradiation level of 80.6 EFPD, a value of 40300 MWd/t U was obtained. The latter experiment had to be interrupted prematurely as a result of an operating problem with the axial thermocouple, the readout of which is used to control the experiment

The fuel rod T2-1, containing UO_2, is used as a thermal reference for the composite fuel experiment Fuel rods T2-4 to T2-6, containing standard UO_2, served as a comparison for fission gas release heat treatment; their burnups were 17170, 19080 and 19580 MWd/t U respectively

4 ANALYSIS OF CENTRE LINE TEMPERUTURE - POWER RELATIONSHIPS

Tc(P) curves, showing centre line temperature as a function of linear power, are plotted on the basis of pairs of experimental values. The centre line temperatures are those measured by the thermocouples during irradiation. The linear powers are readjusted at the end of irradiation by comparison between the calculation and inventory measurements of certain fission products quantified by g spectrometry.

In addition, a simplified modelling procedure was developed to plot the Tc(P) laws calculated and to compare them to points obtained experimentally. This model involves resolving the static heat equation by considering the hot geometry of the rods and the change in thermal properties, expansion and conductivity, with temperature. The conductivity laws of fuels other than standard UO_2 are evaluated as a function of the microstructural changes made [2]. The thermal conductivity law for composites was calculated by Maxwell-Eucken's law of mixtures from the conductivity law of each component [3] This modelling procedure was used to check certain damaging effects of the thermal conductivity of fuels (hyperstoichiometry, porosity, additives, cracking, temperature) It is hoped that by refining the model it will be possible to determine the conductivity laws applicable to fuels

The thermal study of composite fuels is summarised on Figure 2 which gives the experimental points and the calculated laws in the (Tc, P) plane for fuel rods T2-1 to T2-3. The following facts were noted ·

- the CERCER (T2-3) has a thermal response very close to that of a conventional UO_2 (T2-1);
- the CERMET (T2-2) is at much lower temperatures regardless of the linear power (Tc ≤ 565°C); the difference increases continuously as power increases : a gain of a factor of 2 is obtained on centre line temperatures measured at 300 W/cm;
- there is good agreement between measurements and calculations for UO_2 and for the CERMET; on the other hand, for the CERCER, a 20% better thermal conductivity is predicted compared to that observed under irradiation.

This thermal analysis provides a wealth of information. It confirms the benefit of a metallic matrix, in this case molybdenum, for obtaining a significant increase in the thermal conductivity of a composite fuel. The ceramic matrix, $MgAl_2O_4$, does not match this performance, its conductivity being 10 to 20 times lower than that of molybdenum. The CERMET therefore remains relatively "cold" during irradiation whereas the CERCER behaves like a conventional UO_2 fuel. Our calculations do not corroborate this point, probably as a result of the insufficient knowledge of the thermal conductivity of the $MgAl_2O_4$ spinel and perhaps also because of an imperfect composite structure which does not satisfy the conditions of application of the Maxwell-Eucken type law of mixtures This law does nevertheless provide a good evaluation of the CERMET conductivity, a fact that was verified from the experimental measurements made on a CERMET Mo + 60 vol % UO_2 by COLLINS and al. [4]

Fig. 2 : Centre line temperature versus linear power diagram
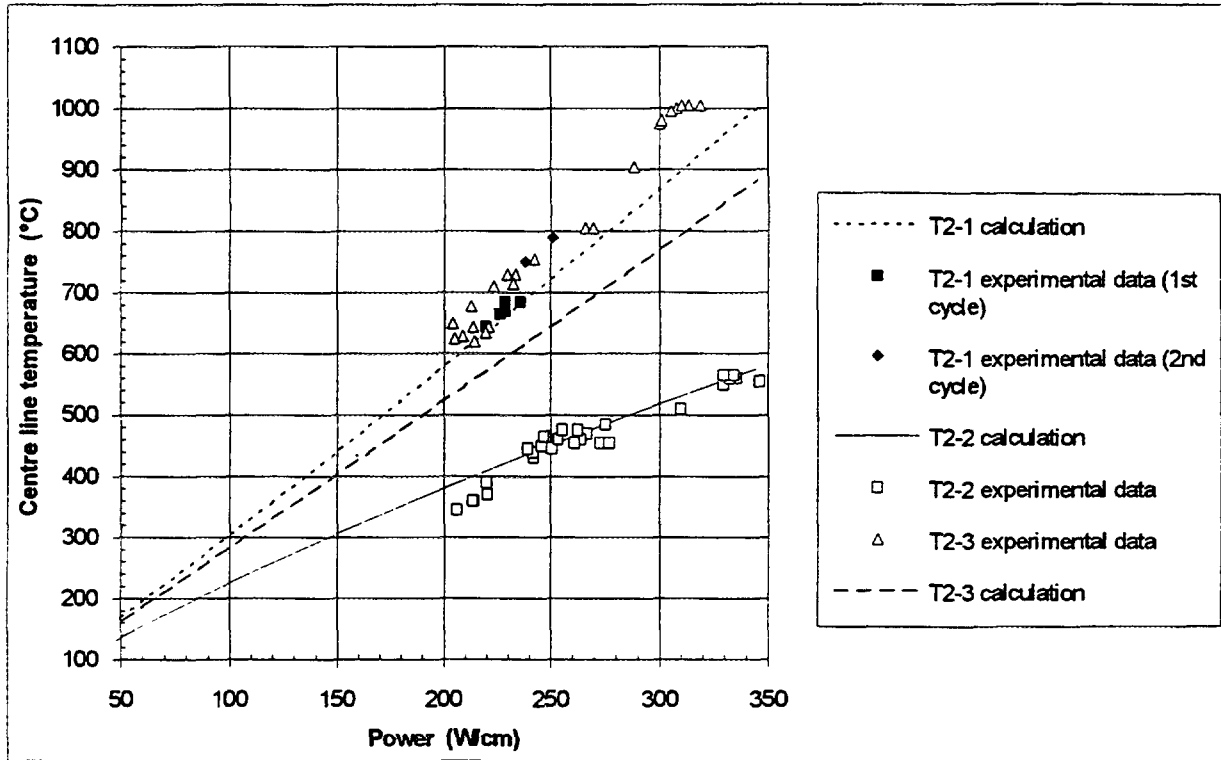
5. POST-IRRADIATION STUDIES OF FISSION GAS RELEASE

The fuel rods are drilled in order to measure the quantities of fission gases released during irradiation. They are then opened to recover the fuel pellets one by one. The individual irradiated pellets are then heat treated so as to encourage the release of gaseous and volatile fission products.

5.1. Drilling of the cladding and opening of fuel rods

For the CERMET, fuel rod T2-2, the fraction of [85]Kr released during irradiation is 2.1%. Considering the relatively low temperature of this fuel, this release may be assumed to result only from fission product atoms emitted by ejection and recoil, originating from UO_2 granules emerging at the pellet surface and central bore. The cladding was cut open along three generating lines and revealed integral, well identified fuel pellets with external appearance very similar to that observed before irradiation.

For the CERCER, fuel rod T2-3, the fraction of [85]Kr released during irradiation is 0.7%. This value, three times lower than that for the CERMET, is surprising and can only be explained by the existence of a strong contact between fuel and cladding during most of the irradiation period. This is borne out by the fact that, when dismantling the T2-3 fuel rod, fuel was torn away from the outer edge of the pellets, with some remaining bonded to the cladding and some being lost in the form of tiny fragments. It is thus evident that a high degree of interaction occurred between the fuel and the cladding, but also between the fuel pellets themselves as some of them were bonded together (Fig. 5a). This specific behaviour must be due to swelling of the CERCER under irradiation, because thermal expansion of the fuel and cladding alone would not lead to total closure of the pellet/cladding gap. Section 5.3 shows that a transformation of the $MgAl_2O_4$ matrix occurred around the UO_2 particles on the edge of the pellets and this may have been the cause of swelling.

Fig. 3a : Along a pellet radius

150 μm
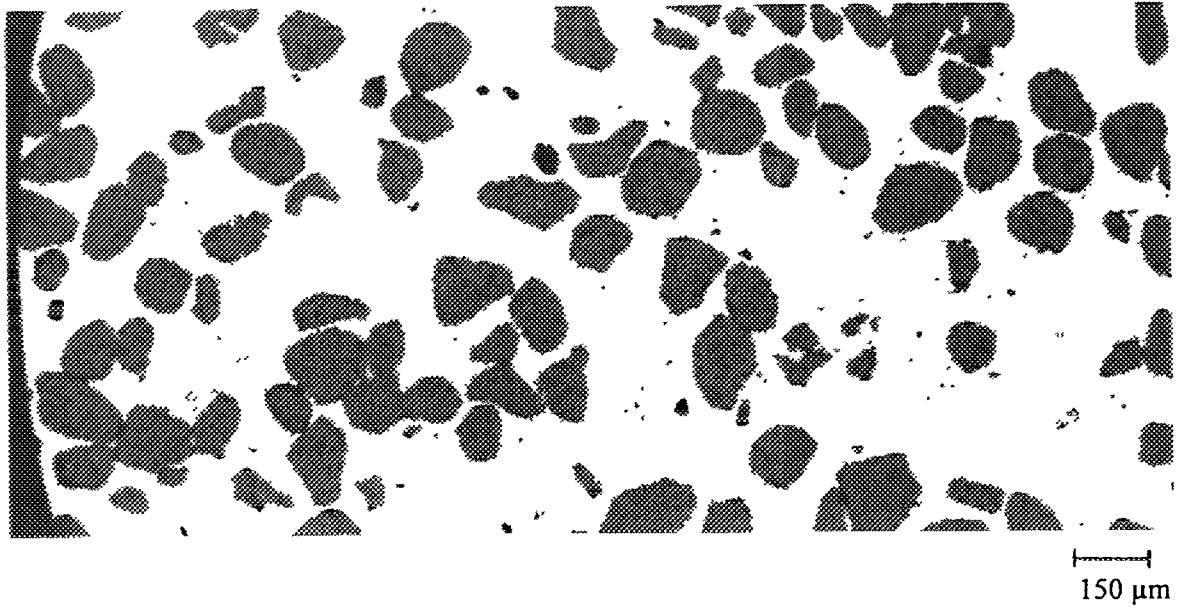
Fig. 3b : Details of UO$_2$ particles embedded in the Mo matrix

30 μm

30 μm
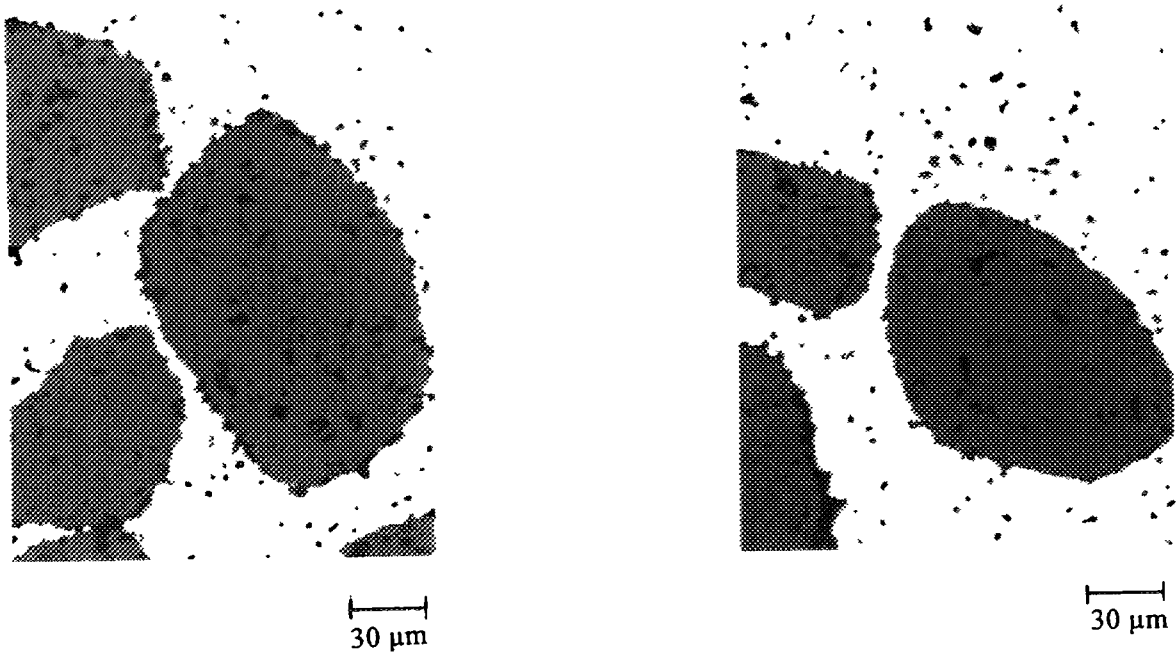
Fig. 3 : Microstructure of the CERMET fuel after irradiation

Fig. 4a :
General view of the
heat treated pellet
(cross-section)

1 mm
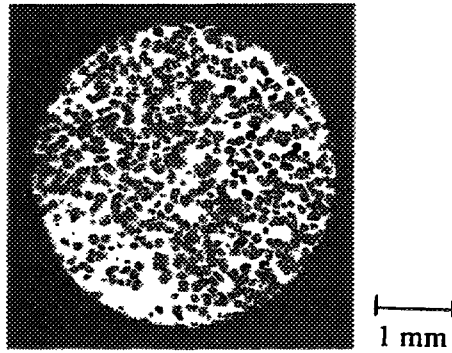
Fig. 4b :
Along a radius of the pellet

150 µm
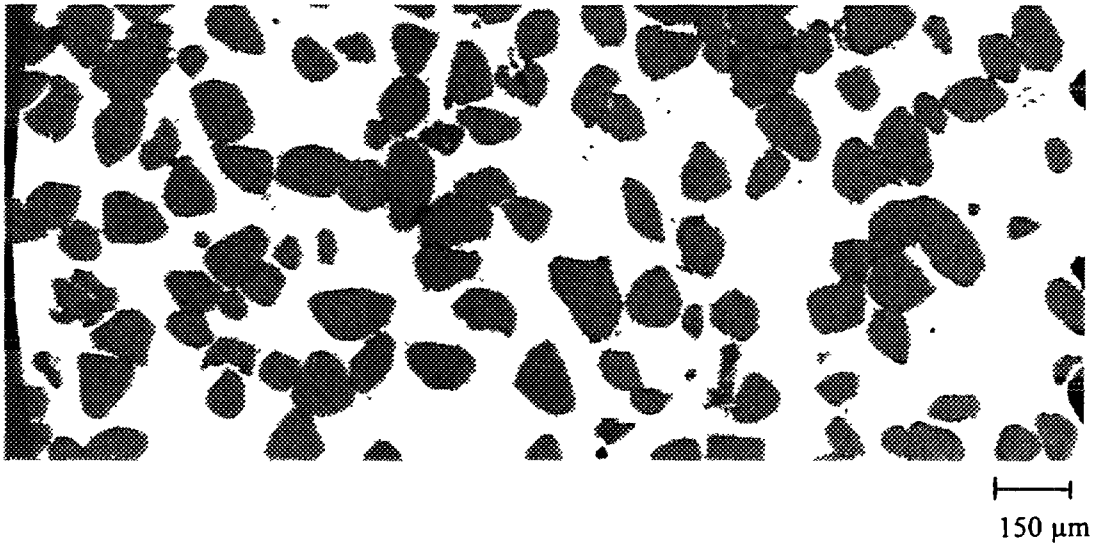
Fig.c :
An UO$_2$ particle and its interface with the matrix

30 µm   15 µm
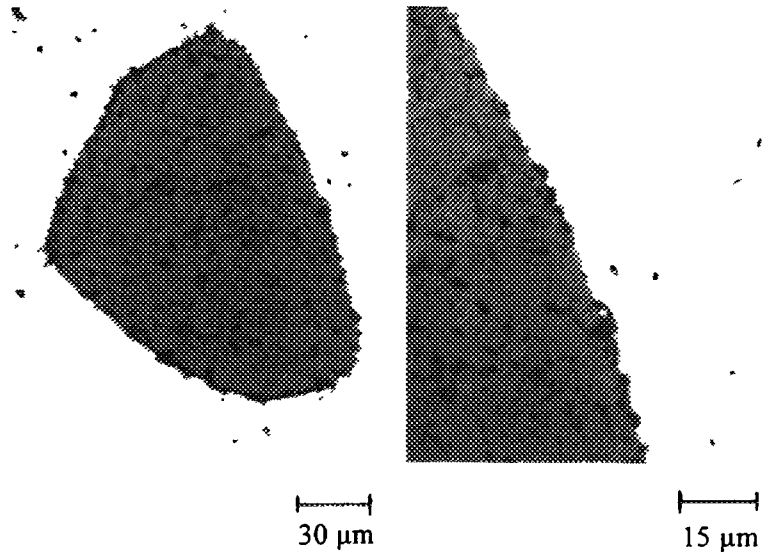
Fig. 4 : Microstructure of the irradiated CERMET fuel after an
annealing test at 1580°C for 30 minutes

Fig. 5b : Through the pellet
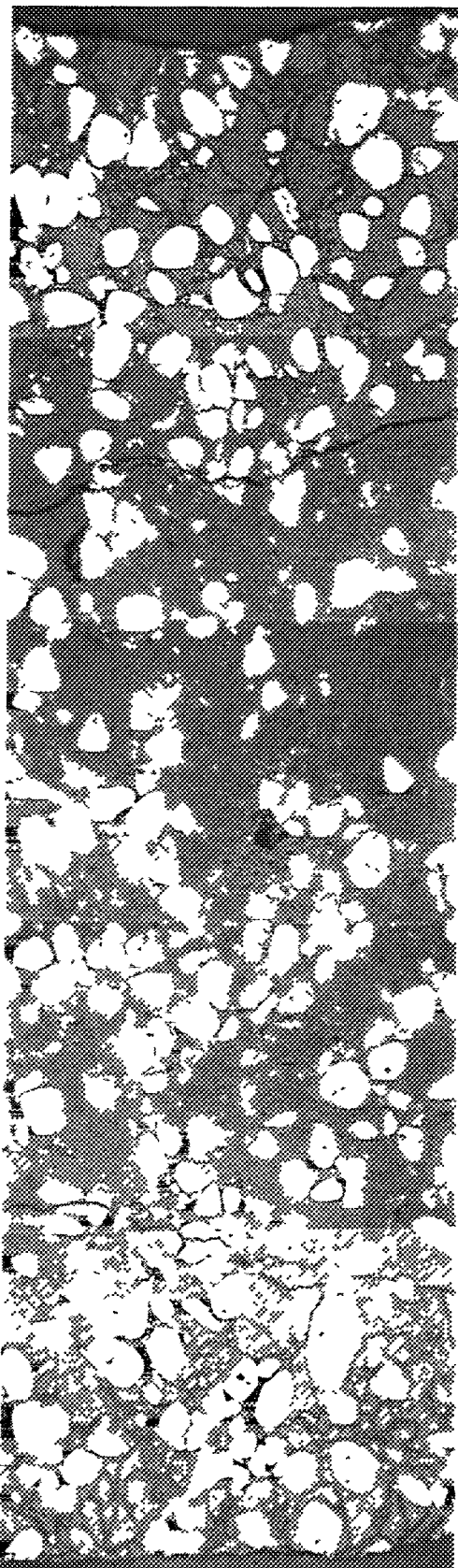
Fig. 5a :
Two linked pellets
(longitudinal section)
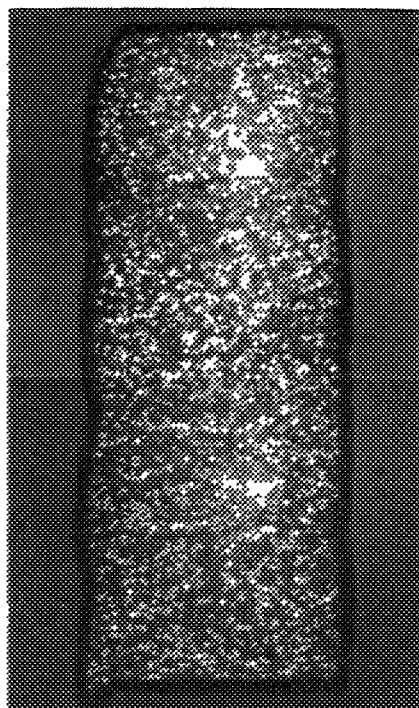
1 mm

Fig. 5d :
At the pellet centre
(after chemical etching)

30 μm

150 μm

Fig. 5c :
At the pellet periphery
(after chemical etching)
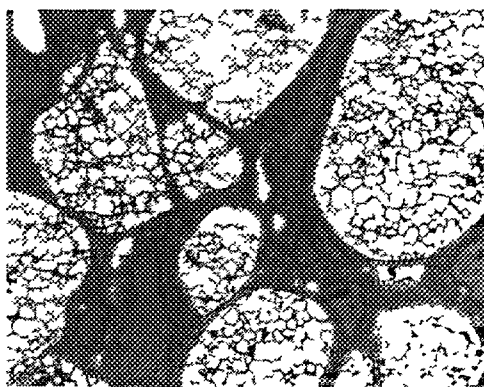
30 μm

Fig. 5 : Microstructure of the CERCER fuel after irradiation

5.2. Release of ^{85}Kr by high-temperature annealing

Heat treatment is performed under vacuum in an HF furnace located in a hot cell. The temperature are hold at 1580°C or 1700°C last 30 minutes during which the gases escaping from the annealed pellet are collected in a glass capsule by means of a Toeppler pump installed in the glove box. The capsule is then analysed by g spectrometry to count the ^{85}Kr atoms. This number of released atoms divided by the number of ^{85}Kr atoms present in the pellet on the heat treatment date gives the fraction of released ^{85}Kr. The values obtained for composite fuels and for a standard UO_2 are presented in Table II. Given that the burnups are different, an immediate comparison is not obvious. However, there can be no denying that the CERMET has very low release rates : at 1700°C and 55400 MWd/tu, the release rate is less than that of a UO_2 at about 18000 MWd/tu. Moreover, the heat treatment temperatures will never be reached by the CERMET during irradiation. The CERCER presents higher release rates than the UO_2 references which is in agreement with the burnups. These results validate the dual barrier concept, UO_2 + matrix, with respect to fission gas release for the CERMET but not for the CERCER.

5.3. Irradiated microstructures before and after heat treatment

Optical microscopy observations on a polished section are made on an as-irradiated pellet and on heat treated irradiated pellets.

The irradiated CERMET keeps an integral structure without any really perceptible trace of damage on a UO_2 particle scale (Fig. 3a). The matrix is not affected by irradiation and the UO_2/Mo interfaces remain adherent (Fig. 3b).

After heat treatment at 1580°C, the CERMET pellet retains its general original appearance (Fig. 4a and 4b). Fission gas bubbles mark the UO_2 grain boundaries (Fig. 4c). Intragranular bubbles also appear but they are much more visible after the heat treatment at 1700°C. The UO_2/Mo interfaces are also the origin of gas bubble precipitation. A slight overall increase in interfacial porosity is observed.

The irradiated CERCER is not fractured but contains a network of longitudinal and transverse cracks that is less extensive than in a standard UO_2 (Fig. 5a). The strong contact with the cladding no doubt led to closure of the existing cracks and prevented the initiation of new ones. Observations were made on a longitudinal section of two joined CERCER pellets (Fig. 5b) where the outer layer was destroyed when opening the fuel rod (cf. § 5.1). The transversal change in microstructure is visible on figure 5b which shows the presence of a phase surrounding the UO_2 particles in the outer part of the pellet. Taking into account the fact that part of the fuel was torn away when opening the rod, this phase would be located in an annular area about 1.5 mm thick where the temperature remains lower than about 1000°C. Its thickness around the UO_2 particles is constant and equal to 5 μm (Fig. 5c). According to our WDS (Wave Dispersive Spectrometry) analyses by SEM (Scanning Electron Microscope) the layer does not contain any elements that are not already in the

Tab. II : ^{85}Kr release fractions during annealing tests at 1580°C and 1700°C for 30 minutes

Fuel	Rod	Burn-up MWj/tu	^{85}Kr release fractions	
			1580°C - 30 min	1700°C - 30 min
UO_2	T2-4	19080		0.24
UO_2	T2-5	17170		0.38
UO_2	T2-6	19580	0.1	0.40
CERCER	T2-3	40300	0.25	0.51
CERMET	T2-2	55400	0.12	0.17

CERCER. Consequently, we have rejected the hypothesis of the formation of a new phase in favour of a transformation of the matrix by amorphisation due to the fact that the fission products are stopped. In the middle of the pellet in UO2 the inter- and intra-granular bubbles of fission gases are already widely present, as revealed by chemical etching (Fig. 5d).

After heat treatment of pellet fragments at 1580°C (Fig. 6a), numerous micro-cracks appeared in the matrix, their density being particularly high in the pellet edge zone where the phase

Fig. 6a :
General view of the
heat treated pellet
(cross-section)

⊢————⊣
1 mm
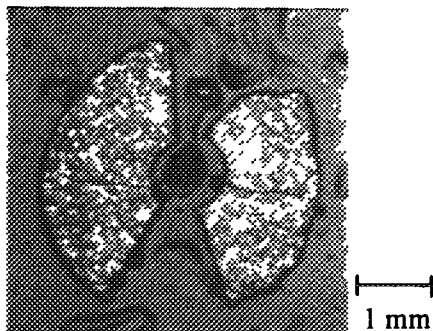
Fig. 6b : Along a radius of the pellet

⊢————⊣
150 µm
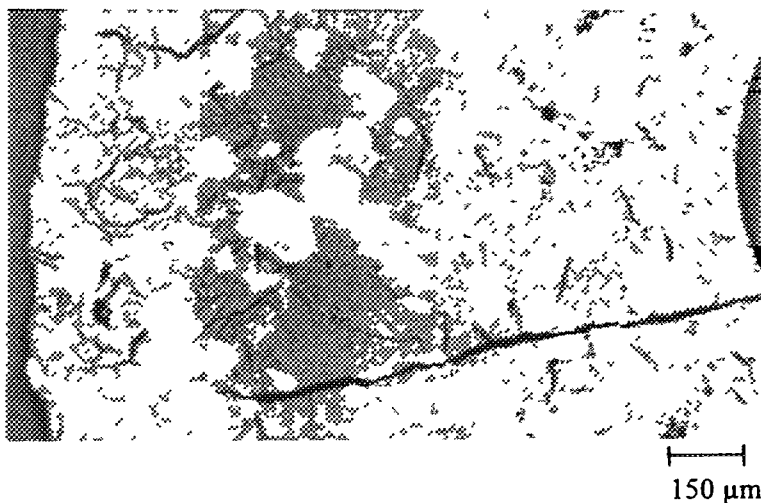
Fig. 6c : At the pellet periphery   Fig. 6d : At the pellet centre
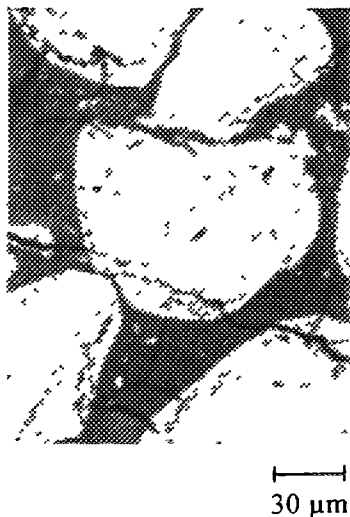
⊢————⊣   ⊢————⊣
30 µm   15 µm

Fig. 6 : Microstructure of the irradiated CERCER fuel after an
annealing test at 1580°C for 30 minutes

that appeared during irradiation was observed (Fig. 6b). This cracking causes percolation of the UO_2 granules which promotes fission gas release. The heat treatment causes the phase around the UO_2 granules to disappear: the regular and homogeneous surround is replaced by a granular and porous structure (Fig. 6c) which is also found in the middle of the pellet (Fig. 6d): this supports the recrystallisation theory.

6. CONCLUSIONS

The results presented in this article show a particularly interesting behaviour of the CERMET in terms of enhanced thermal conductivity and fission gas retention (^{85}Kr) during high-temperature annealing. The CERCER has a thermal conductivity close to that of standard UO_2 and ^{85}Kr release rates that are considerably higher than those measured on the CERMET, twice as high at 1580°C and three times as high at 1700°C, for a lower burnup.

The CERMET microstructure does not change during irradiation. Intergranular fission gas bubbles appear during subsequent annealing.

The CERCER microstructure is significantly modified during irradiation, leading to swelling and strong pellet/cladding and pellet/pellet interactions.

REFERENCES

[1]   DEHAUDT, Ph., CAILLOT, L., DELETTE, G., EMINET, G., MOCELLIN, A., Irradiation of UO_{2+x} fuels in the TANOX device, IAEA TCM on Advances in Pellet Technology for Improved Performance at High Burnup, Tokyo, Japan, 28 oct.-1 nov. 1996.

[2]   MARTIN, D.G., A re-appraisal of the thermal conductivity of UO_2 and mixed (U, Pu) oxide fuels, J. Nucl. Mater. 110 (1982) 73-94.

[3]   STORA, J.P., Thermal conductivity of two-phase solid bodies, Nucl. Technol., 17 (1973) 225-233.

[4]   COLLINS, J.F., FLAGELLA, P.N., Fabrication and measurement of properties of Mo-UO_2 CERMETS, General Electric, Nuclear Technology Department, Nuclear Energy Division, report GEMP-545 (1967).

RESULTS OF EXPERIMENTAL INVESTIGATIONS FOR SUBSTANTIATION OF WWER CERMET FUEL PIN PERFORMANCE

V.V. POPOV, A.D. KARPIN, I.A. ISUPOV, V.N. RUMYANTSEV,
V.M. TROYANOV, V.N. SUBONYAEV, N.A. MELNICHENKO
Institute of Physics and Power Engineering,
State Scientific Centre of the Russian Federation,
Obninsk, Russian Federation

Abstract

The out-of-pile experiment results on interaction of the cladding and matrix materials and uranium dioxide at cermet fuel temperature for normal operating conditions of the WWER-440 reactor are analysed. Cermet fuel element behaviour under the maximum designed damage of the WWER-440 reactor is considered. In the AM reactor loop a fission product output from the unsealed cermet fuel elements have been studied.

Introduction

The cermet fuel pin shown in fig. 1 has a monolithic type design that is as follows: a fuel core consisting of uranium dioxide particles ("middlings") surrounded by metallic matrix with good physical, thermophysical and corrosion-resistant properties is rigidly bonded with a Zr + 1 % Nb clad in a metallurgical or diffusional way.

Thermal resistance at a "cermet fuel - clad" boundary is to be minimized, and a cermet fuel core must have good thermal conductivity, so that the maximum fuel temperature should not exceed the matrix melting point as well as the temperature at which strong interaction of fuel pin components begins. The cermet fuel composition must have good corrosion and erosion resistance in the coolant to ensure safe reactor operation even if some unsealed fuel pins are available.

In the present paper consideration is given to results of pre-reactor and post-reactor tests of pins with cermet fuel consisting of uranium dioxide particles in the silumin matrix.

1. Investigations of thenrnophysical properties of cenmd fuel pins

1. 1. Measurement of fuel thermal conductivity

Cermet fuel specimens 7,8 mm in diameter and 20 mm in height consisting of 60% vol. UO_2 + 40% vol. silumin have been investigated. Cermet thermal conductivity measurements have been carried out in the experimental unit "KS" in steady state by the plate method using as a primary standard an Armco-iron specimen having known thermal conductive. The measurements have been carried out in a vacuum of $\sim 10^{-3}$ Pa in a temperature range 100 - 500°C.

The measurement relative error was 12% at the 100°C temperature level and 7% at higher temperatures.
Average values of cermet fuel thermal conductivity are given in Table. 1.

1.2 Measurements of the resistance of clad-fuel bonding

Testing of "fuel composition-clad" bonding degree has been carried out by the active thermal method with moving of a fuel pin through the central hole of a tubular furnace. Evaluation of the bonding degree was carried out by the time of heating a external surface is less fuel pin external surface up to a specified temperature. If there exists a thermal resistance in a zone of contact, the heating up time of the than if an ideal thermal contact takes place. For temperature registration the thermal indicator of melting (TI-85) was used that was applied on entire surface of a fuel pin. By increasing the heating time and locating the thermal indicator melting zones, one can reveal zones with still lower and lower thermal resistance at the clad-fuel boundary.

Table 1.

Values of cermet fuel composition thermal conductivity (λ)

Type of composition	λ, W/m·°C								
60% vol. UO_2 +	100	150	200	250	300	350	400	450	500
40% vol. Silumin	39,0	38,1	37,4	36,6	35,9	35,1	34,3	33,7	32

For quantitative evaluation of thermal resistance a program "SKOPO 3" has been developed that was intended for calculation of temperature field in a fuel pin. According to this program relationships of time, during which the fuel pin surface attains the thermal indicator melting point, to a value of the contact thermal resistance (Fig. 2) were obtained; taking them as a basis, by the intervals of times, found experimentally, heat transfer conditions were being determined.

Analysis of test results showed that in investigated fuel pins thermal resistance at the fuel-clad boundary is less than $1 \cdot 10^{-5}$ m²·oC/W (the limit of this method's sensitivity).

Calculations of temperature fields in cermet fuel pins with use of received thermophysical characteristics shawed that a ma)dmum temperature in the centre of a cermet fuel pin (60% vol UO_2 + 40% vol. silumin) is: $(T_{fuel})_{max}= 442°C$ - in the WWER reactor.

Pre-reactor isothermal tests were carried out at temperatures close to this one.

2. Investigations of compatibility of fuel pin materials in the process of a prolonged isothermic exposure

For this purpose simulators of cermet fuel pins (60% vol. UO_2 + 40% vol. silumin) have been subjected.

Fuel pin simulators were placed into argon-filled containers filled with argon and tested in the process of a prolonged isothermic exposure (τ =2700 hours) at the temperature 500°C.

After the test no cracks, bowings, distortions or other defects have been discovered in the fuel pin simulators.

The simulators have retained their geometric stability. The clad diameter changes were within the limits of measurement error.

Autoradiographic investigations have showed that at T = 500°C in the time τ = 2700 hours the diffusional penetration of uranium into the silumin matrix does not exceed 10 µm.
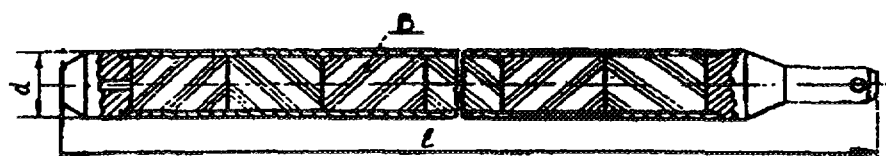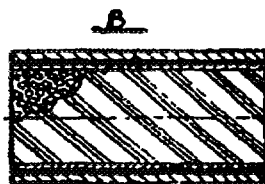
Cermet fuel

Fig 1 Cermet fuel rod for WWER-440 reactor
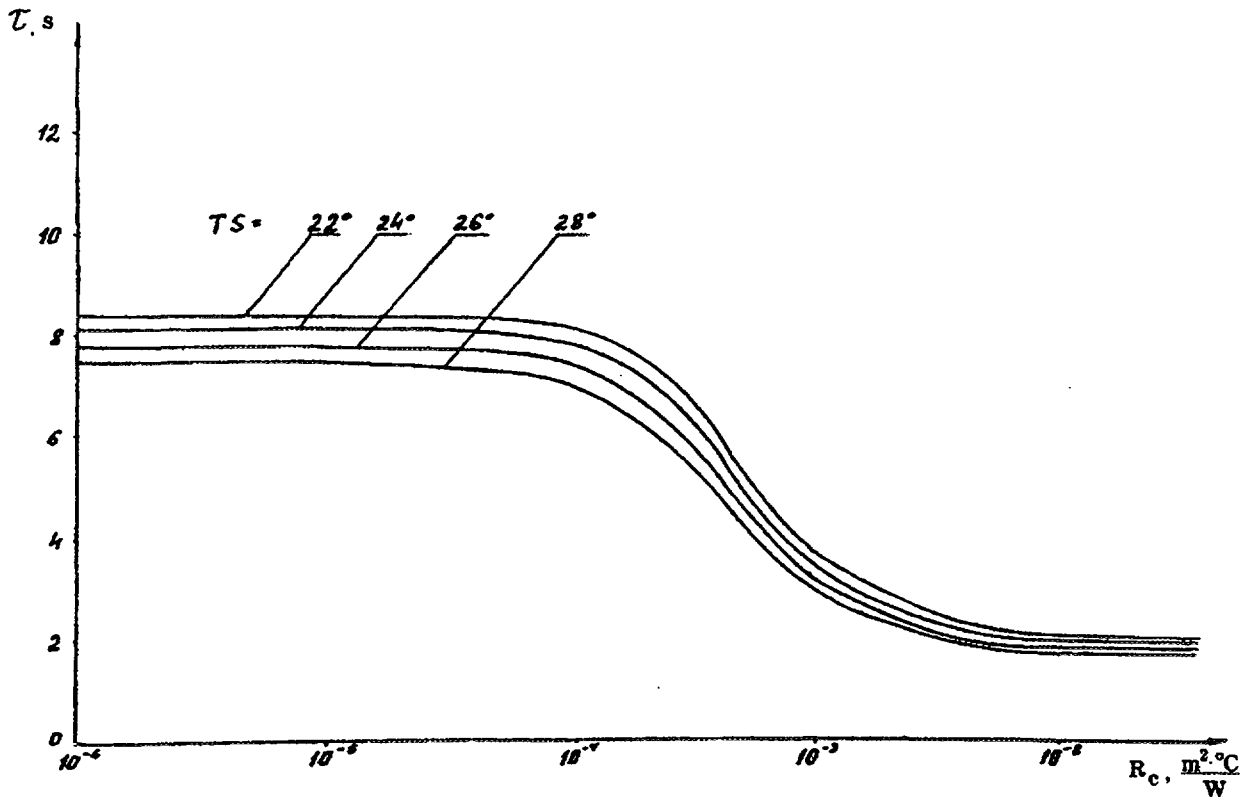
Fig. 2 Dependence of heating time (to 80 °C) of a fuel pin with 60% vol. UO_2 + 40% vol. silumin on contact thermal resistance

Metallographic anabpis of the fuel composftion has shown that the exposure of fuel pins under isothermal conditons does not lead to crack and void formation in the fuel composftion. No difference in fuel structure has been revealed in comparison with initial structure. Isothermic exposure of fuel pin simulators at the temperature 500°C causes no rise of the silumin microhardness both in the matrix base and immediately near the dioxide particles, and it remains comparable with microhardness of silumin in initial state (Table 2).

The distribution of main elements of fuel compositions after tests is presented in Fig. 3. One can see that uranium concentration at the UO_2 particles - matrix boundary reduces practically to zero values in areas having extent of no more than 10-15 μm.

Concentration of aluminium and silicium at the matrix-UO_2 particles boundary reduces to zero values in areas having extent of no more than 10-12 μm. Diffusional penetration of aluminium and silicium into UO_2 particles at the temperature 500°C does not take place.

X-ray phase analysis of cermet fuel has shown that main phases of the fuel compositions tested at the temperature 500°C are the initial components of the cermet fuel: UO_2, Al, Si. Exposure of fuel pin simulators under the temperature 500°C leads to appearance of such phases as UAl_3 and $USiO_4$. But their quantity is insignificant and they can be registered not in all zones of the cermet fuel.

Table 2

Microhardness of areas of fuel composition.

Matrix material	Particles	Matrix microhardness, kg/mm^2	
		close to particle	base
Initial silumin	-	-	50-90

37
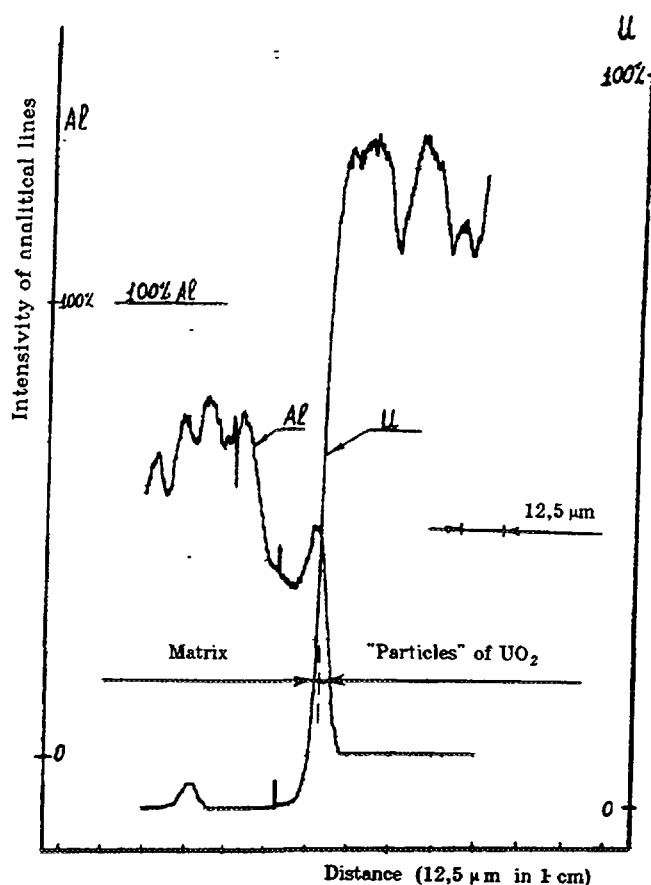
Fig. 3. Distribution of Al and U at the boundary "particle UO₂-matrix" after tests at temperature 500°C (a model)

3. Tests of fuel pin simulators with cermet fuel under conditions of design-basis accidents

Calculation investigations carried out previously showed that in the process of a maximum design-basis accident (MDBA) cermet fuel pins can attain the temperature up to 400-500°C (Fig. 4, 5).

Tests with fuel pin simulators have been carried out in the atmosphere of superheated water steam under the pressure of 0.15-0.25 MPa and at the temperature 500°C during 6 hours.

Exposure of fuel pins to superheated steam at the temperature 500°C during 6 hours leads to formation of dense dark-coloured oxide films on the surface of clad of Zr + 1 % Nb alloy. Received experimental results concerning the weight gain of fuel pin simulators investigated and of reference fuel pin simulator have shawn that corrosion resistance of fuel pin clads is on the level of corrosion resistance of a reference pin (wfth clad of fuel pin of standard design).

Fuel pin simulators have not changed their dimensions in the resuft of tests.

4. Tests of unsealed cermet fuel pins

4.1. Autoclave tests

With the purpose of determining of cermet fuel composition resistance in the coolant the autoclave tests with unsealed clads of fuel pin simulators and fuel composition specimens have been carried out in the following conditions: temperature 310°C, coolant pressure 10.6 MPa.

Autoclave tests of fuel pin simulators with artificial defects have been carried out during 72 hours. After autoclave testing the fuel pin clads have acquired the even black colour. Changes of fuel pin external diameter have not taken place. Dimensions of slots in specimens practically have not changed.

Analysis of water in which these fuel pin simulators has been tested showed absence of uranium in it (the sensitivity of method is 0.3 mg/m).

38

РАЗРЫВ ДУ 500. 1 ГЕ 1 НВД 1 ННД. ВЫБЕГ ГЦН ВМЕСТЕ С ГСР
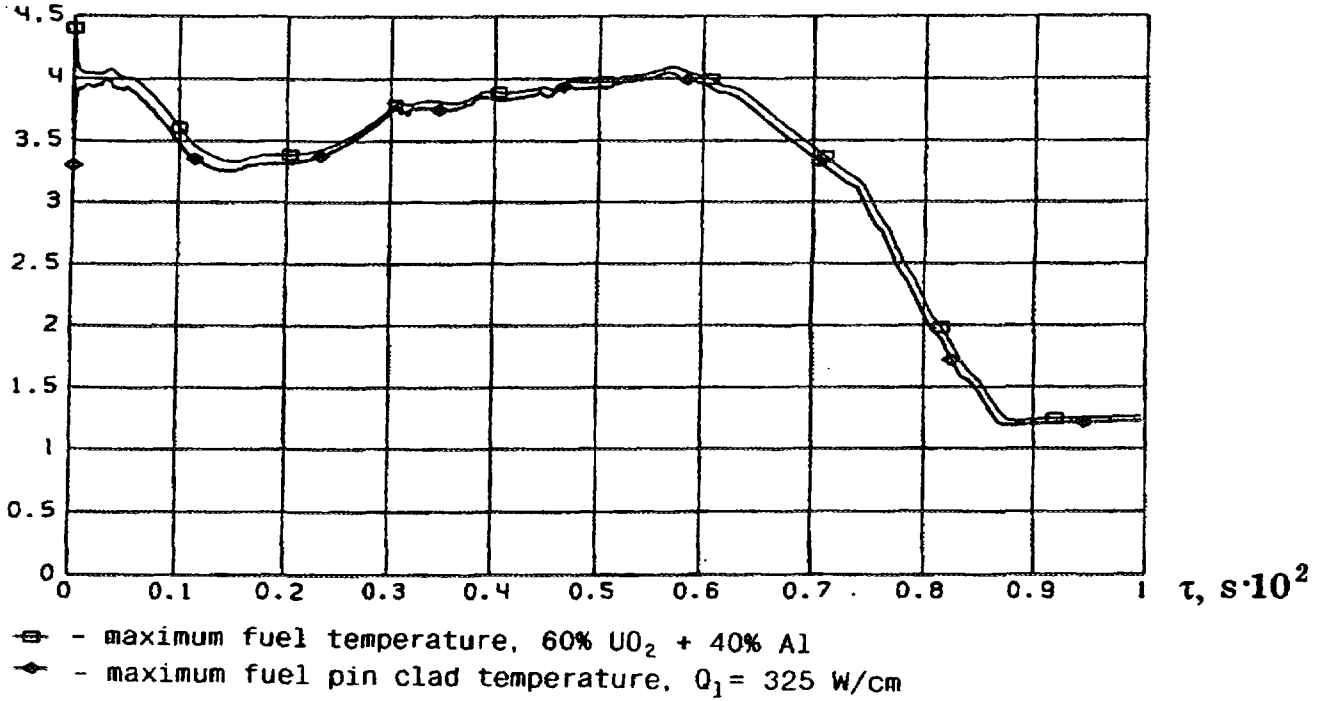
-⊟- - maximum fuel temperature, 60% UO_2 + 40% Al

-◆- - maximum fuel pin clad temperature, Q_1 = 325 W/cm

Fig. 4. Fuel rod temperature in the process of a maximum design-basis accident.

B-230

T, °C·10²

РАЗРЫВ ДУ 500. 2 ГЕ(Ъ НКР и Ъ СКР) 1 НВД 1 ННД (Ql=325 Вт/см)

-⊟- - maximum fuel temperature, 60% UO_2 + 40% Al

-◆- - maximum fuel pin clad temperature, $\lambda/(\delta_{gap})$ =3·10^6W/(m^2°C)
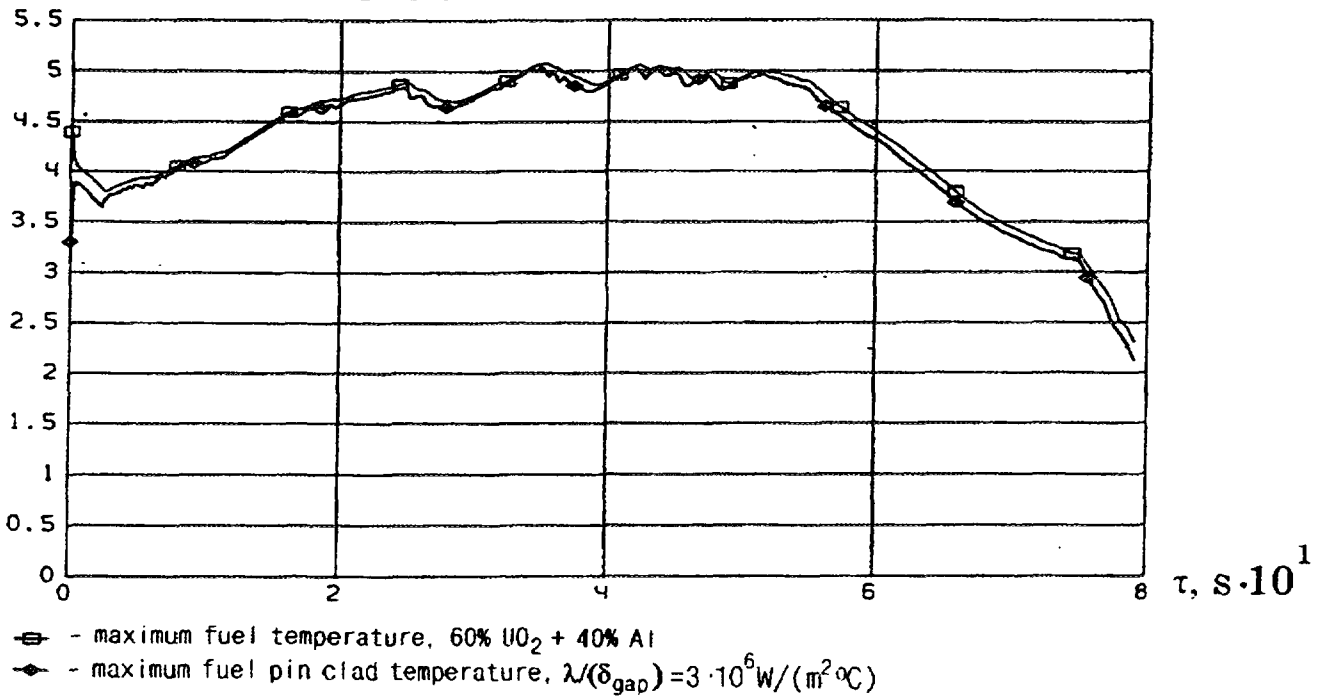
Fig. 5. Fuel rod temperature in the process of a maximum design-basis accident.

Autoclave tests have been carried out as well with a cermet fuel composition (60% vol. UO_2 + 40% vol. silumin) without cladding during 10 hours. After autoclave tests specimens have not changed their weight, they retained their form and microstructure. With these specimens more prolonged tests (τ = 50-200 hours) were also carried out. Investigations of tested specimens have shown that with the increase of contact time of specimens and coolant a non-significant increase of oxides in matrix takes place.

4.2. In-pile tests

A good corrosion resistance of cermet fuel composition (60% vol. UO_2 + 40% vol. silumin) in the coolant having operating parameters had been revealed in autoclave tests and made a basis for realization of unsealed fuel pins in-pile testing. For this purpose a special channel-loop has been created in the AM research reactor. The channel contained 3 fuel pins. Every fuel pin consisted along its length of three parts fully isolated one from another (Fig. 6), a summary length of a fuel pin being 930 mm. Dimensions of its clad were 9.15 mm x 0.7 mm. Its middle part 60 mm long had in its clad a through slot imitating a crack. Its dimensions were 0.45 x 9.0 mm.
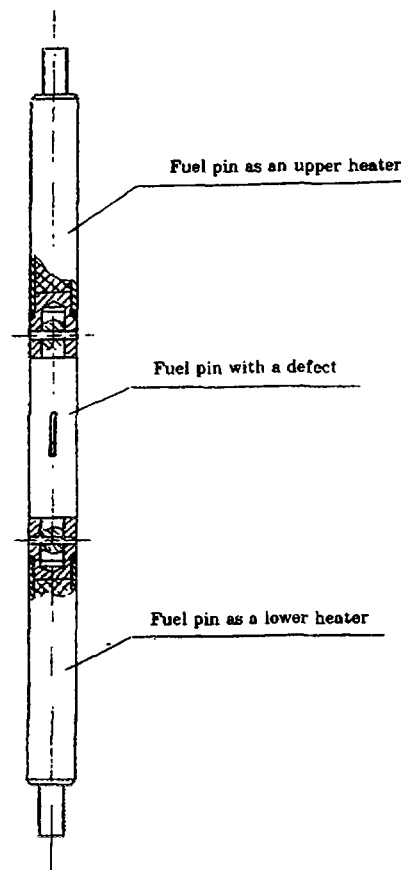
Fig. 6. A sectional fuel rod with an artificial defect.

Table 3

Temperature distribution along the radius of a cermet fuel pin

q_l, W/cm	T_{clad}, °C	$T^{fuel}_{surface}$, °C	T^{fuel}_{centre}, °C
138	296.0	314.0	344.0

40

When the reactor operated with power N = 28% of nominal, the linear thermal load of a fuel pin was q_l = 138 W/cm.

The outlet coolant temperature was 227-230°C.

The temperature distribution along the fuel pin radius in the process of a test is given in the table 3.

For investigation of release of fission products from a cermet fuel the following methods have been used:

- A gamma-spectrometer method (without sampling) for analysis of radionuclides that release out of a fuel composition and enter into the coolant. For this purpose a microcircuit to the channel-loop, a detector and a sensor of the exposition dose rate have been created. Pulses from the detector output were fed to the input of a multichannel pulse analyzer connected with a control and information processing unit;

- Sample-taking with subsequent gamma-spectroscopic analysis of radionuclides;

- Continuous measurement of exposition dose rate on the operational section (a standard method). In-pile tests were being carried out during two months.

5. Conclusions

The analysis of fission products release into the coolant allowed to make following conclusions:

a) During two-month fuel pin operation most fission products were retained by the cermet fuel rather firmly. The main mechanism of the fission products release is a direct emission.

b) A strong influence of acidity of the coolant medium on "washing-away' and "healing" of the fuel composition through clad cracks is noted to exist. During the operation in a stationary regime the operation).

41

SIMULATION OF FISSION GAS RELEASE DURING TEMPERATURE TRANSIENTS

A. DENIS
Departamento Combustibles Nucleares,
Comisión Nacional de Energia Atómica,
Buenos Aires, Argentina

Abstract

Paper discusses the release of fission gases Xe and Kr as a diffusion process. It takes into account gas generation due to fission, gas precipitation in bubbles within the grains, diffusion of gas towards the grain boundaries, formation of grain boundary bubbles, its saturation and subsequent gas release, resolution of the gas contained into both types of bubbles and grain growth.

Temperature profile calculations have allowed to evaluate the gas distribution in fuel pellet and in each grain. Analytical and numerical methods are used.

Several experiments are simulated with the code and a good agreement between the measured Paper discusses the release of fission gases Xe and Kr as a diffusion process. It takes into and calculated results has been obtained.

The influence of the initial grain size and density on fission gas release has been evaluated. It has been found that larger grain size and lower density both yield lower release, but density variation has a minor effect on the release.

Introduction

It is a well-known fact that the fission gases, Xe and Kr, produced in the nuclear fuels due to irradiation affect negatively the fuel performance. They diminish the heat transfer between the fuel and the cladding, which provokes fuel temperature increase. They rise pressure within the fuel element, which may cause cladding failure. They also cause fuel swelling since they occupy a larger volume then the original solid material, which may lead to contact between the fuel and the cladding in localized regions.

The technological importance of this subject has been recognized long time ago and many works have been devoted to its characterization. Most of the essential aspects have been elucidated but, due to the large number of phenomena involved, certain points are not fully understood yet. However, the clear necessity of having simulation codes able to predict the state of a fuel element submitted to a given power history justifies to continue devoting efforts in this direction.

The model that will be presented here was already outlined in some previous works [1,2]. It is based on the following hypotheses:

☆ The UO_2 fuel is considered as a collection of spherical grains where, due to continuous irradiation, noble gas atoms are produced by fission of the U atoms.

☆ In reason of the virtually complete insolubility of these gases in the UO_2 matrix, they either precipitate within the grains forming bubbles of a few nanometers (intragranular bubbles) or are released to the grain boundaries forming intergranular, lenticular bubbles, with sizes of some microns.

☆ Diffusion is the rate controlling step.

☆ Intragranular bubbles are considered immobile and acting as traps for the diffusing gas.

☆ Irradiation can cause destruction of both types of bubbles.

☆ The gas atoms contained in the destroyed intragranular bubbles return to the diffusion process. Due to kinetic reasons, a dynamical solubility, much higher than that predicted by the equilibrium diagram is established.

☆ Destruction of intergranular bubbles acts as an additional source of gas atoms that affect mainly the region of the grain adjacent to the grain boundary.

☆ The amount of gas stored in the grain boundary bubbles grows up to a saturation value. Then, these bubbles interconnect and the gas in excess is released to the plenum and to the gap between fuel and cladding.

☆ The grains grow due to the high temperature of the fuel, especially near its centerline. The grain boundary traps the gas, either free or in bubbles, in the swept volume.

The rate of gas release is calculated by means of the diffusion equation in spherical coordinates, with sources and traps:

$$\frac{\partial c}{\partial t} = D\left(\frac{\partial^2 c}{\partial r^2} + \frac{2}{r}\frac{\partial c}{\partial r}\right) - gc + bm + \beta \tag{1}$$

together with the balance equation for trapped atoms:

$$\frac{\partial m}{\partial t} = gc - bm$$

where c and m are the concentrations of free and trapped gas atoms (at/m^3), ß is the gas generation rate (at/m^{3}s), g and b are the probabilities of capture and release by traps (at/s) and D is the diffusion coefficient of the single gas atoms in the UO$_2$ matrix. Assuming stationary trapping conditions: gc-bm=0 and defining the total gas concentration of gas in the grain ψ=c+m and the effective diffusion coefficient D'=Db/(b+g), the equivalent equation

$$\frac{\partial \psi}{\partial t} = D'\left(\frac{\partial^2 \psi}{\partial r^2} + \frac{2}{r}\frac{\partial \psi}{\partial r}\right) + \beta \tag{2}$$

is obtained, with the boundary conditions: ψ(r=a)=0, i.e., the grain boundary at r=a acts as a perfect sink, and $\partial\psi/\partial r$=0 at r=0 due to spherical symmetry.

The diffusion coefficient D was given by Turnbull et al.[3]; the bubbles' size and concentration, the saturation level of the grain boundary, N_s, and the trapping parameters, g and b, are due to White et al. [4], the equiaxed grain growth rate is that used by Ito et al.[5].

The function representing the gas production rate, ß(r), was already given in [1] It contains the uniform gas generation rate due to irradiation, obtained from the fission rate, F (fissions/m^{3}s), times the gas production yield, y, and the contribution due to resolution of intergranular bubbles, which is proportional to the occupation of the grain boundary, N. Its expression is:

$$\beta = \begin{cases} yF & \text{for} \quad 0 \leq r \leq a-2\lambda \\ yF+h(r) & \text{for} \quad a-2\lambda < r \leq a \end{cases}$$

where a is the grain radius, λ represents the penetration depth of the redisolved atoms and the function h(r) is such that

$$\int_{a-2\lambda}^{a} h(r)4\pi r^2 dr = 4\pi a^2 b' \frac{N}{2}$$

The proportionality constant b'(1/s) represents the probability of release of the intergranular bubbles and is one of the parameter of the model.

Under certain particular conditions the diffusion equation admits analytical solution. In the present case, the presence of the source term ß(r) makes necessary a numerical method to solve equation (2) The finite difference method was used in this work.

Fission gas release during power transients

In previous works [1,2] a very simple expression was derived for the fractional release, adequate to simulate gas release under constant power conditions ,i e., constant fission rate. That

44

formula cannot be used to simulate the gas release of a fuel element in a reactor under normal operation conditions. The expression valid in a general case is obtained as follows:

The time is divided into intervals Δt_k, where k indicates the time step. All the time dependent quantities are labeled with a subscript k

The gas content of one grain and its boundary at time t_{k-1} is

$$C_{k-1} + 4\pi a_{k-1}^2 \frac{N_{k-1}}{2}$$

where C_{k-1} is the total gas number of gas atoms contained in the grain, either free or in intragranular bubbles, and is given by:

$$C_{k-1} = 4\pi \int_0^{a_{k-1}} r^2 \psi_{k-1} dr$$

The quantity of gas generated in one grain during Δt_k, is

$$G_k = 4\pi a_k^3 y F_k \Delta t_k$$

and that generated by all the grains contained in a volume V is

$$V y F_k \Delta t_k$$

The amount of gas incorporated to one grain and its boundary due to grain growth is

$$\left(C_{k-1} + 4\pi a_{k-1}^2 \frac{N_{k-1}}{2} \right) \frac{a_k^3 - a_{k-1}^3}{a_{k-1}^3}$$

The quantity

$$Q_k = \left(C_{k-1} + 4\pi a_{k-1}^2 \frac{N_{k-1}}{2} \right) \frac{a_k^3}{a_{k-1}^3} + G_k - C_k$$

represents the number of gas atoms not contained within the volume of one grain. Before saturation, the surplus Q_k is the grain boundary content. After saturation, Q_k is the sum of $4\pi a_k^2 N_s$ plus the number of released atoms. This means that the content of the boundary of one grain per unit area is

$$N_k = \begin{cases} \left[\left(C_{k-1} + 4\pi a_{k-1}^2 \frac{N_{k-1}}{2} \right) \frac{a_k^3}{a_{k-1}^3} + G_k - C_k \right] \frac{1}{2\pi a_k^2} & \text{before saturation} \\ N_s & \text{after saturation} \end{cases}$$

and the number of gas atoms released during Δt_k, by one grain is equal to

$$L_k = \begin{cases} 0 & \text{before saturation} \\ Q_k - 4\pi a_k^2 N_s & \text{after saturation} \end{cases}$$

45

The total release during Δt_k is L_k times the number of grains in the volume V given by

$$\frac{V}{\frac{4}{3}\pi a_k^3}$$

The fractional release at time $t = \sum_{k=1}^{n} \Delta t_k$, divided for numerical iteration into n time steps Δt_k, is given by:

$$f_n = \frac{\sum_{k=1}^{n} \frac{L_k V}{(4/3)\pi a_k^3}}{\sum_{k=1}^{n} V y F_k \Delta t_k}$$

Although the real power histories of fuel elements used in power reactors are complex, they can be conveniently averaged for simplicity. In the present work, the power histories have been divided into a number of linear steps. The instantaneous value of the fission rate F is determined from the corresponding value of the linear power P (W/cm).

$$F(t) = \frac{P(t)}{\pi(R^2 - R_0^2)E_f},$$

where E_f is the energy released in a single fission event and R and R_0 are the radii of the pellet and of the central hole

Every time step the burnup, B_u(MWd/Ton U), is increased by

$$\Delta B_u(t) = \frac{P(t)\Delta t}{\pi(R^2 - R_0^2)\delta_U},$$

where δ_U is the real Uranium density in the fuel.

Temperature gradients

Among the large number of phenomena that determine fuel performance, the thermal processes belong to the more representative since temperature has a determining effect on most of the fuel parameters. Local temperatures and temperature gradients are relevant for mechanical, physical and chemical processes. The space and time variation of temperature in a fuel are represented by the heat diffusion equation:

$$c\rho\frac{\partial T}{\partial t} = \nabla \cdot (\kappa \nabla T) + E_f F$$

where c is the specific heat, ρ is the density, κ is the thermal conductivity, $E_f F$ is the local power density and T is the absolute temperature. c, ρ and κ are, in general temperature dependent. Under steady-state operation conditions, the first term disappears and the relevant parameter is the thermal conductivity. However, during temperature transients the specific heat and the density become of capital importance.

The following analysis will be restricted to steady-state conditions. In this case and considering the cylindrical symmetry of the fuel pellet, the above equation transforms to:

$$\frac{1}{r}\frac{d}{dr}\left[\kappa(T)r\frac{dT}{dr}\right]+E_f F = 0,$$

.

The thermal conductivity of UO_2 has been extensively studied by several authors. They generally coincide in identifying two main contributions. The thermal conduction due to lattice vibrations which decreases with increasing temperature and is dominant at low and intermediate temperatures. This yields a term of the form $(A+BT)^{-1}$ At high temperatures the electronic contribution governs thermal conduction. Different correlations with temperature are found in the literature for this term.

Delette et al.[6] give for the thermal conductivity of fully dense, fresh fuel the expression

$$\kappa(T) = \frac{1}{A+BT}+\frac{C}{T^2}\exp\!\left(-\frac{W}{kT}\right) \tag{3}$$

valid in the range 100 to 2500°C, with

A=3.4944x10^{-2} m K/W;

B=2.2430x10^{-4} m/W;

C=6.157x10^9 W K/m ;

W=1.41 eV

and k is the Boltzmann constant.

Both contributions yield a minimum value of about 2.4W/mK around 1650°C for the thermal conductivity

Beside the temperature dependence, κ also depends on the burnup. The presence of solid and gaseous fission products decrease the thermal conductivity expected for fresh fuel since they act, like lattice point defects, as phonons scatterers. The constant A in equation (3) needs to be replaced by A+A'B$_u$. According to Kolstad et al.[7], A' is (0.015 ± 0.001)mK/W per at%U. In what follows, for simplicity in the notation, A will represent in reality A+A'B$_u$.

In equation (3), by integrating once in r from R_0 to a generic radius r and assuming that F is independent of r, the expression

$$\kappa(T)r\frac{dT}{dr} = -E_f F(r^2 - R_0^2)$$

is obtained, where the boundary condition $\dfrac{dT}{dr}\bigg|_{R_0} = 0$ of cylindrical symmetry has been applied. A second integration, together with the boundary condition $T(R)=T_s$ yields:

$$\frac{1}{B}\ln\!\left(\frac{A+BT}{A+BT_s}\right)+\frac{Ck}{W}\left[\exp\!\left(-\frac{W}{kT}\right)-\exp\!\left(-\frac{W}{kT_s}\right)\right] = \frac{P}{4\pi[1-(R_0/R)^2]}\left[1-\left(\frac{r}{R}\right)^2+\left(\frac{R_0}{R}\right)^2\ln\!\left(\frac{r}{R}\right)^2\right]$$

that gives T(r). Although this equation has a rather complicated form, it can be solved by means of the Raphson-Newton method.

In order to simplify the numerical calculations, the fuel element was divided into N=5 concentric cylinders, in each of which the temperature was considered constant. The equation for T(r) was solved for the radial coordinates of the boundaries between the zones. The mean value of the temperature in each zone was then determined and assigned to the zone.

Results

With the procedure outlined above, several experiments were reproduced. At first, a series of isothermal experiments performed by Zimmermann [8] were simulated, which made possible to select the more appropriate set of parameters of the model. These results have already been presented in [1].

Then, the space and time variation of temperature were introduced in the model and a number of experiments were simulated: those performed by Notley [9] and the tests 1, 2 and 6 of the FUMEX series for which the experimental value of the gas release was reported [10].

As an example, some results obtained for the FUMEX 2 experiment are shown in Figures 1 and 2. In Figure 1 the time variation of the fractional release is plotted as a function of burnup, along with the averaged linear power. A final value of 2.8% was obtained in the calculations, which compares well with the measured value of 3%.
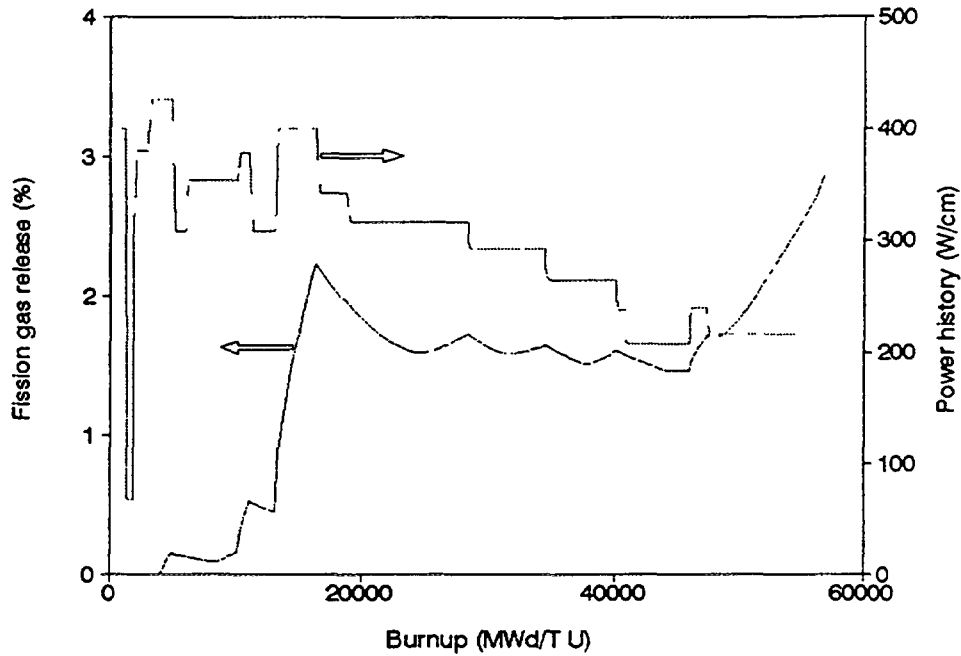
Figure 1 Fission gas release vs. burnup. The simplified linear power used in the calculations was obtained from the experiment FUMEX 2 and is also displayed.
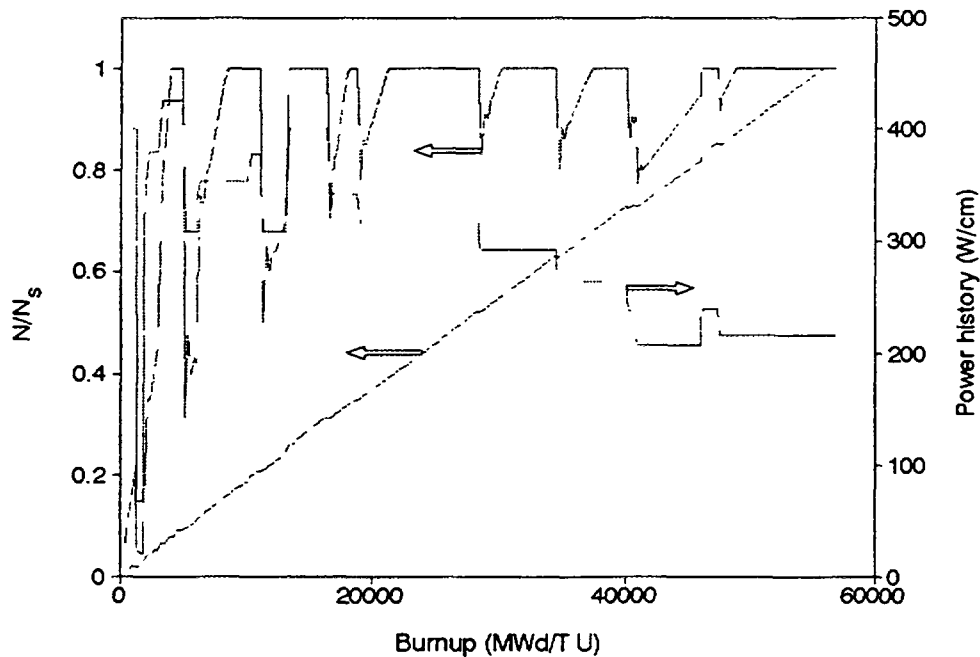
Figure 2 Number of gas atoms per unit area relative to the saturation density vs. burnup. The upper curve corresponds to a grain in the hotter region of the fuel; the lower one, to a grain in the colder region. The simplified linear power obtained from the experiment FUMEX 2 is also displayed.

The grain boundary occupation depends on several parameters like temperature and grain size, among others. The saturation density (number of gas atoms per unit area necessary to saturate the grain boundary) is also temperature dependent. The calculations show that saturation is reached after a different burnup in each pellet region. In the higher temperature zone, saturation may be achieved after a short irradiation period at standard linear power (say 400 W/cm) while in the outer region of the pellet saturation may not be reached in the whole duration of the experiment. In Figure 2 the relationship between the occupation and saturation densities is plotted as a function of burnup for the more internal and the more external rings of the fuel considered in the calculations. (The others were not displayed for the sake of clearness in the representation). The simplified power history is also shown.

Figure 3 shows the comparison between some experimental determinations of the fractional release end the results calculated with this code. It can be seen that the agreement is quite good.
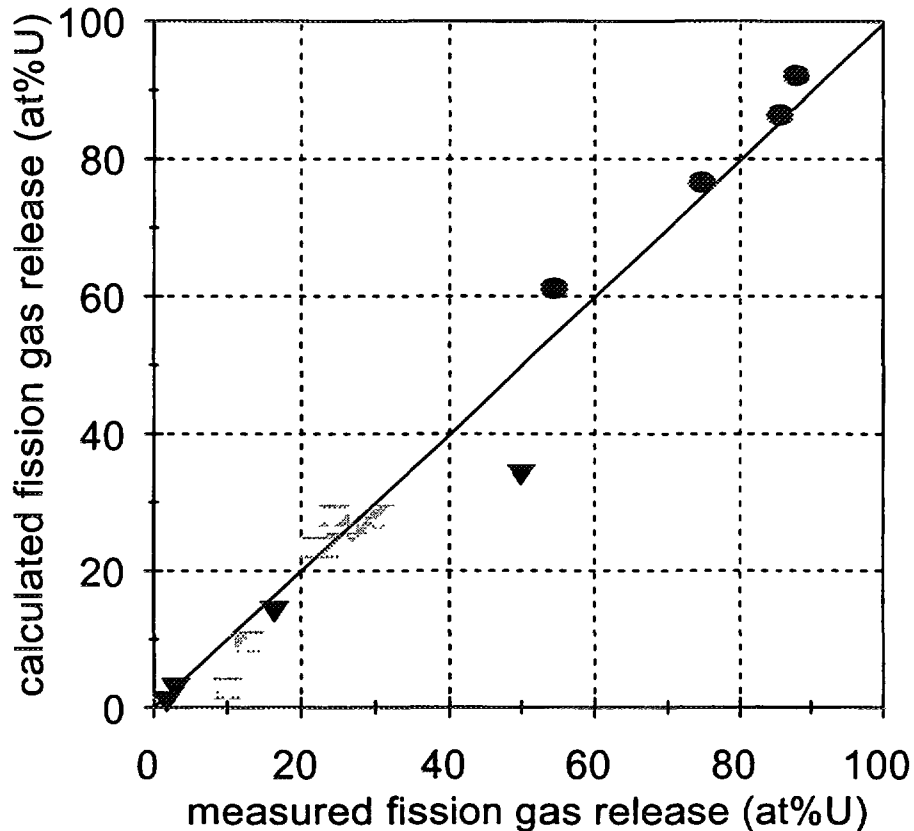
Figure 3 Comparison between calculated and measured fractional fission gas release. ● correspond to the experiments performed by Zimmermann [8]; ■ to those by Notley [9] and ▼ to the experiments 1, 2 and 6 (the last one for two different burnups) of the FUMEX series [10]

In order to evaluate the influence of some physical parameters on the rate of gas release, a comparative analysis was made. In Figure 4 the influence of the initial grain radius is shown. It becomes clear that a larger grain size yield lower release. Comparison of the end-of-life releases in these four cases indicates that the relationship is not linear.

The influence of the Uranium density was also explored. When δ_U was varied from 8.7 to 10.6 (18% increase), an increase of 6% was obtained for the release.

The calculation time is considerably lower than with the previous version of this code. This was accomplished by taking long time steps (of 2 days) during the constant linear power periods. Short time steps (of about 1 minute) were used only when a steep variation of power took place. The calculation time is at present of a few minutes, depending on the complexity of the power history.
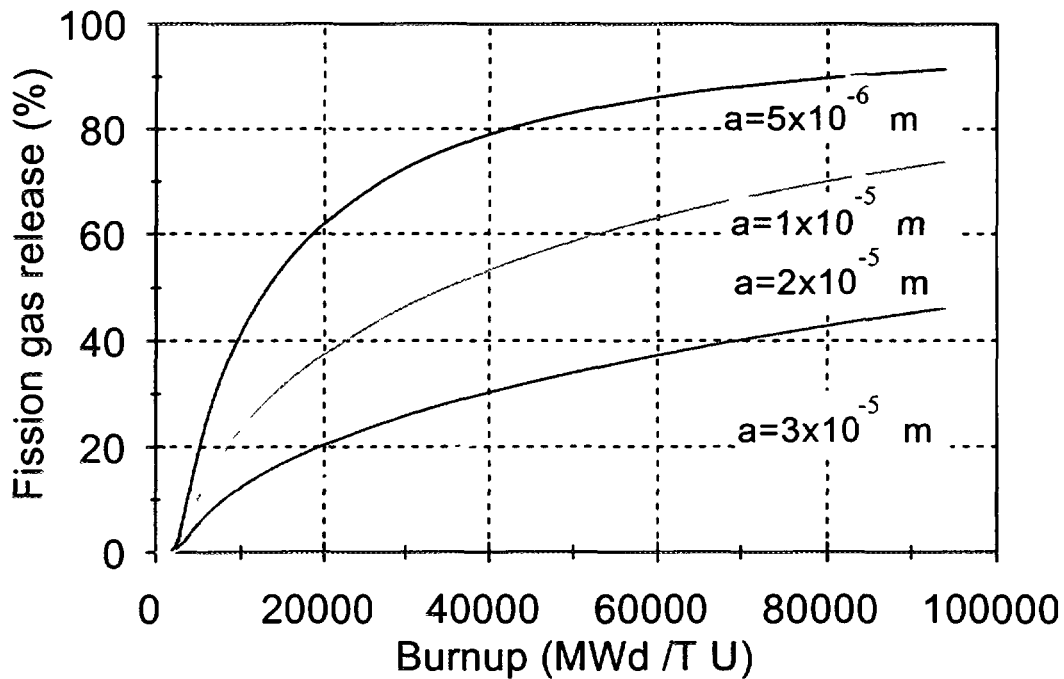
Figure 4 Comparative study of the influence of the initial grain radius on the fractional gas release

Discussion

The gap conductance, i.e., the heat transfer between the fuel and the cladding, is important in defining the fuel temperature. Its influence is more significant at low than at high burnup since, after a long irradiation time, the gap becomes closed. Gas release changes the gas composition within the gap and consequently, the thermal conductivity of this mixed gas. Swelling has an effect too since it modifies the gap size and may produce contact between fuel and pellet. Other phenomena also affect this region of the fuel element. Elaborated models on gap conductance have been stated which consider its dependence on temperature, gas composition, gas pressure, contact pressure, surface morphology and emmisivity, all of them dependent on burnup. The value of the temperature at the external fuel surface is one of the boundary conditions used to solve the differential equation for heat diffusion Uncertainties in T_s cause error in the determination of fuel temperature, which has a determinant effect in the results. However, this aspect has not been included in this model yet and a constant surface temperature $T_{s=}$ 300°C was used in the present calculations.

Another approximation present in this model is referred to the stationary-state condition assumed for the heat diffusion equation, which is a source of error in the temperature determination every time the power level is varied.

From the comparisons described above, it may be concluded that, in order to lower the fission gas release several actions may be followed. One of them is to try to increase the grains' size. Large grains mean large diffusion distances, that make difficult the arrival of the gas atoms to the grain boundary. During irradiation, due to the high temperatures, the grains tend to grow up to a saturation value. This effect contributes favorably to lower the release. But, for very high burnups, higher that about 68000MWd/T U, the 'rim effect' is observed: near the pellet surface very fine grains appear and an enhanced release is produced

Although decreasing the density would have a beneficial effect on the gas release, it does not seem a convenient proposal since it would mean to increase the fuel volume in order to obtain the same mass of fissionable material.

50

References

[1] A.Denis and R.Piotrkowski, Journal of Nuclear Materials 229(1996)149-154.

[2] A.Denis and R.Piotrkowski, *A fission gas release model*, Technical Committee Meeting on Water Reactor Fuel Element Modeling at High Burnup and Experimental Support, IAEA, Windermere, England, September 1994.

[3] J.A.Turnbull, R.White and C.Wise, *The diffusion coefficient of Fission Gas Atoms in UO$_2$* , IAEA TC 659/3.5(1987)pp.174-181.

[4] R.White and M.Tucker, Journal of Nuclear Materials 118(1983)1.

[5] K.Ito, R.Iwasaki and Y.Iwano, Journal of Nuclear Science and Technology 22(1985)129.

[6] G.Delette and M.Charles, *Thermal conductivity of fully dense unirradiated UO$_2$: a new formulation from experimental results between 100 and 2500°C, and associated fundamental aspects*, IAEA TCM, Windermere, England, Sept.1994

[7] E.Kolstad and C.Vitanza, Ju\ournal of Nuclear Materials 188(1992)104.

[8] H.Zimmermann, Journal of Nuclear Materials 75(1978)154.

[9] M.Notley, *Zircaloy-sheathed UO$_2$ fuel irradiated with a declining power history to determine its effect on fission product gas release*, AECL-6585 (1985).

[10] *Fuel modelling at extended burnup (FUMEX)*, IWGFPT/43, Vienna, Austria (1995).

NEXT PAGE(S)
left BLANK

FISSION PRODUCT RELEASE FROM FUEL PINS
OF THE BILIBINO NUCLEAR POWER PLANT

L.I. MOSEEV, A.N. RYZHKOV,
B.C. KIRIANOV, S.I. POROLLO
Institute of Physics and Power Engineering,
State Scientific Centre of the Russian Federation,
Obninsk, Russian Federation

Abstract

The paper presents experimental results on fission products release from burned up fuel rods and from parts of open fuel at Bilibino nuclear power plant

Introduction

There are number of calculating codes for discription of fission products (FP) release from metal, oxide, carbide and carbonitride types of nuclear fuel. But the variety of thermal, strength, hydraulic, chemical processes, conversions in burning fuel during FP release leads to significant uncertainties in calculations, especially for cermet nuclear fuel So that the experimental study of FP release from specific types of nuclear fuel becomes especially important. The paper presents experimental results of investigations of FP release from fuel rods with dispersive fuel composition (uranium dioxide pellets dispersed into magnesium matrix) such as in reactors at Bilibino and in The World's First Nuclear Power Plant (WFNPP) at Obninsk. Such an investigation was needed to meet the security criteria accepted for water-graphite reactors at Bilibino NPP

The operating limit for fuel pins of Bilibino NPP is temperature 703 K or if only one fuel pin will have leakage in its cladding The maximum design limits for fuel pin cladding are:
-temperature 1373 K for fuel pin without inner pressure;
-temperature 1203 K for fuel pin under heat carrier operating pressure

1. Characteristics of tested fuel pins and their operating conditions.

The fuel pins for testing were taken from driver fuel assembly of The First World's NPP. They are of a pipe construction with inner pipe, circle fuel layer and outer cladding. The matrix material is magnesium firmly connected to inner pipe and outer cladding (both pipes were fabricated from stainless steel). The fuel is of uranium dioxide pellets (60% of volume) and magnesium (40% of volume). The density of uranium dioxide pellets is 6,5 g/cm^3, the size of uranium dioxide pellets is 0,2-1,2 mm. Fuel pin sizes: outer cladding - 14 x 0,2 mm, inner sheath - 9 x 0,4 mm. The fuel pins both at The First World's NPP and at Bilibino NPP are of the same design. They were manufactured according to regular technology and ere used in reactor at The WFNPP at refernce conditions. The fuel pins with burnups of about 19-26 MWd/kg U that are close to project values for fuel at the Bilibino NPP have been tested At operating conditions in the Bilibino NPP core the steam of pressure of 6,3 MPa is generated, heat removal is provided by boiling water, heat flux from fuel rods reaches 0,8 MW/m^2. The temperature on fuel pins and fuel composition is about 300-380°C at the operation conditions. Short ten seconds) temperature jumps not higher then 1500-1600°C at fuel material may take place in Bilibno NPP reactors (in case of accidents). In case of accidents without destruction of the fuel pin inner cladding fission products evolve into pure nitrogen environment. In case of accidents accompanied by destruction of inner cladding and heat carrier leakage the reactor environment will be a mixture of the steam and hydrogen

2. FP release during fuel pin heating.

The scheme of device for fuel pin investigations is given in Fig.1 The fuel pin was put into hermetical ampule and was heated in nitrogen or steam environment. Each temperature was kept for 120 minutes Nitrogen or steam continuously circulated with rate ~0,04 m^3/hour Containment of FP in nitrogen or steam was measured by gas radiochromatography.

The scheme of device for investigation of fission
products release from fuel rods.
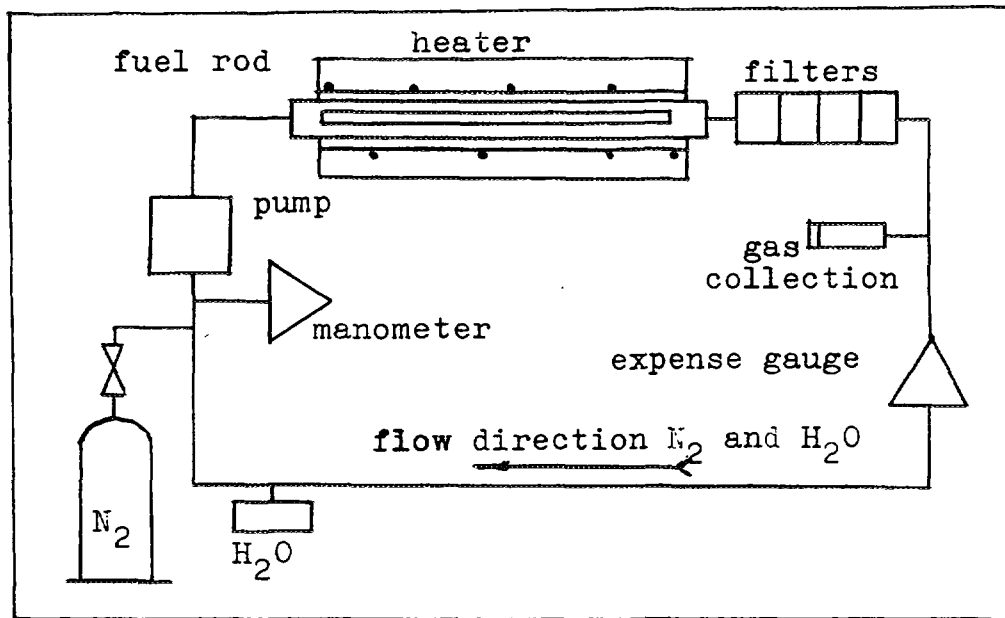
Fig.1.

After testing four fuel pins with burn-up 19.7; 21.2; 23.3; 25.8 MW d/kg U it was found:

1. The fuel pin cladding kept its leak-proofness at temperature range 770-1020 K; the shape and diameter of outer fuel pins cladding were change at region of maximum temperatures. It was observed the thritium release into nitrogen or steam, but no nitrogen or steam interaction with fuel pin materials was been detected.

2. It was observed that magnesium emerges on outer cladding of fuel pin at 1070 K (this phenomenon wasn't observed for nonirradiated fuel pins); the diameter of cladding increased on ~0,7%; the thritium release continued; nitrogen/magnesium interaction at outer cladding started.

3. It was observed that nitrogen and steam interaction with magnesium occured in temperature range 1070-1270 K; the kripton-85 and xenon-133 release was detected at ~1270 K.

4. Microcracks appeared at outer fuel pin surface at ~1370 K; it is observed an intensive kripton-85, thritium and xenon-133 release; it was detected iodine-131, caesium-134, -137 and antimony-125 with ruthenium-106 release into nitrogen and steam.

The kinetics of thritium release is shown at Fig.2. The total kripton-85 and xenon-133 release up to 1400 K was 2,1% of accumulated ones in fuel pins. A different FP persentage in nitrogen and steam is not more then 0,07% of accumulated ones in fuel pins.

Thus, FP release from fuel composition (except thritium) wasn't observed till fuel pin cladding were leak-proofed. Thritium had a high diffusibility in stainless steel at 870-1400 K.

3. FP release from open fuel composition

The scheme of device for the study of FP release from parts of fuel pins in argon, nitrogen and steam environment is shown in Fig.3. Investigations are based on method of argon nitrogen and steam passing with constant rate (~0,05 m³/h) over fuel composition which was preliminary heated up to 585-1900 K with

54

Thritium release from fuel rod.
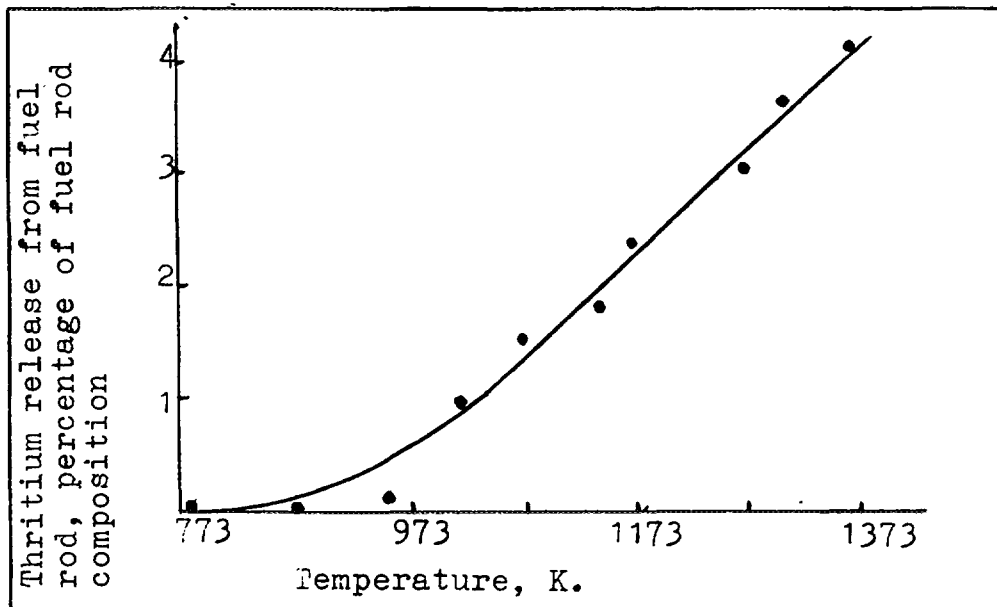
Fig.2.

The scheme of device for investigation of fission products release from parts of open fuel.
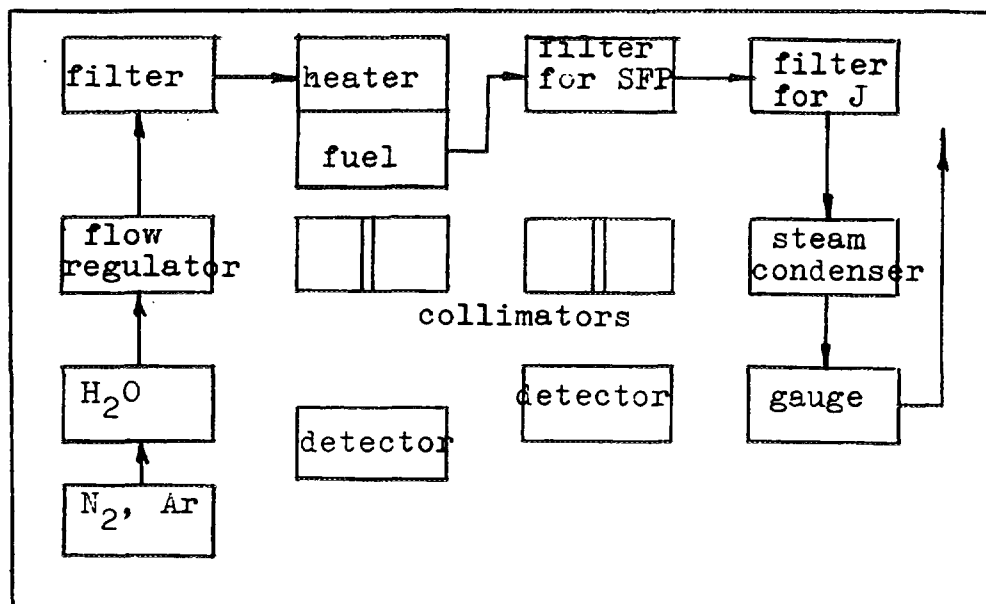
Fig.3.

simultaneous measurements of FP. The mass of tested fuel was 8-12 g, the exposure time at each temperature was 120 min. The measuremets of FP in argon, nitrogen and steam have been performed using a semiconductor gamma spectrometer and gas radiochromatography. Porous zirconium and aluminium oxides were used for the solid FP deposition from gas environment.

The results are presented at Fig.4-7.

The release of ^{131m}Xe and ^{85}Kr in nitrogen environment.
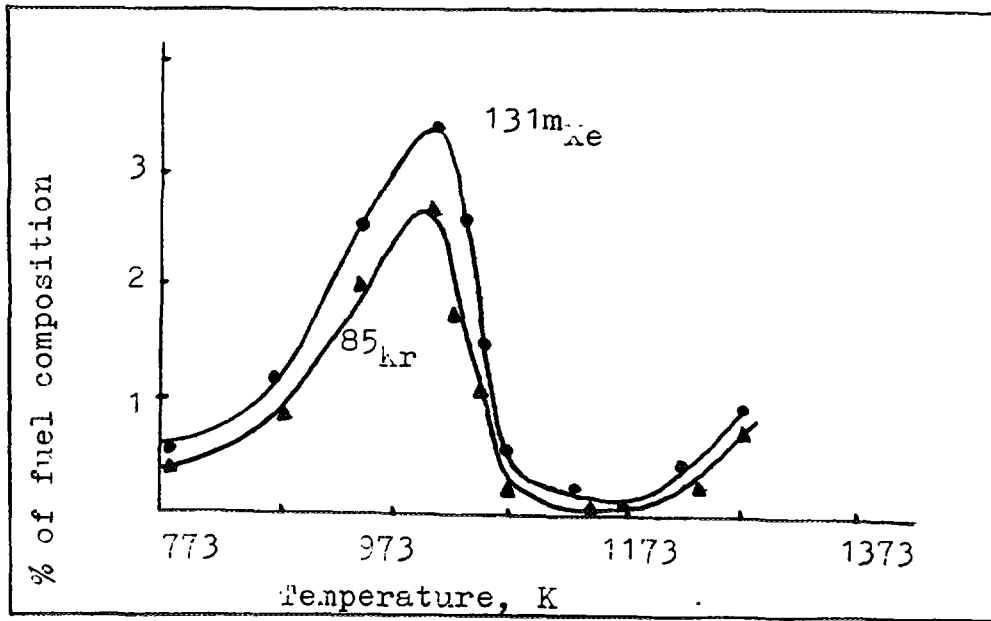
Fig.4.

The release of iodine-131 from fuel in A_2, N_2 and steam environments (burning 21,2 kw day/kg.
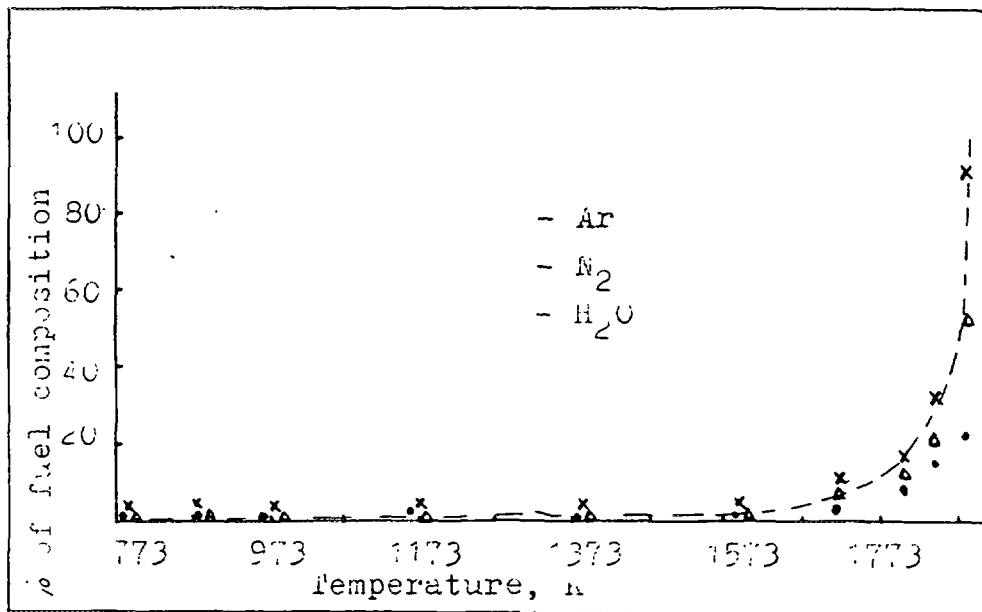
Fig.5.

The release of caesium-137 from fuel in A_2, N_2 and steam environments (burning 20,8 Mw day/kg).
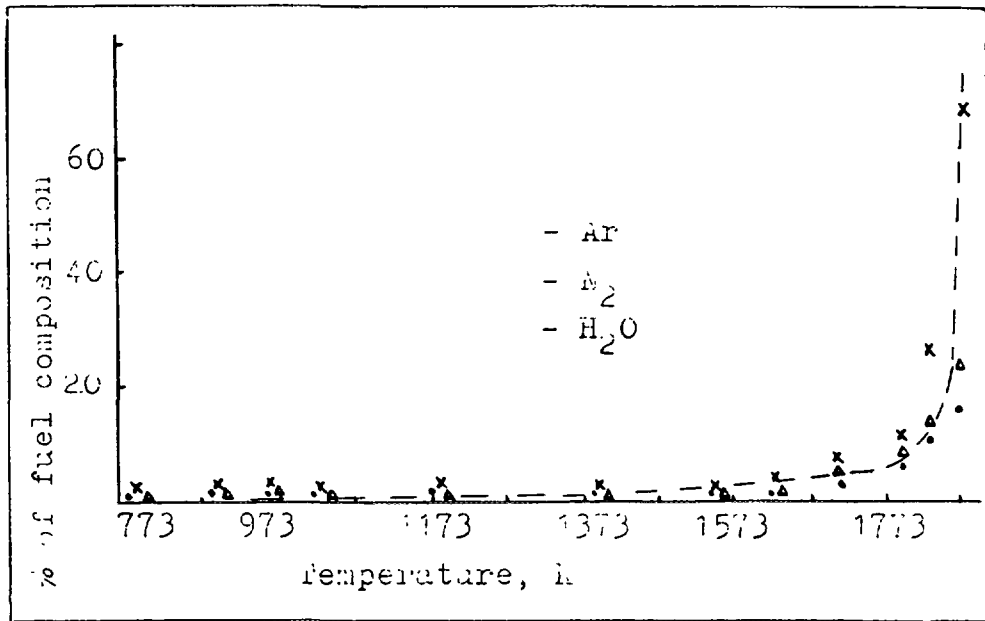
Fig.6.

The release of different radionuclides from fuel in A_2, N_2 and steam environments (burning 20,8 mw day/kg).
(% of fuel composition).

Tempe- rature. °C	95 (Zr+Nb)	103 Ru	134 Cs	140 (Ba+La)	144 Ce
500	$8.7 \cdot 10^{-6}$	$2.6 \cdot 10^{-5}$	$2.8 \cdot 10^{-4}$	$5.1 \cdot 10^{-6}$	$4.4 \cdot 10^{-5}$
600	$1.0 \cdot 10^{-5}$	$3.0 \cdot 10^{-5}$	$3.3 \cdot 10^{-4}$	$5.1 \cdot 10^{-6}$	$5.2 \cdot 10^{-5}$
670	$3.8 \cdot 10^{-4}$	$5.3 \cdot 10^{-4}$	$3.9 \cdot 10^{-4}$	$5.0 \cdot 10^{-5}$	$7.8 \cdot 10^{-4}$
750	$1.1 \cdot 10^{-5}$	$3.8 \cdot 10^{-5}$	$3.3 \cdot 10^{-4}$	$9.3 \cdot 10^{-6}$	$3.5 \cdot 10^{-5}$
900	$1.3 \cdot 10^{-5}$	$7.7 \cdot 10^{-5}$	$8.3 \cdot 10^{-4}$	$1.1 \cdot 10^{-5}$	$1.5 \cdot 10^{-4}$
1000	$1.1 \cdot 10^{-5}$	$2.6 \cdot 10^{-5}$	$1.4 \cdot 10^{-4}$	$1.1 \cdot 10^{-5}$	$3.5 \cdot 10^{-5}$
1120	$1.4 \cdot 10^{-5}$	$2.7 \cdot 10^{-5}$	$3.3 \cdot 10^{-4}$	$1.2 \cdot 10^{-5}$	$4.3 \cdot 10^{-5}$

Fig.7.

From the figures one can see that peak of krypton-85 and xenon-133 release from fuel composition occurs at the magnesium melting temperature (924 K).

When fuel composition was heated in steam environment a higher FP release was observed as compared with argon and nitrogen environment at similar conditions. The magnesium oxidative reaction begining at 920 K is governing this process:

$$Mg + 2\ H_2O = Mg(OH)_2 + \uparrow H_2$$
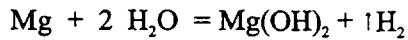
The interaction between magnesium and nitrogen at this temperature according to reaction:

$$3Mg + N_2 = Mg_3N_2$$
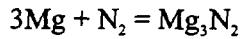
is less strong.

It was also noticed that the second peak of FP release appeared at 1173 K. It is particularly perceptible with following magnesium hydroxide convertion according to reaction:

$$Mg(OH)_2 = MgO + H_2O$$
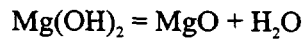
at 1100-1200 K.

In Fig.8-10 the dependences of release rates for different radionuclides on temperature are shown. One can see that rate of FP release in oxidative environment (steam) is larger at all temperatures. It is clearly seen in the case of iodine release.
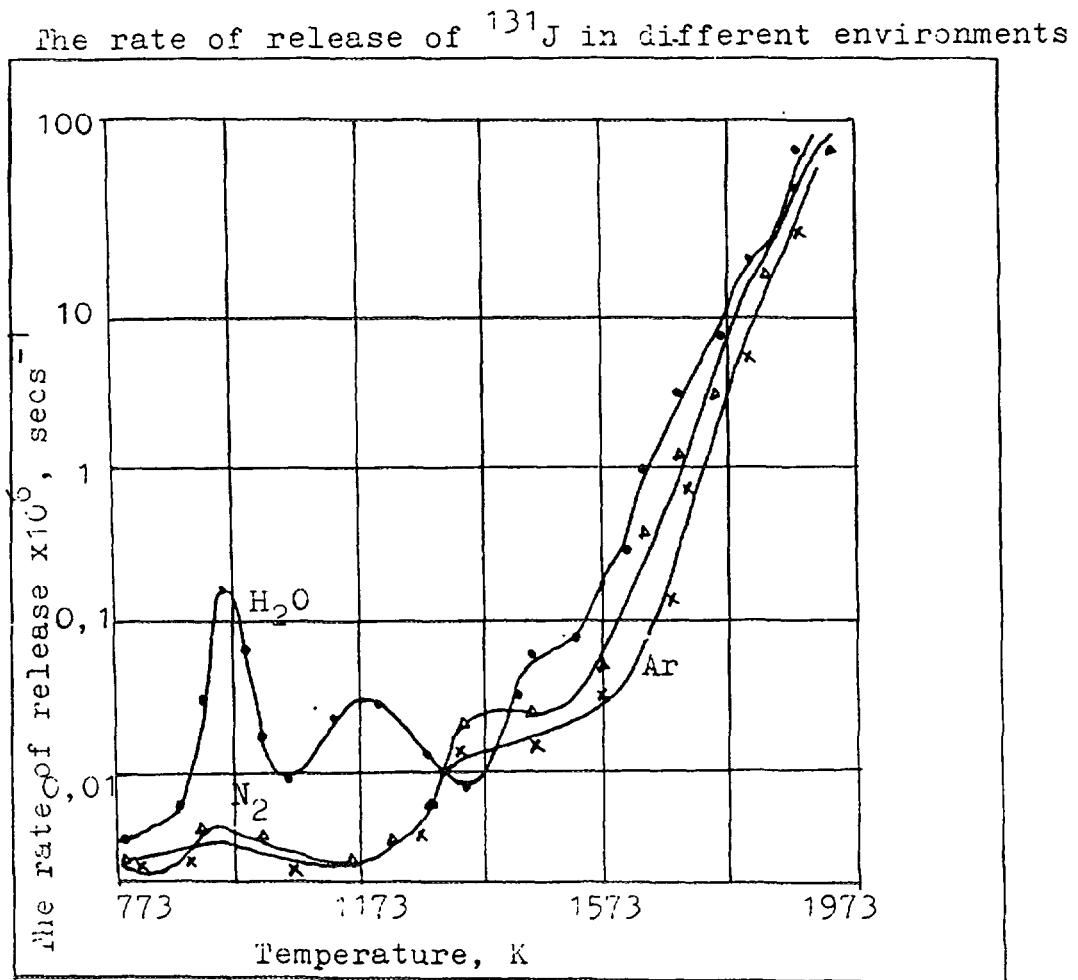
Fig.8.

The rate of release of ^{137}Cs in different environments
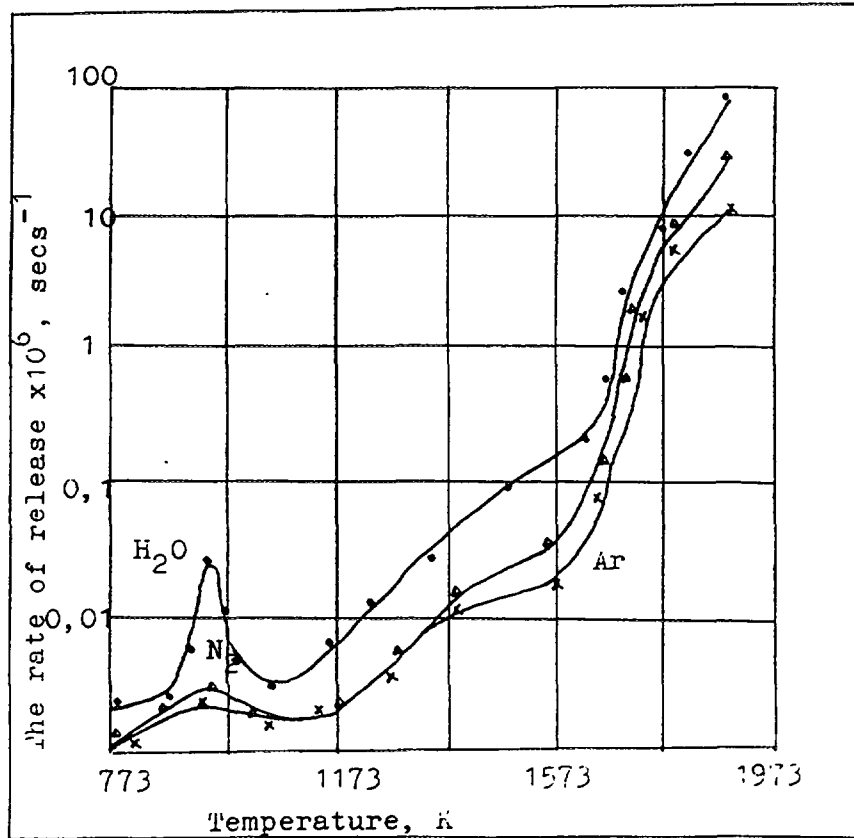
Fig.9.

The rate of release of different fission products in steam environment
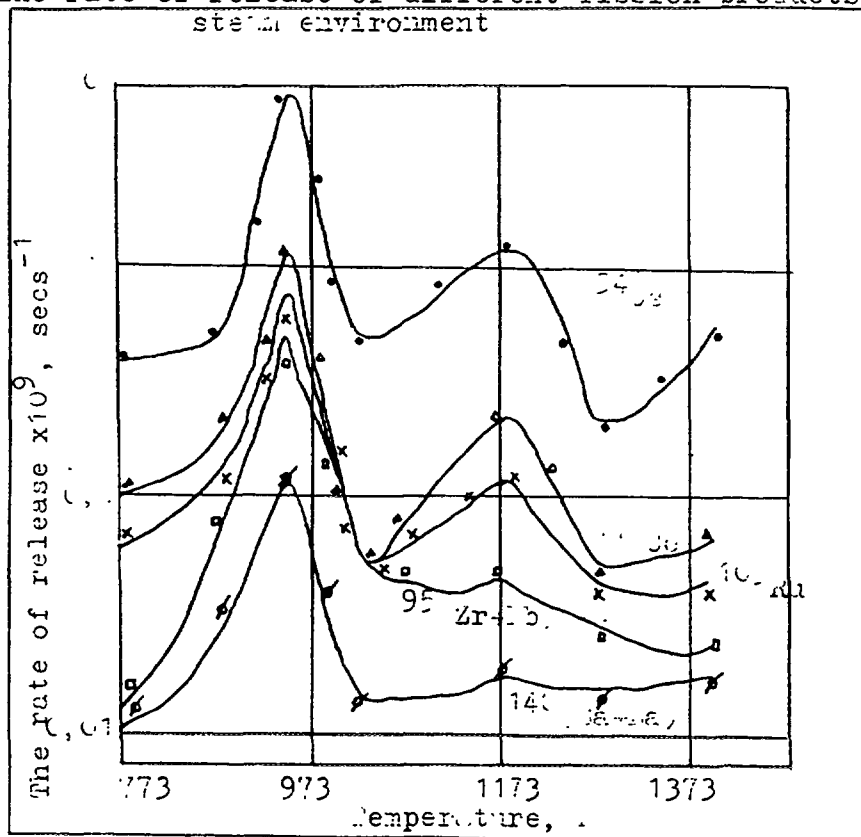
Fig.10.

A significant increase of FP release rate is observed at 1400-1970 K, caused by their diffusion from uranium dioxide pellets.

At Fig.11 the dependence (found experimentally) of kripton-85 diffusion coefficients on fuel composition temperature is shown. From this curve kripton-85 activation energy was calculated and it is equal to $3,1 \cdot 10^5$ J/mol. This value is close to the kripton-85 activation energy in uranium dioxide.

At Fig.12 the averaged experimental results oh the Xe-133 release and their comparison with evaluations made on the base of diffusion model (code CORSOR) for uranium dioxide are given.

The ^{85}Kr diffusion coefficients dependence on temperature.
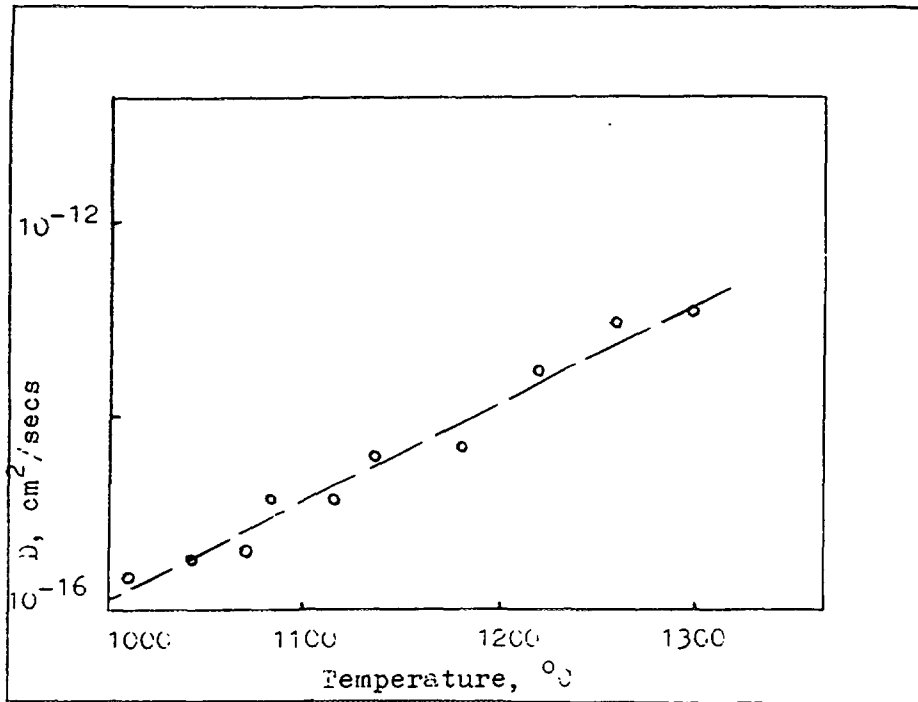
Fig.11.

The comparison of experimental data and calculated results of xenon-133 release.

Fig.12.

60
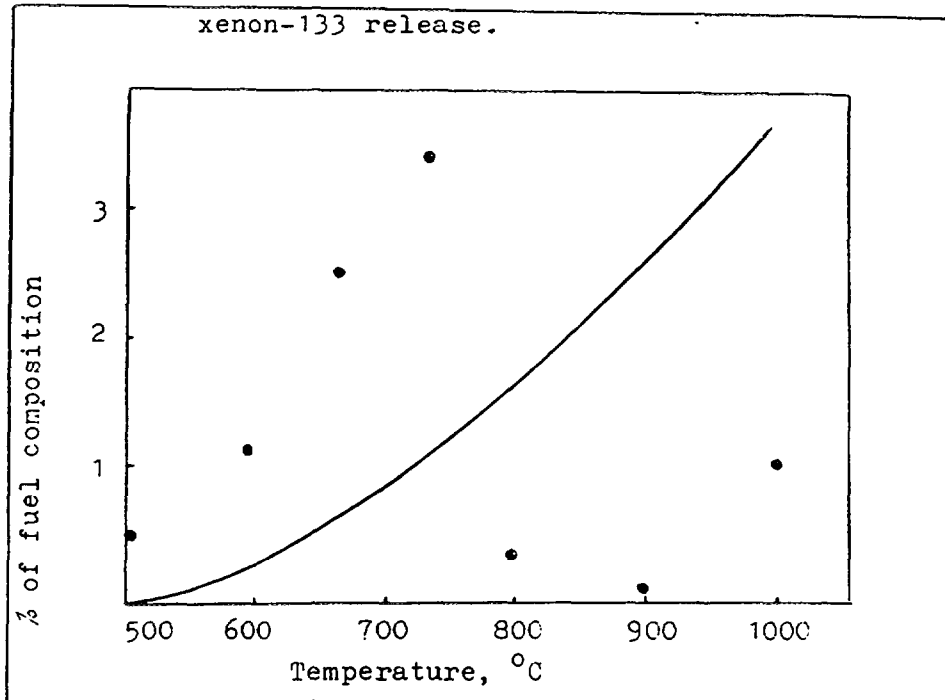
4. Conclusions

1. When burned up fuel pins with composition of uranium dioxide pellets without heat carrier pressure are heated the leakage of outer cladding of fuel pin occurs at 1070 K. This temperature is approximately 420 K higher then the melting temperature of of fuel composition matrix (magnesium). The FP release was detected at ~1270 K. The failure of outer cladding of fuel pin and magnesium release were observed at 1370 K.

2. When open fuel composition was heated, the FP release begins in a moment of magnesium (matrix material) melting. FP release before 1370 K (magnesium boiling temperature) is conditioned by FP release from magnesium. The FP release from uranium dioxide pellets occurs at temperatures above 1390 K, and the rate of FP release exponentially increases with temperature.

SOME FEATURES OF FISSION GAS RELEASE FROM IRRADIATED UO₂ AND CERMET FUELS

Yu.M. GOLOVCHENKO
Institute of Atomic Reactors,
State Scientific Centre of the Russian Federation,
Dimitrovgrad, Russian Federation

Abstract

This paper presents the results of some experiments performed recently at SSC RIAR. These experiments concerned particular features of fission gas release from such types of fuel as UO_2, UO_2+Cu, U. The first and the second fuels represent fuel types with low swelling and low fission gas release.

1. Experimental procedures

In our experiments UO_2 fuel was studied as identical fuel element fragments cut out from the same VVER-1000 fuel element. The fuel burnup was 40 MWd/kg UO_2 (about 4% of heavy atoms). The fuel element fragments were heated in helium or $He+H_2O$ mixture. Temperature and gamma-activity of the gas-carrier were determined as a function of time at the outlet of the furnace.

2. Experimental results

Fig. 1 demonstrates the relation of temperature and gamma-activity of the gas-carrier versus time at the outlet of the furnace. The following features can be pointed out:

- ^{85}Kr release begins at T=800°C;
- ^{85}Kr release increases at T=965;
- signs of burst release of the accumulated gas are available (the volume of the released gas was not measured);
- replacement of the inert environment (helium) with a gas-water vapour mixture does not result in an increase of ^{85}Kr release. It gives the evidence of the absence of the irradiated UO_2 intensive corrosion by water vapour at 800-965°C. One can see the absence of corrosion in Fig.2.
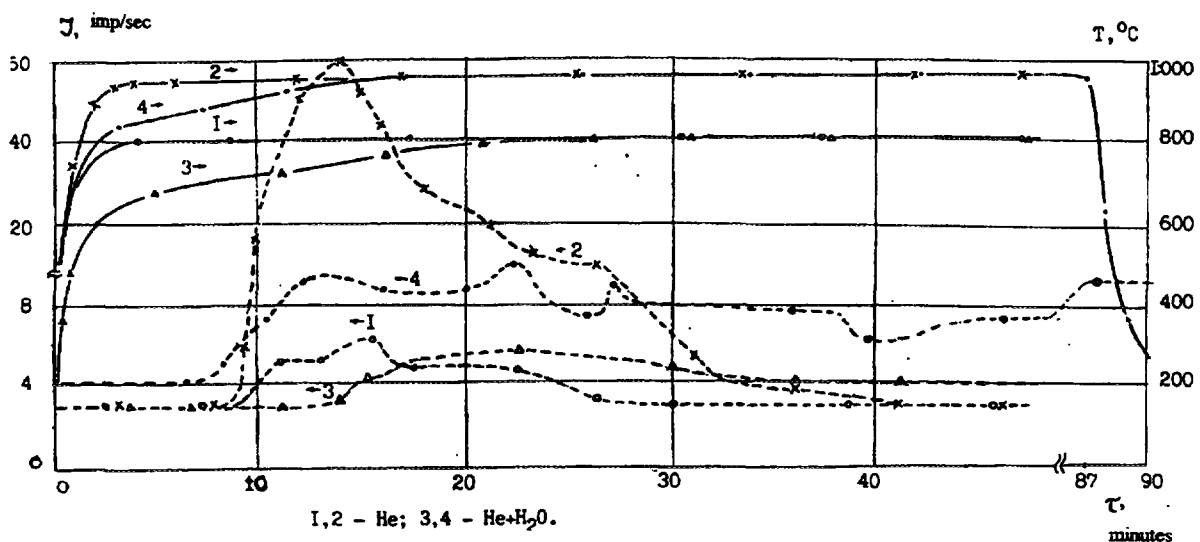
Fig. 1. Variation of temperature and ^{85}Kr release in heating the WWER-1000 fuel element fragments (fuel assembly No. 0329 from Zaporojie NPP).
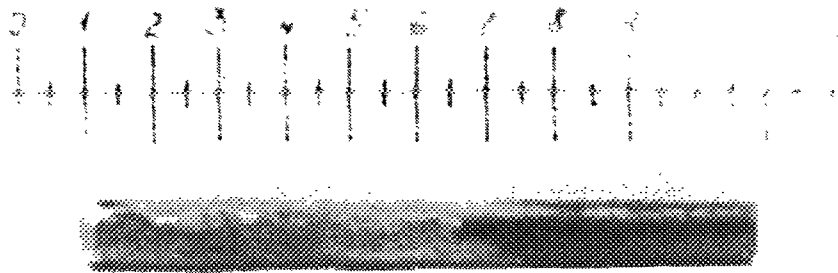
a)
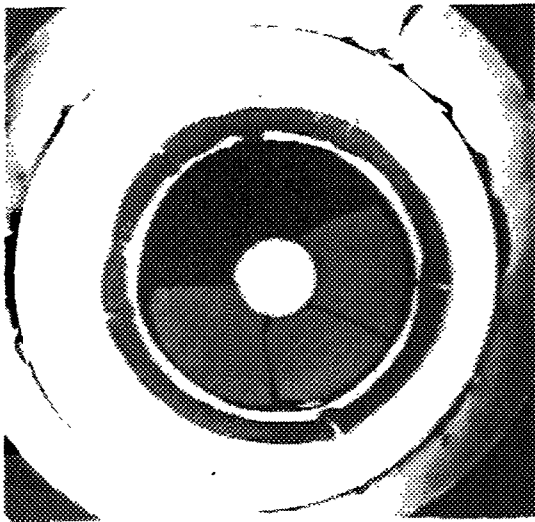
b)
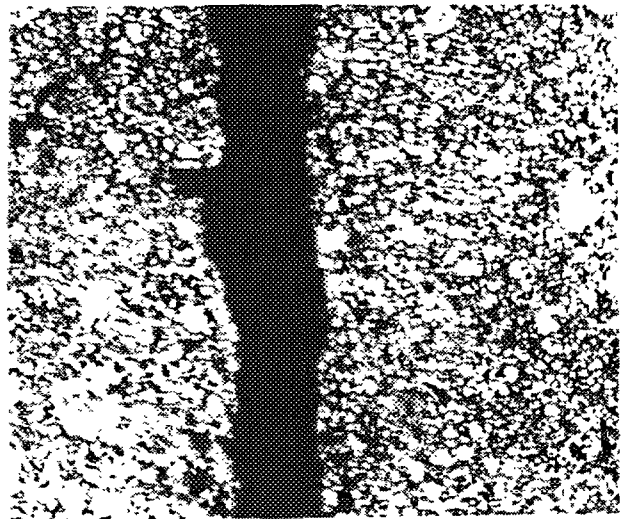
c)

d)

Fig.2. Appearance (a, x1),macro (b, x5) and microstructure (c-fuel, d-cladding, x100) of the WWER fuel element heated in vapour-gas mixture at 950°C, 72 min.

We suppose that there is a burst release of fission gases from the circumferential part of fuel pellets, i.e. from that part of fuel where an operating temperature was lower than that of the subsequent overheating.

An increase of the burnup in oxide fuel may be assumed as a cause of the decrease of the burst release temperature of the retained fission gases.

This assumption was confirmed during post-irradiation overheating of the irradiated SM-2 fuel elements (samples irradiated in SM-2 reactor of the RIAR). In these fuel elements the UO_2 particles are situated in a copper matrix. Under normal conditions, when the fuel temperature does not exceed 300°C, the fuel burnup can achieve several tens percent of heavy atoms without any sign of the gas release. On post-irradiation overheating the fuel element behaviour has a number of peculiar features.

Fig. 3 demonstrates the relation of temperature and gamma-activity of the gas-carrier versus time at the outlet of the furnace. One can see a burst release of ^{85}Kr at 800°C.

Fig. 4 shows macro- and microstructure of a cross-section of the SM-2 fuel element irradiated up to a burnup of 10 % of heavy atoms after overheating up to 690°C. It is evident that both the UO_2 particles and fuel composition as a whole have no anomalous swelling. At the same time the fuel element itself has anomalous swelling. Fragile cracks in the fuel composition and in the steel cladding are indicative of the fission gases burst release from UO_2 at 690°C.

Similar effects were detected in the fuel elements having the burnup higher than 10% of heavy atoms at temperatures below 690°C.
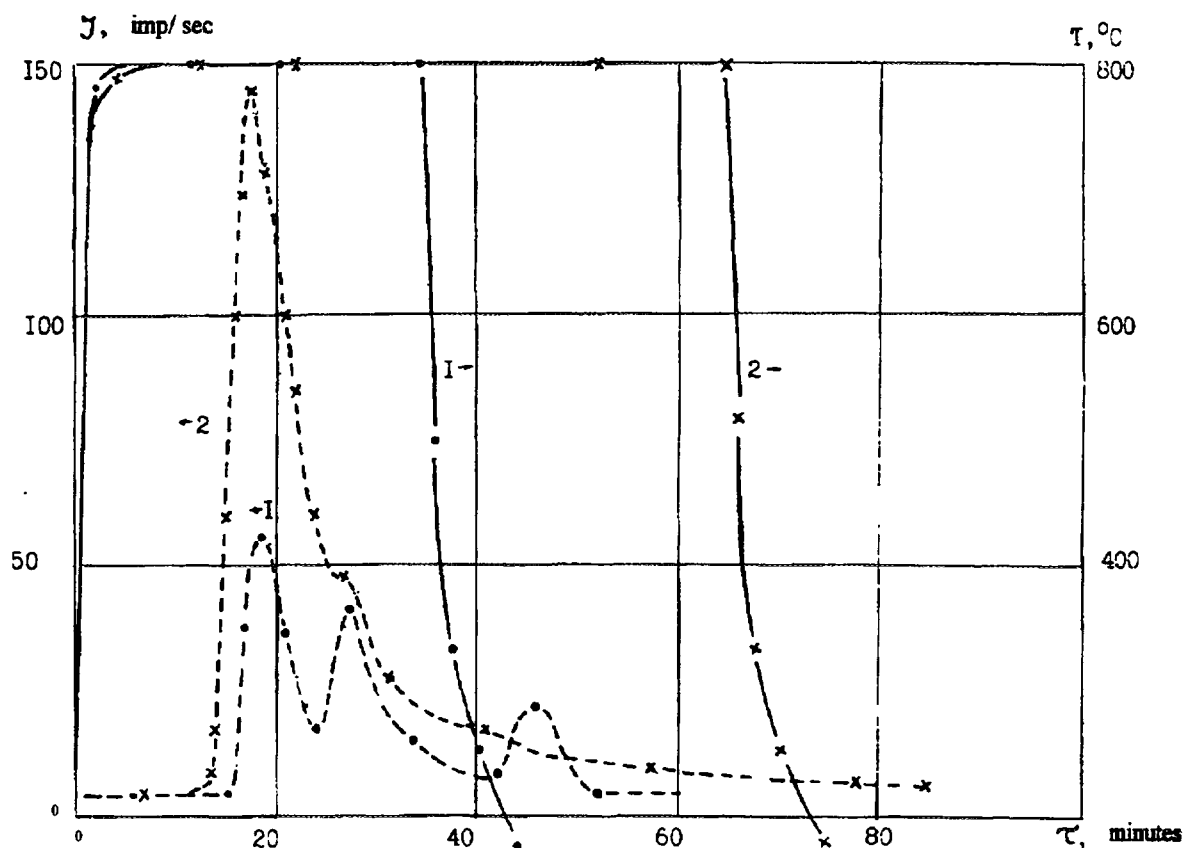
Fig. 3. Variation of temperature and ^{85}Kr release on heating the SM-2 reactor fuel element.

a)

b)

c)

d)
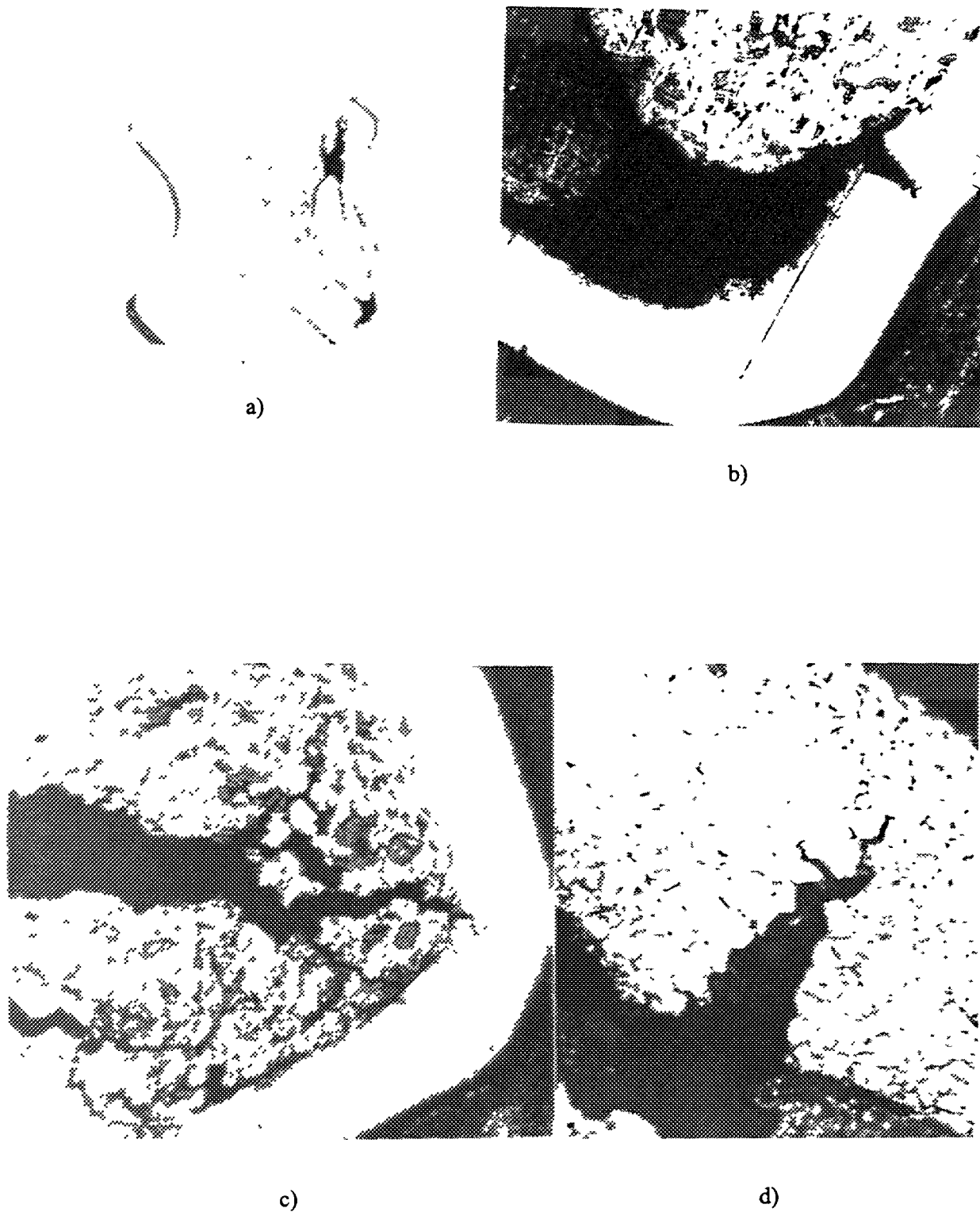
Fig. 4. The SM-2 reactor fuel element No. 2/12 from fuel assembly No. 10100186. Cross-section macro (a, x10 and microstructures (b, c, x100, unetched and d, x400, etched) after heating at 690°C, 30 min.

3. Discussion and conclusions

Hence, these features of the behaviour of fuel with low swelling and low release of fission gases at overheating should be taken into account on developing advanced high- burnup fuel elements. It concerns, first of all, fuel elements of power reactors with water cooling. Just for these reactors different options of the burnup increase are considered due to decreasing gas release from the coarse-grained UO_2 and decreasing fuel temperature as a result of usage of UO_2 + Zr dispersion-type fuel.

The reliability of fuel elements with this type of fuel should be tested not only at normal operating temperatures but also at possible overheating ones.

As for metal fuel, it is usually related to the fuel type having great swelling and gas release. Whereas, under some conditions metal fuel can have a very small gas release even at great swelling.

The experiments performed at ANL (USA) and RIAR have indicated a very small fission gas release from various types of metal fuel, provided swelling does not exceed 20%.

Therefore, on developing fuel elements with a low gas release fuel both metal fuel and dispersion-type compositions with metal fuel should be taken into consideration.

Certainly, with reference to power reactors with water cooling it is not metal uranium which should be considered but its corrosion-resistant Zr- and Si alloys.

FUELS FOR RESEARCH REACTORS
(Session 2)

Chairmen

A.K. SENGUPTA
India

Y.A. STETSKY
Russian Federation

DEVELOPMENT OF HIGH DENSITY FUEL FOR RESEARCH REACTORS

G.A. SARAKHOVA, Yu.A. STETSKY,
V.B. SUPRUN
All Russian Research and Scientific Institute of
    Inorganic Materials,
State Scientific Centre of the Russian Federation,
Moscow, Russian Federation

Abstract

The paper describes the activities on development of high density fuels for research reactors carried out by the ARSRIIM. These activities are performed in the framework of the International Programme RERTR on transfer fuel elements of research reactors to a fuel of reduced enrichment.

Introduction

Russia has been taking part in International Programme RERTR on transfer fuel elements of research reactors to a fuel of reduced enrichment. This problem could not be solved by the dispersion composition based on low density dioxide uranium (UO_2).

The impotant part of this Programme is the development of high density fuels. In our Institute such systems as U-Si, U-Zr-Nb and U-Fe (Fig.1) are considered to this purpose.

R&D activities

The use of high density types of fuel allows to considerably increase the technological effectiveness of the process due to decrease of volume content of fuel in the core (Table 1). Bearing this in mind, development are under way for all types of fuel elements, using high density uranium composition.

The use of high density fuels allows to considerably increase the technological effectiveness of the process due to decrease of volume content of fuel in the core (Table 1). Bearing this in mind, development is under way for all types of fuel elements, using high density composition.
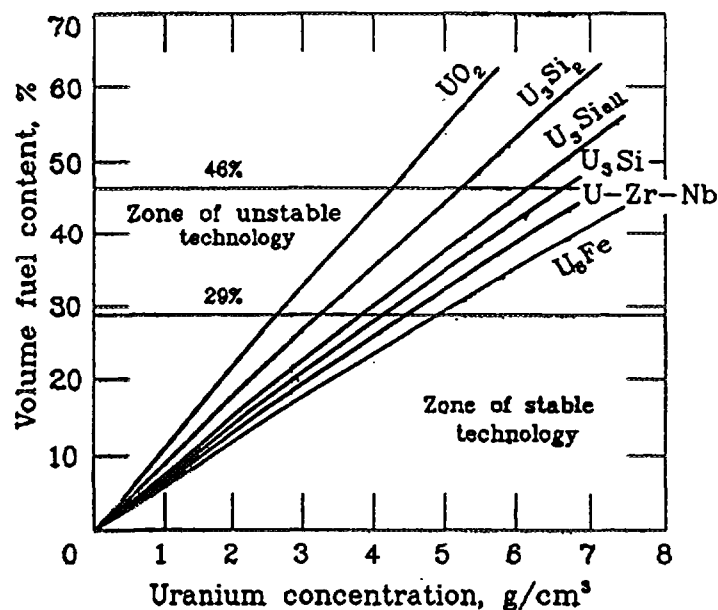
Fig. *1. Volume share of fuel component versus uranium concentration.*

TABLE 1 VOLUME CONCENTRATIONS OF FUEL COMPONENT DEPENDING ON HIGH DENSITY FUEL TYPE OF FUEL ELEMENTS

Type of fuel element	U-235 fuel assembly loading	U total concentr., g/cm3	Volume content of fuel component, %				
			UO_2	U_3Si_2	U_3Si	U, Zr, Nb	U_6Fe
VVR-M2	50.0	2.22	25.4	19.9	15.3	14.6	13.6
VVR-M5	75.3	4.74	54.3	42.6	32.8	31.3	29.0
MR	600.0	3.54	40.6	31.8	24.5	23.4	21.7
IRT-4M	400.0	3.73	42.7	33.5	25.8	24.6	22.8

It can be seen from the data presented in the table that for the main types of fuel elements it is impossible to use not only oxide fuel but uranium silicide of U3Si2 composition as well. That's why the Russian Programme is meant for uranium silicide of U3Si composition. Moreover, a possibility is under study now to use such uranium compositions as U6Fe and compositions of the U-Zr-Nb system.

The research is being currently performed with the objective to increase thermal resistance of these compositions. The major idea here is to receive metastable phases of uranium base, which are produced under quenching from γ-region. So called α"- phase is suppersaturated solid solution in γ- uranium with lattice which preserves of remaining monoclination. The irradiation of such material leads to the creation of more stable high temperature phase. The α"-phase (with b-parameter 5.8 A) formation is confirmed by X-ray analysis. Besides that, the heat of various reactions of uranium alloys with matrix AL have been defined by DTA - analysis. Thedata are as following:

for U3Si with Al matrix   q=5.55 J/g.;

for U3Si doped with Zr and Nb   q=1.22 J/g;

for U6Fe   q=4.1 J/g;

for U6Fe doped with Zr and Nb   q=3.2 J/g.

As a result of these works, the following compositions have been chosen for comparative study of the under-irradiation behaviour:

U - 7.5 wt% Si;

U - 3.7 wt% Si - O.lwt% Al;

U - 1.3 wt% Zr- 1.3wt% Nb - 3.9 wt% Si;   + Al (matrix)

U - 4 0 wt% Fe;

U - 1 1 wt% Zr - 1.1 wt% Nb - 3.9 wt% Fe;

U - 2.5 wt% Zr- 2.5 wt% Nb.

To test fuel structural materials an ampoule device has been developed (Fig.2), which is designed with an internal and external cladding of aluminium alloy AMSN-2.
There are ring spesimens located in the gap between the claddings, which are three layer elements with their

Desing of the ampoule device

Electron—beam welding

∅16,6 −0,1

12^{+1}_{-1}

Ampoule cladding

1

2

3

4

......

Core

0,6 min   0,6 min

14

15

16

$25^{+0,2}_{-0,2}$

17

18

Sealing plug

three—layer specimen

∅ 9,3 +0,1

∅ 13.4 −0,1

504^{+1}_{-1}

$450^{+3,2}_{-3,2}$

25 . 25

25

1,6 min

1,6 min

∅6,0 +0,1

15

12^{+1}_{-1}

∅11,5 −0,1

Electron—beam welding
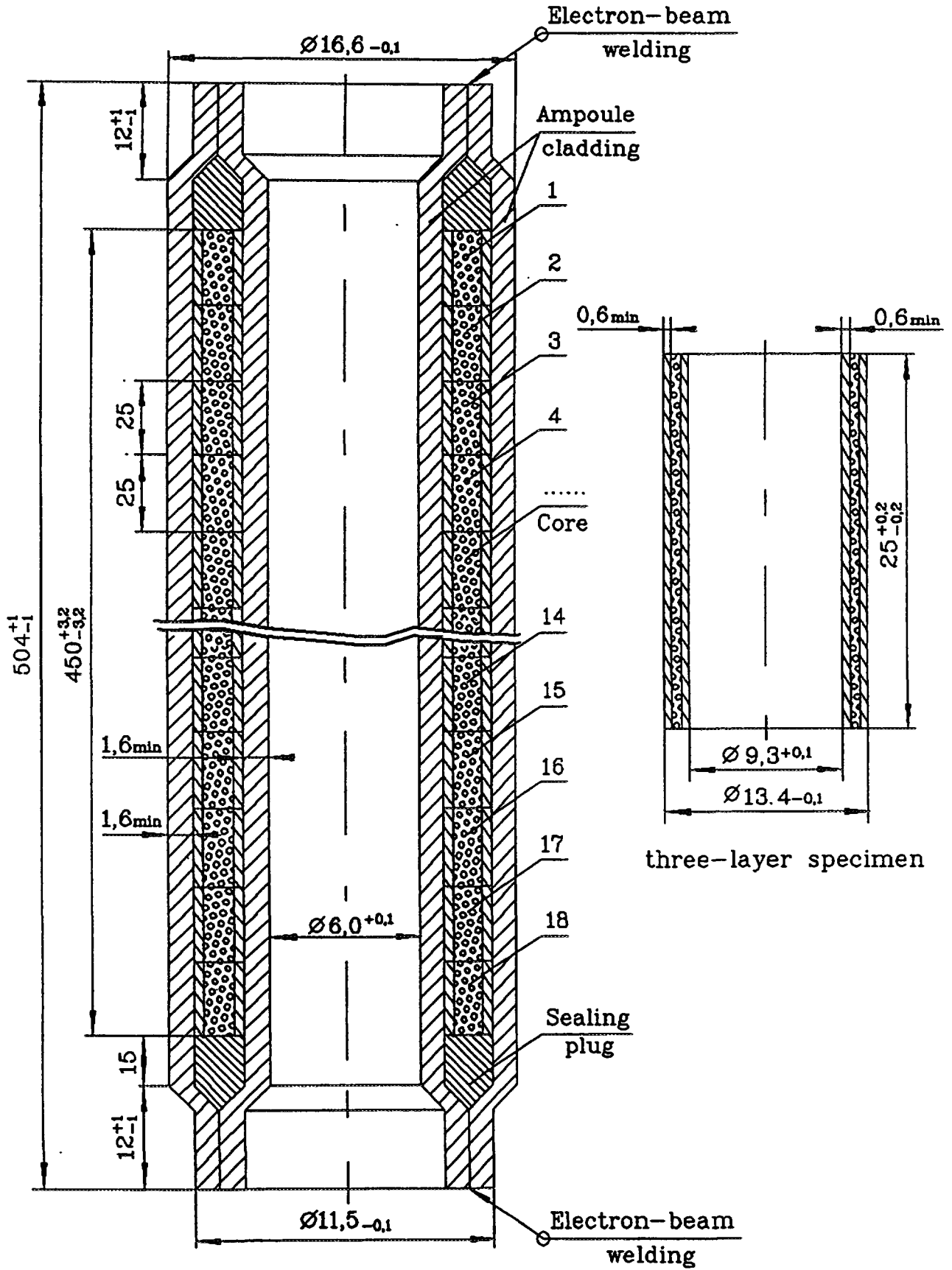
Fig. 2

own plating cladding and the core, produced from the types of compositions under study (Tables 2 and 3) Table 3 shows characteristics of the specimens with oxide fuel. Irradiation of these specimens alongside with new high density materials is explained by, as alreafy mentioned above, by the lack of the experimental data for such concentrations.

TABLE 2 CHARACTERISTICS OF SPECIMENS: DISPERSION COMPOSITIONS BASED ON HIGH DENSITY URANIUM COMPOUNDS IN ALUMINUM MATRIX

No. of specimen	Type of fuel in composition	Density of compound, g/cm3	U content in compound, wt%	Fuel share in composition	
				vol%	wt%
1	U_3Si_2	12.15	92.5	35.6	71.3
2	U_3Si	15.15	96.0	27.5	68.1
3	$(U, Zr, Nb)_3Si$	15.55	93.5	27.5	68.6
4	U_6Fe	17.50	96.0	23.8	67.0
5	$(U, Zr, Nb)_6Fe$	17.40	93.8	24.5	67.6
6	U-Zr-Nb	18.87	95.0	22.3	66.7

Note: Total uranium content in composition 4 g/cm3.

TABLE 3. CHARACTERISTICS OF SPECIMENS: DISPERSION COMPOSISION BASED ON URANIUM DIOXIDE IN AL MATRIX

No. of specimen	Particle size,μm	Content U, g/cm3	UO_2 share in composition	
			vol%	wt%
7	100-250	4.0	47.3	76.3
8	100-250	3.2	37.8	68.6
9	100-250	2.5	32.9	61.3
10	60-100	4.0	47.3	76.3
11	60-100	3.2	37.8	68.6
12	60-100	2.5	32.9	61.3

Table 3 shows characteristics of the specimens with oxide fuel. Irradiation of these specimens alongside with new high density materials is explained by, as alreafy mentioned above, by the lack of the experimental data for such concentrations.

In-core tests are supposed to be conducted in an experimental channel of IVV-2M reactor under the following conditions:

74

U-235 burnup: 50% of regular burnup,
90% of regular burnup.

Duration of tests: 150 and 300 effective days.

Calculated maximum temperature in core: 188°C.

Thermal neutron flux: app. $1 \cdot 10^{14}$ n/cm^2

Loadiing of the ampoules into reactor is scheduled for the end 1996.

DEVELOPMENT OF URANIUM-SILICIDE AND U-Mo ALLOY FUELS BY CENTRIFUGAL ATOMIZATION

Kihwan KIM, Don Bae LEE, Chang Kyu KIM,
Il Huyn KUK
Korea Atomic Energy Research Institute

Kyung Wook BAEK
Korea Advanced Institute of Science and Technology

Taejon, Republic of Korea

Abstract

U_3Si and U_3Si_2 powders for application dispersant for research reactor dispersion fuel elements are produced by atomizing alloy melt instead of comminuting. Many benefits are introduced by applying the atomization technique : reduction of the process, increase of the thermal conductivity, decrease of the thermal reaction with aluminum due to the spherical shape of particle, and increase of the uranium loading. Also, in order to improve the uranium loading of fuel, high density U-Mo powder is prepared by centrifugal atomization. U-Mo powder has spherical shape, narrow size distributions, high density and fine grain structure with isotropic γ-U phase. U-Mo fuel meats, especially U-10wt.%Mo, show good thermal compatibility with Al matrix and maintain microstructure stability.

1. Introduction

Research on the intermetallic compounds of uranium has been continued since 1978 with the decision, by the international research reactor community, to develop proliferation resistant fuels. The reduction of 93% ^{235}U (High Enrichment Uranium or HEU) to 20% ^{235}U (LowEnrichmnt Uranium or LEU) necessitates the use of higher U-loading fuels to accommodate the additional U in the LEU fuels [1]. Intermetallic compounds are well suited for use in research reactor fuel elements, which typically consist of small-particulate fuel dispersed in aluminum. Intermetallic compounds of uranium, in particular U_3Si and U_3Si_2, dispersed in aluminum have been the preferred choice as a fuel for high flux research reactors [2-6].

Korea Atomic Energy Research Institute has been developing the uranium silicide fuel for the HANARO of the 30 MW research reactor since 1988. Uranium-silicide particles have been prepared conventionally by the comminution of cast alloy ingot [7]. It is well known that U_3Si is very tough and the alloy billet is hard to be machined into fine powder. Labors and many steps of tedious work are needed in comminution. The comminuted powder is susceptible to contain impurities such as ferrous particles from the machining tools. In addition, the sharp of comminuted particles is generally irregular with shape edges. In order to overcome the difficulties in comminuting the tough billet and to eliminate the contaminations of impurities, the rotating disk atomization method has been applied for the preparation of uranium silicide particles [8] It is known that the powder has a rapidly solidified microstructure, a relatively narrow particle size distribution, and that the powder is finer and spherical in shape [9-10]. Especially, the spherical powder could give the desirable effects of improving plastic flowability and could not show any appreciable directional orientation after mechanical processing. Also the specific surface area of atomized particles is less than that of comminuted particles, so that the reaction swelling between uranium-silicide particles and aluminum matrices is expected to be reduced.

In addition, the conversion from high enriched uranium (HEU) to low enriched uranium (LEU) for use in research reactor fuel requires a large increase in the amount of uranium contained in a fuel element to compensate for the reduction in enrichment. The development of commonly used aluminum-based dispersion fuels using U^3Si^2 as the fissile component has been rather successful in onverting reactors with the fuel element loadings of up to about 4.8 g U cm^3 [1-4]. U_3Si_2 has been found to possess very stable irradiation behavior, butlimitations in fabricability do not allow loading conversion to LEU any higher than ~6 g U cm^3 [11-12]. While the majority of reactors can be satisfied with U_3Si_2-Al dispersion fuel, several high performance reactors require still increasing the loadings up to 8~9 g U cm^3.

Consequently, in the renewed fuel development program of the Reduced Enrichment for Research and Test Reactor (RERTR) Program, attention has shifted to high density uranium alloys. Early irradiation experiments with uranium alloysshowed promise of acceptable irradiation behavior if these alloys could be maintained in their cubic γ-U crystal structure [13] Alloys with tendency to form this gamma phase are: U-Cr, U-Mo, U-Nb, U-Re, U-Ru, U-Ti, U-V, U-Zr, etc Among these, the alloy which has a relatively large range of gamma phase is U-Mo. In addition Mo has a relatively low neutron caption cross-section. Below 570° C the stable structure of U-Mo alloys is a mixture of α -U and δ- phase (U_2Mo). However, by rapid cooling from he gamma phase, U-Mo alloy easily retains this phase in a metastable state. If this metastable gamma phase can be maintained during fuel element fabrication and irradiation, and if the alloy has good thermal compatibility with aluminum, U-Mo alloy would be a prime candidate for dispersion fuel for research reactors.   In this study, U_3Si and U_3Si_2 powder for application in research reactor fuel elements are prepared by rotating disk centrifugal atomization and are characterized in comparison with the comminuted powders for application as a dispersant for research reactor fuel elements. Also two kinds of fuel meats are prepared with atomized and comminuted U_3Si/U_3Si_2 powders by extrusion or rolling process The effects of atomized spherical powder on fuel meat are investigated. Further U-Mo powders prepared by centrifugal atomization are characterized. The fuel meats are prepared with the atomized powder by extrusion. Especially, the characteristics related to the microstructure stability and the thermal compatibility of fuel meats are examined.

2. Experimental procedure

Uranium-silicide and U-Mo alloy was induction-melted in graphite crucibles with proportioned charge of depleted uranium lump with purity 99.9%, silicon chip with purity 99.9999% or molybdenum buttons with purity 99.7% The molten metal was fed through a small nozzle onto a rapidly rotating graphite disk under an argon atmosphere In order to obtain the suitable size distribution and shape, the atomization parameters, such as the feeding rate of melt, the revolution speed of disk etc., were adjusted. The atomized powder was collected in a container at the bottom of the funnel shaped chamber. On the other hand, for the preparation of comminuted uranium-silicide particles an alloy ingot was made by induction melting and casting using depleted uranium and silicon as raw materials, and then comminuted. And U_3Si alloy was heat-treated at 800°C in order to transform as-cast ingot into U_3Si phase ia peritectoid reaction. Both extruded rods and hot-rolled miniplates were fabricated using comminuted and atomized (spherical) powder.

The powder size distribution of the atomized powder was determined by sieve analysis and light diffraction method. The density of powder and fuel meat were measured by Archimedean immersion method. The morphology and microstructure of powder and fuel meat were characterized with an optical microscope and a scanning electron microscope after polishing and etching. Composition was analyzed done by energy dispersive spectroscopy with the SEM. The phase transformation temperature of the atomized powder was determined using a differential scanning calorimeter (DSC), generally the rate of temperature increase was chosen as 20 °C min-1. The area fraction of the pore was examined by the image analyzer with the micrographs The alloy phases of as-atomized or heat-treated powders and fuel meats were analyzed by X-ray diffraction, using Cu K_α wave length.

3. Results and discussion

The typical shape of the atomized U_3Si, U_3Si_2 and U-Mo alloys particles as observed by scanning electron microscope is shown in Fig. 1. Most of the particles have a spherical shape with few attached satellites [9]. A few fine particles (below 45 μm) have a lengthened, flake-like morphology. Spherical shape of the atomized particles is attributed to the surface tension of the melt droplet [10]. Fig. 2 shows the typical size distribution of atomized U_3Si, U_3Si_2 and U-Mo alloys particles in terms of weight fractions The size distribution of the powder is relatively narrow, and the median particle size was about 80μm. Such a mono-modal size distribution is frequently seen in the ligament disintegration mechanism [14-15]. Fig. 3 shows the particle density versus particle size of U-2wt.%Mo, U-10wt %Mo alloy. The average densities of U-2wt %Mo, U-10wt.%Mo alloy are about 17 3 g/cm³ and 16.8 g/cm³, respectively It is found that the density of atomized powder decreases as the particle size increases irrespective of alloy composition. This is due to the increase of internal pores with the increasing particle size [16]

78
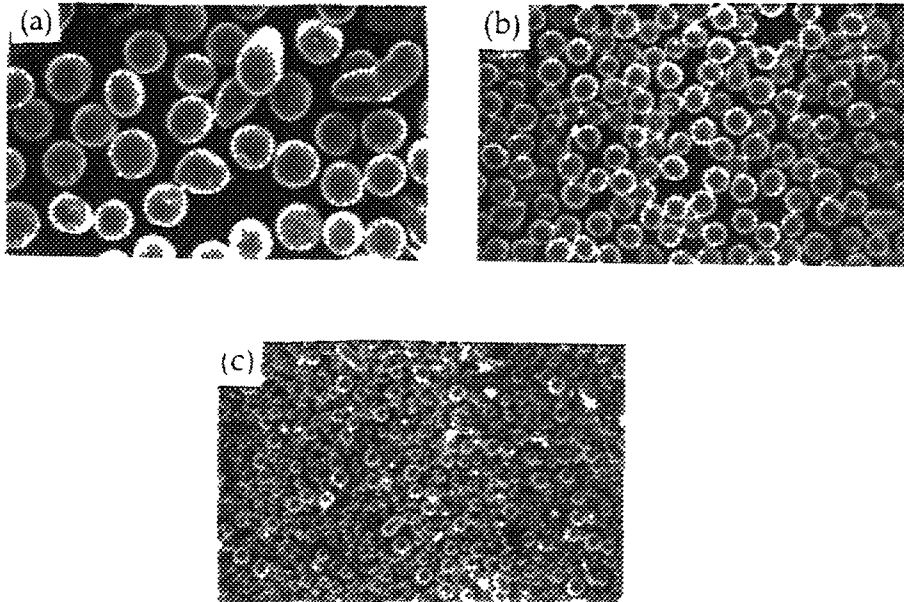
Fig. 1. Photographs showing the shape of atomized powder (x100);
(a) 120-140 Mesh, (b) 200-240 Mesh, (c) -325 Mesh.
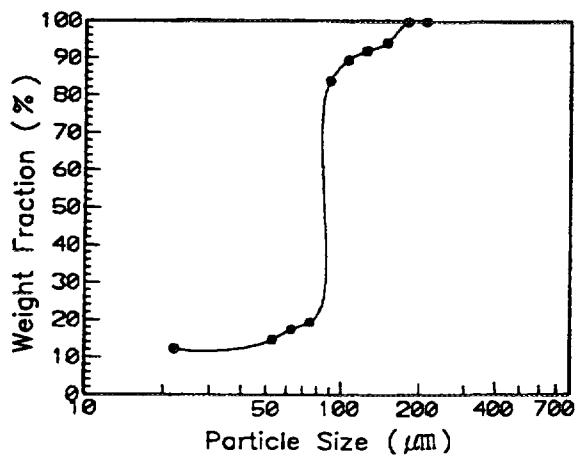
Fig. 2. Particle size distribution of atomized alloy powder.
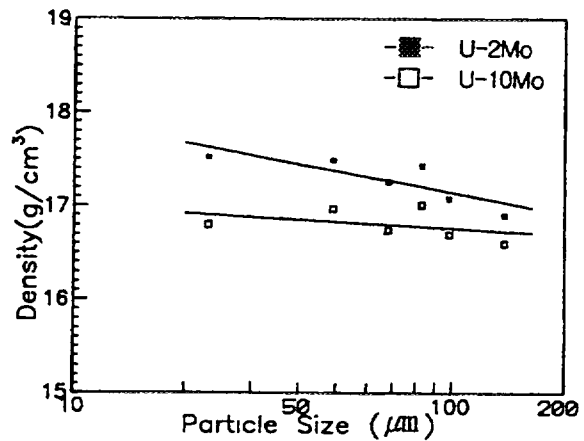
Fig. 3. Variation of density according to particle size in the atomized U-Mo alloy powder.

The minimum width of primary U_3Si_2 precipitates decreased from about 20 μm in the comminuted powder to about 2 μm in the atomized powder due to the effect of rapid solidification. Primary U_3Si_2 precipitates tends to be finer with the decrease of the powder size. This suggests that the finer particles cool rapider due to the increase of the specific area. As the cooling rate increases in a finer melt drop, the time available for solidification decreases The size of primary U_3Si_2 precipitates becomes finer. Fig. 4 shows the isothermal transformation curves for the specimens of different primary U_3Si_2 precipitates sizes in the heat-treatment at 800°C [16]. The heat-treatment period for the formation of U_3Si by a peritectoid reaction was reduced from 72 hours to 6 hours owing to the refinement of microstructure [17]. The curves are typical for phase transformations by nucleation and growth. Nucleation occurs more rapidly in the fine structure than in the coarse one, whereas the slopes which means the transformation rate are almost the same It is assumed that the short peritectoid reaction time is introduced from the large interfacial area of fine primary particles and the rapid nucleation of U_3Si phase[18-19] In addition, the microstructure of heat-treated atomized powder appears to be much finer, about one fifth, than that of heat-treated ingot.
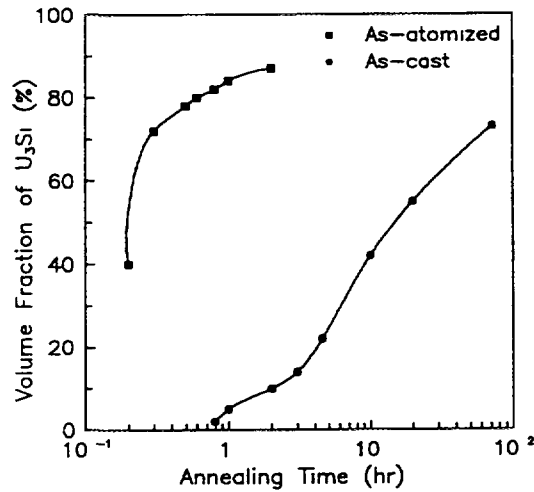
Fig. 4. The isothermal transformation curves for the specimens of different primary U₃Si₂ precipitates size in heat-treatment at 800℃.

The typical cross-sectional micrograph of atomized U-Mo alloy particles, with the EDX analysis result, are illustrated in Fig. 5. It is seen that the micro-structure of the atomized particles is polycrystalline, with many non-dendritic grains below 5 μm in size. The grain size becomes smaller s the particle size becomes finer. This suggests a rapider cooling of finer powder due to the increase of the specific surface area. Because the cooling rate in finer droplet is higher, the time available for solidification decreases and the phase particles get finer.

The X-ray diffraction patterns of atomized U-2wt.%Mo and U-10wt.%Mo alloy powder are shown in Fig. 6 All phases of atomized alloy powders below 150 μm are found to be the isotopic-metastable Γ-U (bcc) phase. It is known that U-2wt.%Mo and U-10wt%Mo alloy frozen slowly consists of α-U phase and δ-U₂Mo intermetallic compound with lamellar structure [20]. On the other hand, Γ-U (bcc) phase, which is the stable phase above about 570°C, can be retained in a metastable state at room temperature by rapid solidification. Fig. 7 shows a differential scanning calorimeter (DSC) trace of atomized U-Mo powder during continuous heating to 750°C at a rate of 20°C min⁻¹. The DSC trace in continuous heating of U-2wt.%Mo alloy shows a large and broad endothermic peak at about 600°C associated with decomposition of metastable γ-U. The continuous heating DSC trace of U-10wt.%Mo alloy shows no peak over the temperature range associated ith decomposition of γ-U. X-ray diffraction of U-10wt.%Mo powder after the continuous heating demonstrates that the alloy powder remains as the metastable Γ-U (bcc) phase.
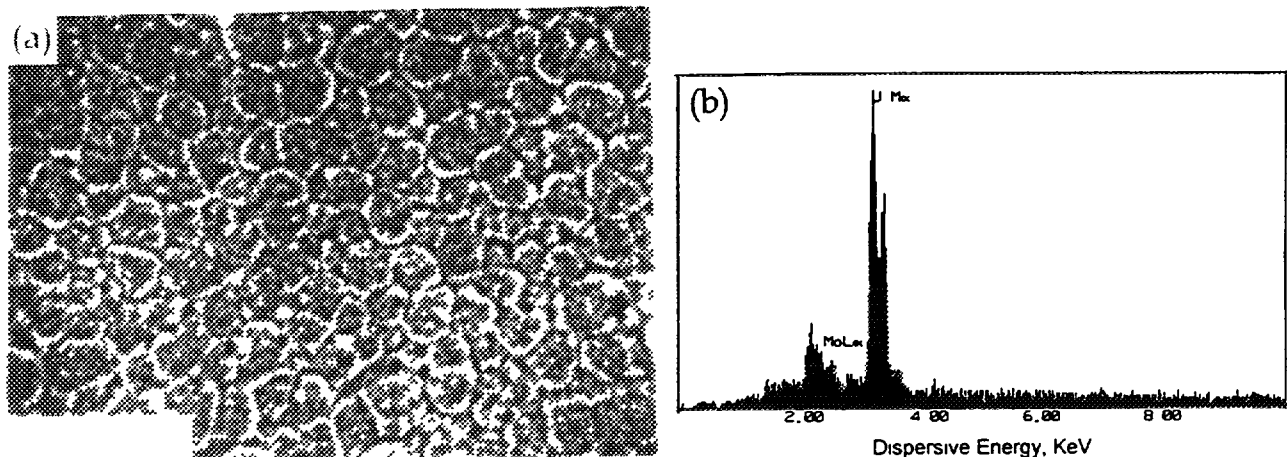
Fig. 5. Micrograph (a) and energy dispersive spectra (b) from the matrix of atomized U-2wt.%Mo powder.

As shown in Fig. 8, the use of spherical U_3Si_2 powder, however, results in somewhat higher porosity in the rolled plate but drastically lowers porosity in the extruded rod. Such results are attributed to the random fracture of spherical particles under the planar stress imposed by rolls, which evidently causes more porosity. The force on spherical particles in a circular extrusion die is more uniform leaving the particles largely intact, thus generating less porosity. The evidence to this widely different behavior can be found in metallographic sections shown in Fig. 9.

On the other hand, U_3Si fuel particles with a certain aspect ratio lie along the working direction in forming, i. e., extrusion or rolling direction. Fig. 10-a shows the cross-section of the fuel meat with comminuted particles in which the fuel particles are reoriented along the working direction of the fuel meat. In contrast, the atomized particles shall never have an aspect ratio since they are spherical. Regardless of rolling or extruding, they have no chance of anisotropic orientation along the working direction in forming. Fig. 10-b shows the atomized particles without anisotropic orientation in the fuel meat in comparison with the comminuted particles aligned to the working direction.

Shape of the fuel particle greatly effects on the fuel properties in relation with the orientation in the fuel meat. Direction of heat transfer in the fuel meat in reactor operation is perpendicular to the plate, which means heat is dissipated perpendicular to the working orientation of the fuel particles in the meat with the comminuted powder. Table 1 shows the difference in thermal diffusivity between the fuel meats with the comminuted powder and the atomized one. The meat with the atomized particles has 15% higher thermal diffusivity in the heat-transfer direction of reactor operation than the one with the comminuted particles does. Thermal diffusivity (α) has a relation with thermal conductivity (K) ; K = ϱ Cp α, where ϱ: density, Cp = thermal capacity. These data of diffusivity show the great difference to say that thermal conductivity increases in a sufficient amount by using the atomized powder.
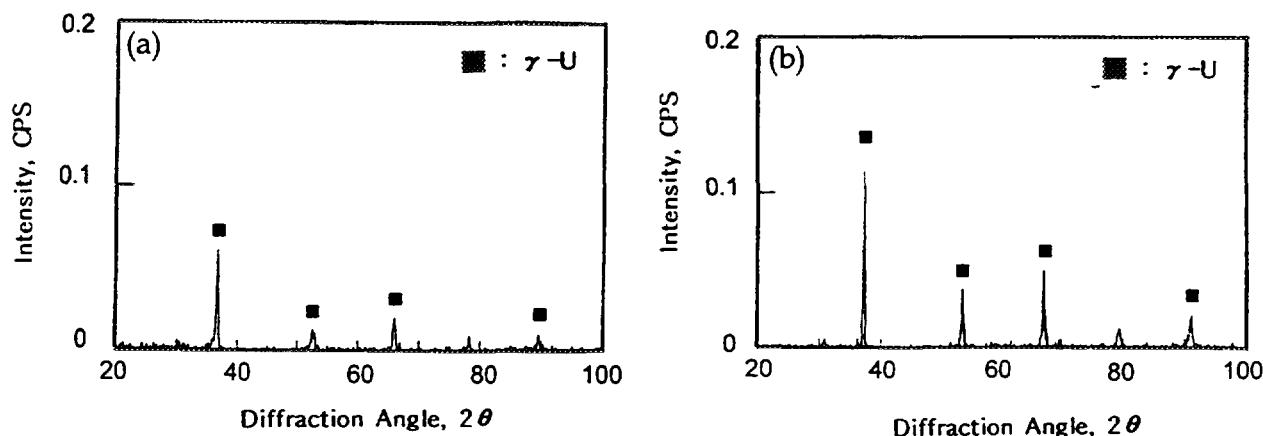
Fig. 6. X-ray diffraction patterns of atomized U-2wt.%Mo powder (a) and
    U-10wt.%Mo powder (b).
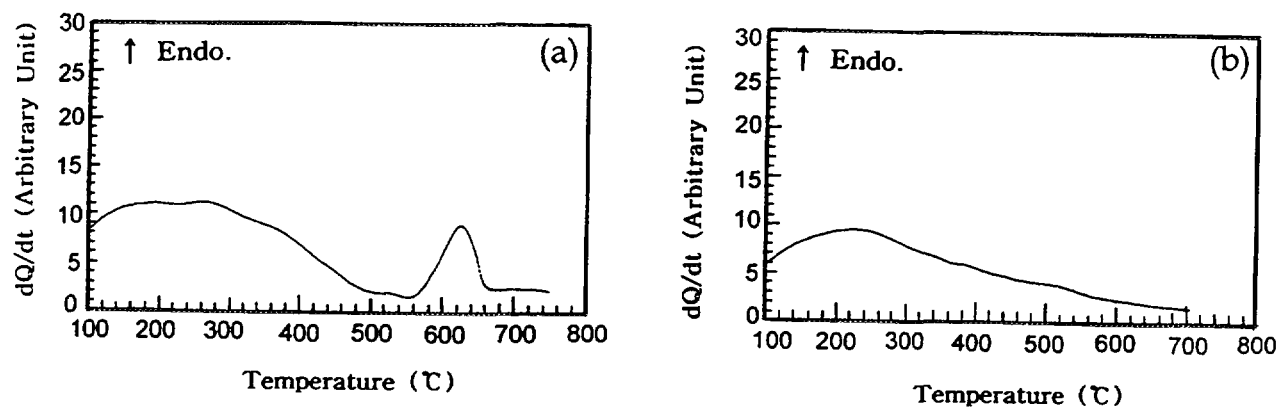
Fig. 7. DSC curves of atomized U-2wt.%Mo powder (a) and U-10wt.%Mo powder (b)
    during continuous heating.

81
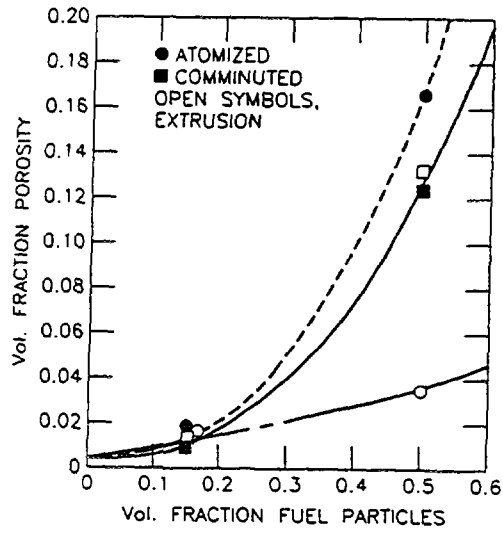
Fig. 8. Fabrication porosity in hot-rolled and extruded dispersion cores with U_3Si_2 particles.
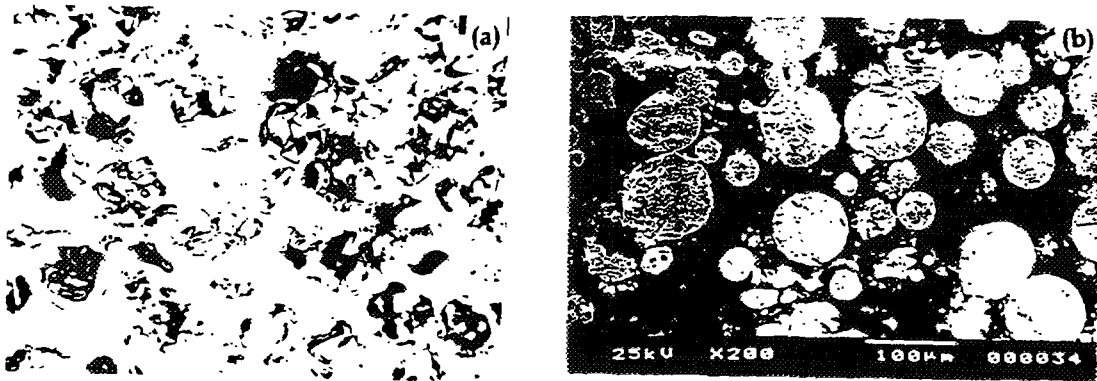
Fig. 9. Microstructure of hot-rolled cores (a) and extruded cores (b) containing
50 vol.% atomized U_3Si_2 powder.
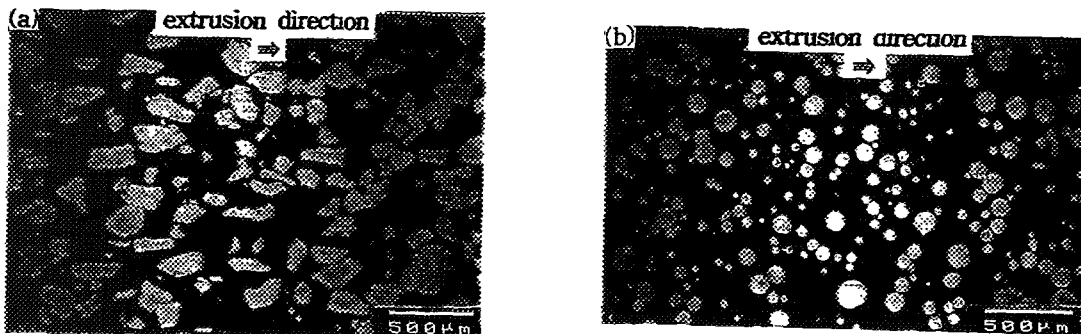
Fig. 10. U_3Si fuel particles reoriented by extrusion; (a) Comminuted particles,
(b) Atomized particles.

82

Swelling phenomenon happens by the reaction between dispersed particles and Al matrix in the dispersion fuels It is shown in Fig 11 that the fuel meat with the atomized particles changes its volume by 15% less than the one with the comminuted particles in thermal reaction. It is supposed that such a difference
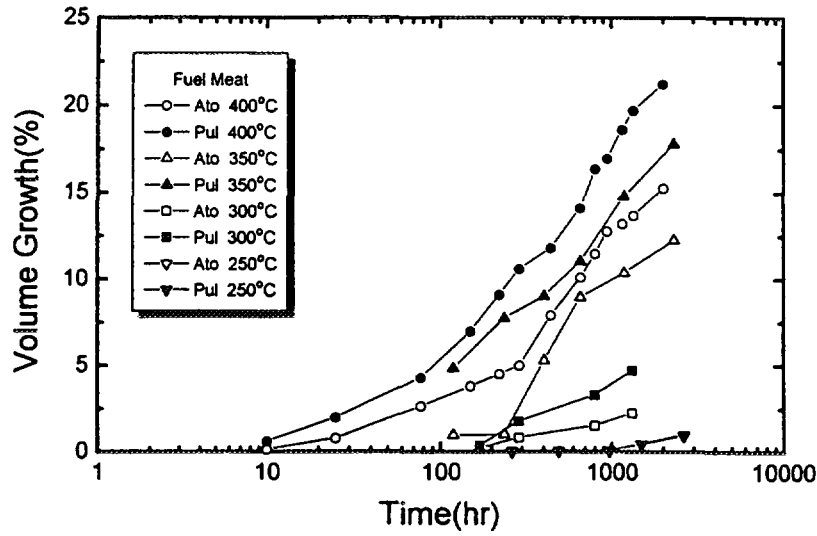
Fig. 11. The rate of thermal reaction between fuel particles and aluminum matrix at various temperatures in comparison between the atomized powder and comminuted one.
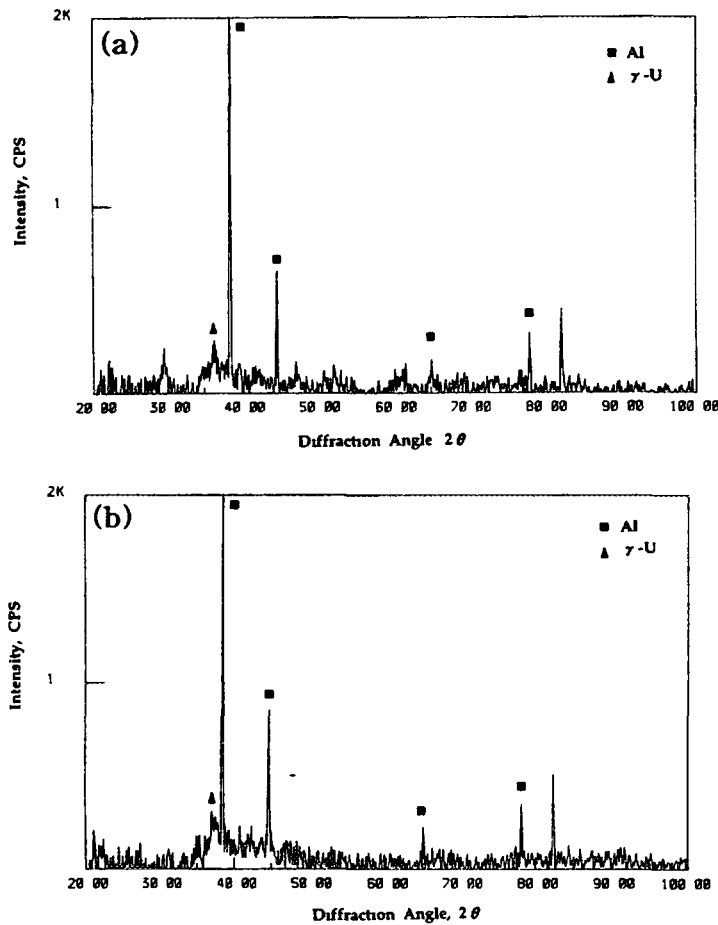
Fig. 12. X-ray diffraction patterns of U-Mo alloy fuel meats after annealing at 400℃; (a) U-2wt.%Mo alloy, (b) U-10wt.%Mo alloy.

is resulted from the smaller specific surface area of atomized spherical powder relative to comminuted powder.

Table 2 shows the results of swelling test for the fuel meat of two kinds of U-Mo alloys (U-2wt.%Mo and U-10wt.%Mo) with 24 vol.% at 400°C. U-2wt.%Mo and U-10wt.%Mo fuel meats are not greatly swollen after holding at 400°C for 1000 hours. U-10wt.%Mo fuel meat almost does not swell, below 5%, but U-2wt.%Mo fuel meat is largely expanded after annealing at 400°C for 2000 hours. X-ray diffraction patterns of fuel meats after annealing at 400°C are shown in Fig. 12. Most of γ-U phase in two kinds of U-Mo fuel meats remain as they were. This confirms that the γ-U phase of atomized U-Mo powder can be retained for the extended times, presumably because the diffusion-controlled transformation is retarded [20-21].

Table 1. Thermal diffusivity varying with U-loading the meat with comminuted particles and with the atomized particles.

powder contents vol%	comminution fuel meats (cm^2/sec)		atomization fuel meats (cm^2/sec)	
	longitudinal	transverse	longitudinal	tranverse
10.6	0.64	0.50	0.64	0.49
15.1	0.61	0.41	0.57	0.46
21.7	0.55	0.36	0.54	0.42
29.2	0.50	0.30	0.48	0.31
41.5	0.31		0.34	

Table 2. Dimensional changes of Al-24vol.%U-Mo alloy fuel meats after annealing at 400°C.

(Unit: %)

Time (hr)	U-2Mo Alloy			U-10Mo Alloy		
	$\triangle \ell$	$\triangle$ d	$\triangle$ V	$\triangle \ell$	$\triangle$ d	$\triangle$ V
11	-0.15	-0.17	-0.49	-0.09	-0.18	-0.45
40	-0.03	-0.30	-0.63	-0.02	-0.06	-0.14
107	+0	-0.23	-0.46	-0.14	-0.05	-0.24
350	+0.19	+0.06	+0.31	-0.07	0	-0.07
1000	+1.83	+0.39	+2.61	-1.04	-1.52	-4.08
2000	+4.28	+10.86	+26	0.12	-0.11	-0.34

4. Conclusion

Rotating disk centrifugal atomization technique was applied in producing the fuel powder of uranium-silicide and uranium-molybdenium alloy.

The particle size distribution could be controlled by adjusting the atomization parameters irrespective of alloy composition. The resulting particle shape is near perfectly spherical with relatively narrow distribution which gives no chance of anisotropic alignment of the particles along the working direction.

Most of the nuisances in the fabrication process of uranium-silicide fuels could be eliminated by obtaining the powder directly from the molten alloys, which enhances the production economy and results in the product powder with less impurities Thermal conductivity increases in the radial direction due to the isotropic distribution of particles in U_3Si fuel rod. Formability increases in the extruded U_3Si_2 fuel rod using spherical powders, which improves U-loading drastically.

U-Mo powder has high density and fine grain structure with isotropic γ-U phase. In addition, U-Mo fuel meats, especially U-10wt.%Mo, show good thermal compatibility with Al matrix and maintain microstructure stability. γ-U phase in U-Mo fuel meats shows relatively good microstruture stability in the operation temperature.

Therefore atomized uranium-silicide and U-Mo powder are suggested to be the potential candidates for high uranium-loading fuel for the purpose of reducing enrichment for research and test reactors.

Acknowledgment

References

1 A. Travelli, Proc. of 9th International Meeting on Reduced Enrichment Research and Test Reactor, Gatlinberg, Tenessee, USA, Nov 2-6, 1986 (ANL/RERTR/TM-9)

2. S. Nazare, J. Nucl. Mater., 124 (1984) 14.

3. R.C. Birther, C.W.Allen, L.E. Rehn and G.L. Hofman, J. Nucl. Mater., 152 (1988) 73.

4. G.L. Hofman, J. Nucl. Mater., 140 (1986) 256.

5. G. L. Copeland, G.L. Hofman, J. L. Snelgrove, Pro. of 9th International Meeting on Reduced Enrichment Research and Test Reactor, Gatlinberg, Tennessee, USA, Nov 2-6, 1986 (ANL/RERTR/TM-9).

6. G. L. Hofman, J. Nucl. Mater., 140 (1986) 256.

7. D. F. Sears, L. C. Berthiaume and L. N. Herbert, Pro. of 9th International Meeting on Reduced Enrichment Research and Test Reactor, Gatlinberg, Tennessee, USA, Nov 2-6, 1986 (ANL/RERTR/TM-9).

8. C.K. Kim, K.H. Kim, C. T. Lee, I. H. Kuk, Pro. of 14th international Reduced Enrichment for Research and Test Reactor, Jakarta, Indonesia, Nov. 4-7, 1991.

9. T. Kato, K. Kusaka, Materials Transactions, JIM. 31 (1990) 362.

10. T. Kato, K. Kusaka, H. Horata and J. Ichikawa, Tetsuto-Hagan , 6 (1985) 719.

11. J P. Durand, Pro. of 19th International Meeting on Reduced Enrichment Research and Test Reactor, Paris, France (1995).

12. J. P. Durand, P. Laudamy K. Richer, Pro. of 18th International Meeting on Reduced Enrichment Research and Test Reactor, Williamsburg, USA (1994).

13. G. L. Hofman and L.C. Walters, Materials Science and Technology, Vol. 10A, Nuclear Materials, B.R.T. Frost ed. VCH Publishers, N.Y. (1994).

14. B. Champagne and R. Angers, Modern Developments in Powder Metallurgy, 12 (1980) 83.

15. B. Champagne and R. Angers, The International Journal of Powder Metallurgy & Powder Technology, 16 (1980) 359.

16. J. E. Flinn and G. R. Smolik, J. Mater. Sci. & Eng., A124 (1990) 39.

17. A. Horata, T. Kato and K. Kusaka, Progress in Powder Metallurgy, 41 (1985) 479.

18. C. K. Rhee, S. I. Pyun, and I. H. Kuk, J. Nucl. Mater., 184 (1991) 146.

19. G. Kimmel, A. Tomer, and A. Barror, J. Nucl. Mater., 40 (1971) 242.

20. K. H. Ekelmeyer, Microstrutural Structure, Vol. 7, Fallen, McCall, eds., (1977).

21. D.E. Thomas, et al., Proc. Second International Conference on Peaceful Uses of Atomic Energy, 5, 610 (1958).

ESTIMATION OF THERMAL CONDUCTIVITY OF AL–U3SI2 FUEL PLATES FOR RESEARCH REACTORS

A.K. SENGUPTA*, R. KESWANI*, G.J. PRASAD*,
C. GANGULY**, D.S.C. PURUSHOTHAM*

* Radiometallurgy Division,
Bhabha Atomic Research Centre,
Trombay, Mumbai

** Central Glass and Ceramic Research Institute,
Calcutta

India

Abstract

Thermal conductivity of Al-36 vol% U_3Si_2 fuel meat in Al/Al-36 vol% U_3Si_2/Al plate fuel was calculated from ambient to 450°C from the estimation of thermal diffusivity by laser flash method, specific heat from literature and density. Thermal conductivity varied from 0.35 W/cm.K to 0.47 W/cm.K in this temperature range.

Introduction

Aluminium clad Al-36 Vol% U_3Si_2 dispersion type fuel is a candidate fuel for water cooled research reactor and is being developed at BARC, India for the proposed 5-10 Mwt reactor. The fuel is being designed to operate without any fission gas release. Thermal conductivity being one of the most important property for prediction of fuel performance, has been derived from ambient to 450°C from the experimentally measured thermal diffusivity by the laser flash method, literature value of specific heat and density. The fuel meat of Al+U_3Si_2 is being fabricated by hot rolling between two Aluminium plates which is likely to introduce structural changes in the fuel meat. This may cause changes in the ultimate thermal properties of the fuel.

Material

U_3Si_2 dispersoids have been prepared by vacuum induction melting taking stoichiometric amounts of uranium and silicon. The Al-36 Vol% U_3Si_2 dispersed fuel meat was prepared by powder metallurgicl route in the form of billet. The fuel meat (billet) was subsequently cladded with Al-Mg alloy by picture frame technique. The details of the fabrication flowsheet developed at BARC, India is given elsewhere[1]. The plate assembly so obtained has satisfactory bonding between the meat and the clad and had a bulk density of about 88% TD. Fig. 1 shows the photomicrograph of the final product.

For measurement of thermal diffusivity of the fuel meat, the sample in the shape of circular disk of diameter 10mm and thickness 1.7mm consisting of 3 layers i.e. Al/Al-36 vol% U_3Si_2/Al was made by machining the fuel plate. Subsequently one of the Aluminium cladding layer of the circular disk was ground off to make the actual sample which has the final dimensions of 10mm in diameter and thickness 1.2mm. Another sample of Aluminium alloy of diameter 10mm and thickness 1.7mm was also prepared by machining from an Aluminium plate.

Measurement

Thermal conductivity of the rolled fuel was estimated from the time-temperature response data of a two layered composite consisting of Al and Al-36 vol% U_3Si_2 using the approach of Hubert[2].
Measurement of the thermal diffusivity was carried out by laser flash method in two steps :

i) Obtaining the time temperature response of the two layer composite by the laser flash method at different temperature interval.

ii) Ascertaining the most suitable values of thermal diffusivity and conductivity of the fuel meat at each temperature by iterating solving the Hubert's model for different values of the thermal diffusivity and conductivity of Al-36 vol% U_3Si_2 layer.
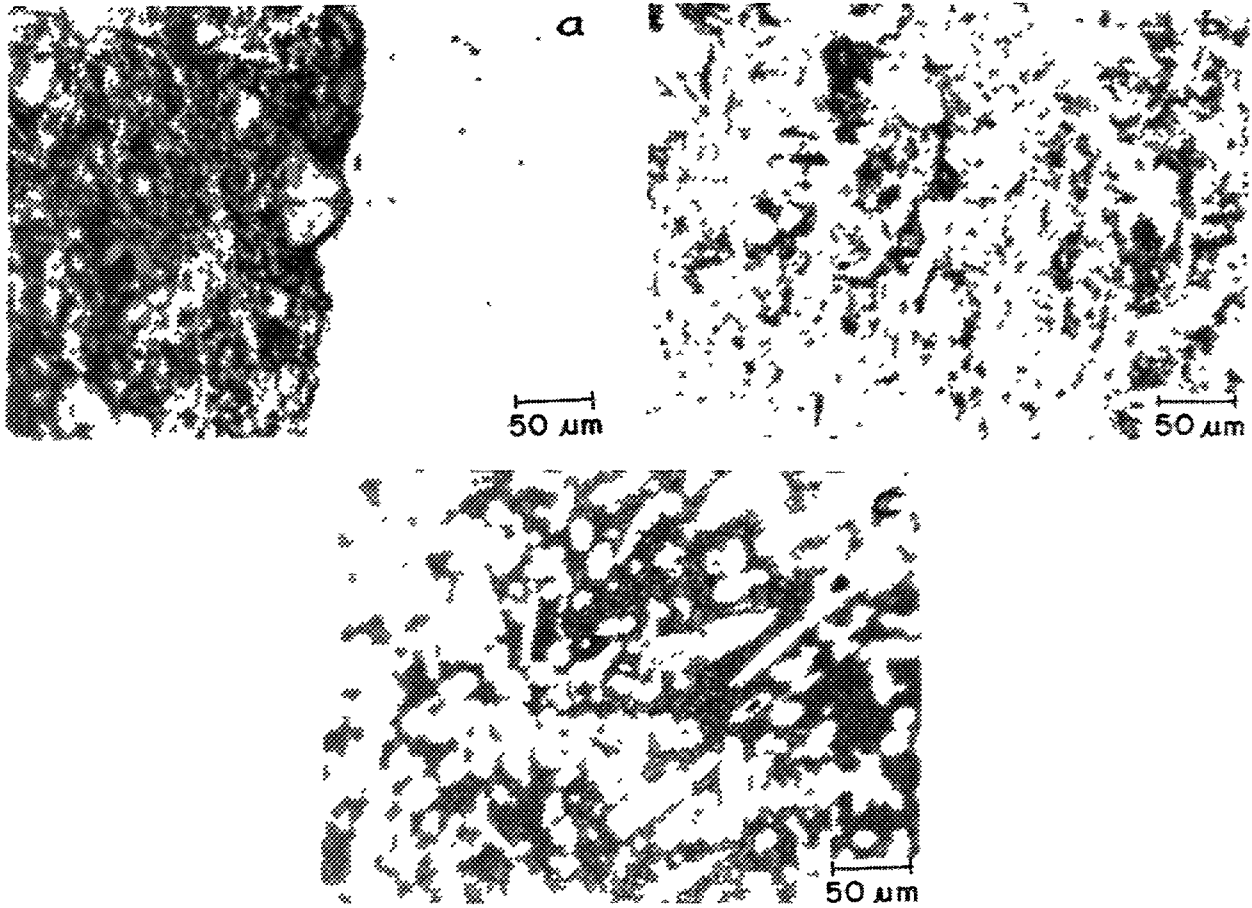
Fig. 1. Photomicrograph of Al-36 vol% U3Si2 fuels:
   a)   Fuel meat with cladding
   b)   Fuel meat
   c)   Fuel meat at a section perpendicular to b)

Thermal diffusivity and conductivity can be expressed by the following relations :

$$a(cm^2/s) = 0.1309 + 1.5197 \times 10^{-5} \times T - 6.9558 \times 10^{-8} \times T^2 - 1.4461 \times 10^{-10}T^3$$

$$k(W/mk) = 0.3259 + 4.3025 \times 10^{-4}T + 6.2735 \times 10^{-7}T^2 - 1.8642 \times 10^{-9}T^3$$

The specific heat data used for thermal conductivity calculation are given below :

$$C_p(J/gm\,°C) = 0.892 + 0.00046 \times T - Wu(0.749 + 0.00038 \times T)$$

where Wu is w% uranium.

The thermal conductivity of the Al-36 vol% U_3Si_2 composite was also calculated from the specific heat and thermal conductivity data of Al-U_3Si_2 using Bragmen method by assuming the disperoids as spherical in shape and are randomly distributed. Thermal conductivity so calculated was

found to be 0.66w/cm.K which is higher than that obtained in this study. The lower thermal conductivity of Al-36 vol% U_3Si_2 obtained in this study may be attributed to the presence of porosity and structural changes entailing hot rolling. The thermal conductivity estimated by the present method more precisely describes the actual thermal characteristics of the fuel meat and should be more reliable for predicting inpile formation. It is seen that the design of the plate fuel is such that all the fission gases are retained in the fuel meat. The 10-12% porosity existing in the fuel meat contained the fission gases. However the thermal conductivity vs. temperature plot [Fig. 2] shows there is a slight positive deviation with temperature which saturates at around 350°C which has also been reported by Saito et al[4]. In the absence of post irradiation data it is presumed that this increase in conductivity will not cause any appreciable rise in temperature as it will be transmitted through highly conducting Aluminium in the matrix alloy and aluminium cladding material.
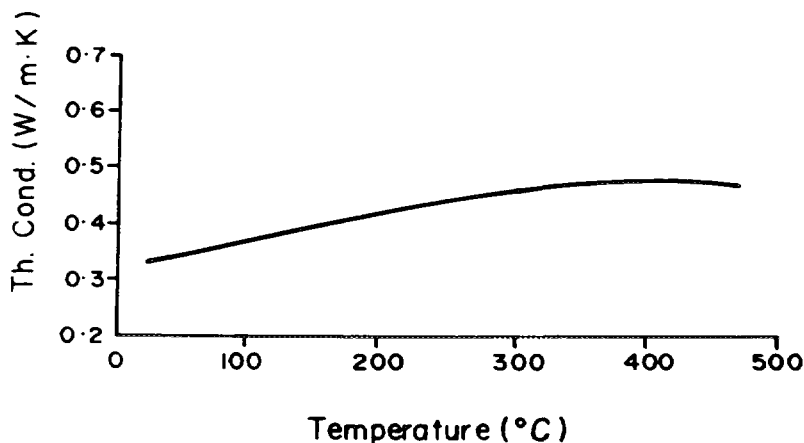
Fig. 2. Thermal conductivity of Al-36 vol% U3Si2 as a function of temperature in the rolled condition.

References

1. P.V. Hegde, G.J. Prasad and C. Ganguly : Trans. PMAI, Vol. 20, p 27 - 31 (1993)

2. Hubert M. James : High temperature high pressures Vol. 17, p 481 - 490 (1985)

3. Braggemen D.A.G. Almn. Phys. 24, 636 - 679(1935)

4. Saito, Junichi; Komori, Yoshihiro; Sakuri, Furnio; Audo, Hiroei: JAERI - M - 91 - 065

FUELS FOR FAST REACTORS
(Session 3)

Chairmen

Yu.K. BIBILASHVILI
Russian Federation

M. COQUERELLE
European Commission

SURVEY OF POST-IRRADIATION EXAMINATIONS MADE OF MIXED CARBIDE FUELS

M. COQUERELLE
Institute for Transuranium Elements,
European Commission,
Karlsruhe

Abstract

Post-irradiation examinations on mixed carbide, nitride and carbonitride fuels irradiated in fast flux reactors Rapsodie and DFR were carried out during the seventies and early eighties.

In this report, emphasis was put on the fission gas release, cladding carburization and head-end gaseous oxidation process of these fuels, in particular, of mixed carbides.

1. Introduction

During the seventies and early eighties, the European Institute for Transuranium Elements has been involved in the development of potential fuels for LMFBR. These studies covered a large spectrum going from the fabrication to the determination of the thermodynamic and thermophysical properties, irradiation in fast flux reactors and, finally, post-irradiation examinations associated with modelling works.

Advanced liquid-metal fast breeder reactor (LMFBR) fuels of the type $(U, Pu)C_{1-x}N_x$ (carbide, carbonitride, and nitride) have been studied in the DN1 and DN2 irradiation experiments carried out in Rapsodie and Dounreay. This paper presents information on fission gas release and a correlation with the different structural regions of these highly rated MX-type fuels. Complementary information concerning the cladding carburization and the head-end gaseous oxidation as possible reprocessing procedure are shortly discussed.

2. Fission gas release

The DN1 and DN2 experiments investigated and compared the behavior of advanced fuels in a fast flux under conditions of high linear power ($X_{max} = 1.3 \times 10^2$ kW $\cdot$ m^{-1} with a pellet diameter of 8.3 mm). The DN1 experiment was performed in DFR and investigated helium-bonded (U, Pu)N, (U, Pu)C and $(U, Pu)C_{1-x}N_x$ fuels (x = 0.2, 0.5 and 0.8); the maximum burn-ups achieved ranged from 1.3 to 7.8 at. %.

The DN2 experiment was carried out in Rapsodie and investigated helium-bonded $(U, Pu)C_{1-x}N_x$ fuel (x = 0.2 and 0.5); the maximum burn-ups attained ranged from 1 to 4 at. %. Fuel pin specifications are summarized in Table I.

2.1 Experimental

Analysis of Released Gas

The released gas contained in the plenums of all sound pins from the DN1 and DN2 experiments was analyzed. The amount of gas in the plenum was measured volumetrically, and mass spectrometry was used to determine the isotopic composition of the gas. The equipment used for puncturing the cladding and collecting the gas has been described elsewhere [1].

Analysis of Retained Gas

Gas chromatography was used to determine the integral amount of gas present and the concentrations of xenon and krypton. The local concentration of bonded xenon (that dissolved in the fuel

lattice and present in gas bubbles) and its variation with radial position was determined by electronprobe microanalysis (EPMA) The analysis of krypton is not possible because interference exists between the krypton $L\alpha_1$ X-ray line and the uranium 2 $M\alpha_1$ line from the fuel matrix Furthermore, the krypton $L\alpha_1$ line is difficult to detect above the active background of the specimen

The analysis of retained gas by chromatography was restricted to six pin sections (five sections of carbonitride and one of nitride fuel, see Table II) Likewise, the analysis of bonded xenon by EPMA was carried out on three sections of sodium-bonded carbonitride fuel (two sections from pin CNP and one from ENP), one section of helium-bonded nitride fuel (from pin AP3), and one section of helium-bonded carbide fuel (from pin DP1)

Gas Chromatography

The fission gas retained in pellet size samples of known weight was liberated in a two-stage operation First, the fuel was ground to a powder with a grain size < 1 μm, and then the powdered fuel was dissolved in concentrated nitric acid At each stage, the gases escaping were collected on a cold trap and analyzed for Xenon and krypton The first stage (grinding) gave information about the amount and composition of the fission gas contained in pores < 1μm in size, the second stage (dissolution) gave similar details for the bonded gas

TABLE I

Fuel Pin Specifications

Experiment		DN1			DN2	
Fuel	U/(U + Pu) (wt%)	20			20	
	^{235}U/U (wt%)	93			88	
	Form	Pelletized	Vibrocompacted	Coviprated	Pelletized	Coviprated
	Fuel density (%TD)	85-89	---	---	86-89	---
	Smear density (%TD)	81-85	79-80	78	82-85	80-83
	Pellet diameter (mm)	8 3	---	---	8 3 8 0	---
	Fuel stack length (mm)		475		320	
Fuel to-cladding	Bonding	He			Na	He
	gap (μm)	200			500	200
Cladding	Material	DIN 1 4919 stainless steel				
	o d (mm)	9.5				
	i d (mm)	8 5				
Fuel pin	Overall length (mm)	790			726	
	Void volume in plenum (cm³)			10		

TABLE II

Concentrations of Xenon and Krypton in Retained Gas

1	2	3		4		5	6	7
		Gas in Pores		Bonded Gas				
		Kr	Xe	Kr	Xe			Xe/Kr
Pin Section	Fuel Type					Xe/Kr Bonded Gas	Xe/Kr Gas in Pores	Gas in the Plenum
		(mm³/g fuel)						
CP2 7 2	MC$_{0 5}$N$_{0 5}$	16 68	104 9	54 23	391 2	7 21	6 28	6 42
ANP/3 2	MN	20 98	126 7	55 56	395 1	7 11	6 03	
ENP'4 2	MC$_{0 8}$N$_{0 2}$	13 20	77 9	86 32	616 4	7 14	5 90	5 587
CNP'1 7	MC$_{0 5}$N$_{0 5}$	15 68	94 55	58 31	439 0	7 52	6 02	6 082
CNP'3	MC$_{0 5}$N$_{0 5}$	13 76	81 41	28 54 (?)	317	11 11	5 91	6 082
CNP'6	MC$_{0 5}$N$_{0 5}$	7 29	44 59	82 73	590 7	7 14	6 10	6 082

94

EPMA

The electronprobe microanalyzer at the Institute for Transuranium Elements is a shielded Cameca MS46 Xenon analysis was carried out at electron acceleration potentials > 15 kV and at beam currents of 300 and 500 nA Since a suitable standard material for xenon analysis by EPMA does not exist, the $L\alpha_1$ X-ray intensity from pure xenon was obtained by interpolation of the $L\alpha_1$ intensities from a series of elements on each side of xenon in the periodic table To compensate for small day-to-day changes in the operating conditions of the machine, the intensities measured were related to the intensity from pure antimony

The analysis results were corrected using the ZAF program of Tong The $L\alpha_1$ absorption coefficients for xenon absorption in uranium and plutonium were interpolated from the values for iodine and cesium $L\alpha_1$ absorption A detailed description of the analytical method is given elsewhere

2 2   Xenon Release from Helium-Bonded Pins

At low burn-up (< 1 5 at %), xenon release is dependent on the chemical composition of the fuel (Fig 4) Release is greatest from (U, Pu)C (~ 75 %) and least from(U, Pu)N (35 %) The fraction of xenon released from (U, Pu)C$_{1-x}$N$_x$ fuel is between that from (U, Pu)N and (U, Pu)C fuels (Fig 4) For these fuels, xenon release increased sharply with carbon content up to x = 0 5 Further increase in carbon content did not significantly change the fraction of xenon released (Fig 1)

For carbide and carbonitride fuels with x < 0 8, the fraction of xenon released is larger at low burn-up than at medium burn-up For carbon-rich fuels, x < 0 5, the difference in the fractions of xenon released at low and medium burn-up was ~ 30 % absolute The lower xenon release at medium burn-up is most probably due to a drop in fuel centerline temperature (~ 400 K) following fuel-cladding contact

Concentrations of Xenon and Krypton in Retained Gas

The results of gas chromatography are given in Table II It is evident from the ratios of the xenon and krypton concentrations (cf, columns 5 and 6) that gas in pores contains proportionally more krypton than bonded gas For the purpose of comparison, column 7 lists the xenon/krypton concentration ratios for the gas contained in the plenums of the pins As expected, the ratios are very similar to those given in column 6, corroborating the fact that the gas travels to the plenum by way of interconnected pores Furthermore, a comparison of the gas concentrations listed in columns 3 and 4 of Table II reveals that for carbonitride fuel, < 20 % of the retained gas is held in pores, the bulk of the gas is contained in bubbles or dissolved in the fuel lattice

2 3   Fuel Restructuring

In the DN1 and DN2 irradiations, the radial temperature difference between the center and the surface of the fuel was in the range from 700 to 1000 K Furthermore, consideration of the cladding temperature and the fuel-cladding heat transfer coefficient, h, indicates that the fuel surface temperature lay between 1000 and 1300 K This gives a range for the in-pile fuel temperature of 1000 to 2300 K

Figures 2 and 3 show examples of the structural zones in the carbide pin DP1 and the nitride pin AP1 after 6 5 and 5 at % burn-ups, respectively The kinetics of fuel restructuring are faster in carbon-rich fuels because the coefficients of self-diffusion for uranium, plutonium and carbon are larger than in nitrogen-rich fuels

Ceramographic analysis of the 21 pins irradiated revealed the presence of four distinct structural zones, each of which is associated with well-defined restructuring processes These zones, which have been designated I through IV, are characterized by the following structural features

Zone IV Stable grain size and relatively stable fabrication porosity Densification, if present is associated with a decrease in the number of pores with a size smaller than 2 µm The upper temperature limit for this zone, T_{IV}, is a function of burn-up and of the chemical

composition of the fuel. In the case of (U, Pu)C fuels, T_{IV} is ~ 1000 K for a fuel irradiated to a burn-up of 6 at. % and ~ 1300 K for a fuel irradiated to a burn-up of 1 at. %. In MN fuels, TIV is ~ 250 K higher than in MC fuels irradiated under similar conditions.

Table 3. Details of the oxidations and final reaction products

Fuel composition	average burn-up (a/o)	Oxidation conditions				O/M from X-ray diffraction	Structure of final products
		Atmosphere	average temp. ($^\circ$C)	Total time (h)	Complete oxidation		
(U,Pu)N	1.41	CO/CO$_2$	800	8	$\checkmark$		.
"	1.41	"	816	13	$\checkmark$		
"	4.46	"	750	8	Na in Pin		
"	1.20	"	800	19	**	2,01±0,01	(single
(U,Pu)C$_{0.8}$N$_{0.2}$	1.04	"	800	11	$\checkmark$	2,01±0,01	(phase (fluorite
"	2,83	"	800	12	**	2,01±0,01	(structure
(U,Pu)C$_{0.9}$N$_{0.1}$	1,02	"	750	8	$\checkmark$		
"	1.81	"	880	18	$\checkmark$		
(U,Pu)C	1.41	"	750	8	$\checkmark$	2,00±0,01	
(U,Pu)N	4,46	Ar-20%O$_2$	590	13	Na in Pin		single phase fluorite
"	3,45	"	"	23	$\checkmark$		
(U,Pu)C$_{0.8}$N$_{0.2}$	1.04	"	"	16	$\checkmark$		
"	2.83	"	"	16	**		)two phase)MO$_{2+x}$(50%))and M$_3$O$_8$
(U,Pu)C$_{0.9}$N$_{0.1}$	1,02	"	"	20	$\checkmark$		) 50%)
"	1,81	"	"	12	$\checkmark$		

* Samples were weighed at intervals during the oxidation. Oxidation was. considered to be complete when there was no further change in weight of the sample. Particles were removed from the reaction vessel during weighing intervals for examination by optical microscopy.
** Small quantity of material lost from reaction vessel.

O EHVC3
ΔAV2   Δ EHVC2
+AV4   X BP3   + CP2   + EHP2
●AP3   ● BP2   ● CP1   ●EHP1 ●FHP1 ●DP2
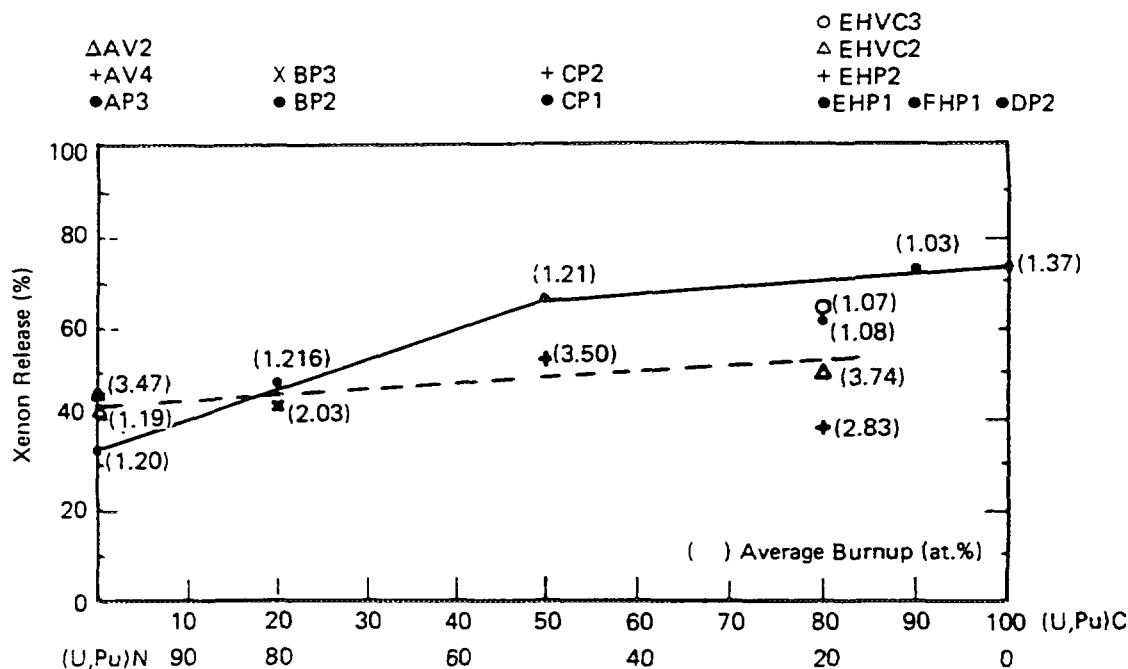
Fig. 1.   Xenon release related to fuel composition and burnup.

96

Zone I at Relative Radius $\frac{r}{r_0}$ = 0.26

Zone III at Relative Radius $\frac{r}{r_0}$ = 0.71

Zone II at Relative Radius $\frac{r}{r_0}$ = 0.56

Zone IV at Pellet Surface
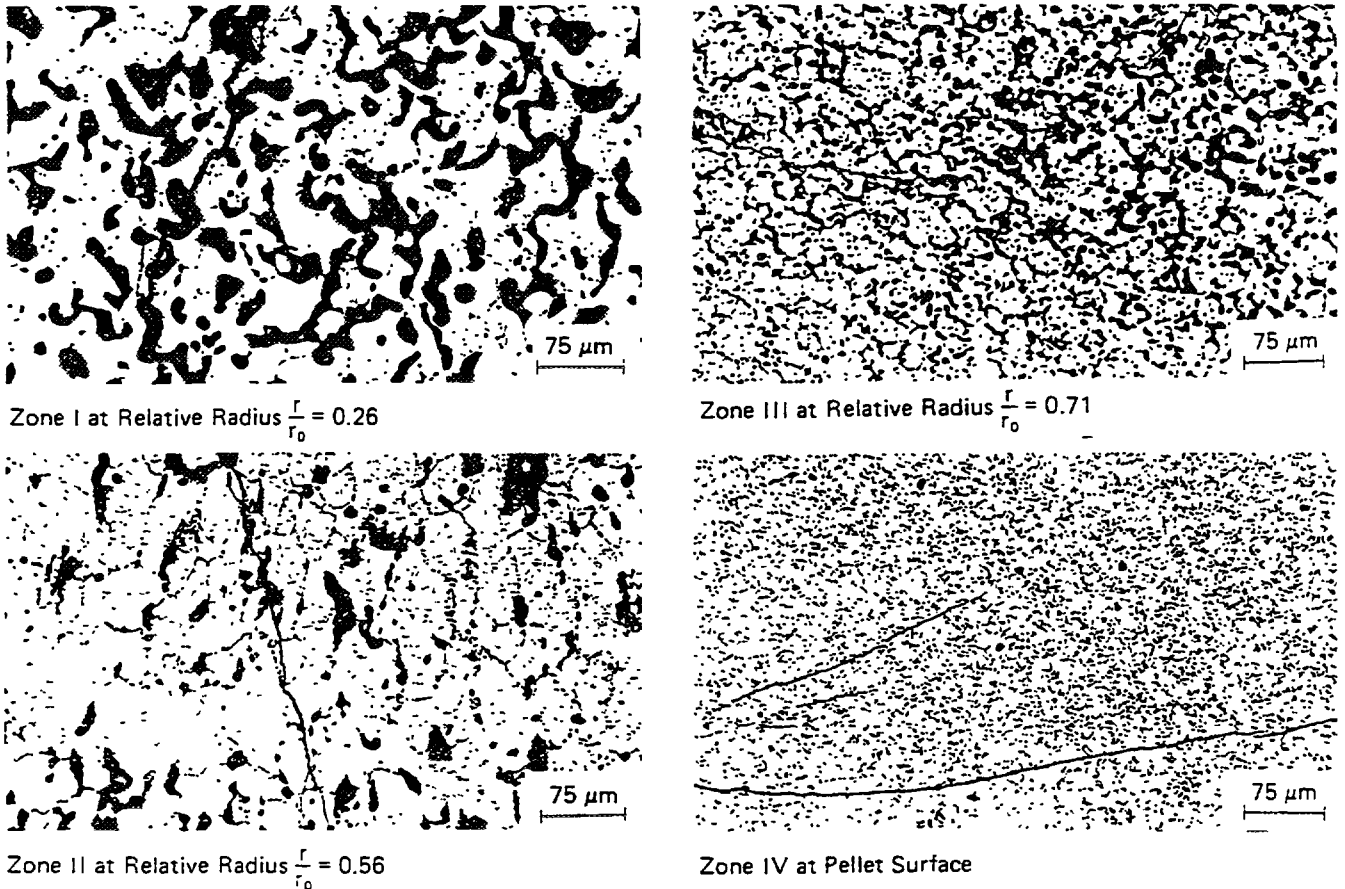
Fig 2   Restructuring as a function of radial position in a mixed carbide fuel. Local linear power 90 kW·m⁻¹. Local burnup 6 5 at.%.

Zone III. Restructuring occurs mainly by coaxial grain growth. This is associated with an increase in porosity, which takes place in the following stages, given in the order of increasing radial temperature·

1.   increase in the population of pores with diameters < 1 μm and > 5 μm

2.   pore precipitation at grain boundaries as a consequence of enhanced gas mobility

3.   coalescence of pores at grain boundaries perpendicular to the thermal gradient leading to broadening of such boundaries and to break-away swelling.

Zone II. Preferential grain growth occurs parallel to the radial temperature gradient, and radial alignment of fission gas porosity takes place at grain boundaries This zone resembles the columnar grain structure generally found in mixed-oxide fuels, and is particularly well developed in carbon-rich fuels where evidence for pore migration has been observed (see Fig. 4).

Zone I Region of coarse fission gas porosity and high gas release. Large asymmetric (globular) pores form that are similar in size to the fuel grains (≤ 20 μm) As in zone II, grains may possess a fine 'porosity' (< 1 μm in diameter) due to fission gas precipitation in a heterogeneous distribution

The zones are described in the order in which they appear in the fuel with increasing distance from the surface (i e , in the order of increasing radial temperature)

Finally, it is pointed out that a small central hole formed in the nitride fuels and in nitrogen-rich carbonitride fuels with x > 0 8. In contrast to oxide fuels, where the central hole results from the migration of lenticular pores up the radial temperature gradient, the central hole in nitride fuels is apparently created by a sintering mechanism

97
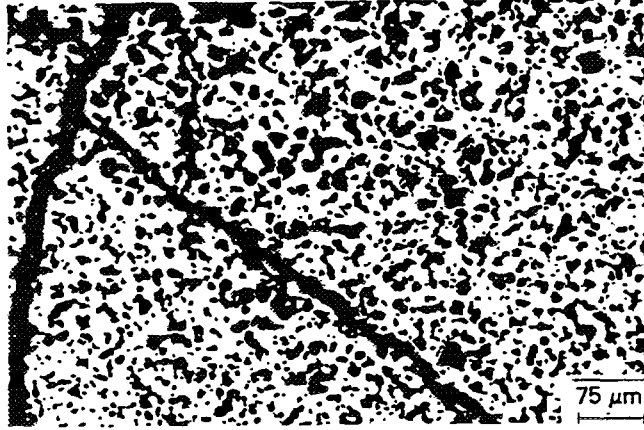
Zone I at Relative Radius $\frac{r}{r_0} = 0.10$
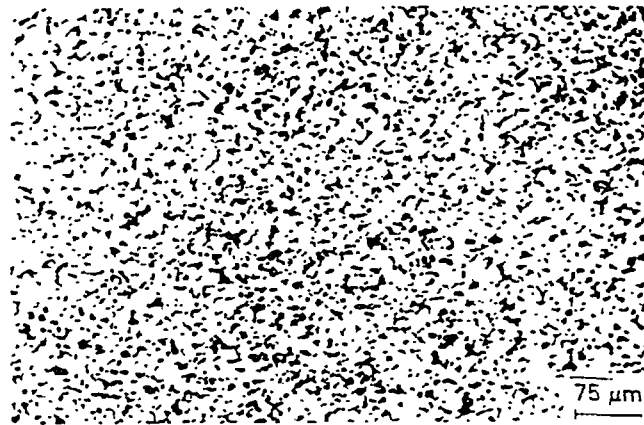
Zone III at Relative Radius $\frac{r}{r_0} = 0.54$

Zone IV at Pellet Surface

Fig. 3. Restructuring as a function of radial position in a mixed nitride fuel. Local linear power 120 $kW \cdot m^{-1}$ Local burnup 5.0 at.%.

98
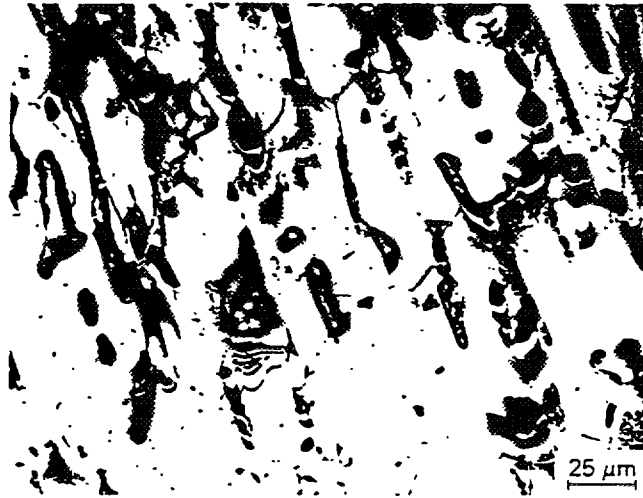
Fig. 4. Pore migration in a mixed carbide fuel. Local linear power 130 kW·m⁻¹. Local burnup 1.5 at.%.

2.4 Radial Distribution of Retained Xenon: Correlation with Fuel Structure

(U, Pu)C₁ ₊ ₓ (Helium-Bonded)

The general form of the distribution profile shown in Fig. 5 is similar to that of xenon profiles obtained from sodium-bonded carbonitride fuels (Fig. 6). The fuel exhibited the four structural zones first defined by Ronchi and Sari (Ref. 2); their radial positions are also marked in Fig. 5. The dense outer fuel (zone IV) consisted of regions with high and low concentrations of xenon. Accordingly, on the left side of the profile, the concentration of xenon approaches the nominal fast fission yield of 0.62 wt % (value after a cooling period of 3 yr.); on the right side, over a distance of 650 μm , the xenon concentration falls sharply from 0.57 to 0.26 % at the fuel surface. In the central porous fuel region (zones I and II), the concentration of xenon was ~ 20 % of the amount created by fission. As in the case of the nitride and carbonitride fuels, the transition from xenon concentrations close to the fission yield to the low concentrations found in the central porous fuel occurred in zone III. The integrated xenon release for the pin section was 50 %, which is slightly lower than the gas release value extrapolation from Fig. 1.

The reason for regions of low xenon concentration at the fuel surface is not well understood. Such regions, however, had a lower density than fuel regions with xenon concentrations approaching the nominal fission yield. This suggests that the observed decrease in retained xenon concentration could, in part, be due to a fall in the amount of xenon created.

The decrease in fuel density was associated with the formation of two actinide containing phases. One phase was confined to a region within 100 μm of the fuel surface and was apparently an oxide; the other phase was probably sesquicarbide.

It is worth noting that the forms of the cesium and xenon profiles measured along the same diameter were almost identical. This indicates that the cesium, which results mainly from the decay of ^{133}Xe and [135]Xe, is trapped in small gas bubbles and pores. More significantly, the finding suggests that in advanced fuel the behavior of cesium closely resembles that of xenon.

(U, Pu)(C₀.₅N₀.₅) (Sodium-Bonded)

The radial distribution profile contained in Fig. 6 exhibits two distinct concentration regions:

1. a region in the porous fuel zone between r/r₀ = 0.6 and the fuel center, in which the xenon concentration is ~ 40 % of the created amount

2   a region in which the amount of bonded xenon is close to the calculated fast fission yield of 0 42 wt % (value after a cooling time of 3 yr)
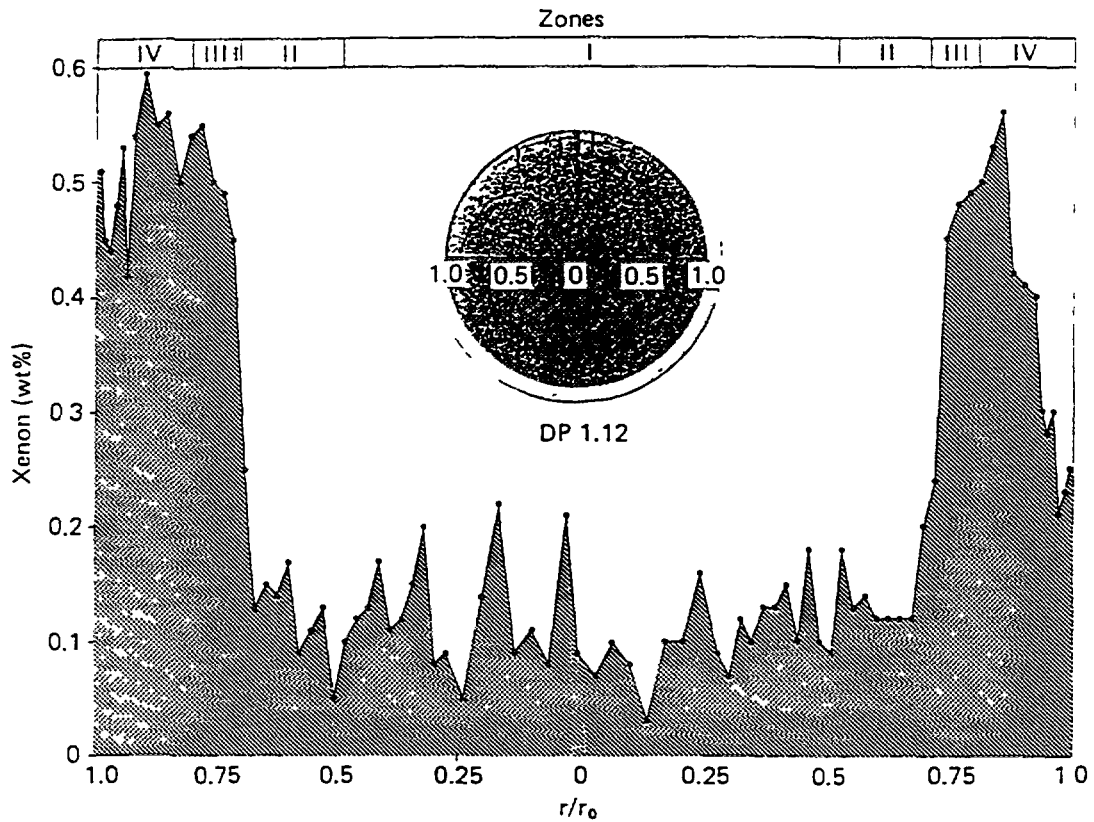
Fig 5   Radial distribution of xenon in a helium-bonded fuel of composition $(U_{0.8}Pu_{0.2})C_{1+x}$ Local linear power 105 kW m^{-1} Local burnup 5 8 at %
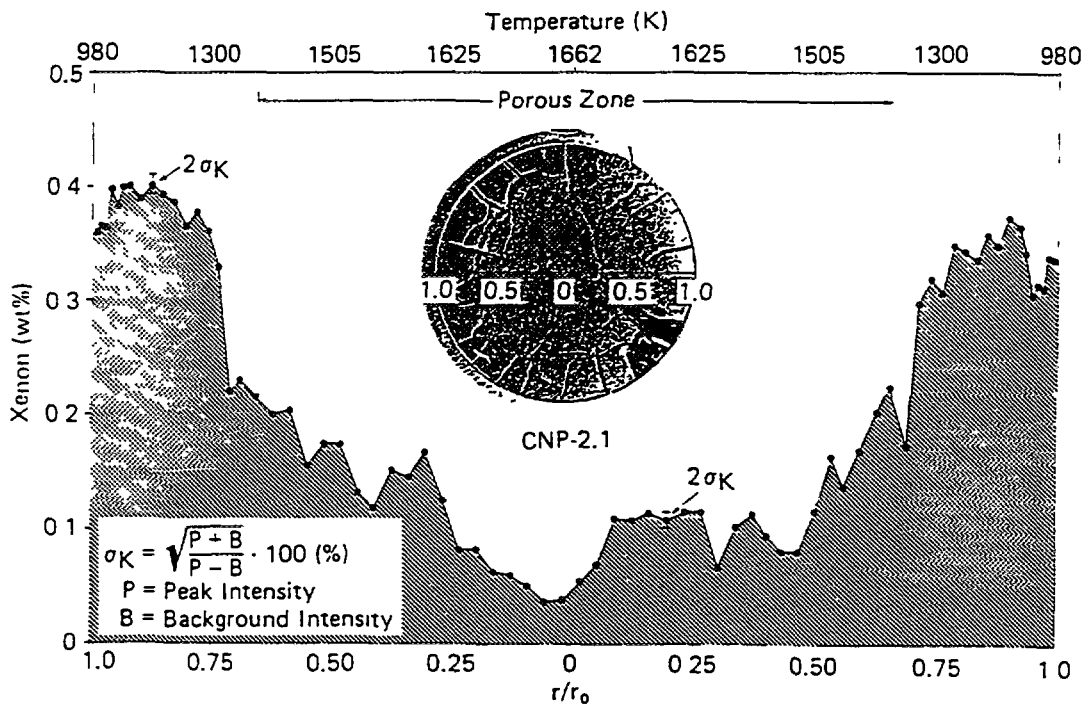
Fig 6   Radial distribution of xenon in a sodium-bonded fuel of composition $(U_{0.8}Pu_{0.2})(C_{0.5}N_{0.5})$ Local linear power 125 kW m^{-1} Local burnup 3 8 at.%

100

This region extends almost from the fuel surface to r/r₀ = 0 75 in the outer dense fuel zone, within 50 μm of the fuel surface, a small decrease in xenon concentration occurs

The region 0 6 < r/r₀ < 0 75 is a transitional zone in which the xenon content of the fuel falls sharply from concentrations approaching the fission yield to the low concentrations found in the central porous regions The range of this zone is not well defined, although the main concentration step occurs in structural zone III The integrated xenon release for the pin section was 36 %

(U, Pu)N (Helium-Bonded)

The radial distribution profile shown in Fig 7 indicates that release behavior in a nitride fuel is similar to that outlined for carbide and carbonitride fuels In contrast to the last two fuels, however, the nitride fuel contained a small central hole and exhibited only two of the four structural zones, namely, zone III (intergranular porosity) and zone IV (unrestructured fuel) The bulk of the fuel consisted of structural zone III This extended from the central hole to r/r₀ = 0 85 In this region xenon release was on the order of 45 %, whereas in the remaining structural zone IV, which occupied the outer part of the fuel, only ~ 15 % of xenon created was released The integrated xenon release for the pin section was 30 to 35 % This is in good agreement with the gas release value obtained by chromatography (see Fig 1)

Some Comments on the Mechanisms of Gas Release

Most irradiation experiments undertaken to investigate mixed carbide and nitride fuels have been carried out at a power below 90 kW · m⁻¹, which produced a fuel centerline temperature lower than 1400 K The pins dealt with in this paper were mainly helium-bonded and were irradiated at high linear power (135 kW · m⁻¹ maximum) This led to high central temperatures of 2300 K at the start of irradiation and 1900 K after gap closure Thus, the DN irradiations can be considered to have consisted of two stages that were characterized by pin operation under distinct different temperature conditions. In the first stage of irradiation, when the gap was open (h = 0 5 to 1 0 ×10⁻⁴ W · m⁻² · K⁻¹), fuel restructuring occurred and the formation of interconnected porosity took place at fuel temperatures above 1100 K From the standpoint of fission gas release studies, the latter constitutes the structural feature of principal interest

The second stage of the irradiation, which we consider to be the steady-state temperature condition, was associated with the closure of the gap and an increase in value of the thermal transfer coefficient, h, to 2 × 10⁻⁴ W · m⁻² · K⁻¹ The subsequent drop in fuel temperature of ~ 400 K modified the rate of all thermally activated mechanisms It is to be noted, however, that the structural features developed in the first stage of the irradiation were retained in this second stage
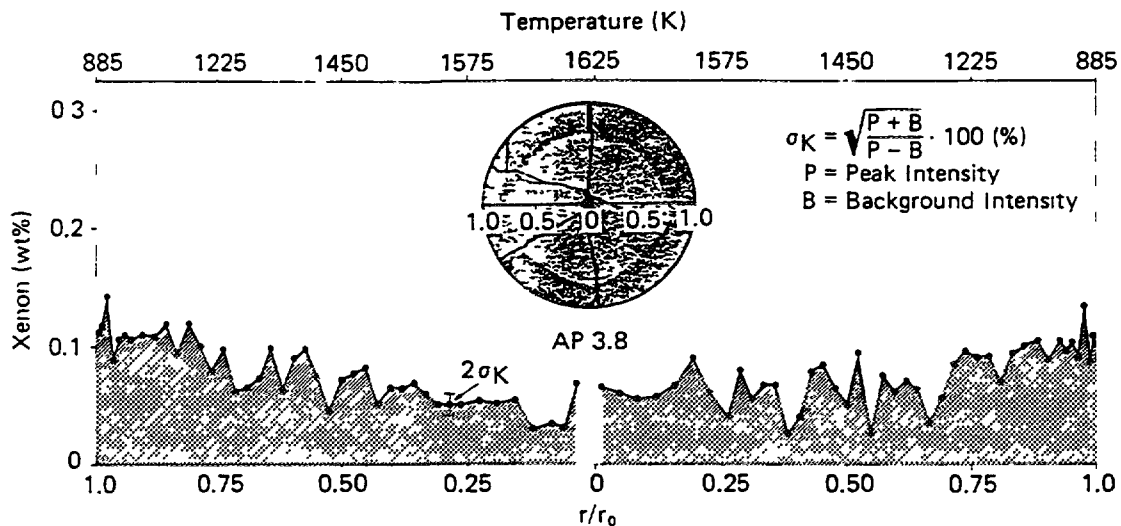
Fig 7   Radial distribution of xenon in a helium-bonded fuel of composition $(U_{0.8}Pu_{0.2})N$ Local linear power 115 kW m⁻¹ Local burnup 1 1 at %

The mechanisms that can be postulated for fission gas release are of two different kinds

1   mechanisms such as atomic diffusion and pore migration (by diffusion or evaporation-condensation) that are thermally activated

2   mechanisms such as transport by recoil and knock-on that are related to the fission process, these can play a role in the central region of the fuel where the free surface offered by the interconnected porosity becomes important

From the post-irradiation examination of the DN pins, evidence has been obtained for gas transport by atomic diffusion Gas chromatography of bonded xenon has revealed that the gas in pores contains proportionally more krypton than bonded gas (Table II) This finding can be explained if it is recognized that in fuel the diffusion rate of krypton is faster than that of the larger atom, xenon It is unlikely that bubble migration, if it occurs, can produce such a shift in the composition of the retained gas

Fission gas bubbles in carbide and nitride fuels grow rapidly to size at which their mobility becomes extremely low Both theory and experimental observation indicate that in technologically significant periods of time the motion of bubbles > 100 Å in size is confined to negligible root-mean-square distances In fact, during irradiation the walls of large bubbles become contaminated by precipitated or segregated fission products, and, consequently, the truly effective mechanism of bubble migration is volume diffusion, which produces slow migration rates [e g , between 10^{-12} and 10^{-13} ms^{-1} at 2300 K in (U, Pu)C with $\Delta T = 1300$ K $\cdot$ cm^1 (Ref 3)]

A second mechanism, bubble sweeping, is provided by the direct motion pores that, by evaporation-condensation, migrate at higher rates than small bubbles The sweeping of bubbles has the effect of transferring gas and void volume to grain boundaries or to interconnected porosity Post-irradiation work indicates that this mechanism occurs in carbide fuel and carbonitride fuels with low nitrogen contents (x < 0 2) It operates in a limited temperature range corresponding to structural zone II (Ref 7), where bubbles grow rapidly to a large size, but does not play a determining role in the total gas release because sweeping does not occur at a sufficiently high rate Thus, it can be concluded that bubble migration makes only a small contribution to fission gas release

A more detailed discussion on the mechanism aspects can be found in Ref 4

2 5   Conclusions

The investigation of fission gas release from carbide, carbonitride, and nitride fuels irradiated in a fast flux under conditions of high linear power has enabled the following conclusions to be drawn

1   At low burn-up, xenon release from helium-bonded advanced fuel is dependent on the chemical composition of the fuel

2   At medium burn-up, closer fuel-cladding contact in helium-bonded pins leads to a decrease in the fraction of gas released from (U, Pu)C$_{1-x}$N$_x$ fuel with x < 0 8

3   In advanced fuels, more than 75 % of the retained fission gas is contained in gas bubbles and in the fuel lattice The remaining gas that is trapped in pores contains proportionally more krypton than the bonded gas Gas is mainly released to the plenum by way of interconnected pores

4   The most important parameter determining fission gas release is fuel structure The fraction of xenon released from the outer unrestructured region of the fuel is generally lower than 15 %, the mechanism controlling the release appears to be atomic diffusion The fraction of xenon released from the central porous region is 50 % and more, and is highly dependent on the composition of the fuel and on burn-up In this region, the role of interconnected porosity is determining Besides diffusion, such supplementary mechanisms as bubble sweeping by grain

boundary or pore migration as well as recoil and knock-on due to fission promote the transfer of xenon and krypton to the interconnected porosity.

References

1. M. Coquerelle, 'The Alpha-Beta-Gamma Laboratory of the European Institute for Transuranium Elements: Equipment Used for the Post-Irradiation Examination of Plutonium Fuels', *Proc. 15th Conf. Remote Systems Technol.*, 246 (1967)

2. C. Ronchi and C. Sari, 'Swelling Analysis of Highly Rated MX-Type LMFBR Fuels. 1. Restructuring and Porosity Behaviour', J. Nucl. Mater., **58**, 140 (1975)

3. C. Ronchi, I. L. F. Ray, H. Thiele, and J. van de Laar, 'Swelling Analysis of Highly-Rated MX-Type LMFBR Fuels', J. Nucl. Mater., **74**, 193 (1978)

4. M. Coquerelle and C. T. Walker, 'Fission Gas Release and Microscopic Swelling in highly rated Advanced Fuels', **48**

3.   Cladding carburization

3.1   Experimental analyses of irradiated stainless steel cladding of sodium-bonded pins

The cladding material used in the irradiation experiments examined were two solution annealed Type 316 (17 Cr, 14 Ni) type steels. Stabilized steels (DIN 1.4790, DIN 1.4988) were also tested or analyzed occasionally. The irradiations were carried out in the Rapsodie and Dounreay fast reactors.

Chemical analyses of the total carbon content, electron microprobe analysis, and microhardness measurements were carried out on the cladding steel of pins irradiated at burn-ups ranging from 2.6 to 12.5 % fima and linear powers between 80 and 100 kW/m.

The following results were obtained:

1.   In the range up to 120.000 Mwd/ton, the total carbon content of the cladding increases linearly from 300 to 5000 ppm. The carburization stops at high burn-up, when all the excess carbon (4 % M_2C_3 was typically present in the starting fuel) is transferred to the cladding.

2.   After an irradiation time of ~ 200 days, the carbon concentration at the cladding surface attains a value of 1.5 % and thereafter does not change appreciably (Fig.8).
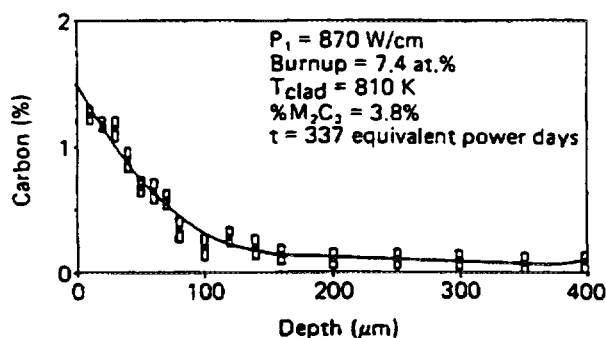
Fig. 8 Typical carbon penetration profile in a stainless steel cladding (from microprobe measurements) of a sodium-bonded pin at high burnup. At first glance this type of profile might be analyzed in terms of a simple linear diffusion process.

3. The shape of the carbon concentration profile as a function of the penetration depth is similar to that obtained in diffusion measurements with constant surface concentration (Fig. 8). This suggests that the carbon is supplied by the fuel at a sufficiently high rate.

4. Microhardness changes produced by carburization were found at various cladding temperatures. Figure 9 shows the average of 12 measurements taken along a circumference at 30 μm from the inner cladding surface, plotted as a function of the cladding inner temperature. The curves display a maximum in the range between 720 to 750 K. In the case of pins irradiated in Rapsodie, where the inner cladding temperature was always > 770 K, the maximum could not be observed.

3.2 Carbon Reactions in Stainless Steel

The major driving force for the reaction between carbon and stainless steel is provided by the very low free energy of formation of various carbides among which those of the type $(FeCr)_{23}C_6$ are found to play the major role in the carburization processes. Figure 10 shows that the equilibrium carbon activity of $Cr_{23}C_6$ is lower than the carbon activity of a hyperstoichiometric uranium carbide by several orders of magnitude.

In the same figure are plotted the carbon activities of some of the more important carbides formed by the fission products.

The dissociation reaction $M_2C_3 \rightarrow 2\ MC + C$ can therefore be thought to control steel carburization. The penetration and reaction of carbon with the steel components take place through a complex pathway, which, in the temperature range of interest, depends to a large extent on two separate reaction kinetics:

1. diffusion of carbon in the austenitic phase

2. formation of $(FeCr)_{23}C_6$ precipitates within the grains and at grain boundaries.
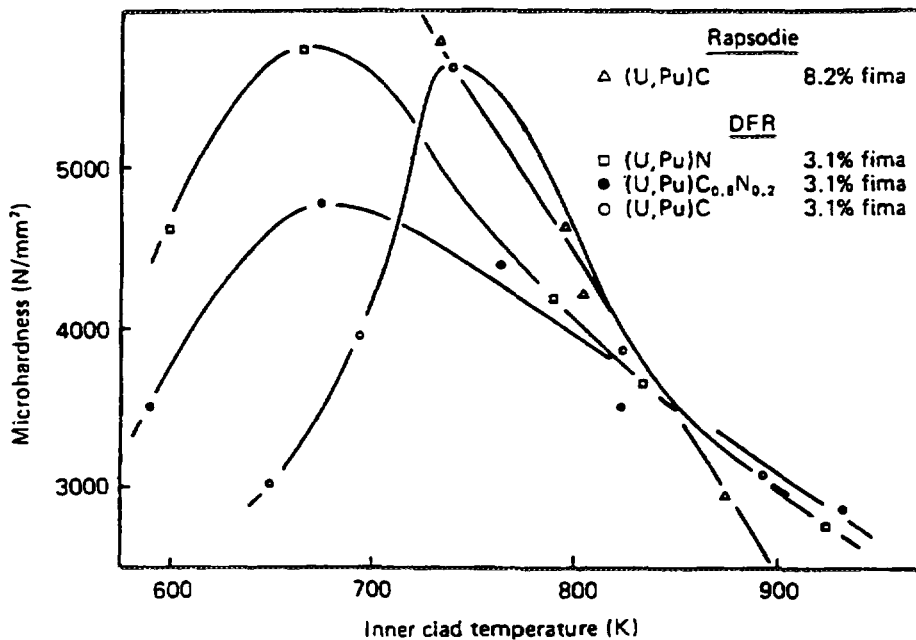
Fig. 9 Average microhardness measured in Type 316 stainless steel claddings, carburized at different temperatures. A maximum hardening is found in a rather well-defined temperature range. See also the section on the interpretation of profiles.
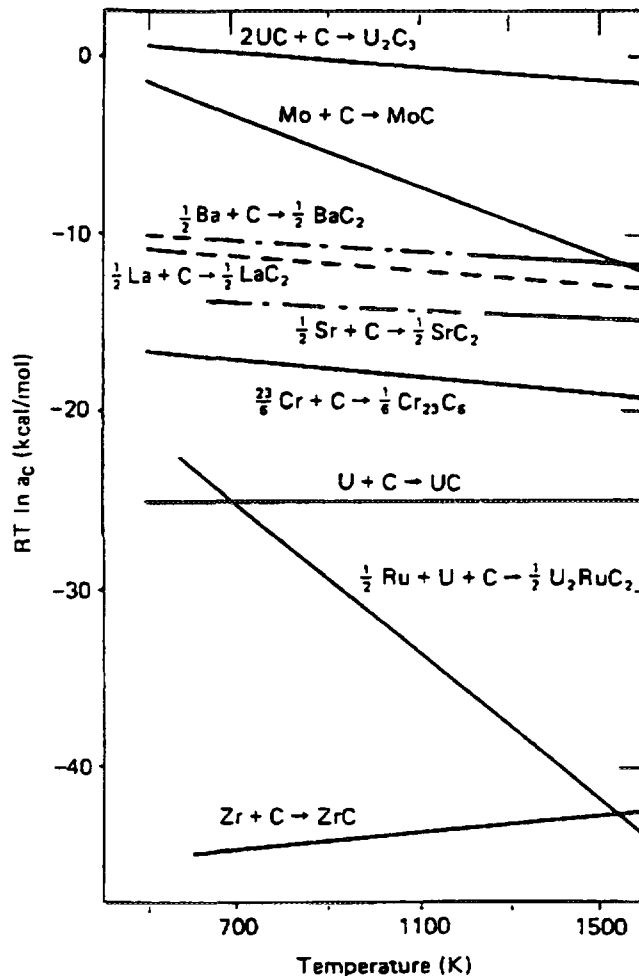
Fig.10 Equilibrium carbon activity as a function of temperature for the most relevant carbon reactions involving fuel components and principal fission products.

The definition and measurement of an effective carbon diffusion coefficient D_{eff} are therefore rather problematic. The shape and the depth of the carbon profile beneath the carburization surface are functions of the space and size distribution of the $(FeCr)_{23}C_6$ precipitates. Therefore, the effective diffusion coefficients obtained from the measured carbon profiles by means of linear diffusion models display a large scatter. Furthermore, the temperature dependence of the diffusion coefficients obtained is very weak; in an Arrhenius plot an activation enthalpy of < 10 kcal/mol is obtained (Fig. 11) that can be hardly attributed to a realistic single activated atomic jump. The analysis of the carbon diffusion equation in the steel from a measured profile should therefore be performed with an adequate algorithm which has been developed by C. Ronchi (Ref. 1).

3.3   Interpretation of the Axial Hardening Profiles of the Cladding

The carburization produces different modifications of the steel mechanical properties, depending on the extent to which the process takes place and on the morphology of the carbides formed.

As shown, the carbon penetration profiles do not change very much in the temperature range 570 to 920 K, in which the cladding normally operates. On the other hand, the microhardness variations as a function of temperature, reported earlier in this paper in observations of sodium-bonded pins, are considerable. They should therefore be attributed to the microstructural changes produced by carburization rather than to the gross amount of carbon diffused into the steel. Starting from Fig.10, three different carburization conditions are expected: These correspond to distinct carburization regimes.

105
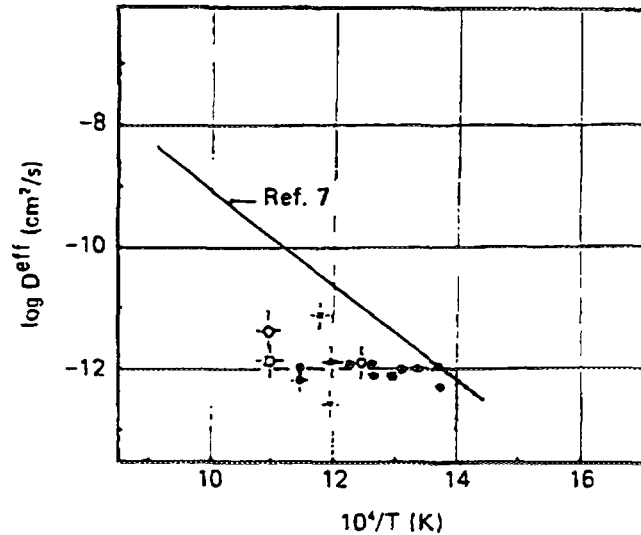
Fig. 11 Arrhenius plot of effective carbon diffusion coefficient in stainless steel obtained from out-of-pile measurements. The data points in the shaded area were deduced from carbon profiles in carburized claddings after irradiation. A different diffusion mechanism is indicated. The line at the top represents the out-of-pile measurements made by Agarwala et al. (Ref. 40).

Low-Temperature Regime (Up to ~ 700 K, see Fig. 9)

This is characterized by an increase of hardness with temperature. At temperatures 550 K the rate of diffusion of carbon is very low ($D_c < 10^{-13}$ cm^2/s), and negligible carbon penetration is expected during typical irradiation times. Only at temperatures > 600 K is the penetration deep enough for carburization to become important.

The optically detected morphological variations of the steel structure produced by carburization are not obvious. In this temperature range the largest microhardness increases are measured, and the carbon penetrating the steel produces a large number of very small intragranular carbide precipitates that are responsible for the observed hardening. The study of precipitation hardening in this temperature range indicates that the amount of carbon precipitated increases strongly with temperature, although the presence or radiation damage was shown to reduce the influence of temperature in the precipitation processes.

Medium-Temperature Regime (700 to 820 K)

The intragranular precipitation of $M_{23}C_6$ attains the maximum extent. At these temperatures the rate of migration of chromium is sufficiently high to produce additional precipitation on the grain boundaries and twins, which increases with temperature. The amount of carbide precipitated on the grain boundaries has little effect on the steel microhardness, which therefore decreases with temperature during this stage in proportion to the fraction of carbon precipitated on the grain boundaries (Fig. 9).

High-Temperature Regime (Above 820 K)

In spite of ist high mobility, the concentration of free carbon and of the submicroscopic carbide particles remains low so that no substantial variations in microhardness with respect to the initial value of 1900 N/mm^2 are expected. On the other hand, the grain boundary reaction with chromium produces a drop of the dissolved carbon concentration in increasingly large zones.

The microhardness curve obtained can be correlated with the frequency of incipient cracks observed in the cladding after diametral deformations of ~ 1 %. Figure 12 shows the frequency of the radial cracks observed in the carburized cladding zone as a function of their depth at different irradiation temperatures. The diagram shows that the largest number of cracks is observed in the temperature zone corresponding to the medium carburization regime, where important hardening is associated with large grain boundary carburization. Actually, the tensile properties of the steel in these conditions are extremely poor. Experiment shows that for carbon concentrations > 0.5 % at temperatures of ~ 750 K the embrittlement is severe and the steel shows very little ductility (Fig. 13) (Refs. 2 and 3).

3.4 Possible Advantages of Cold-Worked Steels

The deterioration of the mechanical properties of the steel caused by carburization is expressed in terms of loss of ductility. If the cladding is expected to be subjected to moderate plastic deformation, however, the major pin failure risks do not arise from precipitation hardening alone but also from severe embrittlement of the grain boundaries. In fact, our observations indicate that the cracks originating at the internal cladding surface have a transgranular character in the heavily carburized zone, but then extend deeper into the steel intergranularly, along carburized grain boundaries. The analysis of the carbon diffusion performed earlier in 'Carbon Reactions in Stainless Steel' suggests that the initial steel defect structure (grain size, twin, and dislocation density) should influence the shape of the carbon penetration profile. Thus, in cold-worked steels a compact intragranular distribution of $(FeCr)_{23}C_6$ precipitates should nucleate and grow on the lattice defects. Finally, a highly carburized layer should be formed down to a certain depth where all the carbon diffusing from the fuel is captured and prevented from penetrating more deeply into the steel.

The effect of cold working on carbon precipitation in sensitizing heat treatments was clearly observed. The carbide precipitation rate is increased by a factor ~ 15 with respect to annealed structures. However, in the presence of radiation damage, the defect structure of the steel is subjected to stubstantial modifications that are not entirely interpreted and quantitatively defined. Generally, the dislocation density of cold-worked steel is observed to decrease with the neutron fluence from typical initial values of 10^{12} to 10^{13} cm^{-2} down to an asymptotical value ρ^* (Refs. 4 and 5).
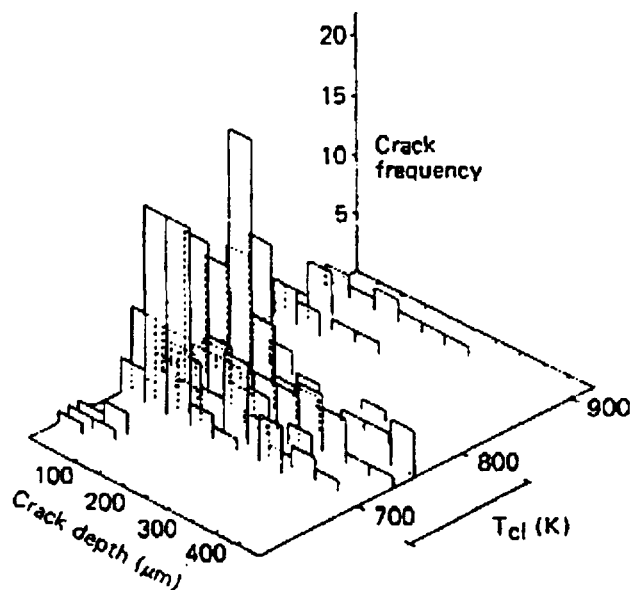
Fig. 12 Frequency of incipient cracks, observed in carburized Type 316 stainless steel claddings, classified according to crack depth and cladding temperature. The cracks were counted in the corresponding sections of 32 mainly helium-bonded pins with burnup ranging between 1 and 8% fima.

107
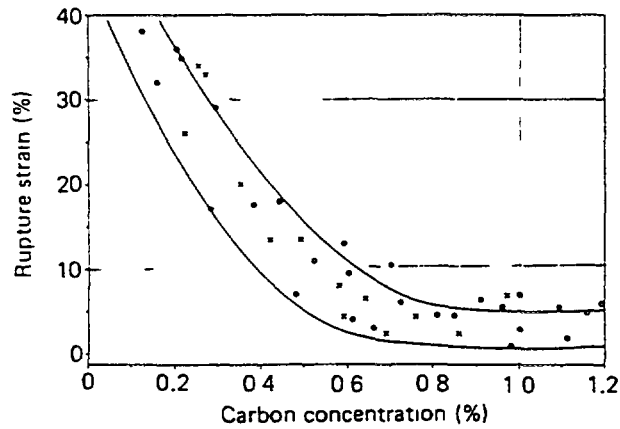
Fig 13 Decrease of rupture strain with increasing carbon
content in Type 316 stainless steel at temperatures
between 770 and 1070 K (Ref 47).

On the other hand, in annealed structures the irradiation produces a progressive increase in dislocation density up to the same value ρ^* , ρ^* corresponds to the steady-state configurations where an equilibrium is established between creation and precipitation of point defects The value of is a function of temperature, however, this dependence has not yet been clearly determined

In some experiments at 770 K and 15 dpa, the dislocation density in cold-worked and solution-annealed Type 316 stainless steel achieves the same order of magnitude of 2 to 5 x 10^{10}/cm^2 In other experiments on niobium-stabilized steels at 870 K and 16 dpa, the cold-worked dislocation structure was still observed ($\rho \sim 1$ to 4 10^{11} cm^2)

At low temperatures the radiation annealing of the cold-worked dislocations occurs, under standard flux conditions, in relatively long times (more than a few weeks) Above a certain temperature the radiation annealing process is rather rapid with respect to the steel carburization rate, hence the effect of cold-working on carburization is expected to be negligible This temperature should lie in the range of 850 to 900 K above which extended radiation-induced recrystallization is observed

It is thus conceivable that up to these temperatures the carbide formation in irradiated steels is accelerated by cold working to form a dense carbide layer preventing a further deep penetration of carbon, but at higher temperatures the extent of this effect remains unclear

At the present time, this argument cannot be fully justified The results obtained in the Los Alamos National Laboratory-Westinghouse tests of fuels fabricated with improved methods seem to confirm that cold-worked steel presents a good carburization resistance In these experiments a burn-up of 16 % fima was safely attained Between 670 and 870 K a carburized layer is observed to be formed, independently of temperature, in the early irradiation period, down to a depth of ~100 μm, (20 % of the cladding volume), afterward the carbon penetration does effectively stop At high burn-up the carburized layer was extensively cracked, but apparently the loss of ductility of the canning was tolerable as diametral strains up to 3 5 % were measured

On the other hand, British irradiation tests with hyperstoichiometric carbide fuels at burn-ups up to ~ 9 % fima showed that the carburization depths in a 20 % cold-worked Type 316 stainless steel do not exceed 100 μm up to 850 K, but above this temperature they increase abruptly Similar observations were made on 15 % cold-worked stabilized steels at burn-ups between 5 and 8 % (see the next section) where from 850 to 950 K the carbon penetration depth increases from 100 to 300 μm

A comparison of the carbon penetration depths in solution-annealed and cold-worked steels is illustrated in Fig 14 Most of the values of the carbon penetration depths were deduced from microhardness profiles, since at temperatures < 850 K these proved to be strictly homologous to the carbon concentration profiles The measurements indicate that at low temperatures the solution-annealed steel was subjected to a somewhat deeper carburization than the cold-worked steel, but at > 900 K this difference vanishes

108

Carburization depth (μm)

300

200

100

700   800   900   1000

Temperature (K)
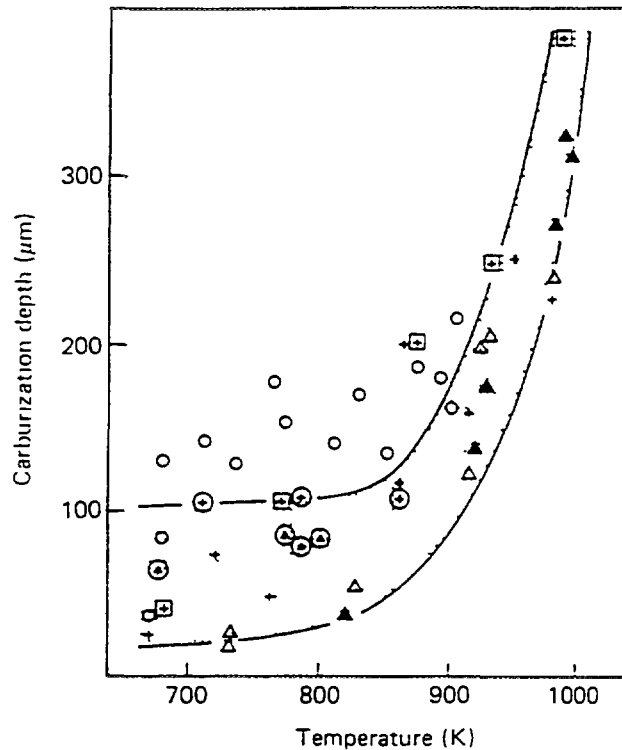
Fig 14 Carburization depth in various cladding steels at medium and high burnup The data pertaining to cold-worked alloys are in the shaded area

o = solution annealed Type 316 stainless stee¹ 8 to 12% burnup

— = cold-worked Type 316 stainless steel 3 to 5% burnup (Refs 58 and 59)

⊟ = cold-worked Type 316 stainless steel 8% burnup (Refs 58 and 59

⊖ = cold-worked Type 316 stainless steel 10 to 12% burnup (Ref 53)

△ = cold-worked titanium stabilized 5% burnup

▲ = cold-worked niobium stabilized 5% burnup

Ⓐ = cold-worked niobium stabilized 7 5 to 9% burnup

3 5   Behavior of Stabilized Steels

Stabilized austenitic steels are being successfully utilized as cladding materials in FBRs because of their low irradiation swelling rates However, their use with carbide fuels was rather limited

Two steels were examined, the (V, Nb)-stabilized DIN 1 4988 and the titanium-stabilized DIN 1 4970 steels The weight concentration of V + Nb in the former amounts to ~ 1 5 %, whereas in the latter the titanium concentration does not exceed 0 6 % In both cases, 15 % cold-worked material was used The carburization behavior of these stabilized steels displays essential differences with respect to Type 316 stainless steel

The measured carburization hardening on the inner cladding surface as a function of temperature shows a maximum located between 750 and 830 K for the titanium-stabilized steel and between 850 and 900 K for the (V, Nb)-stabilized ones (Fig 15), and the hardness values attained are significantly higher than in Type 316 stainless steel However, the carburization depth is comparatively low for temperatures up to 850 K At higher temperatures the carburization becomes deeper, but the hardening decreases (Fig 16)

109
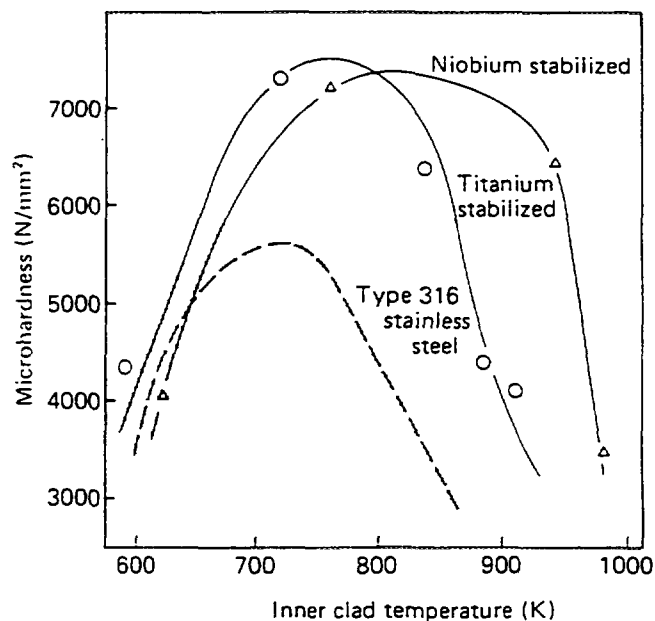
Fig. 15 Maximum observed hardening caused by carburization in sodium bonded pin cladding after a burnup of ~8% fima. The curves represent the behavior of the Ti- and (V,Nb)-stabilized steels, as compared to Type 316 stainless steel (shaded area).
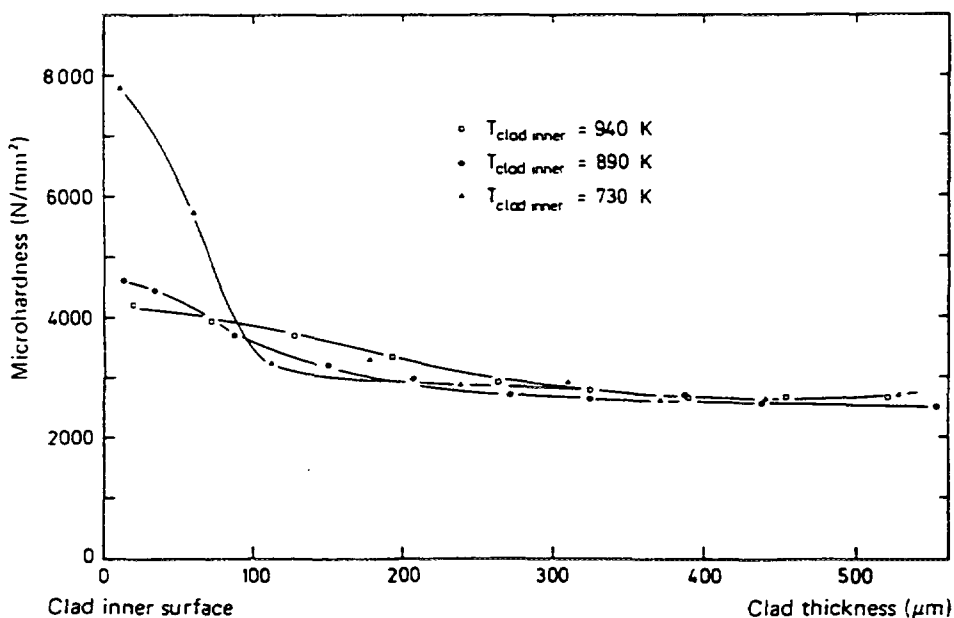
Fig. 16 Microhardness profiles from the inner cladding surface at three temperatures for a titanium-stabilized steel.

In the high-temperature range explored (850 to 1000 K) in the niobium-stabilized steel, grain boundary carbide precipitation is observed beyond the carburization layer over the whole cladding cross section. This effect is less pronounced in the titanium-stabilized steel. Generally, the carburization reactions in stabilized steels are faster than in non-stabilized alloys. In particular, between 850 and 1050 K the precipitation rate of carbide is increased up to one order of magnitude. For instance, in niobium-stabilized steels containing 130 ppm carbon at 850 K, $M_{23}C_6$ is observed to precipitate on the grain boundaries and Nb(C, N) within the grains after only 10 h of annealing.

110

The reaction patterns leading to the precipitation of titanium or niobium carbides are rather complex (see, for example, Ref 6), involving formation of metastable compounds followed by re-solution stages However, since the stabilizing elements have significantly lower diffusion coefficients in steel than chromium, these reactions, in the temperature range of interest (600 to 1000 K) occur with formation of finely dispersed precipitates

These features explain the high degree of hardness achieved by the stabilized steel after carburization Even the displacement of the maximum in the hardening curves toward higher temperatures (see Fig 15) is probably associated with the persisting intragranular precipitation controlled by the less mobile stabilizers These observations indicate that the loss of ductility caused by carburization in stabilized steels is probably more pronounced than in Type 316 stainless steel From the measurement of carburization depths and hardness, it is expected that the highest cladding failure risk, produced by carburization, is encountered in the intermediate temperature range between 800 to 900 K, i e, at a somewhat higher temperature than in Type 316 stainless steel

3 6   Conclusions

The following conclusions can be drawn

1   Solution annealed austenitic steels of Type 316 do not seem to be suitable as cladding materials for MC The carburization produced by standard hyperstoichiometric fuels is very deep At high burn-up, nearly 50 % of the cladding volume is expected to suffer a dramatic loss of ductility Several irradiation tests confirm that claddings of solution-annealed Type 316 stainless steel deformed by 0 5 to 1 % exhibit numerous radial cracks extending from the internal cladding surface through the heavily carburized region, with a depth of > 200 μm Under tensile stresses exerted by the fuel or caused by thermal cycling, these cracks evolve very rapidly into severe cladding breaches
A significant percentage of pins was observed to fail after diametral deformations of < 1 5 %

2   Stabilized steels, which are presently considered because of their low irradiation swelling, display worse carburization properties at temperatures> 900 K
3   Among the cladding materials that are presently customarily used, cold-worked Type 316 stainless steel seems to provide the best resistance to carburization, although this observation is based on incomplete evidence
4   Finally, ferritic alloys could offer substantial advantages with respect to austenitic steel Their carbon content is approximately one order of magnitude higher than that of Type 316 stainless steel (0 3 % maximum versus 0 4 % maximum), and their mechanical properties are little influenced by carburization levels Ferritic steels, which develop maximum softness, ductility, and corrosion resistance in the annealed condition, can be suitably tailored in order to obtain the best compromise between a high room-temperature ductility and an elevated stress rupture strength at high temperature Recently, a 13 Cr-Ti-Mo ferritic alloy was obtained showing low sensitivity to embrittlement and swelling under fast neutron irradiation and an excellent compatibility with sodium Adversely, one could fear that placing pins with ferritic steel cladding in an (presently) otherwise austenitic steel-sodium system would induce a carbon transfer through the coolant channels with possible detrimental effects The experimental results obtained to date are very encouraging, showing a pronounced insensitivity of the carbon concentration in these ferritic alloys to variations of carbon activity in sodium

References

1   C Ronchi, M Coquerelle, H Blank, J Rouault, 'The Sodium-Bonding Pin Concept for Advanced Fuels', Part II Analysis of the Cladding Carburization, Nucl Techn, 67 (1984) p 73

2   G Gotzmann, P Hofmann, and F Sarikaya, 'Mechanical Properties of Cladding Materials after Annealing with Carbide Fuels', KfK-1942, Kernforschungszentrum Karlsruhe (1973)

3.   A. Thorley and C. Tyzak, 'The Carburization of Stainless Steel in Sodium containing Carbon Impurities and its Effects on Mechanical Properties', Proc. Conf. Effects of Environment on Mechanical Properties in Nuclear Systems', British Nuclear Energy Society, London (1971)

4.   H. R. Brager, F. A. Garner and E. R. Gilbert, 'Stress-Affected Microstructural Development and the Creep-Swelling Interrelationship', Proc. Conf. Radiation Effects in Breeder Reactor Structural Materials, Scottsdale, Arizona, p. 727, American Society for Testing and Materials (1977)

5.   W. V. Wayda and K. Ehrlich, 'Radiation-Induced Recrystallization, its Cause and Consequences in Heavy-Ion irradiated 20 % Cold-Drawn Steel of Type 1.4970', J. Nucl. Mater., 113, 149 (1983)

6.   H. Gerlach and E. Schmidtmann, 'Einfluß von Kohlenstoff, Stickstoff und Bor auf das Ausscheidungsverhalten eines Austenitischen Stahles mit 16 % Cr 2 % Mo 16 % Ni und Niob', Arch. Eisenhüttenwesen, 39, 1 (1968)

7.   R. P. Agarwala, M. C. Naik, M. S. Anand and A. R. Paul, 'Diffusion of Carbon and Stainless Steels', J. Nucl. Mater., 36, 41 (1970)

4.   A Head-End Gaseous Oxidation Process for Irradiated Carbide, Carbonitride, Nitride Fuels

4.1   Introduction

Extraction of unspent uranium and plutonium from irradiated oxide fuel is performed by the well established PUREX process. Advanced fuels (carbides, carbo-nitrides, nitrides) could be handled by this process after conversion to the oxide. In principle, this may be performed by a wet chemical process (but this involves the production of complex organic molecules which interfere with the extraction process) or as in the study reported here, by gaseous oxidation (Ref. 1, 2).

For easy reprocessing, the oxidized fuel must be exclusively near stoichiometric (U, Pu)O_2 containing 25 % Pu. Accordingly, samples of advanced fuels have been oxidized in gaseous environments to determine the most appropriate means of achieving the required degree of oxidation. This report summarizes the arguments leading to the choice of oxidizing media used in this study and the analysis of the oxides thus formed.

4.2   Choice of oxidizing media

Thermodynamic calculations indicate that CO/CO_2 mixtures could be used to provide suitable oxidizing media at 700° C - 900° C. Assuming the predominant reaction to be of the type:

$$MC + 3\ CO_2 = MO_2 + 4\ CO$$
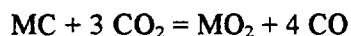
then (U, Pu)O_2 should be formed if the CO/CO_2 ratio is maintained between $\approx$ 10/1 and 1/100 at $\cong$ 800° C. It has been estimated that CO_2 alone flowing at $\cong$ 6 1/h through the furnace which in this case had a reaction chamber of $\cong$ 3 1, would result in gas compositions within this range at $\cong$ 800° C; the permissible range of CO/CO_2 ratios gives considerable flexibility in the operation of this process.

In addition, rapidly flowing (50 1/h) Ar-20 % O_2 at 590° C has been employed in some tests. Such a gas would avoid possible additional contamination by carbon from CO/CO_2 mixtures which would lead to residue problems in the PUREX process. Preliminary tests with unirradiated (U, Pu)C indicated that at less than 600° C a product soluble in nitric acid would be formed in this environment (1).

4.3   Experimental techniques and results

Starting materials consisted of sections up to 60 mm long of mixed (U-20 % Pu) irradiated carbide, carbonitride and nitride pins with maximum burn-ups from 1 to 7 at. %; the maximum linear power was 1350 W/cm. During oxidation, the gas was passed continuously over the specimen which was contained in a covered stainless steel crucible in the furnace. Oxidations in CO/CO_2 commenced with an interval of 1 h at 700° C primarily to precipitate carbides in the cladding steel (DIN 1-4970), so that it would fail/crack in a brittle manner from the stresses generated by the volume change on conversion of the fuel to oxide, thus exposing the fuel to the gas. Subsequent oxidation was always at higher temperatures, up to 800° C. Samples of oxidized fuel were mounted, polished and examined on an optical microscope; other samples were studied by X-ray diffraction to determine the O/M rate of the oxide and to determine the presence of other phases.

4.4   Results and discussion

Oxidation in CO/CO " AND Ar-20 % O_2

Table 3 gives details of the fuels which have been oxidized, oxidation conditions and the results of X-ray analysis. Oxidation in CO/CO_2 resulted in exclusive formation of (U, Pu)O_2 with an O/M ratio close to the stoichiometric value. From experience gained previously, little difficulty should be encountered in handling these oxides by the PUREX process. Oxidation in Ar-20 % O_2 resulted (with the possible exception of sample AP1) in two phase oxides containing significant amounts of M_3O_8 (see section 2).

Microscopic examination of reaction products

All oxidations in CO_2 resulted, as expected, in brittle intergranular failure/cracking of the cladding. In cases where a longitudinal (fiducial) mark was present on the outside of the cladding, the brittle crack closely followed this mark. Cladding/failure cracking was not observed during oxidation in Ar-20 % O_2.

The morphology of the reaction product did not depend on the type of fuel or on the oxidizing gas (see below) but rather on the fuel restructuring which had occurred during irradiation.

Oxidation in Ar-20 % O_2 only resulted in a surface attack and in some oxidation along major cracks. Scale formed at the fuel/cladding interface and on the exposed (cut) faces at the ends of the pin section and grew progressively into the fuel.

At the end of the oxidation (little or no further change in weight of the samples), the oxidized fuel consisted of a powder of particle size 10 - 50 µm, regardless of the oxidizing medium and type of fuel.

4.5   Conclusions

1)   Conversion of advanced fuels (carbide, carbo-nitride and nitride) to oxide by heating in flowing CO_2 at $\cong$ 800° C offers a promising alternative to the wet chemical process.

2)   Oxidation in Ar-20 % O_2 carried out at 590° C does not always result in exclusive formation of near stoichiometric (U, Pu)O_2.

3)   Since the particle size of the oxide is 10 - 50 µm, a high percentage of the fission products will be present in the oxide.

4)   Oxidation of the advanced fuel proceeds both at the outer surface and also internally (on the inside of pores, along cracks etc.) when flowing CO_2 is used at $\cong$ 800° C.

References

1. U. Benedict, K. Richter, and G. J. Tuerlinx, Trans. of ENC '79 Conf. of European Nuclear Soc., Hamburg, 1979, 31. TANSA 1-666 (1979) p. 512

2. A. L. Mills and K. Hartley, British Patent 1 205 169 (1968)

The experimental results collected in this report have been obtained by Dr. H. Blank, U. Benedict, C. Ronchi, I. Ray, C. T. Walker, B. Whitlow and M. Coquerelle.

FUEL OF PLUTONIUM MONOCARBIDE AND INERT DILUENT SOLID SOLUTION (54.5% PuC + 45.5% ZrC) FOR FAST REACTORS

B.D ROGOZKIN, N.M. STEPENNOVA,
Yu E FEDOROV, M.G. SHISHKOV
All Russian Scientific and Research Institute of Inorganic Materials,
Moscow

Yu.M. GOLOVCHENKO
Research Institute of Atomic Reactors,
Dimitrovgrad

Russian Federation

XA9745727

Abstract

The problem of efficient and cost-effective use of plutonium without breeding in nuclear power is the urgent scientific and engineering task. Solution of this problem in practice is related to the development of closed fuel cycle and utilization of fast reactors, including Pu and minor actinides burner fast reactors.

Use of plutonium fuel with inert diluent that substitutes ^{238}U and eliminates plutonium breeding is the problem of great practical interest. All properties of solid solutions and composite materials of carbides and nitrides (PuC - ZrC, PuN - ZrN, PuN - AlN etc.) comply with the requirements imposed on nuclear fuel to the greatest extent.

Efficient plutonium burning is aided by increased plutonium content in the fuel.

ARSRIIM was the first to propose the fuel based on PuC - ZrC and PuN - ZrN solid solutions with high thermal conductivity and thermodynamic stability that is now under development.

Methods for synthesising solid solutions of plutonium and zirconium monocarbides through entire range of compositions was developed by the authors, the procedure to produce 54.5 % PuC + 45.5 % ZrC fuel was chosen, irradiation test was carried out in BOR-60 reactor with 400 - 500 W/cm heat rating up to 8.0 % HM burnup.

As a result of irradiation tests it was concluded that all fuel elements remained their serviceability and were suitable for further operation, fuel-cladding interaction was local and did not exceed 100 μm, fuel swelling was about 1 %/% of burnup, gas release was less than 2 %.

It was for the first time, when the possibility to use fuel with high content of plutonium and inert diluent in fast reactor was shown.

1. Introduction

Nuclear power development involves safety assurance cost-efficiency, solution of the problems of high-level wastes, usage of weapon-grade and nuclear-grade plutonium, and transmutation of minor actinides, long-lived isotopes such as ^{128}I and ^{99}Tc. Release of considerable amount of fissile materials in nuclear weapon reduction led to arising the important problem of safe utilisation of weapon-grade plutonium and highly enriched uranium. It is known, that weapon-grade plutonium is supposed to be used as follows.

1. In fast reactors as:

   a)   mixed uranium-plutonium fuel highly enriched to 45 % in plutonium;

b) plutonium fuel with inert matrix,

2 In thermal reactors and HTGR in the form of oxide fuel;

3 In molten salt reactors in the form of halides [1 - 5].

As the majority of researchers guesses, recycling of spent plutonium fuel in fast and thermal reactors is inevitable. Accordingly, the type of chosen fuel should be suitable for the recovery of irradiated fuel.

In our opinion, mixed monocarbides, mononitrides, uranium and plutonium carbonitrides as well as solid solutions or compositions of plutonium monocarbides, mononitrides and inert diluent substituting ^{238}U may be used as the fuel of such type. Use of plutonium carbon-nitride fuel with inert diluent makes it possible to exclude plutonium breeding.

Mixed uranium and plutonium carbon-nitrides feature high content of fissile material in unit volume, of conductivity 17 - 26 W/cm at 600 - 1,500 °C, good compatibility with structural materials and coolant, low volatile fission products release, etc.

There is no data on the properties of solid solutions of plutonium and inert diluent carbide-nitride, for example, zirconium, titanium, niobium in the available references. There is no information on their synthesis as well Available data on properties of UC - ZrC, UN - ZrN allow to suppose that properties of solid solutions of similar plutonium and inert diluent compounds will be close to those (high thermal conductivity of about 20 - 27 W/cm, thermal-chemical stability, good compatibility with structural materials and coolant). Therefore, use of fuel with inert diluent is a problem of great scientific and engineering interest. With this problems concerning environmental safety and reliable storage of plutonium will be solved too.

The paper is devoted to study of the processes of PuC-ZrC solid solution synthesis and meat manufacture, as well as to the results of irradiation tests in BOR-60 reactor.

2. Synthesis of solid solutions of plutonium and zirconium monocarbides

Two methods synthesis were developed for synthesis of starting:

1) Pu and Zr metals;

2) Pu and Zr oxides.

When developing synthesis methods one had to take into consideration that single-phase plutonium monocarbide corresponds to $PuC_{0.88}$ stoichiometry, and wide homogeneity range with carbon content ranging from 8.0 to 11.6 % by weight is peculiar for zirconium monocarbide. Accordingly, quantity of carbon required to exclude formation of sequa-phase of Pu_2C_3 in fuel was needed to be determined by experiments.

We don't know the solid solution synthesis methods for wide range of compositions published earlier. There is only brief information on solid solution with up to 24 % plutonium content synthesized by arc melting [6].

In the first method plutonium and zirconium powders synthesized by hydrogenation and dehydrogenation were used as starting materials. Zirconium powder synthesized by electrolysis was used too. Plutonium and zirconium powders were mixed with DG-100 black in the defined ratio. The charge obtained was pressed and sintered. Exothermic reaction of carbidization with formation of two solid solutions enriched in plutonium and zirconium started up in the process of heating at temperature about 600 °C.

116

The spongy mass obtained was grinded and work-pieces were pressed at 2 - 10 t/cm^2 pressure from the powder obtained. The work-pieces were sintered in the atmosphere of chemically pure argon at 1,750 - 1,850 °C. As a rule the meats obtained included two phases and were fine-grained with grain size less than 15 μm. Grain microhardness made up 1,500 - 1,800 kg/mm^2. Meats containing, for instance, 54.5 % Pu and 45.5 % ZrC were of two phases of solid solution with lattice parameters a = 4.738 $\overset{o}{A}$ and a = 4.911 $\overset{o}{A}$. Non-uniformity in plutonium distribution did not exceed 5 %. Content of oxygen and nitrogen in the meats was less than 0.1 % each.

Meats for irradiation tests in BOR-60 reactor were manufactured by this method.

In the second method starting charge included plutonium oxide, carbon and zirconium monocarbide powders The charge pelletized. The pellets were placed in a furnace and heated gradually, first in vacuum up to 1,400 - 1,500 °C, and then in argon atmosphere up to 1,800 - 1,900 °C. The obtained solid solution also included two phases enriched in plutonium and zirconium. The mass obtained was grinded and the powder was used to press and sinter the meats. Sintering regime is similar to the above mentioned. Composition of the solid solution was levelled over the volume when sintering. Grain size did not exceed 15 μm Grain microhardness was 1,500 - 1,900 kg/mm^2.

The meats of PuC - ZrC solid solution were manufactured by the described methods with compositions within the whole range.

The meats of 56 % UC + 44 % ZrC solid solution for active fuel element portion and 15 % UC + 85 % ZrC solid solution for shielding portion of fuel elements were made for comparative irradiation tests. UC - ZrC solid solution was sinthesized by carbothermal method from uranium and zirconium oxides.

3. 54.5 % PuC - 45.5 % ZrC fuel irradiation tests in BOR-60 reactor

DESCRIPTION OF FUEL ELEMENT AND FUEL ASSEMBLY DESIGN AND MANUFACTURING METHOD

Fuel element design is presented in Fig. 1. The fuel elements are sealed, of rod type. Cladding is made of 6.9 mm O D. tubes with 0.4 mm wall thickness of cold-worked 06Cr16Ni15Mo3Nb steel (TU 14-3-895-80). The meats for fuel rod active length are made of 54.5 % Pu + 45.5 % ZrC solid solution and 56 % UC + 44 % ZrC solid solution. The meats for shielding zone are made of UC - ZrC containing depleted uranium. Helium concentration filling these fuel rods is 96 %. Wire of 06Cr16Ni15Mo3Nb steel 1.05 mm in diameter is wrapped on the central fuel rods and 0.6 mm by 1.3 mm shaped wire is wrapped on fuel rods of peripheral zone to space the fuel rods in fuel assemblies. Helium leak detector was used to test fuel rods for leak-tightness at 350 °C temperature.

Fuel assembly comprises head, internal hexagonal tube, transition joint, tail, fuel rod bundle, external hexagonal tube. Internal tube with wrench dimension of 38 mm and 0.8 mm wall thickness is intended for forming fuel rod bundle. External tube with wrench dimension of 44 mm and 1 mm wall thickness is installed to increase fuel assembly weight and welded by its lower end to the transition joint. Shroud is made of 09Cr18Ni10Ti steel (TU 14-3-592-77).

Main fuel characteristics are presented in Table 1.

IRRADIATION CONDITIONS

Fuel assembly was irradiated during three short fuel cycles Burnup of 8 % HM is reached for irradiation time, neutron fluence in central plane made up 5.48 10^{22} n/cm^2 (E > 0) and 4.43·10^{22} n/cm^2 (E > 0.1 MeV). Linear fuel rating made up 400 - 450 W/cm. Cladding peak temperature taking into account overheating made up 635 ± 25 °C.
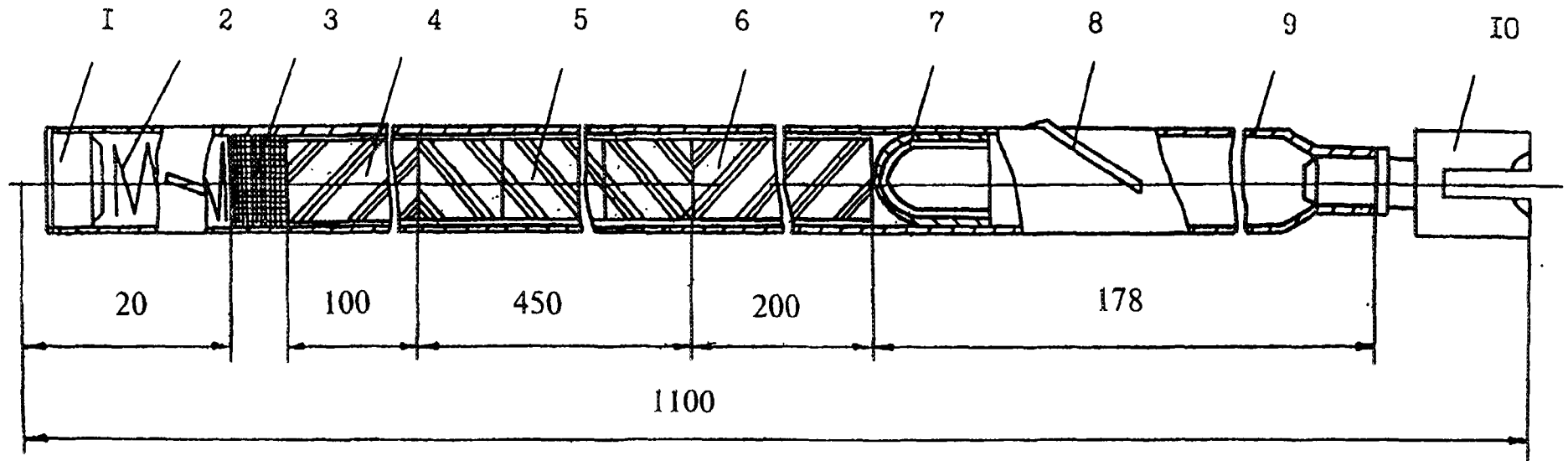
Fig. 1. Fuel element design:

1 - upper cap; 2 - spring; 3 - plug; 4 - meat of the upper shielding zone; 5 - active length meat; 6 - meat of the lower shielding zone; 7 - capsule; 8 - wire wrapping; 9 - cladding; 10 - lower cap

Table 1

Main characteristics of fuel meats of 54.5 % PuC + 45.5 % ZrC and 56 % UC + 44 % ZrC

Composition	Fuel Rod No	Density, g/cm³	Diameter, mm	Column length, mm	Chemical composition, %			Lattice parameter, $\overset{o}{A}$
					Carbon	Oxygen	Nitrogen	
Pu-Zr-C	1	$8.7^{+0,2}_{-0,15}$	$5.92^{+0.02}_{-0.04}$	448.8	6.53	0.1	0.05	4.738 and 4.911
Pu-Zr-C	2	$8.7^{+0,2}_{-0,15}$	$5.92^{+0.02}_{-0.04}$	448.4	6.53	0.1	0.05	4.738 and 4.911
Pu-Zr-C	3	$8.7^{+0,2}_{-0,15}$	$5.92^{+0.02}_{-0.04}$	449.3	6.53	0.1	0.05	4.738 and 4.911
Pu-Zr-C	4	$8.7^{+0,2}_{-0,15}$	$5.92^{+0.02}_{-0.04}$	450.7	6.53	0.1	0.05	4.738 and 4.911
Pu-Zr-C	7	$8.7^{+0,2}_{-0,15}$	$5.92^{+0.02}_{-0.04}$	448.9	6.53	0.1	0.05	4.738 and 4.911
Pu-Zr-C	8	$8.7^{+0,2}_{-0,15}$	$5.92^{+0.02}_{-0.04}$	449.0	6.53	0.1	0.05	4.738 and 4.911
Pu-Zr-C	12	$8.7^{+0,2}_{-0,15}$	$5.92^{+0.02}_{-0.04}$	448.7	6.53	0.1	0.05	4.738 and 4.911
U-Zr-C	5	9.3	5.91 - 5.92	449 ± 1	8.0	0.3	0.02	4.787
U-Zr-C	6	9.5	5.9 - 5.96	449 ± 1	7.9	0.3	0.02	-

Composition	Fuel Rod No	Density, g/cm³	Diameter, mm	Column length, mm	Chemical composition, %			Lattice parameter, Å
					Carbon	Oxygen	Nitrogen	
U-Zr-C	9	9.3	5.89 - 5.94	449 ± 1	8.0	0.3	0.02	4.787
U-Zr-C	10	9.5	5.88 - 5.99	449 ± 1	7.5	0.4	0.02	4.790
U-Zr-C	11	9.4	5.89 - 5.93	449 ± 1	7.8	0.3	0.02	4.790
U-Zr-C	13	9.5	5.88 - 5.99	449 ± 1	7.5	0.4	0.02	4.790
U-Zr-C	14	9.5	5.88 - 5.99	449 ± 1	7.5	0.4	0.02	4.790
U-Zr-C	15	9.5	5.88 - 5.99	449 ± 1	7.5	0.4	0.02	4.790
U-Zr-C	16	9.5	5.88 - 5.99	449 ± 1	7.5	0.4	0.02	-
U-Zr-C	17	9.4	5.89 - 5.93	449 ± 1	7.8	0.3	0.02	4.790
U-Zr-C	18	9.5	5.9 - 5.96	449 ± 1	7.9	0.3	0.02	-
U-Zr-C	19	9.4	5.89 - 5.93	449 ± 1	7.8	0.02	0.02	4.790

POST-IRRADIATION FUEL ROD EXAMINATION

As evident from measurements taken on fuel assembly shrouds, wrench dimension increase did not exceed 1 %.

All fuel rods remained leaktightness. Profilometer was used to measure fuel rod diameter with ± 0.01 mm error. Increase in diameter of the cladding in area of active portion centre was not observed.

Fuel cladding were pierced and gases were extracted inside vacuum chamber enclosing the fuel rod to determine gas volume inside the cladding. As seen from measurement results, gas volume inside the cladding was approximately the same as initial (21 cm^3). This testifies that there is no gas release from fuel.

Densities of claddings and irradiated meats were determined by hydrostatic weighting in carbon tetrachloride. Densities of the meats and claddings are presented in Tables 2, 3.

Fuel swelling makes up about 1 %/% of burnup. Negative swelling appear to be related to decreasing open porosity and after-sintering of the meats. Diametric gap remains in any fuel rod.

As evident from the analysis of macrostructure and microstructure of 54.5 % PuC + 45.5 % ZrC fuel, the meats held fine grained structure and round pores uniformly distributed over meat volume. Two-phase initial fuel of 54.5 % PuC + 45.5 % ZrC composition with 4.738 and 4.911 $\overset{o}{A}$ lattice parameters with predetermined uniformity in plutonium distribution became single-phase, homogenous with lattice parameters of 4.8328 $\overset{o}{A}$ (core top), 4.8270 $\overset{o}{A}$ (core middle), 4.8291 $\overset{o}{A}$ (core bottom) This should lead to improved operational properties. After irradiation the uniformity in plutonium distribution remained.

Cladding swelling was negligible.

Cladding carbonization was local only, did not exceed 100 μm and was observed in upper fuel rod portion. Cladding microhardness tended to increase up to 500 - 600 kg/mm^2 in the interaction area.

Behaviour of fuel rods with 56 % UC + 44 % ZrC meats is similar under the irradiation.

As seen from welded joints study, they do not restrict fuel assembly life.

All fuel rods held serviceability and were suitable for further operation.

In-pile tests conducted have shown for the first time the possibility to use 54.5 % PuC + 45.5 % ZrC solid solution as the fuel for fast reactors

CONCLUSIONS

1. Methods for synthesis of solid solution for all the range of compositions of starting metals and oxides, and methods for manufacturing fuel meats with less than 5 % non-uniformity in plutonium distribution are developed.

2. Irradiation tests of fuel rods with 54.5 % PuC - 45.5 % ZrC fuel meats are carried out in BOR-60 reactor with 400 - 450 W/m fuel rating up to 8 % HM burnup. All fuel rods held their leak-tightness and were suitable for further operation. Fuel swelling and gas release made up less than 1 %/% and 2 % respectively.

3. It was the first time when the possibility of using fuel with high content of plutonium (54.5 % PuC) and inert diluent (45.5 % ZrC) in test fast reactor was shown.

Table 2

Fuel density and swelling

Fuel Rod No	Composition	Initial Density, g/cm^3	Reactor Core Top		Reactor Core Centre		Reactor Core Bottom	
			Density, g/cm^3	Swelling, %	Density, g/cm^3	Swelling, %	Density, g/cm^3	Swelling, %
4	Pu-Zr-C	8.7	7.9	10.0	7.8	9.0	7.9	11.5
12	Pu-Zr-C	8.7	9.1	- 4.7	not measured	not measured	9.43	- 7.8
11	U-Zr-C	9.4	9.2	2.4	8.45	11.2	not measured	not measured
13	U-Zr-C	9.3	9.1	2.2	8.34	11.5	not measured	not measured
18	U-Zr-C	9.5	9.17	3.6	8.99	5.7	9.19	3.3

Table 3

Fuel cladding density and swelling

Fuel Rod No	Fuel	Reactor Core Top		Reactor Core Centre		Reactor Core Bottom	
		Density*, g/cm^3	Swelling, %	Density, g/cm^3	Swelling, %	Density, g/cm^3	Swelling, %
12	Pu-Zr-C	7.9	1.9	not measured	not measured	7.7	5.1
11	U-Zr-C	7.93	2.0	7.9	2.2	7.93	2.0
13	U-Zr-C	8.1	0	7.92	2.0	8.0	0.8
18	U-Zr-C	7.98	1.5	7.9	2.2	not measured	not measured

Note: 06Cr16Ni15Mo3Nb steel initial density is taken to be 8.1 g/cm^3

REFERENCES

1. Dekusar V.M, Kalashnikov G.N., Kunna I.S. "Physical and technological aspects of cermet fuel. Use of plutonium in VVER". IAEA Technical Committee Meeting on Unconventional Options for Pu Disposition, 7 - 11 November, 1994, Obninsk, Russia.

2. Shikava, A. Shono, T. Wakabayashi. "Study on Pu Burner Fast Reactor Cores Without Uranium". IAEA TCM, 7 - 11 November, 1994, Obninsk, Russia.

3. Garnier. "New Fuel Concepts within the French CAPRA Program". IAEA TCM, 7 - 11 November, 1994 Obninsk, Russia.

4. Languille, J.P. Pages. "Review of WP's on Plutonium Burner Fuels". CEA/MINATOM Fast Reactors Working Group Meeting. 6 - 9 September, 1994, Obninsk, Russia.

5. Alberstein. "Combining an Accelerator and Gas Turbine Modular Helium Reactor for Near Total Destruction of Weapon Grade Plutonium". IAEA TCM, 7 - 11 November, 1994, Obninsk, Russia.

6. Furukava, K. Mitachi, S.E. Chigrinov, et al. "Rational Pu-Disposition for ^{233}U Production by Thorims-NES". IAEA TCM, 7 - 11 November, 1994, Obninsk, Russia.

7. Plutonium. Handbook. Ed. O. Vika. V. 11, p.294

IMPORTANT OUT-OF-PILE THERMOPHYSICAL PROPERTIES OF URANIUM–PLUTONIUM MIXED CARBIDE FUELS FOR A FAST BREEDER TEST REACTOR

XA9745728

A.K. SENGUPTA*, T. JARVIS*, T.R.G. KUTTY*,
P.V. HEGDE*, D.N. SAH*, C. GANGULY**,
D.S.C. PURUSHOTHAM*

* Radiometallurgy Division,
Bhabha Atomic Research Centre,
Trombay, Mumbai

** Central Glass and Ceramic Research Institute,
Calcutta

India

Abstract

The out of pile thermophysical and thermomechanical properties of Nuclear fuels are essential parameters for the fuel design, prediction of the in-pile performance and as a reference data for the subsequent post irradiation examination. Importanat properties like thermal conductivity, thermal expansion, thermal toughness(creep) of plutonium rich hyperstoichiometric mixed uranium plutonium monocarbide which is the driver fuel for the Indian fast breeder test reactor (FBTR) have been measured and estimated at BARC, India. The mixed carbide fuel pin has been designed to accomodate fission gases.

The out-of-pile thermophysical and thermomechanical properties of this fuel have been generated upto a maximum temperature of 1500°C and the effect of high "Pu" content on these properties has been discussed with relevance to its inpile performance(fission gas release). The fuel has seen a burn up of about 25000 MWd/t and its post irradiation examination data are expected shortly.

Introduction

Hyperstoichiometric mixed uranium plutonium carbide pellet stack encapsulated in AISI 316 (20% cold worked) tube has been used as driver fuel for sodium cooled fast breeder test reactor(FBTR) in India. FBTR is a loop type experimental reactor of 40 MW (thermal) and 13.2 MWe capacity with two primary and secondary sodium loops and a common steam water circuit which supplies high pressure.

The unique features of the mixed uranium plutonium carbide fuel which prompted us to go for this fuel are :

- Excellent compatibility with pure sodium,

- Higher thermal conductivity permitting high linear power,

- Good irradiation behaviour reported by other countries for suitably designed mixed carbide fuels(with   Pu upto 20%)

- Good breeding ratio and short doubling time

The composition of the uranium plutonium mixed carbide fuel has been chosen in a phased manner depending upon the experience gained. Hyperstoichiometric plutonium rich mixed carbide (70%PuC-30%UC) was chosen as fuel for Mark I core. Since the fuel was new it was proposed to

125

ascertain its performance through post irradiation examination and increase linear heat rating and burn up in phased manner as follows:

Phase I   Mark I Core, (70%PuC - 30%UC) low power operation

Phase II   Mark I Core, intermediate power operation upto 10.5 MWt

Phase III   Mark II Core (55% PuC - 45%UC), 40 MWt nominal power operation

Main characteristic features of Mark I and Mark II cores are given in Table I. The target burn up of the fuel has been realised in two stages. Initially it is upto the fuel-clad gap closure due to free swelling. The estimated fuel swelling rate for the Mark II fuel is given in Table II. Subsequently, once the fuel-clad contact is established, fuel-clad mechanical interaction (FCMI) starts. The clad exerts pressure on the fuel and both the clad and the fuel undergoes creep deformation and the extent of creep deformation is determined by the smear density of the fuel. Fig. 1 shows the schematic diagram of a FBTR fuel pin.

Out of pile thermophysical and thermomechanical properties of these fuels were essential to evaluate the usefulness of these fuels in reactor. It further helps to predict the inpile performance and computer modelling for calculation of whole core accident analysis, fission gas release, fuel-clad interface temperature etc. Reported literature(1-13) on the thermophysical and thermomechanical properties of mixed carbide fuel are mostly limited to compositions with plutonium content < 40%. In the present investigation certain properties like linear thermal expansion, thermal toughness and thermal conductivity of $(U_{0.3}Pu_{0.7})C$ and $(U_{0.45}Pu_{0.55})C$ have been measured experimentally as a function of temperature. In the absence of in-pile thermophysical property data attempts have been made to understand qualitatively the effect of these properties on the fission gas release and in general the fuel performance.

Material preparation and characterisation

The mixed carbide was prepared by vacuum carbothermic reduction of mechanically mixed UO_2, PuO_2 and graphite powder in the form of clinkers. The clinkers were then crushed and milled and the powders were cold pressed and sintered at 1923K for 4h in Ar-8vol% H_2 atmosphere. The details of the fabrication steps and characterisation procedures have been reported elsewhere [14]   The nominal compositions of the fuels are given in Table III.

In addition to the radiotoxicity associated with plutonium bearing material, mixed carbide fuel pellets are prone to oxidation and hydrolysis in the presence of oxygen and moisture. Carbide powders are also very much pyrophoric hence these materials were handled in leak-proof glove boxes flushed continuously with a high purity once through nitrogen atmosphere having oxygen and moisture content of ≤ 25 ppm each. The equipment used to measure the thermophysical properties was specially modified to suit glove box installation, keeping in mind easy operation, maintenance and safety.

Out of pile thermophysical properties

THERMAL TOUGHNESS

Thermal toughness is an indirect way of predicting the thermal creep behaviour of the fuel. In the absence of conventional creep data of these plutonium rich carbide fuels (Pu : 70% and 55%), high temperature microhardness data were generated as a function of temperature(Fig.2 & 3). From the plot of Hardness vs temperature, the transition temperatures were determined. The mechanism for softening below the transition temperature is stated to be athermal and major mode of deformation mechanism in the region are slip and twinning. Above the transition temperature deformation occurs by thermal process such as dislocation climb or glide process. Knowing the melting temperature of the carbides, the transition temperature in terms of T/T_m was estimated and it was presumed that the material will be softened enough to undergo sufficient creep deformation both during free swelling and restrain swelling of the fuel The Mark II fuel which contain 55%PuC has higher M.P.(1984°C) compare to that of fuel

126

containing 70%PuC(1825°C), however the creep behaviour at a particular(T/T_m) is not expected to be markedly different [T_m = melting temp.].

Table I.

Main Characteristics of FBTR Cores

Parameters	Small Core (Mark I)	Nominal Core (Mark II)
Research power (Mwt)	10.5	40
(Mwe)	2	13.2
Fuel	70%PuC-30%UC	55%PuC-40%UC
Theoretical density(g/cc)	13.6	13.5
Pellet density (PD)	90% TD	86% TD
Smeared density	85% TD	79% TD
No. of subassemblies	26	76
No. of pins/subassembly	61	61
Fuel pin diameter(mm)	5.1	5.1
Maximum Linear heat rating (W/cm)	250	350

Control rods :
 Material   : B_4C (90% enriched in B^{10})

 Nos.   : 4

Temperature :

Nominal Maxmimum clad temperature(°C)   : 607, 622

Hot spot clad midwall temperature(°C)   : 699

Design limit for clad hot spot temperature(°C): 700

Nominal maximum fuel centre temp.(°C)   : 1381, 1415

Design limit for fuel central temperature : melting point

Melting point of fuel   : 1825, 1984

Table II.

Fuel swelling rate [15] as a function of centre temperature

Fuel Centre Temp.(oC)	Swelling rate (% V/V) per Atom% B.U)
1578	98
1455	19
1332	7.2
1208	4.2
1085	2.9
961	2.2
776	1.7
468	1.4

TOP PLUG

SPRING

SPRING SUPPORT

INSULATOR PELLET

FUEL PELLET

INSULATOR PELLET

PELLET SUPPORT TUBE & DISC

TOP PLUG WELD

CLAD

SPACER WIRE

LENGTH OF THE PIN — 531·5 mm

O·D OF THE CLAD — 5·10 mm.

I.D. OF THE CLAD — 4·36 mm

BOTTOM PLUG

FBTR FUEL PIN SHOWING THE COMPONENTS
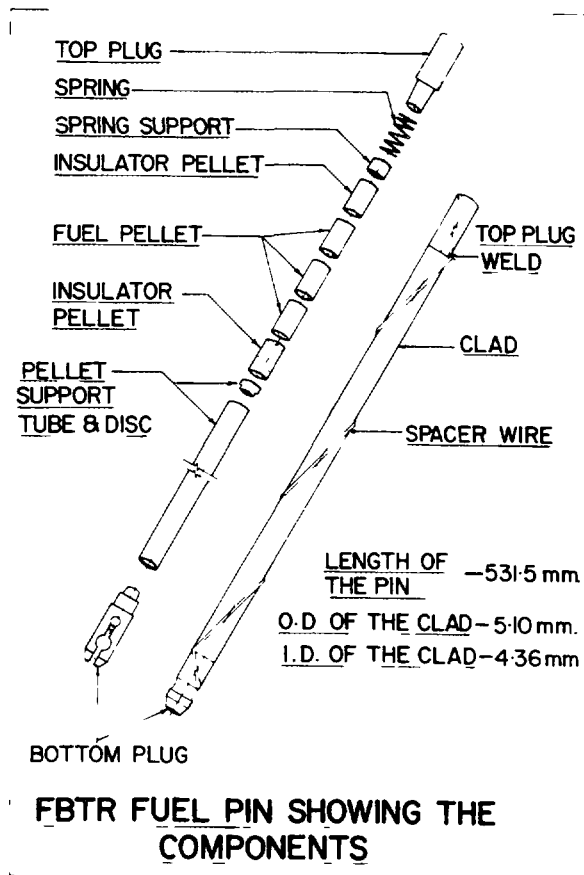
Fig. 1 A schematic diagram of FBTR fuel pin

Table III.

Nominal Compositions of Mark I and Mark II fuel

	$(Pu_{0.7}U_{0.3})$ (Mark I)	$(Pu_{0.55}U_{0.45})C$ (Mark II)
Pu	66wt%	52wt%
C	<5.06	<5.03
D	< 6000 ppm	< 6000 ppm
N_2	< 1000 ppm	< 1000 ppm
M_2C_3	5-15%	5-15%
Density	91% TD	86% TD

The hardness vs. temperature relationship for both the fuel are given below by the following equations:

$(U_{0.3}Pu_{0.7})C$ (Mark 1):

$H = 11548 \exp (-1.30 \text{ E-} 03 \text{ T})$ (ambient to 1123 K)
$H = 24316 \exp (- 2.12 \text{ E-} 03 \text{ T})$ (1123 K to 1573 K)

$(U_{0.45}Pu_{0.55})C$ (Mark II) :

$H = 14520 + 04.5T - 0.036 T^2 + 27.6 \times 10^{-6} T^3 - 6.23 \times 10^{-9} * T^4$

COEFFICIENT OF THERMAL EXPANSION

The coefficient of thermal expansion(CTE) is one of the properties that is easier to specify and is very useful data for the fuel designers There are many results to draw from e g.:

- temperature,
- alloy composition,
- stoichiometry,
- manufacturing process.

The CTE of these fuels containing 70% and 55% PuC were measured using a horizontal dilatometer from ambient to 1500 K. The relation between L/L_0 (L_0 being the initial length) and T can be expressed by the following relation :

$(U_{0.3}Pu_{0.7})C$ (Mark I):

$L/L_0 = 16.59 \times 10^{-4} + 4.17 \times 10^{-6}T + 4.60 \times 10^{-9}T^2$

$(U_{0.45}Pu_{0.55})C$ (Mark II) :

$L/L_0 = 37.08 \times 10^{-4} + 1.032 \times 10^{-5}T + 9.85 \times 10^{-11}T^2 + 4.567 \times 10^{-13}T^3$

The average linear expansion coefficient were 9.2 x 10^{-6}/K and 11.2 * 10^{-6}/K for Mark I and Mark II fuels respectively.

Thermal conductivity (k) of the fuel was calculated from the relation

k = a x C

where a, and C are the thermal diffusivity, density and specific heat respectively. The thermal conductivity data if required for 100% dense material are corrected using the conventional relation used for carbides

$K_{Th\ density} = K_m\ (1+P)/(1-P)$

where "p" is the fractional porosity and $K_{Th\ density}$ is the thermal conductivity of the 100% dense material.

Thermal diffusivity has been measured from ambient to 1773K by transient pulse or flash method of Parker [16] using Ruby pulse laser as the flash source. The thermal diffusivity were calculated using Clark and Taylor's [17] method. The specific heat was calculated from the specific heats of the constituent UC and PuC from literature [18] and using the Kope's Law of mixture.

Thermal conductivity of Mark I and Mark II sintered fuel pellets are shown in Fig.4 and Fig. 5 respectively and can be expressed by the following relations :

$(U_{0.3}Pu_{0.7})$ (Mark I):

$k = 10.34 - 2.0 \times 10^{-2}T + 3.25 \times 10^{-5}T^2 - 8.22 \times 10^{-9}T^3$

$(U_{0.45}Pu_{0.55})C$ (Mark II).

$k = 27.92 - 7.1 \times 10^{-2}\ T + 6.92 \times 10^{-5}\ T^2 - 1.85 \times 10^{-8}\ T^3$
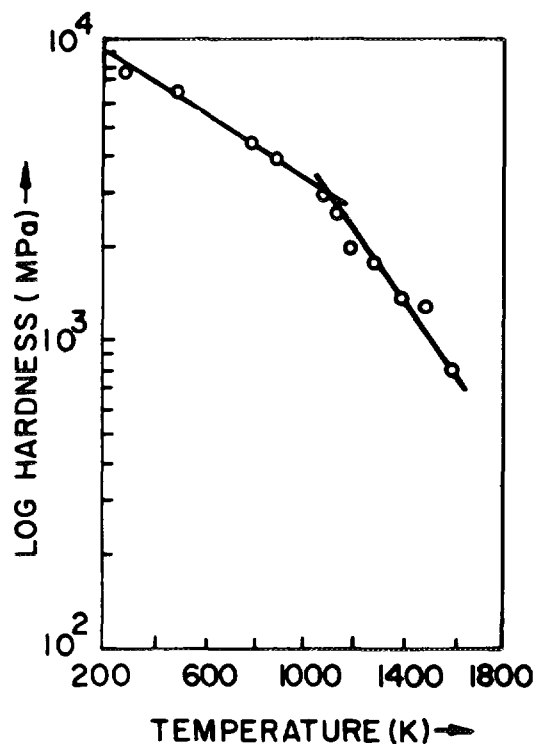
Fig. 2 Hot Hardness of $(U_{0.3}Pu_{0.7})$ C as a function of temperature
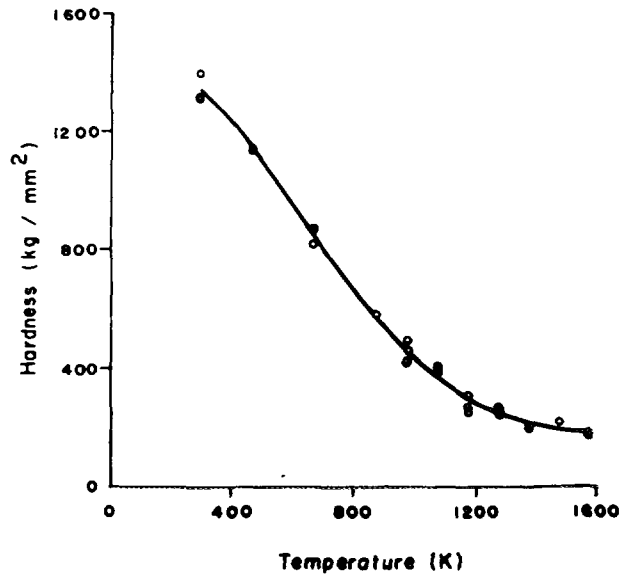
Fig. 3   Hot Hardness of $(U_{0.45}Pu_{0.55})C$ as a function of temperature
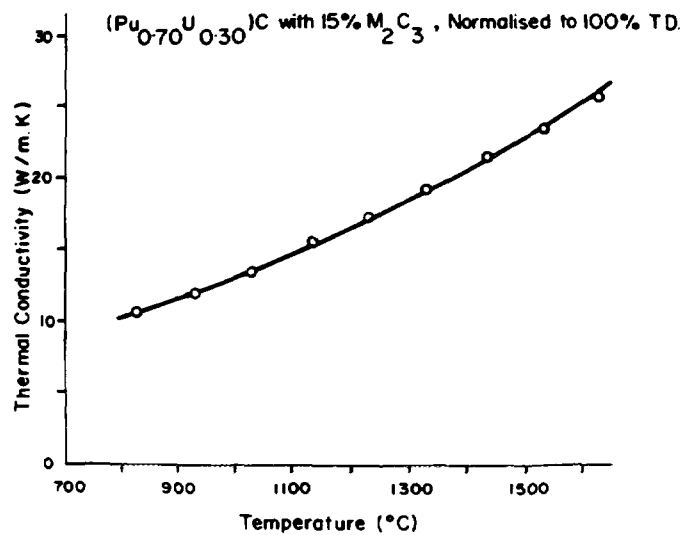
Fig. 4   Thermal conductivity of $(U_{0.3}Pu_{0.7})C$ as a function of temperature

Thermal conductivity of Mark I fuel is close to that of PuC whereas that of Mark II fuel is less compare to Mark I. It has been observed that when "UC" is being replaced by PuC the overall thermal conductivity decreases. However the lower thermal conductivity of Mark II fuel containing less amount of PuC, compare to that of Mark I fuel could not be explained at the moment.

One of the most important phenomena as seen from these figures is that the thermal conductivity of both Mark I and II fuel are low at lower temperatures but increases very rapidly with temperature. This sharp positive temperature coefficient helped in flattening the temperature gradient, across the fuel pin.

131

∇ RMD Measurement (1993)

RMD Measurement (1995)
(O Heating ● Cooling)
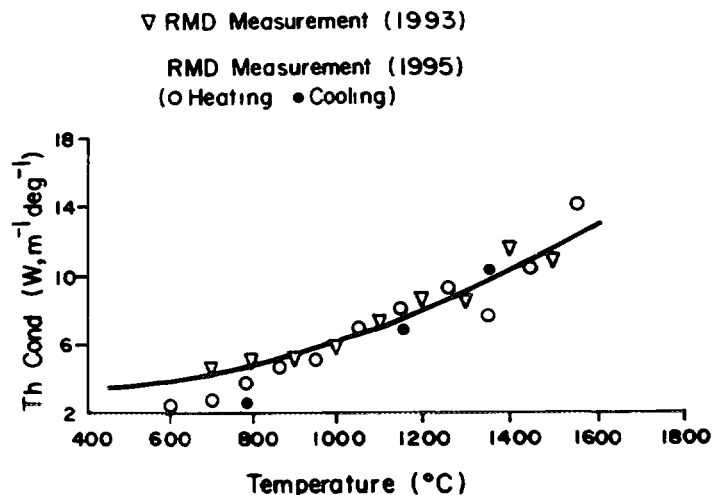
Fig. 5   Thermal conductivity of $(U_{0.45}Pu_{0.55})C$ as a function of temperature

Fuel performance modelling

The mixed carbide fuel is exposed to severe operating conditions which consist of high fission rate, high temperature and temperature gradient, fast neutron flux, high energy charged particles etc. A number of thermal, mechanical, chemical and metallurgical processes go on simultaneously inside the fuel and they interact with each other in a complex manner. In order to evaluate the performance of the fuel element during its irradiation in the reactor, a computer code is required. The out-of-pile thermophysical and mechanical properties of the fuel and cladding are important inputs for the fuel modelling codes. The out-of-pile materials property data generated in our laboratory are being utilised for the development of computer models for the FBTR fuel.

Thermal conductivity is one of the most important parameters for the calculation of the fuel centre temperature and radial temperature profile which in turn govern all the important processes e.g., fission gas atom diffusion and release, creep and swelling, restructuring, fuel and fission product redistribution etc. occuring inside the fuel are governed strongly by the temperature of the fuel. The out-of-pile data generated on thermal conductivity, linear thermal expansion, cladding thermal expansion and fuel density, along with other data taken from literature are being utilised to develop a computer programme based on finite difference method for calculating the fuel centre temperature and radial temperature profile in the FBTR fuel, as a function of its linear heat rating and burnup.

A microstructure dependent advanced fission gas release model is currently available in our laboratory for oxide (UO_2) and UO_2 $-PuO_2$ mixed oxide fuels. An attempt has been made in this model to include most of the important physical processes involved in the fission gas release mechanism operating in the fuel during irradiation. These include:

- diffusion of fission gas through the fuel grain,
- either as atoms or bubbles,
- sweeping of fission gas by the fuel grain boundary
- during grain growth process,
- irradiation induced resolution of gas bubbles,
- accumulation of gas atoms on the fuel grain boundary,
- nucleation and growth of bubbles on the grain boundary,
- interlinkage of grain boundary bubbles, and
- release of fission gases to the void space inside the fuel pin.

An output from the model is shown in Fig.6 which illustrates the behaviour of fission gas inside the fuel at an isothermal local temperature of 1600 K The straight line marked A in the plot represents
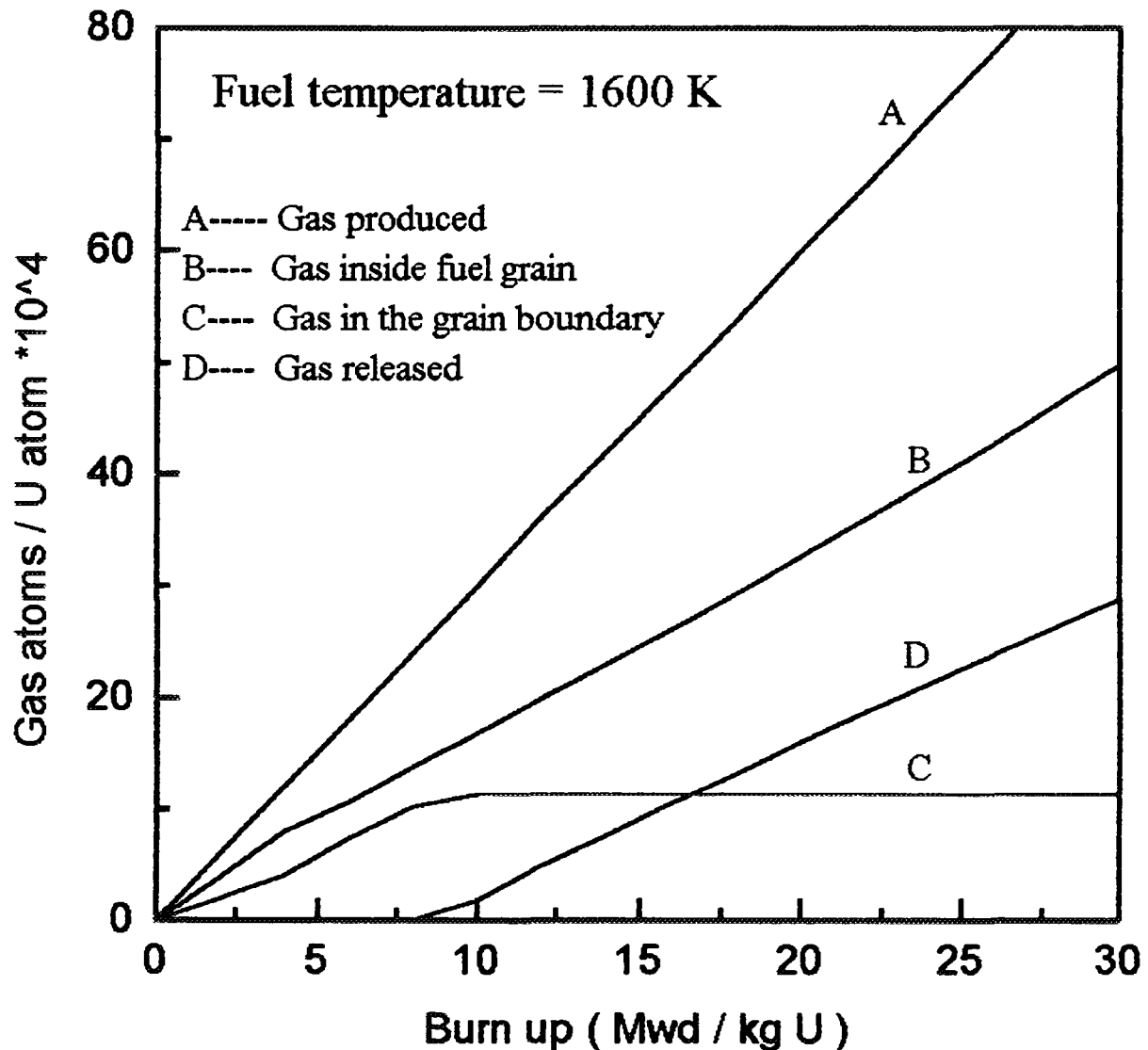
Fig. 6 Microstructure based fission gas release model

the fission gas generation in the fuel at a constant rate which is dependent on the local fission rate. Curve B and C show the partitioning of the fission gas between the grain interior and the grain bounadary. Curve D shows the gas release to open void space. It is observed from the plot that the fuel grain boundary gets saturated at a certain fuel burnup (which depends on the local fuel temperature) and there is no further increase in the grain boundary gas content thereafter. As soon as the grain boundary gets saturated, any further gas atom reaching the grain boundary is released to the open void space as the grain boundary cannot contain any more gas.

Discussion

The FBR's operate at higher fuel temperature and hence it is expected to release more fission gas. In oxide fuels most of the gases are released but in carbide fuels most of the fission gases are retained in the fuel matrix. The fission gas pressure has been calculated in two steps. First the fission gas generated is calculated and then the pressure developed in the plenum area and the temperature existing there by. The fission gas pressure calculated as a function of burn up for the FBTR fuel pin is

$P(Kg/cm^2) = 5.48146 \times 10^{-4} \times B + 2.6156$ (B in MWd/t)

For 50,000 MWd/t, fission gas pressure will be 30 bar.

The mixed carbide fuel has seen a burn up of about 25000 MWd/t and the post-irradiation data are yet to be obtained In the absence of the post irradiation data it is difficult to make definite conclusion quantitatively on the effect of the different thermophysical and thermomechanical properties on the control of fission gas relase. A model of fission gas release has however been developed for mixed $(U,Pu)O_2$ fuel. The same is considered to be used to predict the level of gas release in the mixed carbide fuel after its validation with post irradiation data on mixed carbide fuel.

The mixed carbide fuel having FCC(NaCl) structure is closed packed structure and is expected to swell more and hence fission gas relase will be less compared to that of mixed oxide fuel having more open CaF_2 structure.

The higher thermal conductivity of the carbide fuel and its strong positive temperature coefficient causes a flattening of the temperature gradient across the fuel cross-section. The mean volumetric temperature of the fuel will be low and hence fission gas release will be less

As already discussed the burn up has been divided into two stage. In the first stage there is fuel-clad gap closure by free swelling and in the second stage FCMI occurs For both free swelling and restrained swelling to occur, the material must be soften enough at the mean volumetric temperature of the fuel to undergo creep deformation so that the growth of fission gas bubble can be accomodated and its release can be prevented. Since for the relase of the fission gas, it has to migrate to the grain boundary a large grained fuel would give lower gas release. Similarly following the same reason a high density fuel retains more of fission gases, while porous fuel releases more of fission gas.

The high thermal conductivity of the carbide fuel minimises the mean volumetric temperature of the fuel which means the fuel becomes less prone to thermal creep deformation in the absence of sufficient thermal activation. However, for both free swelling and restrained swelling to occur the material should undergo creep deformation It has been found from the plot of hot hardness data with temperature that both the Mark I & Mark II fuels become soft enough to undergo creep deformation.

Thermal conductivity is one of the most important parameter for calculation of the central temperature and the radial temperature development. The accuracy and reliability of these data is an important factor in determining the strongly temperature dependent physical effects such as fission gas diffusion and relase, restructuring, creep deformation and thermal expansion.

Conclusions

Out-of-pile thermophysical and thermomechanical properties eg. thermal conductivity, thermal expansion and thermal toughness of mixed $(U_{0.3}Pu_{0.7})C$ and $(U_{0.45}Pu_{0.55})C$ carbide fuels for FBTR have been measured upto 1500°C These data are being utilised for development of models for performance evaluation of the fuel.

References

1   N.H. Brett and L.E. Russell, "The thermal expansion of PuO_2 and some other actinide oxides between Room temperature and 1000°C. Plutonium 1960, Clever Hume; London 1961, pp 397-410.

2   P G Palmer, USAEC Report HW 72245 (1962)

3.   M.A. De Crescent and A.D. Miller, "High temperature properties of Uranium Carbide", Proceedings of a symposium on carbide in Nuclear Energy, Harwell, U.K (1963) pp 342-57.

4   D Stahl and A Strasser, "Properties of solid solution of Uranium Plutonium carbides ibid, pp 373-91

5.   A E Ogard, C.C. Lawd and J.A Leen, "The thermal expansion of PuC and PuC-UC solid solution",   LA 2768 (1962).

6   M Tokar, A W Nutt and J.A. Leary, "Mechanical properties of carbide and Nitride Reactor fuels", LA 4452 (1970)

7.   M. Tokar, "High temperature compressive creep and Hot Hardness of Uranium - Plutonium carbides   LA - 4704 (1971).

8.   M. Tokar LA - DC - 72 - 187(1970).

9.   F.M. French and D.J. Hodkin, "Mechanical properties and compatibility of uranium-plutonium carbide", Plutonium 1965, Institute for Metals, London (1967) pp 697 - 720.

10.   J.A. Leary and K.W.R. Johnson, "Thermal conductivity of Uranium - Plutonium carbide Fuels", Nuclear Metallurgy 13, International symposium on Plutonium Fuels Technology, 1967 pp 309 - 21.

11.   J.B. Moser and O.L. Krugger, "Thermal Diffusivity of Actinide compounds" in Proceedings of the   7th Thermal conductivity Conference, Gaitherburg, Maryland, NBS Special Publication 302, 1967   p 461.

12.   M.J. Wheeler , E. King, C. Manford and H.J. Hedger, "Thermal diffusivity of U,(U,Pu) Carbides and   U oxide AERE-R-6499 (1970).

13.   H.D. Lewis and J.F. Kerrisk, "Electrical and thermal transport properties of Uranium and Plutonium   Carbides LA 6096 (1976).

14.   C. Ganguly, G.C. Jain, P.V. Hegde, U. Basak, R.S. Mehrotra, S. Majumdar and P.R. Roy, "Development and fabrication of 70% PuC-30%UC fuel for the fast breeder test reactor in India" Nuclear Technology Vol. 72, Jan. 1986, p 59.

15.   Fast Breeder Test Reactor Safety Report on Mark II Core (March 1995), IGCAR, Kalpakkam 603102.

16.   W.J. Parker, R.J. Jenkins, C.P. Buttler and G.L. Abbott, "Flash Method of Determining thermal diffusivity, heat capacity and thermal conductivity" J. Appl. Phys. 32[9], 1679-84 (1961).

17.   Clark L.M., Taylor R.E, J. Appl. Phys. 46(2), 714-719 (1975).

18.   "Science of Advanced LMFBR fuels" Ed : Hj. Matzke, North   Holland   Physics   Publishing, (1986).

FISSION GAS RELEASE OF URANIUM–PLUTONIUM MIXED NITRIDE AND CARBIDE FUELS

XA9745729

T. IWAI, K. NAKAJIMA, Y. ARAI, Y. SUZUKI
Department of Chemistry and Fuel Research,
Japan Atomic Energy Research Institute,
Oari-machi, Higashi-Ibaraki-gun, Ibakaraki-ken,
Japan

Abstract

Uranium-plutonium mixed nitride and carbide for advanced fast reactor fuels were irradiated at JRR-2 and JRR-2, and the fission gas release from these fuels were determined. It is confirmed from the irradiation tests that the application of the cold fuel concept to these fuels on the basis of their advantageous thermal properties may realize low fission gas release Furthermore, the introduction of the thermal stable pellets with dense matrix and relatively large pores can lower the fission gas release to a few percent up to the burnup of 5.5%FIMA In spite of the retention of fission gas release in the thermal stable pellets, no significant enhancement of the fuel-clad mechanical interaction was observed in the examined range of burnup It is also suggested that the open porosity would strongly influence the fission gas release from nitride and carbide.

1. Introduction

Uranium-plutonium mixed nitride and carbide fuels have been developed as advanced fuels for fast reactors(FRs) because of the advantage in their thermal stability caused from high thermal conductivity and high melting temperature [1]. Such thermal properties enable us to use these fuels at high heating rates over 800W/cm [2], but it is also an option to apply milder heating rates, according to so-called "Cold Fuel Concept" [3] In case of the irradiation at heating rates similar to those for MOX or metallic fuels, the central temperature of nitride and carbide fuels could be kept less than 1/2 - 1/3 of the melting temperatures in absolute temperature At Japan Atomic Energy Research Institute (JAERI), mixed nitride and carbidefuels have been investigated from the viewpoint of the collection of the basic data of these advanced FR fuels and also fuels for transmutation of minor actinides such as Np, Am and Cm

The research at JAERI covers fabrication technologies [4-6], property measurements [7-10], and irradiation tests [11-12]. Furthermore, studies on the electro-refining of nitride fuel started [13,14] as a pyrometallurgical reprocessing technology With regard to the irradiation tests, thermal stable pellets with dense fuel matrix and relatively large pores have been developed and supplied besides conventional type pellets. This report describes briefly the results of the irradiation tests of uranium-plutonium mixed nitride and carbide fuels, especially focusing on the fission gas release(FGR).

2. Program of irradiation tests

Uranium-plutonium mixed carbide fuel was planned to be irradiated in Japan Research Reactor-2(JRR-2) and Japan Materials Testing Reactor(JMTR) from 1983 to investigate the fundamental behavior of the advanced fuels for FRs. The irradiation tests of mixed nitride fuel were followed by those of carbide fuel and started from 1988. The program of the irradiation tests is shown in Fig. 1, which includes the irradiation at JOYO performed under a collaboration with Power Reactor and Nuclear Fuel Development Cooperation(PNC). Nine fuel pins of carbide fuel and 4 pins of nitride fuel were irradiated at JRR-2 and JMTR and the post irradiation examinations(PIEs) were carried out at the hot cells of Reactor Fuel Examination Facility of JAERI.

3. Fabrication of fuel pins and capsules

3 1 DESIGN OF FUEL PINS AND CAPSULES

All capsules containing nitride or carbide fuel pins were double-sealed, as the conceptual structure is shown in Fig. 2. An inner thermal medium was NaK and an outer one was made of an aluminum alloy so that the cladding temperature would be around 770K at the linear heating rate of 800 W/cm, the value of which is a design limit requested from the regulation for the research reactors. Several sets of thermocouple were inserted into the thermal media to monitor the burning of fuels. Main design parameters of fuel pins are as follows·

The bulk pellet density of about 85%TD(TD; Theoretical Density)
Plutonium enrichment of 20%
Cladding tubes of 20% cold work SUS 316 of 9.40 mm in diameter
Helium gas bonding

3 2 FUEL FABRICATION

Uranium-plutonium mixed carbide was synthesized by carbothermic reduction of the mixture of the dioxides with graphite at 1,723K in a vacuum. For comparison of the effects of carbon contents on the fuel behavior, two kinds of carbide pellets with different compositions were supplied for the irradiation tests; one of them had a nearly-stoichiometric composition; C/(U+Pu)1.00, and almost a single phase of fcc-structured monocarbide, (U,Pu)C. The other one had a hyperstoichiometric composition; C/(U+Pu) 1 10, and contained about 20 % of sesequicarbide, (U,Pu)2C3, in the matrix of monocarbide. The carbide discs obtained by the carbothermic reduction were milled, compacted and sintered at about 2000K in an argon gas stream. In the last irradiation campaign, the thermal stable carbide pellets were fabricated by use of pore former to obtain dense fuel matrix with relatively large pores without any significant change of pellet density of about 85%TD. Nickel metal

138

Test No.	Fuel	Reactor	No. of pins	Dia. (mm)	Linear power (kW/m)	Burnup (%FIMA)	'83	'85	'87	'89	'91	'93	'95	'97	'99
1	Carbide	JRR-2	2	6.5	42	1.2	▬ —								
2	Carbide	JRR-2	2	9.4	64	1.5	▬ —								
3	Carbide	JMTR	2	9.4	59	3.0			▬ —						
4	Carbide	JMTR	2	9.4	60	4.5				▬ —					
5	Carbide	JMTR	1	9.4	64	4.7				▬ —					
6	Nitride	JMTR	2	9.4	65	4.1						▬ —			
7	Nitride	JMTR	2	9.4	73	5.5						▬ —+			
8	Carbide	JOYO*	1	8.5	(80)	(4.5)								▬ —	
9	Nitride	JOYO*	2	8.5	(80)	(4.5)								▬ —	

* Under joint research program with PNC   ▬▬ Irradiation   —— PIE

Fig. 1   Irradiation program of mixed carbide and nitride fuels
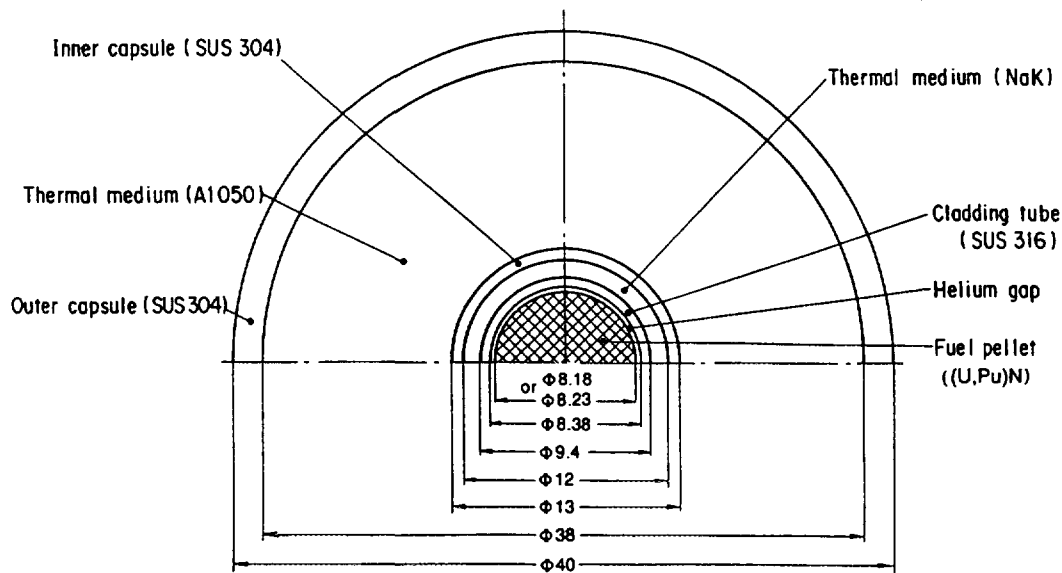
Fig.2   Conceptual design of capsules for irradiation of nitride fuel at JMTR

powder was added to carbide powder as a sintering aid before compacting in order to obtain dense matrix. The details of the fabrication process are described in earlier papers[4]. The microstructure of the conventional type- and thermal stable carbide pellets are shown in Photo. 1 to Photo.3.

Mixed nitride was also prepared by carbothermic reduction of the dioxides with graphite in flowing N_2-8%H_2 mixed gas at 1773K[5,6,11]. The mixing ratio of the dioxides and graphite, C/(U+Pu), was 2.50. The fabrication procedure of nitride pellets was similar to that of carbide fuel except the atmosphere condition for sintering. Pore former was added to nitride powder before compacting to make the thermal stable pellets. Since actinide nitrides originally show poor sintering characteristics, fine nitride powder ground by a tungsten-lining ball-milling was used for obtaining dense fuel matrix. No sintering aid was used in the case of the nitride pellet fabrication. The microstructure of the nitride pellet sintered in flowing Ar-8%H_2 gas is shown in Photo. 4.

The fabrication of fuel pellets was carried out in gloveboxes with an atmosphere of argon gas purified to impurity levels of less than 2 ppm and 5 ppm for oxygen and water, respectively, in order to protect the fine powder of carbide and nitride against oxidation.
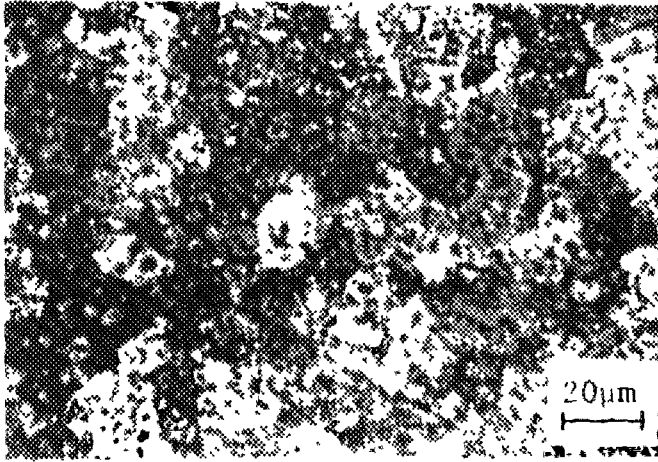
Photo.1 Microstructure of nearly stoichiometric mixed carbide pellet
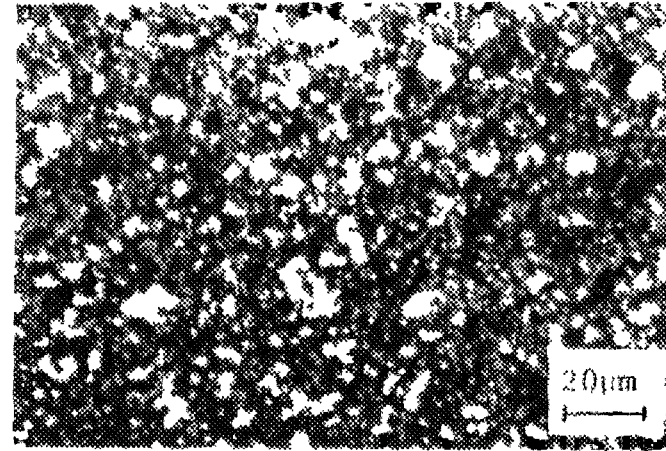
Photo 2 Microstructure of hyperstoichiometric mixed carbide pellet
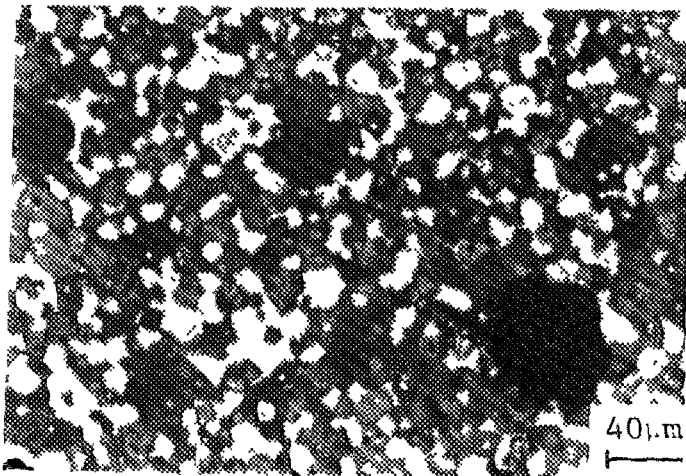
Photo.3 Microstructure of thermal stable carbide pellet
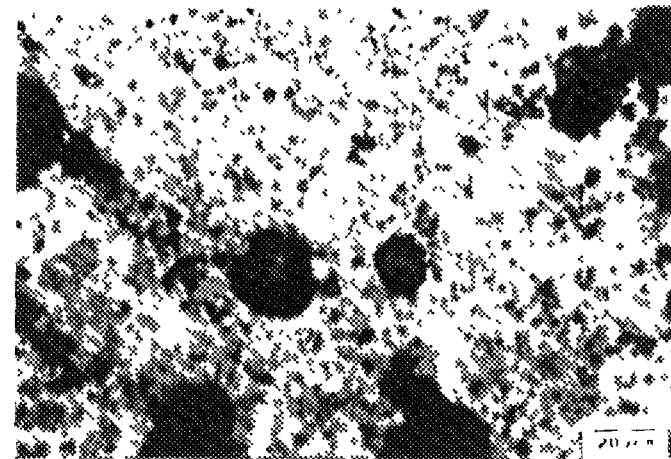
Photo.4 Microstructure of thermal stable nitride pellet

3.3 PIN PREPARATION AND ENCAPSULATING

After centerless-grinding and inspections, the pellets were inserted with thermal insulator pellets of uranium mononitride or uranium monocarbide and a plenum spring into the cladding tube of 20%C.W. SUS316 and an upper endplug was welded by TIG in a helium gas atmosphere. As an except, a cladding tube of 11Cr-2W ferritic stainless steel was used at the final irradiation of nitride fuel to investigate the effects of cladding materials on the fuel-clad mechanical interaction(FCMI). After the fabrication of fuel pins, one or two pins were encapsulated by Mechanical Engineering Division of JAERI.

The characteristics of the carbide and nitride fuel pins are shown in Tables 1 and Table 2.

4. Irradiation

The irradiation and post irradiation examinations(PIEs) were completed as scheduled without any trouble, although the nitride fuel of the last irradiation is still under examinations at present. The irradiation conditions are summarized in Table 3 and Table 4 The heating rate and burnup were estimated from the temperature of NaK and found to be lower than the scheduled one because of conservative capsule design. Therefore, actual heating rates were estimated to be 420 - 730 W/cm The maximum burnup was estimated to be 4 7% FIMA for carbide and 5.5% FIMA for nitride

5. Results of post irradiation examinations

5 1 CARBIDE FUEL

The items of the PIEs were shown in Fig.3. The destructive examinations of irradiated fuel pins were carried out at the cells with an argon gas atmosphere. The maximum burnup in the program was 4.7% FIMA and no pin failure was observed. The typical macrostructure of carbide pellets irradiated at JMTR are shown in Photo 5 to Photo.7. The results of PIEs of the carbide fuel are briefly summarized as follows:

The structure of the outer region was kept as fabricated, but in the inner region porosity increased as shown in the photographs.

No significant migration of actinide and FP elements was observed except fission gas such as Kr and Xe, and Cs.

Maximum diametric increase of fuel pins was in the range of 0.3 - 0.5 % at 3 - 4.7% FIMA as shown in Fig. 4.

Slight carburization of cladding material was induced by hyperstoichiometric carbide and a slight reaction of cladding material with fuel material was observed in the case of nearly-stoichiometric carbide

Table 1 Characterization of mixed carbide fuel irradiated at JRR-2 and JMTR

Capsule Name		ICF-37H		ICF-47H		84F-10A		84F-12A		87F-2A
Pin Number		37-1	37-2	47-1	47-2	10-1	10-2	12-1	12-2	-
Fuel										
Carbon content	(wt%)	4.70	5.21	4.66	5.09	4.67	5.16	4.67	5.19	5.09
Oxygen content	(wt%)	0.27	0.14	0.25	0.16	0.29	0.12	0.30	0.14	0.48
Ceq/(U+Pu)		1.00	1.09	1.00	1.10	1.02	1.10	1.02	1.10	1.14
Diameter (mm)		5.40	5.40	8.23	8.23	8.23	8.23	8.23	8.23	8.23
Density	(%TD)	89.7	93.3	83.1	83.7	84.6	81.5	83.0	82.2	86.7
Pu/(U+Pu)		0.201	0.201	0.194	0.194	0.194	0.197	0.202	0.198	0.196
Stack length	(mm)	96	96	60	60	100	100	100	100	180
Cladding Tube										
Outer diameter	(mm)	6.50	6.50	9.40	9.40	9.40	9.40	9.40	9.40	9.40
Thickness	(mm)	0.47	0.47	0.51	0.51	0.51	0.51	0.51	0.51	0.51
Pin										
Gap size (mm)	0.16	0.16	0.15	0.15	0.15	0.15	0.15	0.15	0.15	
Smear density	(%TD)	84.6	88.0	80.2	80.7	81.6	78.6	80.1	79.3	83.6
Total length	(mm)	185	185	170	170	250	250	250	250	390

Ceq; Carbon equivalent
%TD; % of Theoretical Density

Table 2 Characterization of mixed nitride fuel irradiated at JMTR

Capsule name		88F-5A		89F-3A	
Pin Number		5-1	5-2	3-1	3-2
Fuel					
Nitrogen content	(wt%)	5.56	5.56	5.42	5.42
Oxygen content	(wt%)	0.12	0.12	0.14	0.14
Carbon content	(wt%)	0.20	0.20	0.20	0.20
Neq/(U+Pu)		1.04	1.04	1.03	1.03
Diameter (mm)		8.18	8.23	8.23	8.25
Density	(%TD)	83.1	83.0	85.8	86.1
Pu/(U+Pu)		0.196	0.196	0.209	0.209
Stack length	(mm)	100	100	100	100
Cladding					
Materials		20%C.W.316SS		←	Ferritic SS
Outer diameter	(mm)	9.40	9.40	9.40	9.40
Thickness	(mm)	0.51	0.51	0.51	0.50
Pin					
Gap size (mm)		0.20	0.15	0.15	0.15
Smear density	(%TD)	79.2	80.1	82.5	83.2
Total length	(mm)	250	250	250	250

Neq; Nitrogen equivalent

Items	Pins	Pellets	Cladding
Visual inspection of fuel pins	O		
Profilometry	O		
Gamma scanning	O		
Puncture & FP gas collection	O		
Density measurement		O	
Metallography		O	O
Pore distribution		O	
Grain size measurement		O	O
Micro-gamma scanning		O	
Auto-radiography		O	
Hardness			O
Electron probe microanalyses		O	O
X-ray diffraction analyses		O	

Fig.3 Items of post-irradiation examinations of carbide

and nitride fuels at JAERI
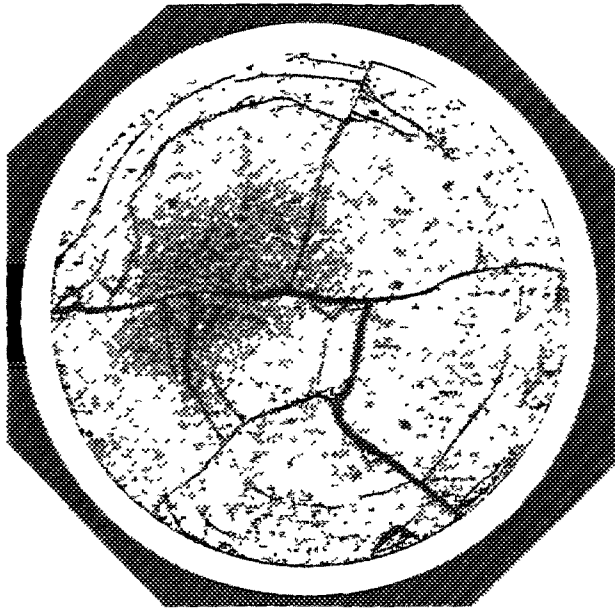
Photo.5 Macrostructure of nearly stoichiometric
mixed carbide pellet irradiated up to
4.5%FIMA
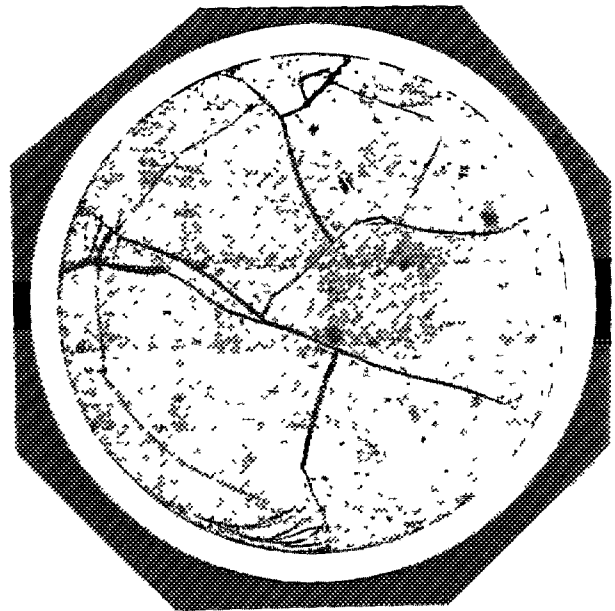
Photo.6 Macrostructure of hyperstoichiometric
mixed carbide pellet irradiated up to
3.7%FIMA
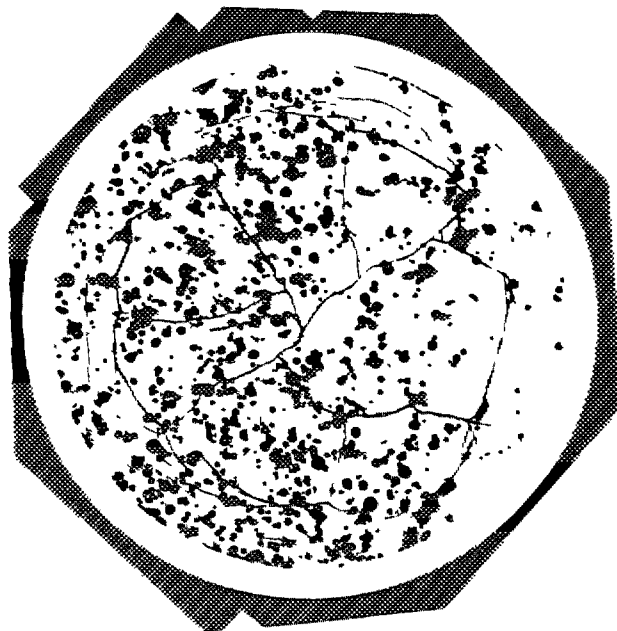
Photo.7 Macrostructure of thermal stable carbide
pellet irradiated up to 4.7%FIMA
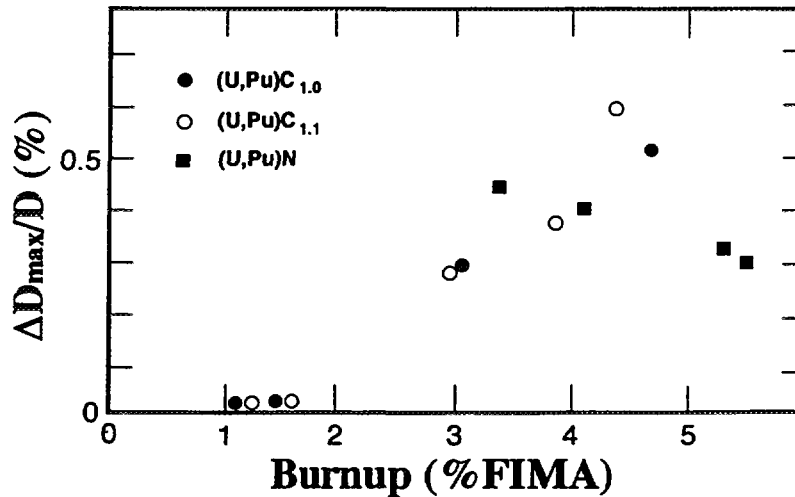
Fig.4   Maximum diameter increase of carbide and nitride fuels irradiated at JRR-2 and JMTR

Segregation of plutonium was measured in the fuel containing sesquecarbide.
Precipitation of Pd and Mo was observed.

The FP gas released from the pellets to plenum was collected by puncturing and its amount and composition were determined. The results are summarized in Table 5, where the first irradiation at JRR-2 was preliminary, so the pellets of high density of 90%TD and cladding tubes of 6.5 mm in diameter were used. It can be seen from the table that the carbide fuel shows the FGR rates of 2 - 3%/% FIMA except the irradiation of the first preliminary campaign and the last one. The latter irradiation test was carried out by using the thermal stable pellets and showed very low FGR; less than 1% at 4.7% FIMA.

The results on the FGR obtained by the irradiations in USA and European countries lie in the range of 10 - 30 % at 5% FIMA at the heat rates of 700 - 1200W/cm and smear densities of 75 - 80% TD[15]. Of course, FGR strongly depends on the fuel design and irradiation conditions, especially the fuel density and heating rate. The tests in USA and European countries were basically performed around the heating rates of 800W/cm or more. Considering the difference in heating rates, the present results obtained by us are considered to be in fairly good agreement with those reported previously except the case of the thermal stable pellets.

5.2 NITRIDE FUEL

Four pins of nitride fuel were irradiated at JMTR only by using the thermal stable pellets. The typical macrostructure after irradiation is shown in Photo.8, but it seems to be quite strange. It is presumed that such structure might be caused from an incomplete treatment of pore former at fuel fabrication although the structure before irradiation, which is shown in Photo. 4, was not so strange.

145

Table 3 Irradiation conditions of mixed carbide fuel

Capsule Name		ICF-37H	ICF-47H	84F-10A	84F-12A	87F-2A
Pin Number					12-1	12-2	
Reactor		JRR-2	JRR-2	JMTR	JMTR		JMTR
No. of cycle		6	10	12	17		17
Irradiation time	(hr)	1,543	2,655	6,143	8,748		8,924
Linear heat rate	(W/cm)	420	640	590	600	490	640
Central Temperature	(K)	1,270	1,420	1,490	1,530	1,370	1,510
Burnup	(GWd/t)	10	13	26	39	32	40
	(%FIMA)	1.2	1.5	3.0	4.5	3.7	4.7

Table 4 Irradiation conditions of mixed nitride fuel

Capsule name		88F-5A		89F-3A	
pin number		5-1	5-2	3-1	3-2
Reactor		JMTR		JMTR	
No. of Cycle		15		19	
Time	(hr)	7,626		9,972	
Linear heat rate	(W/cm)	650	535	700	730
Central temperature	(K)	1,770	1,470	1,710	1,740
Burnup	(GWd/t)	35	29	45	47
	(%FIMA)	4.1	3.4	5.3	5.5

Table 5 FGR data of mixed carbide fuel irradiated at JRR-2 and JMTR

| Capsule name | | ICF-37H | | ICF-47H | | 84F-10A | | 84F-12A | | 87F-2A |
Pin Number		37-1	37-2	47-1	47-2	10-1	10-2	12-1	12-2	
FGR	(%)	0.4	0.1	9.4	9.4	6.1	13.7	7.1	15.5	0.6
Porosity										
Before irradiation	(%)									
After irradiation	(%)									
Open porosity		1.3	0.5	11.5	11.0	9.7	12.3	9.7	11.8	2.2
Closed porosity		11.3	8.6	7.8	6.7	9.0	8.4	11.4	8.5	15.1
Grain size										
Before irradiation	(μm)	-	-	6.3	2.8	4.0	2.7	-	-	-
After irradiation	(μm)									
Outer region		10.6	7.9	2.9	2.8	3.7	3.0	2.5	2.8	10.6
Intermediate Region		10.5	7.5	3.8	3.9	4.7	3.1	2.6	3.2	10.6
Inner Region		14.3	7.3	6.3	4.9	5.3	3.2	7.0	3.3	10.9

At present, the results of PIEs of nitride fuel are under analysis, but the features of fuel behavior observed in the present irradiation tests are briefly summarized as follows:

Precipitation of Pd was observed.

Actinide and FP elements did not migrate significantly.

No significant reaction of fuel material with the cladding tubes was observed.

Maximum diameter increase of fuel pins was smaller than those of carbide fuel (see Fig.2).
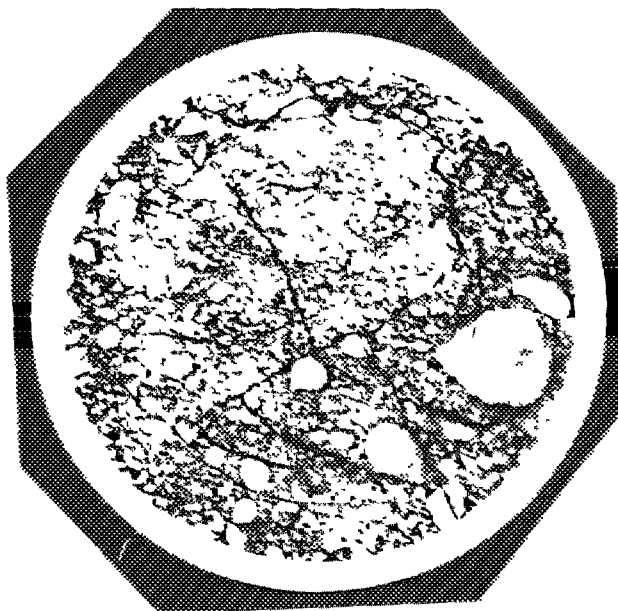
Photo.8   Macrostructure of thermal stable nitride
pellet irradiated up to 5.5%FIMA

The results of the FGR from the mixed nitride fuel irradiated at JMTR are shown in Table 6 and Fig 5 summarizes the results of the FGR from nitride and carbide fuels obtained from the present irradiation program. The factors controlling the FGR from nitride fuel could not be determined in this campaign, since only the thermal stable pellets were irradiated and their structure seemed to be strange. In spite of this negative condition, the nitride fuel was confirmed to show very low FGR of a few percent at about 5%FIMA. Further depression of the FGR of nitride fuel might be expected by proper handling of pore former, as the thermal stable carbide pellets showed the FGR of less than 1%.

This low FGR of nitride fuel observed in the present studies can be explained by both of the low fuel temperature and the stability of the structure. Although the structure shown in Photo.8 seemed strange, the open porosity was much smaller than those of carbide pellets fabricated without pore former. Therefore, it is suggested that the nitride pellets still kept the features of the thermal stable pellets. As pointed out by Blank[3], fuel temperature of carbide and nitride pellets decreases with irradiation up to the burnups of 2 - 3 % FIMA because of the increase of the gap conductance and

148

keeps a constant value after the closing of the gap. Figure 6 shows the change of the central temperature of nitride fuel during the irradiation at JMTR, where the temperature was measured by a set of thermocouple inserted into the central holes of fuel pellets. It is understood from the figure that the gap seemed to close around 2 - 3 % FIMA and fuel temperature continued to decrease till the burnup.
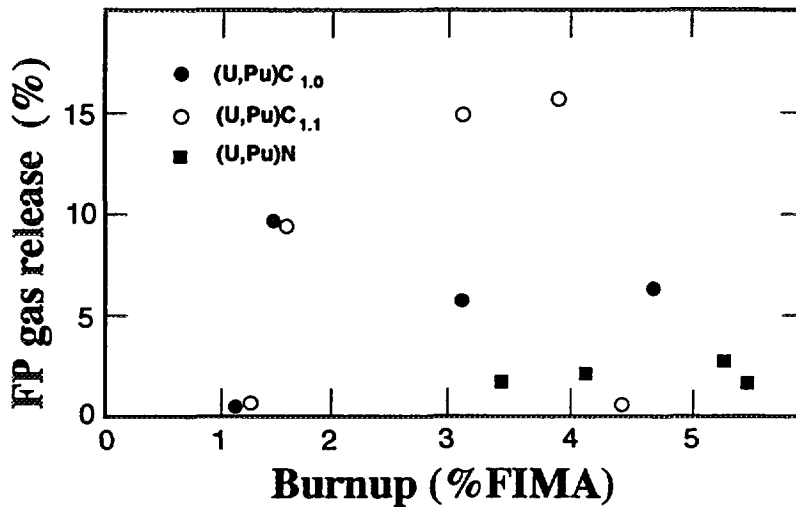
Fig.5   Fission gas release from carbide and nitride fuels irradiated at JRR-2 and JMTR
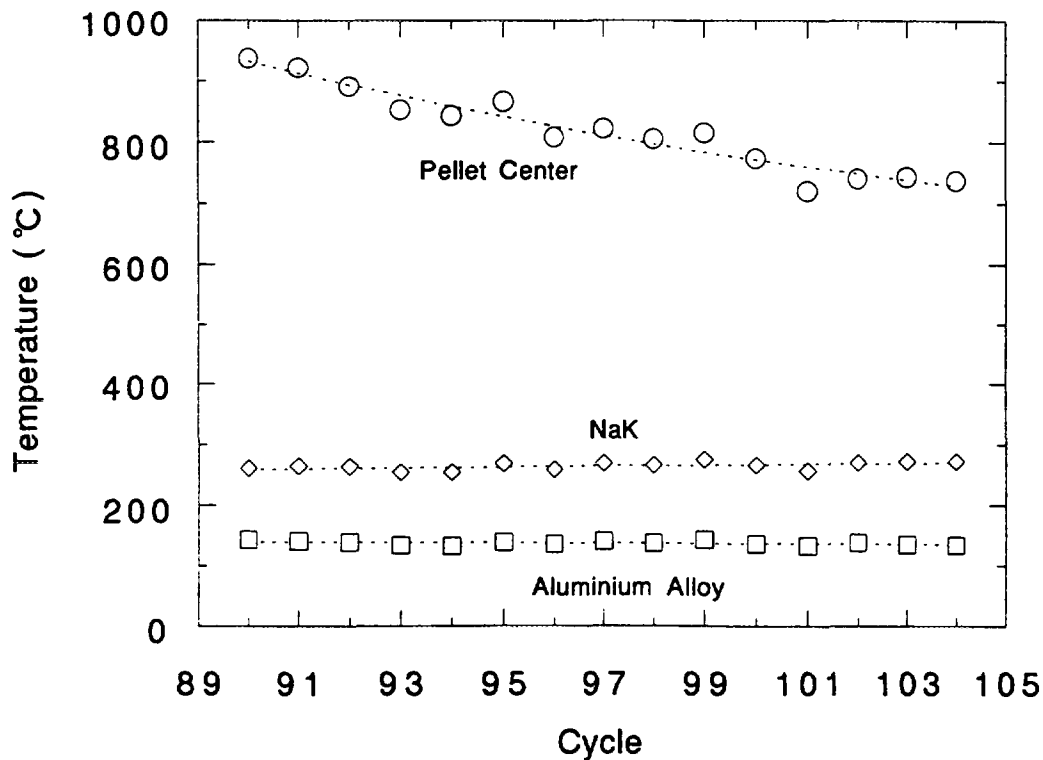
Fig.6   Temperature change at fuel center and thermal media under irradiation of nitride fuel at JMTR

149

6. Discussion

6.1 THERMAL STABLE PELLETS

The thermal stable carbide pellets irradiated at JMTR showed very low FGR of less than 1% at 4 7%FIMA as expected The reason why the pellets showed very low FGR might be explained by the stability of the fuel matrix. It is also found that the FGR from nitride pellets was very low, although the fuel pellets showed a strange structure perhaps because of the improper addition of pore former. Further improvements of fabrication technology of the thermal stable nitride pellets might make the FGR negligibly small. The values of the FGR from the thermal stable pellets of carbide and nitride are much lower than those of carbide pellets fabricated by a conventional route without pore former and also the results of irradiation tests in USA and European countries. It is considered that the lowering of the FGR has been realized by the introduction of the thermal stable pellets as well as the adoption of the cold fuel concept.

6.2 EFFECTS OF SECOND PHASE AND POROSITY

Comparing the FGR of the carbide fuel irradiated in the present program, the pellets containing sesequicarbide as a second phase had a tendency to show larger FGR. The presence of sesquicarbide might disturb the grain growth of the monocarbide during sintering at the fabrication process. It would be common that the small grain sizes have a tendency to enlarge the FGR because of shorter distance for diffusion of fission gases to the boundaries. The reason why hyperstoichiometric carbide fuel showed large FGR might be explained by the presence of sesquicarbide. However, the difference in the grain size between both carbide fuel pellets was not so large. On the other hand, the thermal stable pellets of carbide showed very low FGR as shown in Table 5. These pellets had a hyperstoichiometric composition but large grains because of use of a sintering aid Therefore, it is too easy to explain the difference in FGR only on the basis of the presence of the second phase.

The porosity after irradiation were determined in the present study as shown in Table 5 and Table 6. It is easily understood that the thermal stable pellets have very low open porosity. The pores introduced by the pore former seem to stay close for the pellet surface and the fission gas was considered to be retained in the fuel matrix In the case of carbide pellets fabricated without pore former, hypersotichimetric carbide pellets had larger open porosity. It is suggested from the comparison of the porosity that the FGR depends on the open porosity rather than the presence of a second phase or grain size. The results of the effect of open porosity on the FGR are in fairly a good agreement with those reported on the nitride fuel, which shows rapid increase of FGR when the open porosity exceeds 10%[16]. Of course, there is some possibility that the formation of open porosity might be caused from the pressure of sesquicarbide. The controlling of the open porosity should be a key technology to lower the FGR.

150

Table 6 FGR data of mixed nitride fuel irradiated at JMTR

| Capsule name | | 88F-5A | | 89F-3A | |
Pin Number		5-1	5-2	3-1	3-2
FGR	(%)	2.9	1.8	2.8	1.7
Porosity					
Before irradiation	(%)				
After irradiation	(%)				
Open porosity		8.8	8.7	5.1	4.3
Closed porosity		11.2	10.2	13.3	12.7
Grain size					
Before irradiation	(μm)				
After irradiation	(μm)				
Outer region		4.0	3.7	+	+
Intermediate Region		3.9	3.6	+	+
Inner Region		3.6	4.2	+	+

+: under analysis

6.3 FUEL CLAD MECHANICAL INTERACTION

In the design of MOX fuel, almost all of FP gas generated would be released in the gas plenum, especially at high burnups, although the outer region still keep some fission gas in fuel matrix. In addition the creep rate of MOX fuel is relatively large so that the life of the fuel might be controlled by either the increase of inner pressure and/or the swelling of cladding materials. On the other hand, the FGR from the carbide and nitride fuels are confirmed to be lowered by adoption of the cold fuel concept. Especially FGR of the thermal stable pellets was found to be negligibly small at least up to 5.5%FIMA. It is well known that FP gas retained in the fuel matrix has a tendency to enlarge the fuel swelling. Since nitride and carbide have relatively low creep rates, the FCMI would become important for fuel design.

In the present study, the maximum increase rates of fuel diameter were 0.2 - 0.3%/% FIMA or less after the closing of fuel-cladding gap, as shown in Fig. 4. The values are equivalent to or lower than those reported from the irradiation of carbide and nitride, D/D of 0.3-0.8% at 5% FIMA[17] and 0.48%/% FIMA[18], respectively. Therefore, at least up to the burnup of 5.5% FIMA, the FCMI would be not essential in spite of the depression of FGR. At higher burnups, especially over 10%FIMA, there is some possibility that the FCMI caused from the swelling due to retained gases and solid FPs would become significant. It cannot be concluded that the large pores in the thermal stable pellets can take a role for accommodation of gas swelling. Furthermore, the temperature increase at transition conditions might enlarge fuel swelling. Therefore, it is necessary that the data of irradiation should be collected from the viewpoint of FCMI.

7. Conclusions

The irradiation tests of nitride and carbide fuels at JRR-2 and JMTR have been performed at JAERI to investigate the fuel behavior of these advanced fuels. From the tests we can conclude on the FGR as follows:

(1)   The carbide pellets fabricated by a conventional route showed the FGR rates of 2 -3%/% FIMA, which is considered to be equivalent to those in literature.

(2) The thermal stable pellets of carbide and nitride fuels, which were fabricated by use of pore former, showed very low fission gas release of less than 3 % at 4 - 5.5% FIMA.

(3)   It is suggested that the fission gas release of carbide and nitride fuels might be controlled by open porosity.

(4)   The acceleration of fuel-cladding mechanical interaction by the depression of fission gas release was not essential at least up to 5.5% FIMA.

In addition to the irradiation tests in JRR-2 and JMTR, the thermal stable pellets of carbide and nitride fuels are being irradiated to goal burnups of about 4.5%FIMA at the fast experimental reactor JOYO under collaboration with PNC. The analyses of the FGR and the other behavior of these fuels are programmed by combining the results from the irradiation at JOYO with those at JRR-2 and JMTR.

Acknowledgments

References

1 Hj Matzke, "Science of advanced fuel", North-Hollands, Amsterdam (1986).

2. H. Blank, M. Coquerelle, I.L.F.Ray, K. Richter and C.T. Walker, Proc. on Reliable Fuels for Liquid Metal Reactors, Tucson, Sept. 7-11, 1986, p7-15.

3. H. Blank, J.Less-comm. Met., 121(1985)583.

4 Y.Suzuki, Y. Arai and T. Sasayama, J.Nucl. Sci. Technol., 20(1983)603.

5. Y. Arai, S. Fukushima, K. Shiozawa and M.Handa, J.Nucl. Mater., 168(1989)280.

6. Y. Arai, S. Fukushima, K.Shiozawa and M.Handa, IAEA-TECDOC 466(1987) p.25.

7. Y. Arai, Y.Suzuki, T. Iwai and T. Ohmichi, J. Nucl. Mater., 195(1992)37.

8. Y. Suzuki, A. Maeda, Y. Arai and T. Ohmichi, J. Nucl. Mater., 188(1992)239.

9. Y. Arai, T.Ohmichi, S. Fukushima and M.Handa, J.Nucl. Mater., 168(1989)137.

10. Y. Arai, M. Morihira and T.Ohmichi, J. Nucl. Mater., 202(1989)70.

11. Y. Arai, Y. Suzuki, T. Iwai, A. Maeda, T. Sasayama, K. Shiozawa and T. Ohmichi, J. Nucl. Sci. Technol., 30(1993)624.

12. Y. Arai, Y. Suzuki, M. and Handa, Proc. on Evaluation of Emerging Nuclear Fuel Cycle System; GLOBAL' 95, Paris, Sept. 11-14, 1995, p.538.

13. M. Handa, N. Kobayashi and H. Katsuta, JAERI-RDIPE Seminar on Lead Cooled Fast Reactor, Moscow, Oct.27-28, 1993.

14. Y. Suzuki, T. Ogawa, Osugi, Y. Arai, and T. Mukaiyama, to be published in Proc. on 4th OECD/NEA International Information Exchange on Pertitioning and Transmutation, Mito, Sep.10-13, 1996.

15. R. J. Herbst, R. W. Straton, Proc. on Reliable Fuels for Liquid Metal Reactors, Tucson, Sept. 7-11, 1986, p.7-1

16. A. A. Bauer, J. B. Brown, E.O. Fromn and V.M.Storhok, Proc. on Fast Reactor Fuel Element Technology, New Orleans, Apr.13-15, 1971, p.785.

17. R. L. Petty, T. W. Latimer, Trans. Am. Nucl. Soc., 39 (1981)413.

18. A.A. Bauer, P.Cybulskis, R.L.Petty and N.S. DeMuth, Proc. on Fast Breeder Reactor Fuel Performance, Monterey, Mar. 5-8, 1979, p.827.

MONONITRIDE FUEL AND LARGE SCALE NUCLEAR POWER INDUSTRY

V.V. ORLOV, A.G. SILA-NOVITSKY, V.S. SMIRNOV,
V.S. SKIKUNOV, A.I. FILIN, V.V. NAUMOV, S.V. BULAVKIN
RDIPE,
Moscow

B.D. ROGOSKIN, M.G. SHISHKOV, O.N. DUBROVIN,
N.M. STEPENNOVA, Y.E. FEDOROV
All Russian Scientific and Research Institute of Inorganic Materials,
Moscow

Russian Federation

Abstract

Work to study nitride fuel, conducted in Russia a long time, has indicated interrelation between operational properties, including the data of gas fission release, the content of impurities and synthesis processes. Recommended method production fuel from initial metal, as more profitable that one from initial oxide, needs development of electro-chemical reprocesing with metal as end product and contributory to nonproliferation and cost efficient fuel cycle Irradiation tests UN have shown no fission gaseous bubble within the lead sublayer.

Taking as example the core design of BREST reactor of 300 MW(e) power there have been shown a possibility to put into reality a principle of nature safety in fast reactor by using inherent properties of U-Pu mononitride fuel (high density and thermal conductivity, low fission gas release and swelling) and lead coolant (low neutron absorption and moderation, high density and boiling temperature, chemical passive) as well as original technical solution on core major component (passive self-regulatory).

1. Introduction

Natural safety features of a reactor are largely dependent on the fuel composition properties, such as density (CBR=1), heat conductivity (moderate temperatures, power effect of reactivity, fission gas release and its pressure on fuel claddings), radiation resistance, critical temperature margin (melting, disintegration, interaction with claddings and coolant). It is important to note that increased power density, which previously was a major incentive to studying fuel with high heat conductivity (monocarbide, mononitride, carbonitride, metallic fuel), can no longer motivate its use for inherently safe reactors

With priority given to the fuel properties related to its in-pile performance, it is also necessary to take into account the properties associated with fuel handling outside reactors, such as ability to manufacture and to reprocess with regard to minor actinides incorporated in the fuel and to the economical efficiency of the fuel cycle.

The extent of practical experience with a certain fuel in nuclear engineering and industry is an important, but not a dominant factor for future developments. In the light of all the requirements, mononitride fuel was judged to be the best option for the lead-cooled fast reactor despite its disadvantages associated with considerable neutron absorption in the ^{14}N (n, p) ^{14}C reaction with formation of hydrogen and environmentally hazardous ^{14}N. This shortcoming can be subsequently largely alleviated with the use of nitrogen enriched with the ^{15}N isotope, which economical estimates show to be acceptable and even beneficial.

2. Mononitride fuel

2 1. RADIATION TESTS OF MONONITRIDE FUEL

Radiation tests of uranium and mixed uranium-plutonium mononitride fuels have been carried out in Russia and abroad on a smaller scale than those of monocarbide fuel. The tests involved first individual fuel rods, then fuel assemblies and finally a fully loaded core BR-10 reactor [1, 2, 3].

The irradiated fuel rods had helium and sodium sublayers. Mononitride have be used in the form of pellets with theoretical density of 82...95% and microspheres with bulk density in fuel rods of 10...11 g/cm^3. The oxygen and carbon percentage in fuel varied from 0.05 to 0.6% and from 0.04 to 0.5%, respectively.

Linear heat rate in those tests varied widely from 200 to 500 W/cm. The temperature in the pellet centre ranged from 1450 to 2500 K depending on the fuel rod design and irradiation conditions. Radiation tests of the fuel were conducted with burn up between ~0.5 and 15% h.a. The rod core diameters varied between 5 1 and 7.65 mm. Radiation tests have been carried out at fast and thermal reactors, i.e., BR-10, BOR-60, SM-2, MIR, MTR, ETR, EBR, DFR, RHAPSODY, PHOENIX, etc.

Generalized data from the radiation tests are presented in Ref. [1].

The radiation tests of the mononitride fuel yielded the following main results:

1 All the domestic and foreign experiments showed good compatibility of uranium mononitride and mixed fuel with austenitic steels at surface cladding temperatures of 920...980 K up to the burn-up of 15 % heavy atoms (h.a.), although affected areas on inner surfaces of claddings were detected in many experiments. Chemical analysis pointed to carbonizing as their cause. It may be mentioned besides that use of highly pure mononitride (with oxygen and carbon accounting for less than 0.2% each) resulted in 2.2 to 2.5 times lower carbonizing. No iodine or caesium corrosion was observed. Caesium release from fuel did not exceed 5 % of the quantities produced.

2 Mononitride fuel rods with helium and sodium sublayers tested in the BOR–60 reactor, reached design burn-up at heat rates of 380 to 1300 W/cm, cladding temperatures of 910 to 980 K, and neutron fluence of up to 4.7•10^{22} n/cm^2 (with E>0.1 MeV). At the same time, degradation of mechanical properties of claddings was observed with burn-up above 6 % h.a. The greatest increase in the fuel rod diameter found 10...60 mm above the core centre, did not exceed 1 4 % The cladding ellipticity in this region was 0.05 mm, with outside diameter making 8.3 mm and thickness 0.4 mm.

3. Most important characteristics of fuel are its swelling and release of fission gas depending on the temperature, burn-up and density. It is an established fact that purer fuel in terms of oxygen and carbon content shows less swelling. Thus, swelling of mononitride fuel with density of 91% TD, burn-up of 7.6% h.a., and oxygen and carbon content of less than 0.2% each, amounts to 1.2...1.5% per 1% of burn-up at a temperature of 1710...1740 K in the centre, whereas swelling of fuel containing 0.4...0.5% of oxygen and 0.3...0.4% of carbon, comes to 1.9...2.5% per 1% of burn-up [2].

Under similar conditions, fission gas release is almost half as great with very pure mononitride fuel as it is with fuel containing oxygen and carbon — each in excess of 0.3...0.4% (23...25% and 45...50% of the quantities produced, respectively).

The data presented in [4] practically coincide with the above results. The swelling of mononitride fuel with density of 85% and 95% OD, and burn-up of about 15% h.a. in a thermal spectrum reactor with a heat rate of 1000...1300 W/cm and temperature of 1470...1510 K in the rod core centre, is 1 1% and 1.3% per 1% of burn-up, respectively, in case of fuel rods with a sodium and a helium sublayer.

Thus, mononitride fuel of high purity swells less and has better retention of fission products

Temperature increase in the centre of the rod core leads to greater swelling and fission gas release.

4 In the IVV-2 reactor ampoule irradiation testing UN fuel with content impurities until 0,15 % GFP has consisted less 10 % (burn-up above 0,5 %, temperature in centre less 1100 K) without fission gas bubble creation in lead sublayer (reported by L Menkin on Scientific Meeting Sverdlovsk's Division of RDIPE, Belojarka, 1996)

2.2 TECHNOLOGY FOR PRODUCTION OF MONONITRIDE

The two main methods of mononitride fuel synthesis [5] under development use the following starting materials:

a) uranium and plutonium oxides and

b) metallic uranium and plutonium.

Both methods may be used to fabricate fuel pellets of different density, although fuel fabrication on more than 90 % TD from oxides is more labor-consuming than that of metals Minimum content of impurities were observed in mononitride fuel fabricated of metals.

The technology of fuel fabrication is largely dictated by the chosen regeneration technique and its end product which serves as a source material for fuel refabrication (Fig. 1).

Mononitride fuel can be regenerated with the use of the hydrometallurgical technique (Purex process) which practically has the world monopoly for reprocessing of oxide fuel. Studies carried out in the USA, Western Europe, Japan and Russia show that mononitride fuel can be reprocessed by this method using practically the same equipment as in regeneration of oxide fuel [6, 7, 8] This accounts for most foreign countries using uranium and plutonium oxides as source materials for mononitride fuel production [9, 10].

The advantages of nitride fuel with low oxygen content and the on-site fuel cycle envisaged in the BREST design call for considering and developing nonaqueous reprocessing methods the benefits of which are demonstrated by the results of the US effort with the IFR concept [11] and by the work at NIIAR in Russia [12].

The need for new methods of fuel reprocessing is dictated also by the requirements of nonproliferation of nuclear weapons, associated with the expected expansion of nuclear energy uses in the world.

Mononitride fuel has higher electrical and thermal conductivity, lower Gibbs energy and, apparently, higher solubility in halides. Based on these properties and using the data of the Argonne National Laboratory on electrochemical regeneration of alloyed mixed metal fuel (U+Pu+Zr+Fs) in molten halides, the A. A Bochvar Institute of Inorganic Materials set to develop the electrochemical process of mononitride fuel regeneration in melts. The early results are encouraging, but longer test are required [13]

Electrochemical regeneration of irradiated mononitride in melts, should be implemented, can prevail as the most inexpensive and space-saving process wherefore it is regarded as the basic option for the lead-cooled fast reactor under design.

3. Large-scale nuclear power industry requirements

In view the coming century world energy and fuel problems we should come back the concept of large-scale nuclear power industry (NPI) as the most real way to stabilize and decrease.

Creation of large-scale NPI [14] is possible only in case of radical enhancement of NPP safety and accompanying productions, preserving economic competition capacity of NPI as well as substantial increasing the efficiency of utilization of uranium and going over to fuel breeding Realization of this way depends in our efforts·

- to define the economic and safety requirements and to choose an adequate technology;

- its engineering development and demonstration in next few decades.

Requirement to nuclear technology [15] consists the following main propositions.

Control member characteristics

Parameter	Parameter value			
	Scram 1	AR	S	PAP
Maximum efficiency of a control member, $\Delta K/K$	0.07	0.022	0.025	0.07
Number of control members	8	4	12	16
System efficiency, $\Delta K/K$, per cent	0.52	0.08	0.30	1.06
($)	(1.44)	(0.22)	(0.83)	(2.94)

```
┌─────────────────────┐        ┌─────────────────────┐
│ Fabrication of       │        │ Fabrication of       │
│ mononitride          │        │ mononitride          │
│ fuel from oxides      │        │ fuel from metals      │
└─────────────────────┘        └─────────────────────┘
              ┌─────────────────────┐
              │ Assembly of fuel rods │
              │ and bundles           │
              └─────────────────────┘
              ┌─────────────────────┐
              │ BREST-300 fast reactor│
              │ with lead coolant     │
              └─────────────────────┘
┌─────────────────┐            ┌─────────────────┐
│ Uranium and      │            │ Metallic uranium │
│ plutonium oxides │            │ and plutonium    │
└─────────────────┘            └─────────────────┘
        Nitrogen 15   Fuel reprocessing    Nitrogen 15
┌─────────────────────────┐  ┌─────────────────────┐
│ Hydrometallurgic         │  │ Electrochemical      │
│ reprocessing             │  │ reprocessing in melts│
│ Purex-process            │  │                      │
└─────────────────────────┘  └─────────────────────┘
        Wastes                      Wastes
```

Fig. 1 Schematic of the fuel cycle

- Natural safety is the safety provided mainly by fundamental law of nature and inherent properties of fuel, coolant and other reactor components with deterministic and completely avoiding the most dangerous accidents for example TMI and Chernobyl ones (fast runaway, loss of coolant, fires, steam and hydrogen explosion) with catastrophe release of radioactivity. Due to internal and external causes, including terrorism. Any accident possible to occur is under consideration as design basis one expect nuclear impacts and natural events with reliable determine probability lower than 10^{-6}. With the catastrophes prevented, the problem of NPP safety becomes just a more ecological-economical problem.

- The deterministic safety requirement to radwaste management technology lie in observance of natural radiation equilibrium at their disposal which can be attained by transmutation and storage.

- The problem of nonproliferation, in view of possible U enrichment, has no deterministic solution within the nuclear technology and demands political measures. The new nuclear technology shall contribute to implementation of such measures, making in more difficult to produce and recover Pu from cycle for further weapon application and facilitating the inspection. Fuel cycle technology excluding both weapon-grade Pu and U, Pu and MA separation may be physical protection against fuel thefts.

- Uranium consumption should be reduced by an order as compared to current LWRs, which corresponds to BR close to 1 or higher without requirement short Pu double time.

- Generation of nuclear power shall remain economically profitable both for developed and developing countries. For example, the current LWR generation cost seems reasonable limit.

The requirements seem to be contradicting and difficult to be fulfilled as a whole. However, safety and economy can be harmonized, if the inherent safety points are applied as early as at conceptual design stage.

4. Lead-cooled fast reactor

Realization of the natural safety principles without getting out for of technology mastered current NPI has been demonstrated to substantial extend in conceptual designs of LCFRs of 300-1200 MW(e) power, developed by RDIPE with other Russian institutes participation.

The conceptual calculation and design stage BREST-300 reactor with CBR≈1 has been completed last year and besides a comprehensive experience with LMFR and Pb-Bi cooled naval reactors based on critical assembly experiments, stele corrosion test on Pb loop, technology works and some ones [13, 15, 16, 17, 18, 19].

Fig. 2, 3 present the design scheme of two-circuits cooling BREST-300 reactor. Secondary circuit is using water-steam of supercritical parameters ($T_{inlet}\cong610$ K, $T_{outlet}\cong790$ K).

BREST-300 reactor core (Fig. 4) comprises 185 FAs (Fig. 5) of three types and is surrounded by 164 blocks of lead reflector.

Fig. 5 presents relative distributions of inlet and outlet coolant velocities and its temperature at reactor core outlet.

Control members are taken out of reactor core and located in the fist row of reflector to provide refuelling under control of scram.

Main parameters of fuel elements and FAs loading, determined for fuel microcycle duration of ~1 year, are presented in table 1.

Azimuthal peak power ratio is similar for all the shaped subcores and is 1.18

FA (Fig. 5) comprises 114 fuel rods and 7 bearing elements. FAs are centred and fixed in pits of support cylinders. FA fastening mechanism is controllable one with ball contact bearings, self-tightened under way of operation.

Guiding tubes installed at heads of adjoining FAs are used to load and unload FA out of reactor core. Therewith axes of adjoining FAs are deflected of their vertical position resulting in creation needed gaps for FAs refuelling that excludes damage both adjoining FAs and loading one.

Applied scheme of FAs refuelling and fastening does not provide reassured reactor core stiffness due to loading interval by imposing mechanical interactions, so the present authors applied

hydraulic damper reducing power of which rises as action frequency increases. Therewith stability of entire reactor core is provided for frequency more 1 Hz and lateral overloading up to 1.2 g. Reactor core stability is achieved by terminating the loading onto the shell of stationary reflector. Calculation estimates showed more 12 Hz value of frequency of damped FA that is higher the most hazardous frequency range in case of earthquake.

At the level of FA heads there are spacer devices provided for FA position stability under hydrodynamic effect of coolant.

1—pump   7—separating shell
2—vessel   8—fuel storage
3—thermal shielding   9—steam generator
4—CPS   10—safeguard vessel
5—core   11—rotary plug
6—support posts
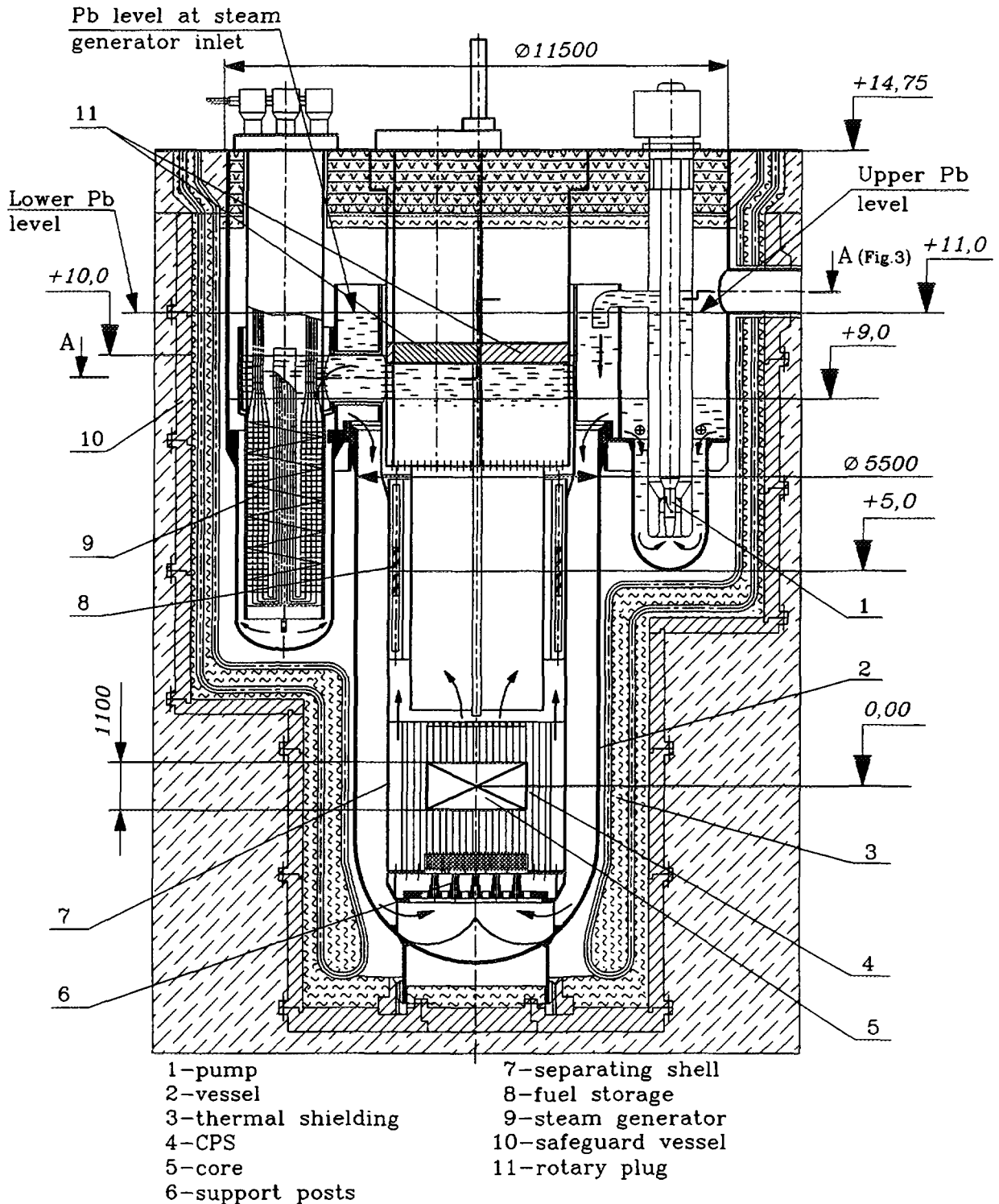
Fig. 2 BREST—300 layout
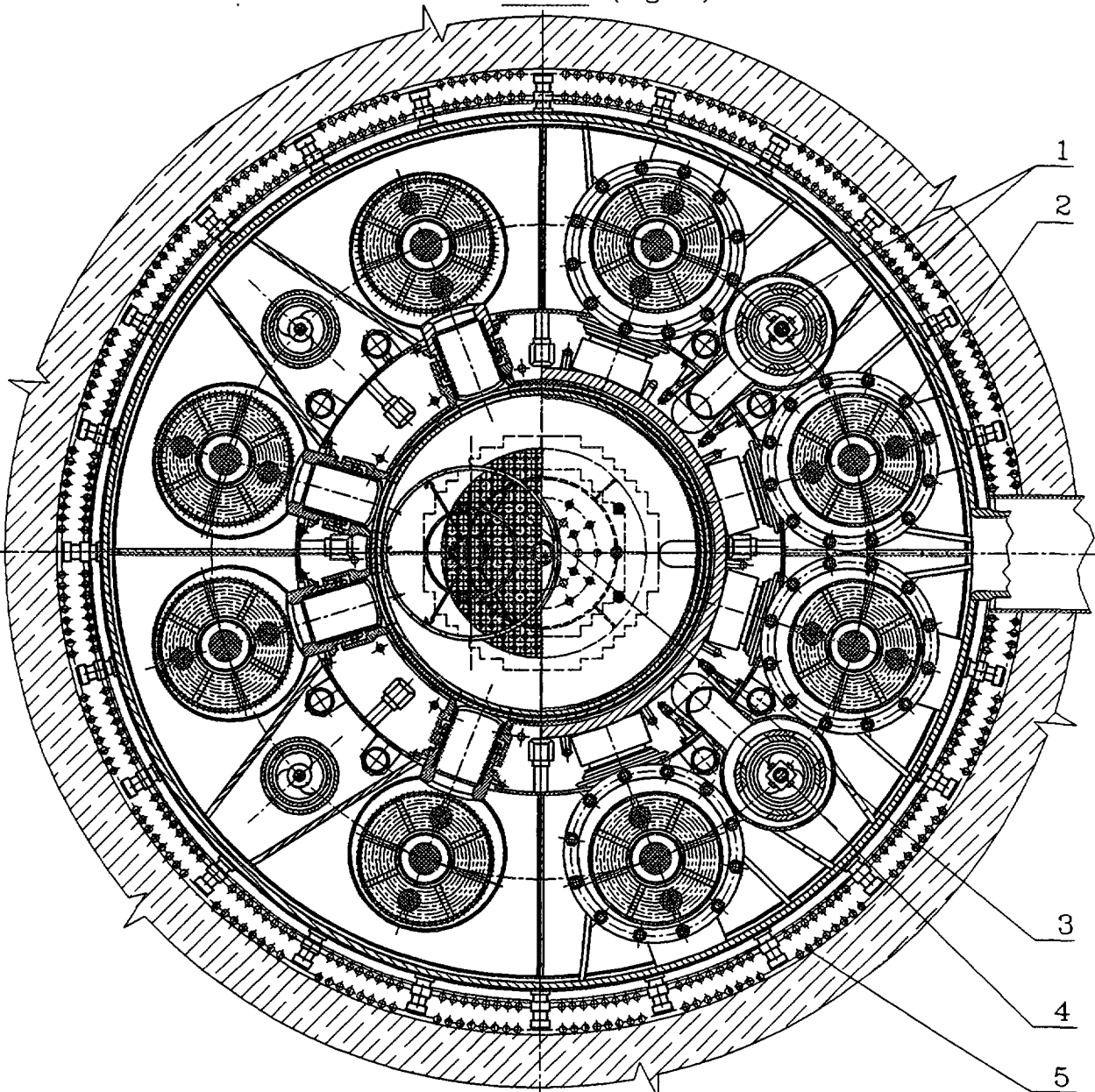
1. charging valve
2. steam generator
3. FA
4. pump
5. pipes of heat removal air system

Fig. 3 Cross—section over header branches
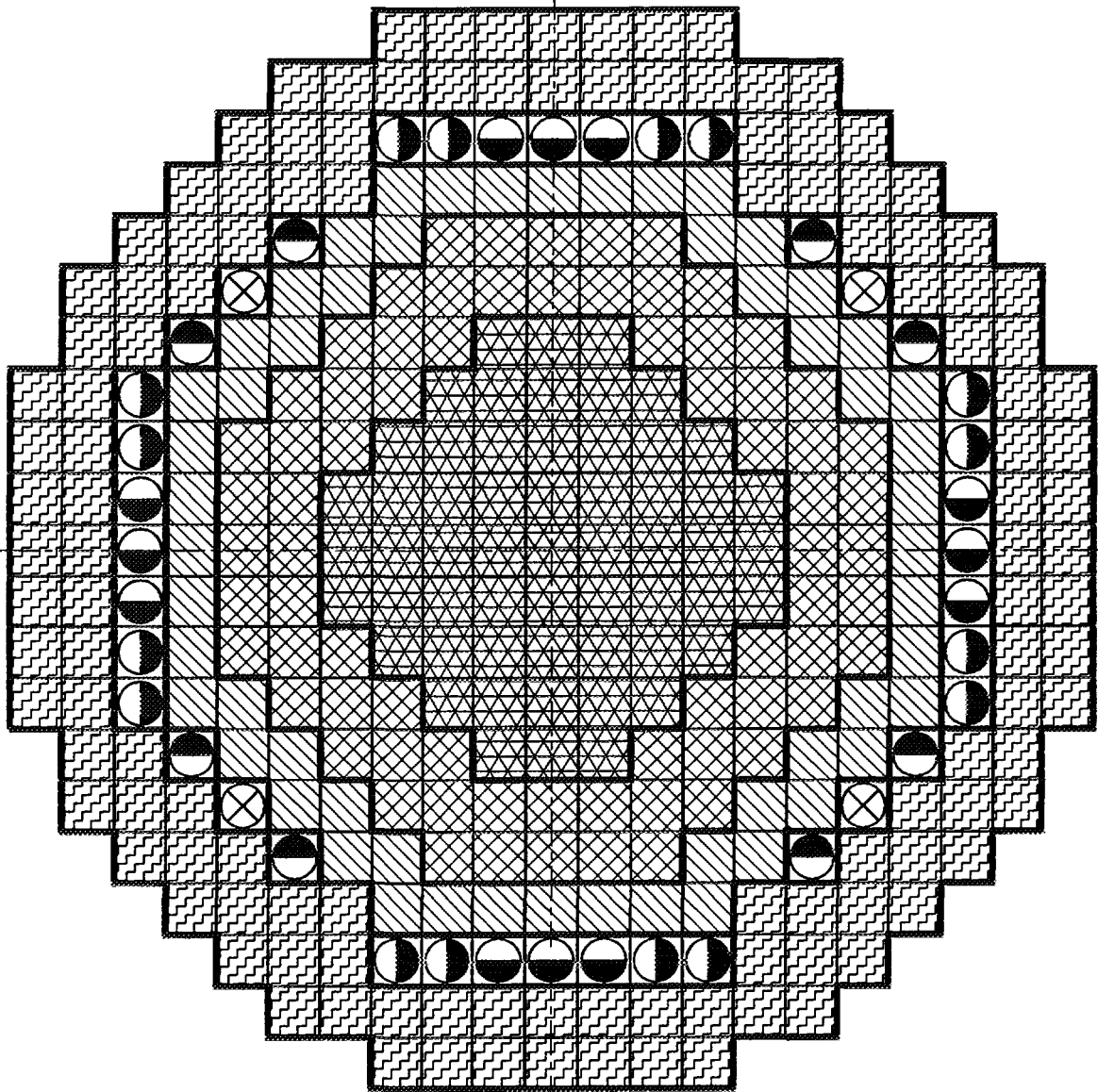
- ▨ — core 1 FA (9.1 mm fuel rod diam.);
- ▧ — core 2 FA (9.6 mm fuel rod diam.);
- ◩ — core 3 FA (10.4 mm fuel rod diam.);
- ◑ — scram regulator (scram 1);
- ⊗ — automatic regulator (AR);
- ◑ — scram passive regulator (scram 2);
- ◓ — shim regulator (S);
- ▨ — block of lead reflector

Fig. 4 BREST−300 reactor core cross−section diagram
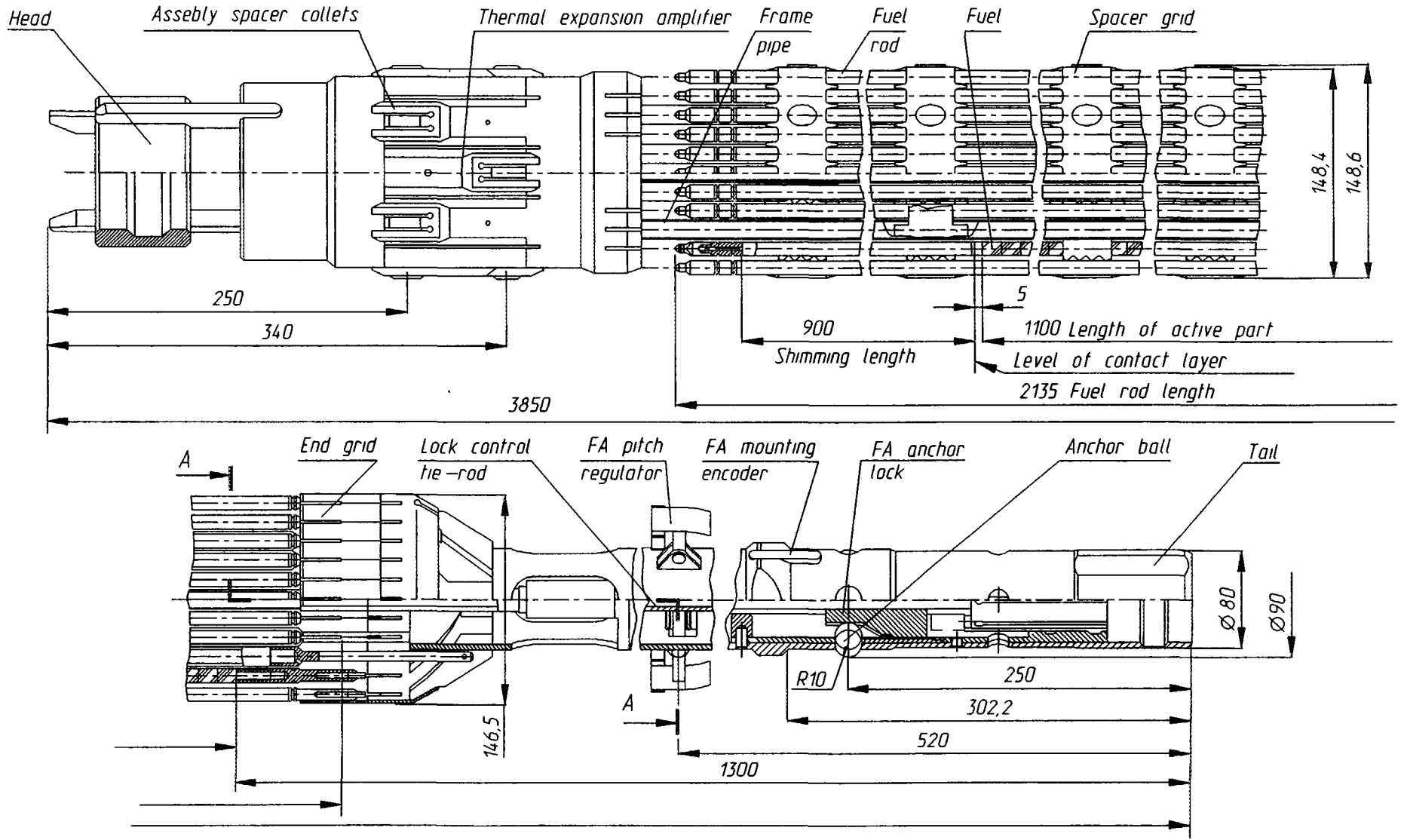
Fig. 5   BREST-300 fuel assembly

Dependency of average FA location pitch in the middle core on inlet coolant temperature is presented in Fig. 4. Such a dependency is conditioned by difference in thermal expansion coefficients of cylinders and FA pitch regulator located at its end.

Thermal expansion amplifier fixed at lateral faces of spacer grids located in FA upper part near the damper. After having reached 870 K outlet temperature it provided drawing adjoining FAs apart. This corresponds to insertion of around $0.3\beta_{eff}$ negative reactivity, when the value of power effect is $\sim 0.44\beta_{eff}$.

As calculations stated flow stopping up to 40 per cent inside FA and up to 100 per cent at outlet causes coolant and fuel cladding temperature growth by less than 40 K. This relates to coolant inleakage from adjoining ductless FAs that rapidly reconditions coolant flow rate in a disturbed FA due to fuel lattice rarefaction.

It should be noted that low GFP yield from fuel and hydrostatic coolant pressure result in squeezing the most portion of fuel rods and only by 5 year of FA operation in central part of reactor core GFP pressure in fuel rods will exceed hydrostatic one (Fig. 8). Share of such the fuel rods in reactor core is 6 per cent. Calculation values of fuel cladding stresses are −10.2 MPa and +12.7 MPa at the start and end of fuel rod lifetime, and thermal stresses are 30 MPa and 20 MPa.

$$\frac{U}{\overline{U}} \cdot \frac{T}{\overline{T}}$$
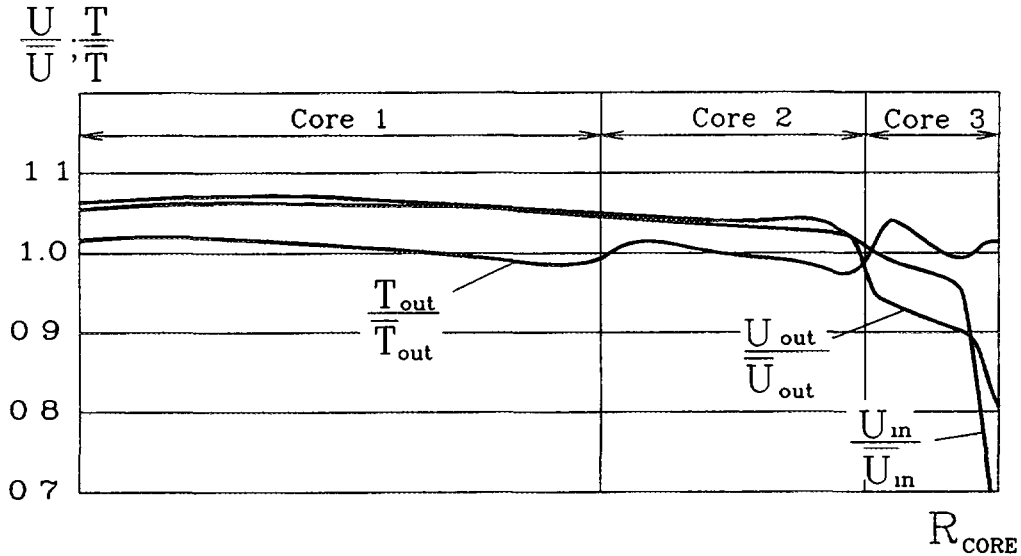
Fig. 6 Reactor core radial nonuniformity of lead flow rate and temperature
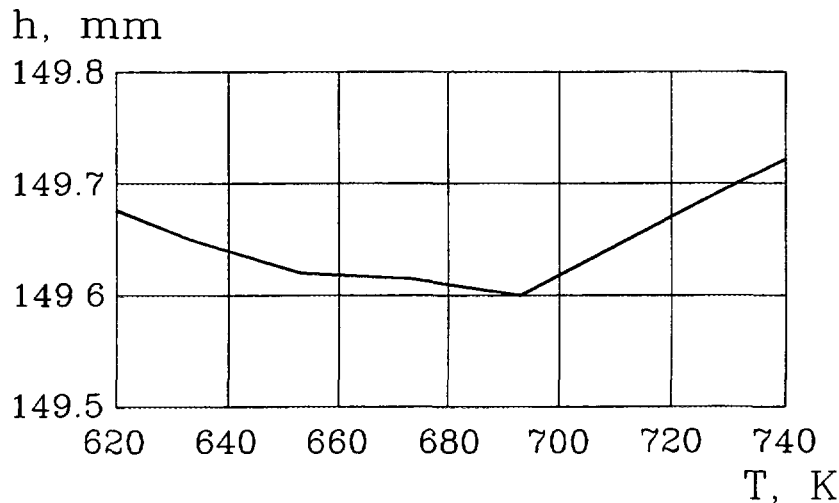
Fig 7 Effect of coolant inlet temperature on average FA pitch value

164

cladding

fission gas

lead

fuel

2000

1100

lead coolant
W=1.8m/s

Shematic of
fuel element

Pressure of fission gas, MPa

2.37

2.0

1.32 1.29

Pressure of lead coolant
in the middle of core

1.07

1.0

0.9

0.75

0.6

0.4

0.3

0.2

12   37   64   89   112   138   160   185

Number of
fuel assembly

$V_{relesed}^{max} = 0.11 m^3$; $t^{min} = 4$ sec
fission gas

$\Delta\rho < 0.5\beta$
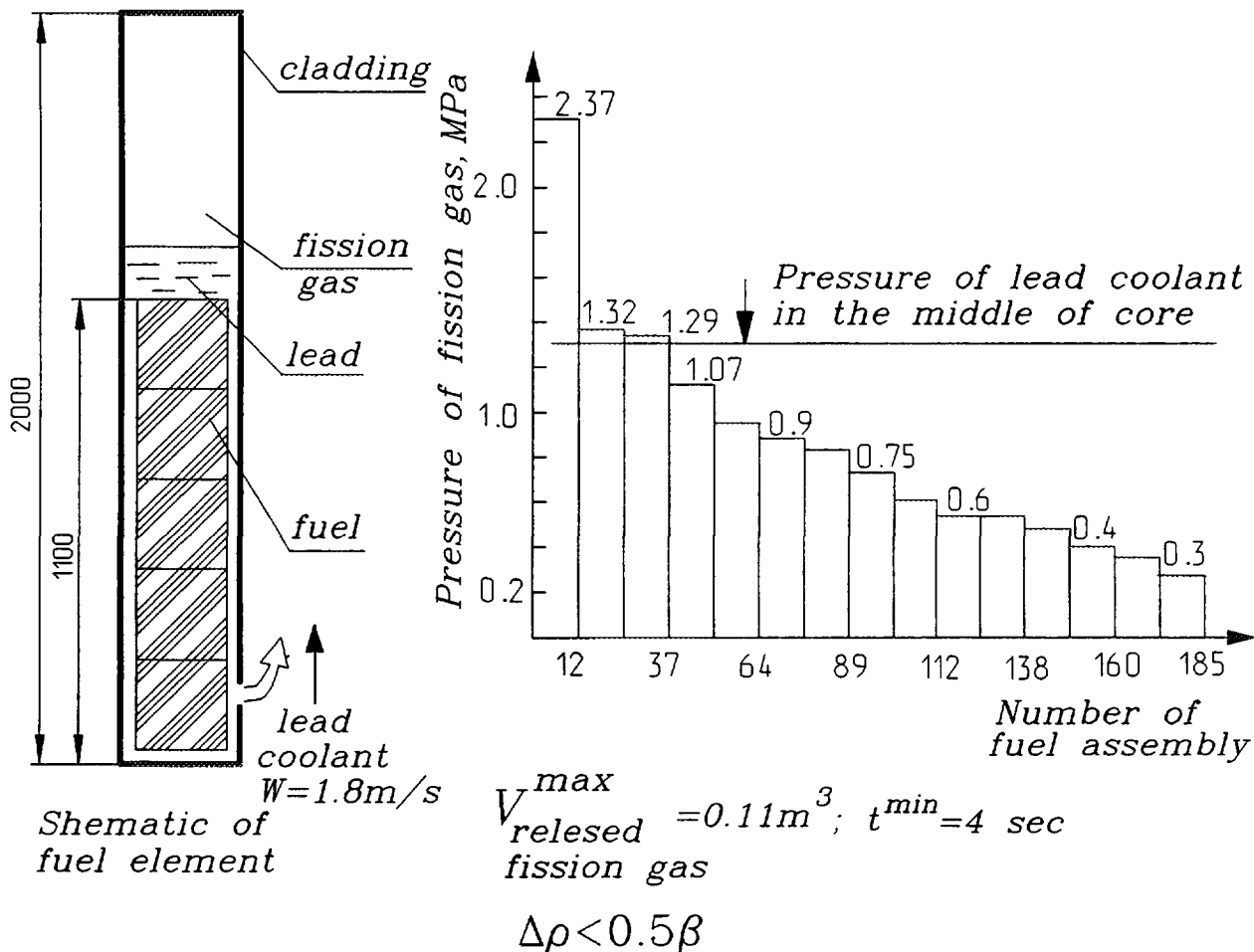
*Fig. 8 Accident with prompt fuel cladding repture
(fission gas release into lead coolant)*

Low lead heating up (120 °C) and good thermal conductivity of fuel cladding specify small values of power and temperature effects equal $1.6 \cdot 10^{-3}$ $\Delta K/K$ and $1.0 \cdot 10^{-3} \Delta K/K$. This determines maximum reactivity margin of around $0.9\beta_{eff}$ corresponding to cooled down reactor core condition. Minimum reactivity margin is around $0.16\beta_{eff}$ in nominal operating conditions.

Fuel loading-unloading results in effect inserted by fresh FA which is approximately equal spent FA effect. This effect for core 1, core 2 and core 3 is 0.182, 0.065 and 0.041 per cent of $\Delta K/K$.

Maximum void reactivity effect does not exceed $0.8\beta_{eff}$ at $\rho_{Pb}=0.75\rho_{oPb}$ when changed lead density. Conservative estimation of lead density changing in case of steam ingress due to steam generator depressurization is 0.06 that corresponds to reactivity insertion of around $0.25\beta_{eff}$.

Naturally, local in-core lead density decrease may result in larger value of the effect, however it is possible only in case of sabotage.

Spontaneous depressurization of all the fuel rods overpressurized with GFP is estimated as $0.5\beta_{eff}$ effect (Fig. 8). Note that conservative estimation of possibility for fuel rods depressurization in accidents of LOFWS and TOPWS type gives us 0.06 per cent of amount of fuel rods in reactor core.

Small values of reactivity margin and effects, high temperature margin to phase transitions (cladding melting and lead boiling), significant thermal capacity of primary circuit exclude emergency reactivity disturbance more β_{eff}. So BREST-300 lead cooled reactor does not require control members of great efficiency and fast response. This allows to control with lead displaces from reflector blocks and use regulators of two positions.

Table 2 presents their characteristics.

165

Table 1

Loading parameters of fuel elements and FAs

Parameter name	Parameter value		
	Core 1	Core 2	Core 3
Fuel rod diameter, mm	9.1	9.6	10.4
Relative pitch in fuel rod lattice:	1.495	1.417	1.308
Volumetric fraction:			
- fuel	0.231	0.264	0.322
- structural materials	0.093	0.097	0.111
- coolant	0.676	0.639	0.567
Breeding ratio:			
- fresh fuel	1.09	1.10	1.11
- onset of fuel microcycle	1.06	1.07	1.08
- middle of fuel microcycle	1.05	1.06	1.07
- end of fuel microcycle	1.04	1.05	1.06
Thermal output, MW			
- onset of fuel microcycle	229.1	265.9	178.9
- middle of fuel microcycle	228.8	265.9	178.2
- end of fuel microcycle	228.8	265.9	178.2
Radial power peaking ratio, K_r	1.09	1.16	1.18
Number of fuel rods	6498	8208	6384
Radius, mm	637	759	1148
Peak linear power rate, kW/m	42.7	41.3	35.3
Peak fuel rod surface temperature, K:			
- nominal	869	879	887
- "hot spot"	902	915	922
Peak fuel temperature, K:			
- nominal	1087	1085	1063
- "hot spot"	1253	1247	1244
Flow relative narrowing by spacer grid	0.199	0.211	0.234
Number of FAs	57	72	56
Number of FAs to be refuelled	11-12	14-15	11-12
Fuel burn-up in FAs to be refueled, HM per cent:			
- average	9.0	6.9	4.8
- peak	11.8* (10.8)	9.8 (8.3)	6.8 (5.8)
Radiation induced damage of fuel cladding, dpa	130 (120)	114 (97)	86 (73)
Plutonium content** in FAs to be loaded in, HM percent:			
- plutonium	14.0	14.0	14.0
- (^{239}Pu+^{241}Pu)	9.7	9.7	9.7

* Fuel burn-up values and radiation induced damage of fuel cladding in case of FAs shuttling inside any shaped subcore during its operation are presented in parentheses.

** Mixed U Pu N mononitride fuel is used with relautionships between different radioactive nuclides are as follows:

$$^{238}Pu/^{239}Pu/^{240}Pu/^{241}Pu/^{242}Pu/^{241}Am/^{242}Am/^{243}Am=0,5/64/28/3,1/1,7/2,1/0,1/0,5$$

It should be noted that Table 1 shows parameters with self-reactor grade Pu in mixed mononitride with nature nitrogen. Weapon Pu loading in BREST-300 reactor needs to rise reactor core height from 1100 to 1400 mm, preserving pellets density equal 95 % TD. Using ^{15}N allows to reduce pellets density above 10 %. If weapon Pu loading in BREST with power more than 600 MW(e), the initial core height does not be increased but the initial pellets density needs increasing.

Due to the characteristics inherent in LMFR (reactivity margin $K \leq \beta_{eff}$, feedback), lead coolant (chemical passivity, high density and boiling temperature, low neutron absorption and moderation), UN-PuN fuel (density, thermal conductivity, thermal-radiation stability) catastrophic course of severe accidents can be avoided.

The inherent safety enables simplifying the reactor design, control system, eliminating intermediate circuits in the main and emergency cooling systems. Economical estimations allow one to expect the NPP cost to be equal or lower to that of NPP with LWR. The NPP closed fuel cycle, electrochemical fuel reprocessing and its recycling together with other actinides in the reactor, transmutation of I and Tc, utilization of Sr and Cs, and long-term storage of the remaining fission products are envisaged, enabling radwaste disposal with their radiation hazard equivalent to that of mined uranium with its decay products.

Closing of the fuel cycle at NPP, combined recycle of all actinides, elimination of uranium blanket and low reactivity margin contribute to nonproliferation and control measures.

CONCLUSION

1. Synthesis process mononitride production from initial metal is more profitable that one from initial oxide. Electrochemical reprocessing mononitride fuel should be developed as contributory to nonproliferation and cost effective fuel cycle.

2. Future large-scale NPI may be build on the lead-cooled fast reactors as the high safe and cost-effective nuclear technology based on current experience (LMFR and Pb-Bi naval reactor).

REFERENCES

1   B. D. Rogozkin, L. V. Arseenkov, O. A. Alekseev, V. A. Zaitsev et al. Overview of the properties, fabrication and reprocessing technology, irradiation testing and compatibility of mononitride fuel. Report. Moscow. 1990.

2.   B. D. Rogozkin, Yu. M. Golovchenko, N. M. Stepennova, Yu. E. Fedorov et al. VNIINM and NIIAR Report. № 7533, 1991. Post-irradiation studies of an experimental fuel assembly KNS with mixed monocarbide, mononitride and carbonitride fuel irradiated in the BOR–60 reactor.

3.   A. G. Vakhtin, V. D. Dmitriev, S. I. Ermakov et al. Operating experience for fuel rods in the nitride zone in the BT–10 reactor. Presentation made at the Soviet-Japanese Seminar. 1990. Obninsk.

4.   A. Bauer. Nitride Fuels. J. Reactor Technology 1972, 15, 2, 87.

5.   B. D. Rogozkin, F. G. Reshetnikov, Yu. E. Fedorov, N. M. Stepennova, M. G. Shishkov et al. Review of the fabrication techniques for monocarbide, mononitride, uranium carbonide cores for fuel rods of fast reactors. Atomnaya energiya V. 35, No 6, 1973, p. 377–386.

6.   C. Pranier, P. Bardelle, J. P. Pages, K. Richter, R. W. Stratton, G. Lederberger. Europen collaboration on mixed nitride fuels. International Conf. on Fast Reactors and Related Fuel Cycle. October 28–November 1, 1991 Kyoto, Japan   V   II, p 15.9.1–15.9.12.

7.   L. V. Arseenkov, V. V. Vetrov, B. D. Rogozkin. VNIINM. Report 6948, 1989.

8. H. Blank, H. Bokelund. Problems expected in the future fuel cycle development of dense fuels for LMFBR. Advanced fuel technology and performance Wurenlingen, Switzerland, December 4–6 1989 IAEA–TECDOC–352, Vienna 1985, p 189–213.

9. V. A. Makhova. Fast reactors abroad. Promising fuels for LMFBRs. AINF 587, No 5, Moscow, 1982.

10. Y. Arai, S. Fukushima et al. Fabrication of UPuN fuel pellets. J. Nuclear Maxer 168 (1989) p 280–289.

11. Y. I. Chang, C. E. Till Advanced breeder cycle uses metalic fuel. Modern Power System, 1991, v.11, №4, p. 59–63.

12. O. V. Skiba et al. Technology of pyroelectrochemical reprocessing and fabrication of oxide fuel. NE'–93, June 28–July 2, N. Novgorod. Abstracts from the meeting, V. 2, p. 777j779.

13. B. D. Rogozkin et al. Properties, Synthesis and Reprocessing Technology of Mononitride Fuel for Inherently Safe Reactors. Proceedings of ARS 94, Int. Top. Meeting, Pittsburgh, PA, USA, April 17–21, 1994, V. 1, p. 382–389.

14. . Атомная энергия, т. 72, вып. 4, стр. 317, 1992. В. В. Орлов, Б. Ф. Громов, М. И. Солонин, Е. О. Адамов и др., "Нетрадиционные концепции АЭС с естественной безопасностью".

15. E. O. Adamov, V. V. Orlov Requirements a new nuclear technology for the large-scale power industry, Proceeding of ARS'94 International Topical Meeting on Advanced Reactors Safety, v. 2, p. 636–642, Pittsburg, PA, USA, April 17–21, 1994 year.

16. V. V. Orlov et al Physical characteristics of lead cooled fast reactor, Proceeding 1994 Topical Meeting on Advances in Reactor Physics, v. 1, p. 348–356, Knoxville, TN April 11–15, 1994 year.

17. E. O. Adamov, V. V. Orlov et al Coceptual design of BREST-300 lead-cooled fast reactor, Proceeding of ARS'94 International Topical Meeting on Advanced Reactors Safety, v. 1, p. 509–515, Pittsburg, PA, USA, April 17–21, 1994 year.

18. V. V. Orlov et al Lead-cooled reactor core, its characteristics and features, Proceeding of ARS'94 International Topical Meeting on Advanced Reactors Safety, v. 1, p. 516–523, Pittsburg, PA, USA, April 17–21, 1994 year.

19. V. V. Orlov et al Study of ultimate accidents for lead-cooled fast reactor, Proceeding of ARS'94 International Topical Meeting on Advanced Reactors Safety, v. 1, p. 538–543, Pittsburg, PA, USA, April 17–21, 1994 year.

RESEARCH AND DEVELOPMENT OF MgO BASED MATRIX FUEL

I.S. KURINA, V.N.I. LOPATINSKY,
N.P. YERMOLAYEV, N.N. SHEVCHENKO
Institute of Physics and Power Engineering,
State Scientific Centre of the Russian Federation,
Obninsk, Russian Federation

XA9745731

Abstract

Study of 15% vol. PuO_2 + 85% vol. MgO without ^{238}U pellet fabrication was carried out. The work has been carried out for uranium dioxide simulator fuel composition fabrication by means of mechanical mixing of individual initial UO_2 and MgO powders and by coprecipitation from aqueous solutions. Optimal technological parameters for the qualitative sintered pellets (with regulating density and without defects) fabrication has been established.

Pre-irradiation testing of specimens has been carried out. The aim consists in examination of fuel-clad interaction for the system UO_2 + MgO - cladding at clad operating temperature (700°C) and at central fuel hole temperature (1200°C).

PuO_2 + MgO pellet fabrication follows under optimal condition states out during R and D of uranium dioxide simulator fuel Mean density of sintered pellets is 4,3 g/cm^3 (i e 90% of the theoretical value) physical configuration of pellets being satisfactory.

Fuel components regeneration was carried out

Introduction

Nowadays some nations (France, Japan as well as Russia) are following research and development of advanced fast reactor core for effective utilization of commercial and weapon grade plutonium In the light of this trend is formed expediency of development and testing of new plutonium-bearing composition in order to replace uranium-238 by any inert diluent
State Scientific Center Institute of Physics and Power Engineering after 1994 within the framework of the Russian-French cooperation for EFR project and later within the framework of the ISTC contract carries out research and development of MgO-base matrix fuel

Magnesium oxide inert diluent has been chosen not by chance as follows
- MgO does not form intermediate phase with PuO_2;
- MgO does not react with sodium,
- MgO exhibits high stability under irradiation;
- MgO may by easily reprocessed,
- MgO possesses satisfactory heat conductance (12 Wt/m °C at 900°C for specimen with porosity level 0%)

This work is dedicated to R&D of PuO_2 + MgO fuel pellets fabrication

Owing to technical complication (high plutonium compounds toxicity and need for dedicated special facilities and premises) has been made decision to use at initial study uranium dioxide fuel for development of all technological procedures, for pre-irradiation study and for post-irradiation examination. Other cause consists in close similarity of technological and physico-chemical properties of uranium and plutonium dioxides

Preliminary physical computations gives actual PuO_2 content in inert matrix as high as 15% (volume) therefore bulk matrix component [(i.e 85% (volume) MgO] being same main PuO_2-MgO and UO_2-MgO composition features become very similar

At first study stage main attention has been devoted to technology choice for compact items fabrication when using UO_2-MgO composition Two alternative route has been considered First conventional route is based on mechanical blending of initial uranium and magnesium oxides, cold

pressing and pellet sintering. Second route is based on coprecipitation of uranium and magnesium compounds from nitric solution, thermal post-treatment and pellet sintering.

Both type of specimens received has been investigated by means of metallurgical, X-ray and other analytical methods and as regards their chemical reprocessing. Basic PuO_2 + MgO fuel pellets fabrication route is coprecipitation procedure from nitric solution. This presentation deals with study scope mentioned.

1. Fuel pellet fabrication from composition 15% vol. UO_2 + 85% vol. MgO

A lot of work has been carried out with UO_2 simulation aiming to elucidate optimal technological regime for fuel pellet fabrication.

The figure 1 gives fabrication scheme of UO_2-MgO composition by conventional route of mechanical mixture of powders (technology 1). The figure 2 gives fabrication scheme of UO_2-MgO composition by co-precipitation of uranium and magnesium compounds from nitric solution (technology 2).

Flow sheet for UO_2 + MgO composition pellet fabrication by mechanical blending of powders
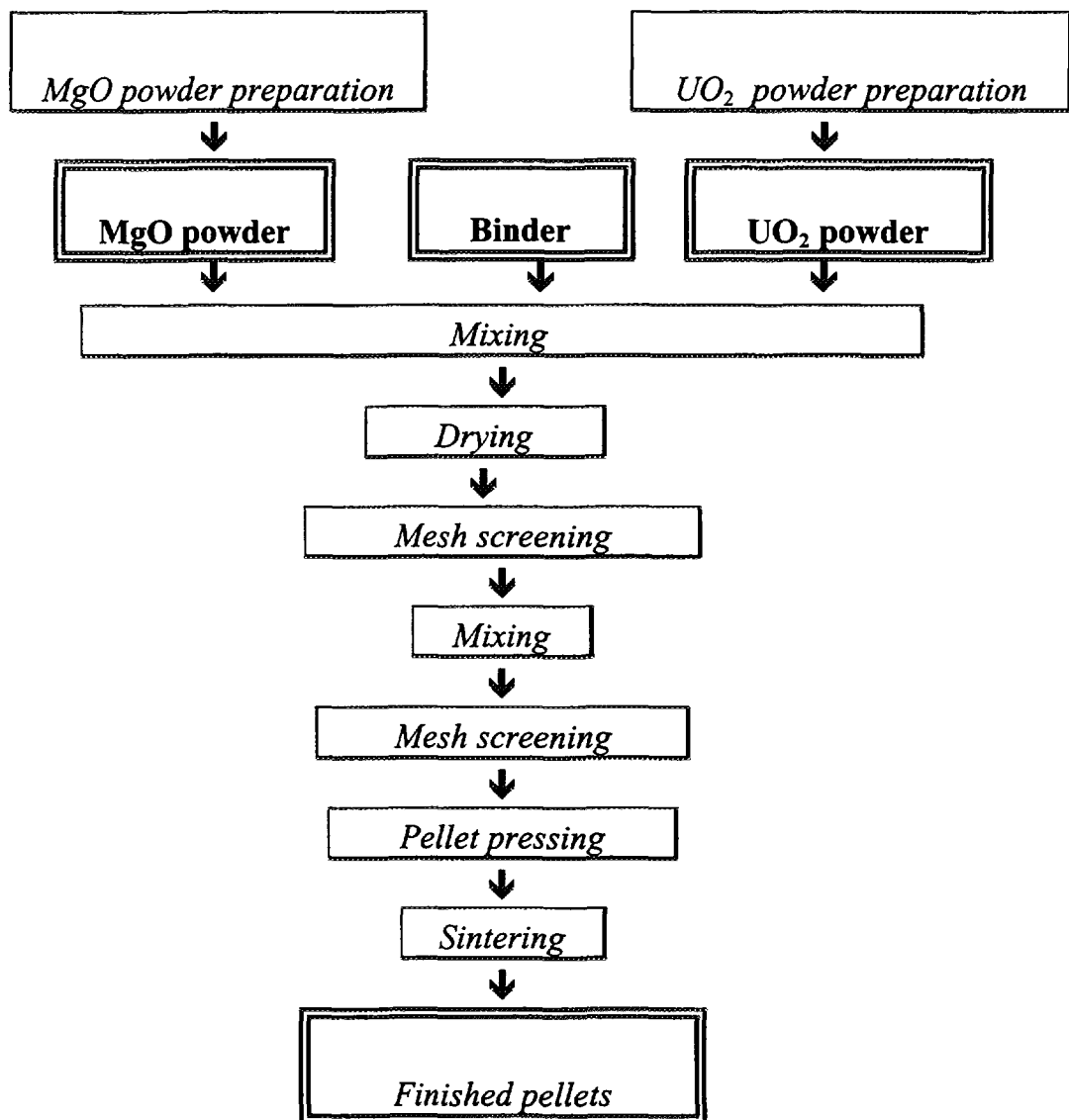
Figure 1

Flow sheet
for UO$_2$ + MgO composition pellet fabrication by coprecipitation of magnesium hydroxide Mg(OH)$_2$ and ammonium polyuranate from solution
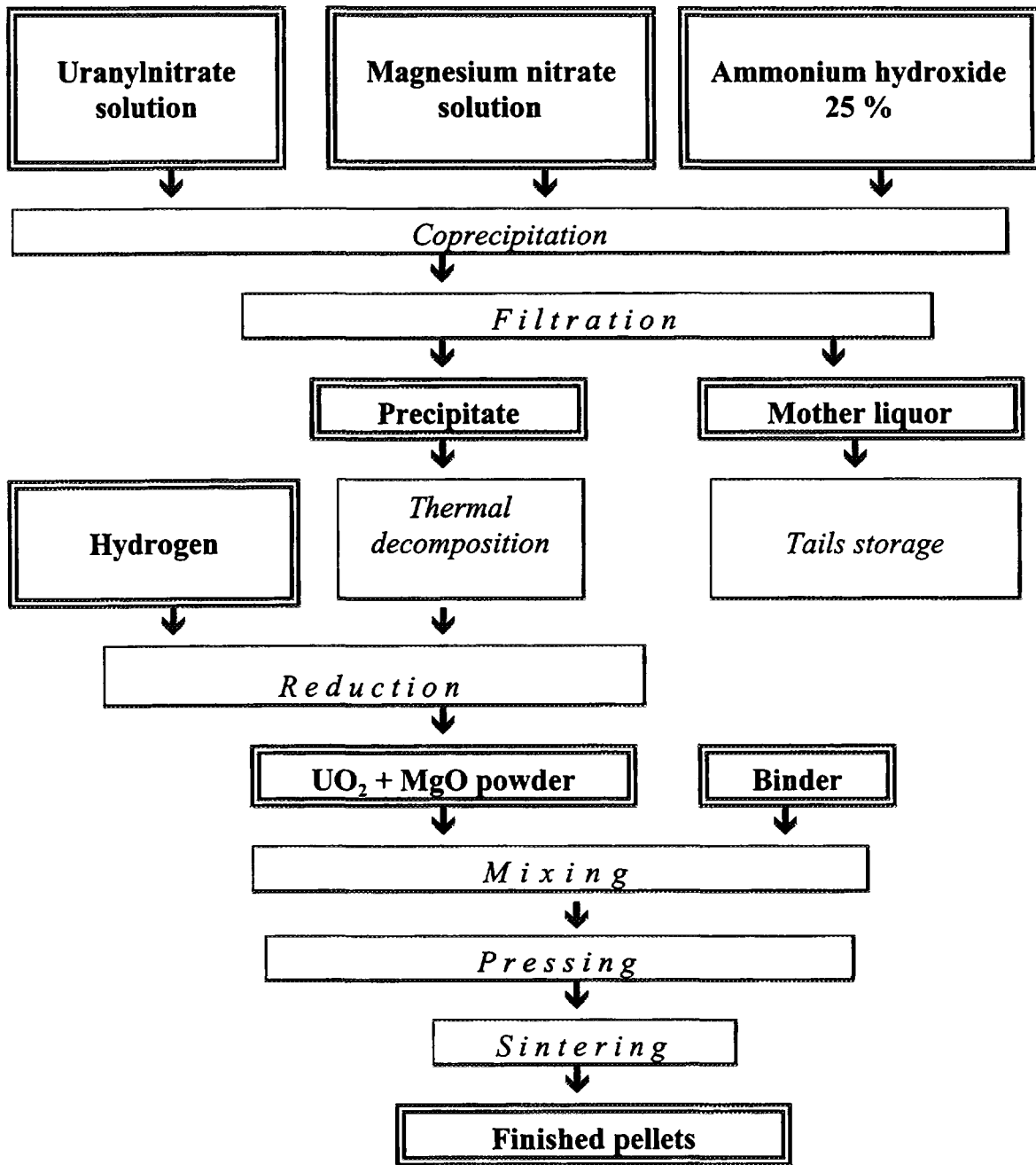
Figure 2

In course of our researches has been proved out as follows. Pressing value, MgO powder properties, temperature and heating rate when sintering have preponderant influence on sintered pellet quality for technology 1. Precipitate heat treatment, pressing value and heating rate when sintering are main parameters of perfect pellet production by technology 2.

Optimal parameters has been chosen for production of perfect fuel pellet with 90% theoretical density value. Pellet density may be controlled by sintering temperature correction. It must be stated out co-precipitated from solution pellets possesses enhanced density value.

At optimal condition of technology 1 and 2 some pellet batches has been prepared. By means of different methods has been investigated their some properties as follows.

2. Examination of composition 15% vol. UO_2 + 85% vol. MgO specimens

2.1. DETERMINATION OF FUEL DISTRIBUTION HOMOGENEITY

Alpha radiographic study has been carried out in order to examine fuel component distribution in composition UO_2 + MgO. Homogeneity distribution of UO_2 in pellets has been corroborated.

2.2. X-RAY COMPOSITION STUDY AT DIFFERENT TECHNOLOGY 2 STAGES OF COMPOSITION PREPARATION

X-ray microprobe and X-ray phase analysis has been implemented for chemical composition and phase composition at all intermediate products of pellet fabrication route. Table 1 presents correspondent data for powder and pellet phase composition.

**Powder and pellet phase constitution of UO_2 + MgO composition
preparated by coprecipitation from solution**

Material	Phase constitution	Lattice spacing, Å	
		UO_{2+x}	MgO
As-precipitated powder from solution	$(NH_4)_2U_4O_{13}$ + $Mg(OH)_2$	-	-
Powder after heating at 900-1200 °C	$MgUO_4$ + MgO	-	-
Powder after heating at 1000 °C and hydrogen reduction	UO_{2+x} + MgO (x=0,15)	5,450	4,215
Sintered pellet	UO_{2+x} + MgO (x=0,02)	5,465	4,215

2.3. METALLURGICAL EXAMINATION AND MICROSTRUCTURE STUDY

X-ray microprobe investigation of pellet surface (mechanical powder blending, technology 1) shows existence of alternating black and white areas with diameter 15 - 80 micrometers (figure 3). It has been established white areas being uranium content phase and black areas being magnesium content phase. Specimen is formed by mechanical mixture of compound UO_2 and MgO uniformly distributed across the specimen.


Figure. 3
Metallographic specimen of the sintered pellet UO_2 + MgO composition surface
(mechanical powder blending, technology 1)

Typical surface appearance of the UO_2 + MgO composition pellet surface (coprecipitation from solution method, technology 2) is shown in figure 4. It has been established surface is formed by white, gray and dark-grayish areas white areas being uranium content phase, dark-grayish areas being magnesium content phase, gray areas being mixed magnesium + uranium content phase. Specimen is formed by mechanical mixture of compound UO_2 and MgO uniformly distributed across the specimen..

Material microhardness determination has been carried out by means of microhardness metering device PMT-3 with 200 gramm loading.

Figure. 4
Metallographic specimen of the sintered pellet surface
coprecipitated from solution (technology 2)

Investigation of pellet specimen (technology 2) shows microhardness of the white matrix from 510 to 830 kg/mm² mean value of 12 measurement being 670 kg/mm². Microhardness of the white matrix is near to that of microhardness of uranium dioxide UO_2

Microhardness of the dark-grayish structural component is varying from 360 to 570 kg/mm² mean value of 10 measurement being 455 kg/mm². Gray component microhardness is not determined their areas being to small to be measured.

Material microhardness determination for technology 1 has been carried out by means of the same microhardness metering device with 200 gramm loading. Microhardness of the black matrix is 670 ± 70 kg/mm²

2.4. DEPENDENCE OF THE HEAT CONDUCTANCE VERSUS TEMPERATURE

Figure 5 gives dependence of the UO_2 + MgO composition heat conductance λ versus temperature when using technology 2. At temperature 1000°C λ value is 8,1 - 8,3 Wt/m· °C. Mechanical UO_2 + MgO powder blending gives material with mean heat conductance λ at temperature 1000°C equal to 5.7Wt/m·°C.

2.5. MELTING TEMPERATURE AND MELTING HEAT DETERMINATION FOR UO_2 + MGO COMPOSITION

In experimental way it was established first liquid phase drop appearing in the temperature range 2250-2300°C. Melting heat for 15% (vol.) UO_2 + 85% (vol.) MgO is 75 - 77 kJ/mol.

2.6. ISOTHERMIC TESTING

TESTING AT 700°C AND 750°C

The testing has been carried out in order to elucidate interaction depth in the system fuel-matrix-cladding at temperature 700 and 750°C. Tube steel CHS-68 is dummy fuel element cladding material Testing run duration is 1000 h.

TESTING AT 1200°C

The testing has been carried out in order to elucidate interaction depth in the system fuel-matrix at temperature 1200°C. Testing run duration is 1000 h.

It was authenticated as follows :

• Dummy fuel elements retain their leak tightness and dummy fuel element cladding has not any geometrical distortion. It was not detected after testing any fuel composition pellet evolution in comparison with initial fuel pellet state.

• Selected cladding material is steel CHS-68 which possesses good compatibility with fuel composition 36% (vol.) UO_2 and 64% (vol.) MgO at temperature 700°C and 750°C during 1000 hours Prepared after mechanical powder blending fuel composition as well as chemically coprecipitated one show none chemical interaction in the system fuel-cladding.

• Post-testing microstructure and mechanical properties of dummy fuel element cladding vary within intrinsic features of that structural material class in annealed state when taking into consideration the testing run duration. Mechanical properties evolution of dummy fuel element cladding material are produced by imposed time-temperature regime of compatibility testing only and any contribution of fuel element material interaction to mechanical properties evolution was not detected.

• Isothermal annealing of fuel composition pellet at temperature 1200°C does not produce any change in fuel phase composition. Maximum geometrical parameters evolution does not exceed 1% for annealed pellet. Post-testing fuel pellet microstructure and microhardness are meeting with their initial state Oxygen-uranium ratio of dispersion composition is decreased from 2,01 till 1,99.

3. PuO_2 + MgO pellet fabrication

The study is aiming to endorse PuO_2 + MgO composition specimen fabrication after route developed by using dummy UO_2 composition Leak tight glove boxes have been applicated in hot laboratory for the study. Scheme of PuO_2 + MgO composition pellet fabrication is illustrated by figure 6 During PuO_2 + MgO pellet fabrication have been implemented the all technology parameters specified at research and development study of dummy UO_2 composition.

3.1. PLUTONIUM AND MAGNESIUM SALTS COPRECIPITATION FROM NITRIC SOLUTION AND PRECIPITATE CALCINATION

Chemical composition 15% (vol.) PuO_2 + 85% (vol) MgO has been specified by nuclear physics computation for plutonium utilization in fast reactor.

18,1 gramm of Pu and 36,3 gramm of MgO have been token for nitrate solution preparation By dissolution in nitric acid has been produced 460 ml of solution with concentration : Mg - 51,5 g/l, Pu - 42 g/l, HNO_3 about 30 g/l.

Simultaneous dosing into coprecipitation facility of initial nitrate solution and 25 percent ammonium hydroxide solution gives rise coprecipitation of $Pu(OH)_4$ + $Mg(OH)_2$ hydroxides It was needed 1030 ml of ammonium hydroxide solution to control constant pH medium value 10,6 during plutonium and magnesium hydroxide precipitation from 460 ml of

After solution dosing the pulp has been agitated 1 hour at temperature 40-42°C and has been settled 1 day. After precipitate filtration mother liquor is 1050 ml and contains less than 1 mg/l of plutonium and 1,5 g/l of magnesium. Moisture content of $Pu(OH)_4$ + $Mg(OH)_2$ precipitate is 70%. Precipitate has been washed out by means of ammonium hydroxide solution on the filter and has been emplaced in a quartz tube. Precipitate calcination has been carried out in a muffle furnace at temperature 1000°C as long as 4 hours. Calcined powder is the substance with khaki color. Chemical analysis gives powder composition 36% (weight) PuO_2 + 64% (weight) MgO.

3.2. PRESSING AND SINTERING OF PUO_2 + MGO COMPOSITION PELLETS

A pressing batch of following composition 17,09 g of PuO_2 + MgO powder, 170 mg of paraffin (0,1 weight %); 85 mg of oleic acid (0,5 weight %), 41 ml of carbon tetrachloride. As-prepared batch has been exposed in the air for 1 day to volatilize CCl_4.

Hydraulic press facility has been used for pellet pressing. Batch has been emplaced into pressing form with inner diameter 7,4 mm. Mean single batch has been as high as 1,61 g; operating die loading was 60-62 kg, loading exposure duration was 10-15 seconds. Table 2 contains data for pressed compacts. Pressed pellets have been loaded into molybdenum crucible which has been suspended in operation space of the muffle furnace.

Sintering parameters:
- vacuum = $(2-4)\cdot10^{-4}$ mm Hg;
- heating rate 100°C /h until 1500°C;
- sintering duration 5 hours at 1500°C;
- compact cooling to 50°C during 3,5 hour;
- compact unloading at room temperature.

Table 2 gives density geometrics data for sintered pellets. Diameter shrinkage after PuO_2 + MgO pellet sintering is 18,9 %. Mockup study of dummy UO_2 composition gives after sintering diameter shrinkage 18,9 % as well.

Compacts of 36% (vol.) PuO_2 + 64% (vol.) MgO composition have satisfactory physical configuration and does not contain fissuration, cleavage, spallation and other type of defects. There are dark-gray pellets. Pellet height exhibits «waist», its length is 97-98 % from total height. Table 2 presents «waist» data. Pellet end diameter is 0,05 mm more than «waist» diameter.

4. PuO_2 + MgO composition pellet study

4.1. CHEMICAL OXYGEN POTENTIAL ($-\Delta GO_2$) IN SINTERED PELLETS

Chemical oxygen potential in sintered pellets and computed on this base oxygen factor (O/Pu) has been measured by electromotive force method using solid electrolyte on the base of thorium oxide. Measurements have been carried out at temperature 1000°Ñ. Measurement error is ±0,001 O unit in factor (O/Pu). PuO_2 + MgO sampling has been made across three pellet section of pellets number 3 and 10 Sampling consists in boring out of about 100 mg of the material from both pellet sides and from equator plane Table 3 summarizes data received.

Table 2

Geometrics and density of PuO_2+MgO compacts and sintered pellets

Pellet number	Compacts				Sintered pellets					
	weight g	diameter, mm	height, mm	density, g/cm^3	weight g	diameter, mm	diameter shrinkage, %	height, mm	density, g/cm^3	
									geometrical	pycnometric *)
3	1,45	7,4	13,6	2,49	1,42	6,0	18,9	11,9	4,22	4,43
4	1,55	7,4	14,3	2,52	1,43	6,0	18,9	12,2	4,14	-
6	1,58	7,4	14,8	2,49	1,54	6,0	18,9	12,8	4,25	-
7	1,56	7,4	14,5	2,51	1,51	6,0	18,9	12,6	4,24	-
10	1,55	7,4	14,3	2,53	1,49	6,0	18,9	12,6	4,19	4,40

*) Footnote: Density has been measured by pycnometric method. Pycnometer volume = 31,2 cm^3 , filling liquid - CCl_4,
temperature = 20±0,05°Ñ. Measurement precision ±0.001 g. Results have been obtained by three single measurement with related error ~ 4,7 %.

Table 3

$(-\Delta GO_2)$ values and $O/_{Pu}$ in pellets

Pellet number	$(-\Delta GO_2)$, kal/mol	$O/_{Pu}$
3 (pellet end)	93,6	1,997
3 (pellet end)	86,4	1,998
3 («waist»)	86,6	1,998
10 (pellet end)	93,8	1,997
10 (pellet end)	86,3	1,997
10 («waist»)	86,5	1,998

4.2. PUO₂ + MGO PELLET ALPHA RADIOGRAPHY

Alpha radiography of the specimen 7 (see table 3) has been realised. Figure 7a shows specimen photo (alpha radiograph) from this analysis.

Plutonium distribution in PuO_2 + MgO specimens is homogene and any segregation of fuel component or of matrix was not observed.

Heat conductance dependence versus temperature
for UO2+MgO composition (technology 2)
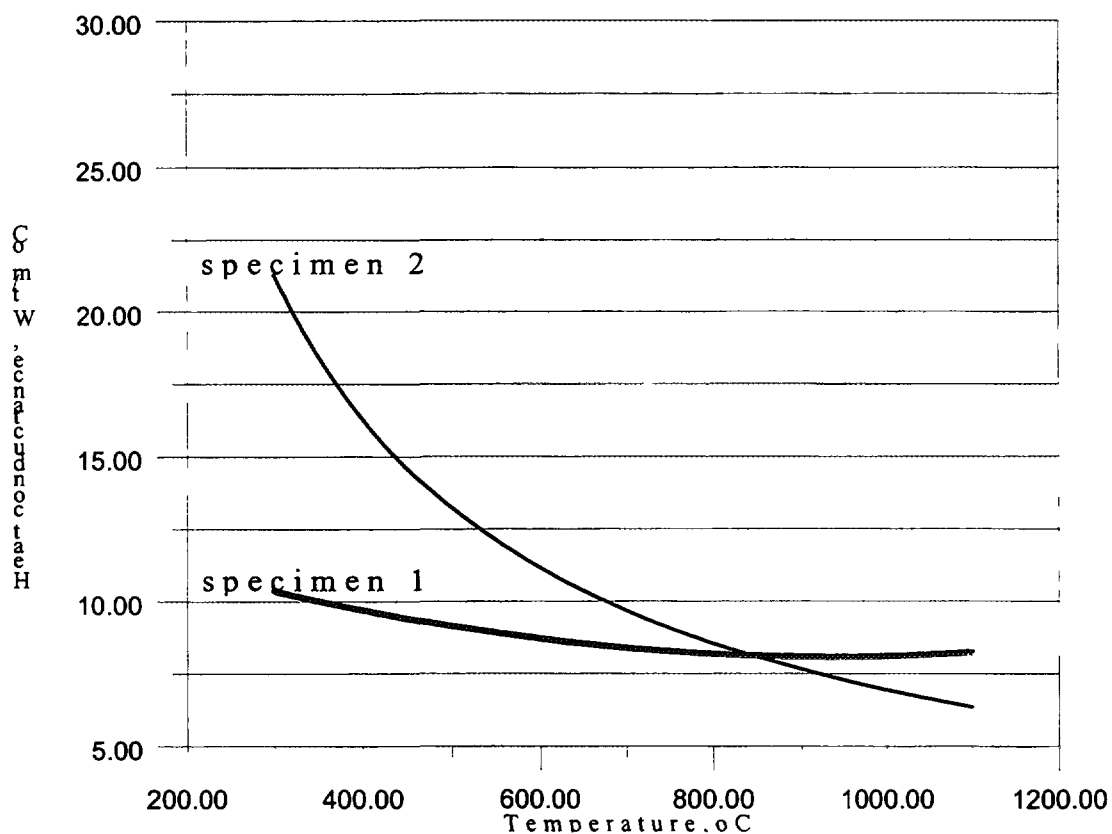
*Figure 5*

Technological route of fuel composition PuO₂+MgO pellet fabrication by coprecipitation of Mg(OH)₂ and Pu(OH)₄ from solution

Technological route of fuel composition PuO_2+MgO pellet fabrication by coprecipitation of $Mg(OH)_2$ and $Pu(OH)_4$ from solution

```
┌──────────────────┐  ┌──────────────────┐  ┌──────────────────┐
│ Pu(NO₃)₄ solution│  │ Mg(NO₃)₂ solution│  │   25% ammonium   │
│                  │  │                  │  │ hydroxide solution│
└────────┬─────────┘  └────────┬─────────┘  └────────┬─────────┘
         ▼                     ▼                     ▼
┌───────────────────────────────────────────────────────────────┐
│                        Coprecipitation                        │
└───────────────────────────────┬───────────────────────────────┘
                                 ▼
        ┌──────────────────────────────────────────────┐
        │                  Filtration                  │
        └──────────┬──────────────────────┬────────────┘
                   ▼                      ▼
            ┌─────────────┐        ┌──────────────┐
            │ Precipitate │        │ Mother liquor│
            └──────┬──────┘        └──────┬───────┘
                   ▼                      ▼
      ┌──────────────────────┐   ┌─────────────────┐
      │ Thermal decomposition│   │  Tails storage  │
      └───────────┬──────────┘   └─────────────────┘
                  ▼
      ┌──────────────────────┐   ┌─────────────────┐
      │  PuO₂ + MgO powder   │   │     Binder      │
      └───────────┬──────────┘   └────────┬────────┘
                  ▼                       ▼
      ┌───────────────────────────────────────────┐
      │                 Mixing                    │
      └──────────────────┬────────────────────────┘
                         ▼
      ┌───────────────────────────────────────────┐
      │                 Pressing                  │
      └──────────────────┬────────────────────────┘
                         ▼
              ┌─────────────────────┐
              │      Sintering      │
              └──────────┬──────────┘
                         ▼
            ┌────────────────────────┐
            │     Finish pellets     │
            └────────────────────────┘
```
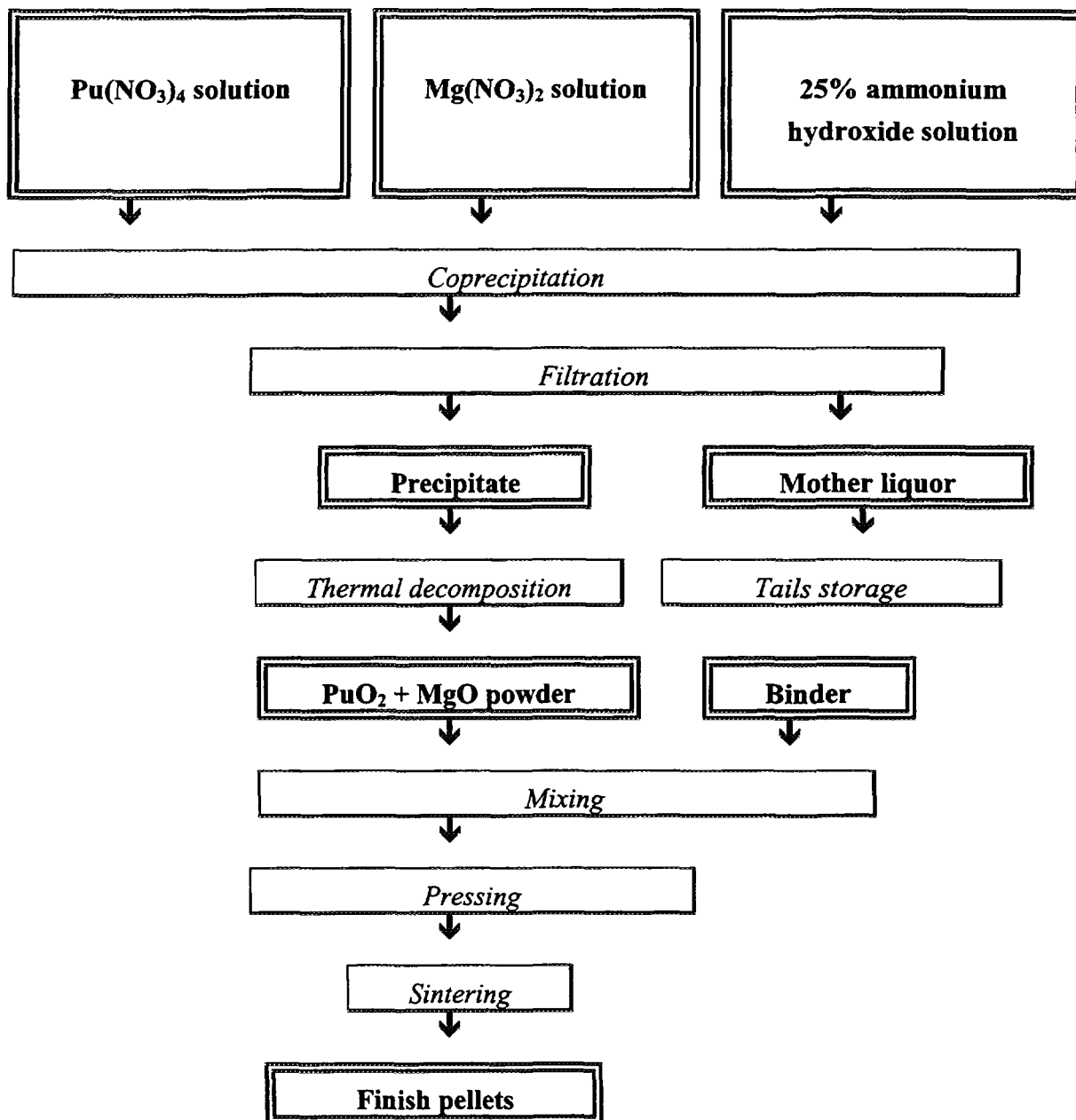
**Figure 6**

4.3. METALLOGRAPHIC STUDY OF PUO₂ + MGO FUEL COMPOSITION

The appearance of $PuO_2 + MgO$ fuel pellet is on figure 8 a and b.

Metallographic study has been carried out with metallurgical specimen cross-sectioned in the plane 1,5 mm from the pellet end. Cross section has been polished mecanically with chromium oxide on wool support. Magnification 100 and 200 was achieved by commercial microscope MIM-15.

Microstructure of material is formed by gray matrix containing uniformly distributed white particle with dimension from 1 to 50 micrometers (figure. 7 b, c).

a)   b)   c)
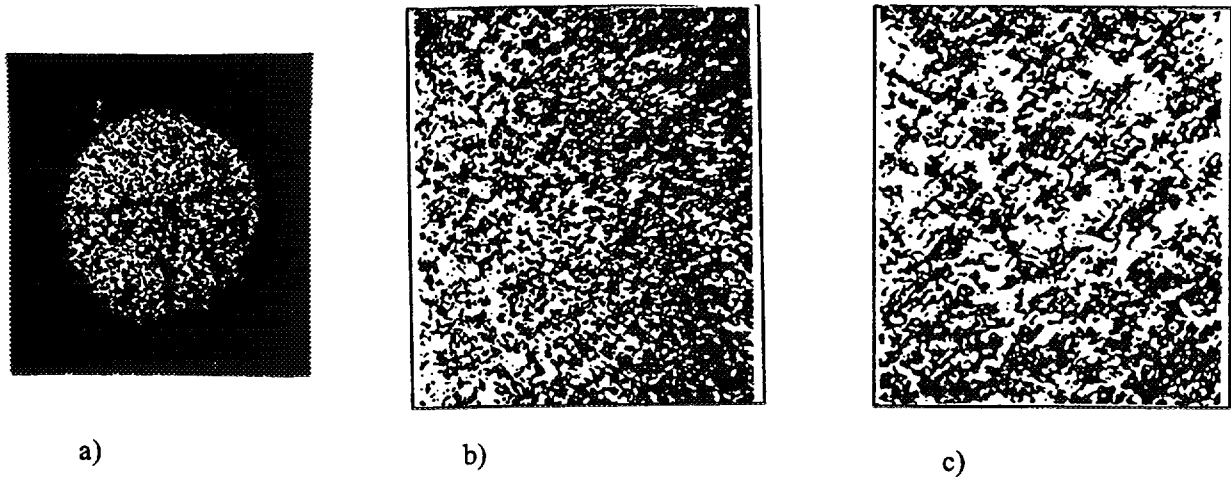
Fig. 7. PuO$_2$ + MgO composition alpha radiograph (a, x5) and microstructure (b, x100 and c, x200)

Fig. 8. The appearance of PuO$_2$ + MgO fuel pellet

4.4. PHASE CONSTITUTION STUDY OF PUO$_2$ + MGO COMPOSITION PELLET

X-ray analysis has been used for phase constitution study of the sintered compact prepared from PuO$_2$ + MgO composition.

X-ray powder pattern has been registrated at facility DRON-2 (reflection monochromatized Co radiation). Data treatment has been carried out by routine procedure. Results prove existance of two oxide phase : fluorite type PuO$_2$ with crystal lattice parameter 5,397 ± 0,001 Å and sodium chloride type MgO with crystal lattice parameter 4,211±0,001Å. Powder pattern does not contains any non interpreted line.

4.5. MEASUREMENT OF PUO$_2$ + MGO PELLET MECHANICAL STRENGTH BEFORE FAILURE

PuO$_2$ + MgO pellet mechanical strength before failure has been evaluated in pellet end direction by means of pressing installation.

Total loading before failure for pellet 3 is 651 kg (± 3 kg), for pellet 10 is 646 kg (± 4 kg).

Compact cross section is equal to 28,26 mm^2.

Specific loading before failure is:

for pellet 3 about 23 kg/mm^2;

for pellet 10 about 22,9 kg/mm^2.

5. Sintered PuO$_2$ + MgO pellet reprocessing study

Dissolution condition for sintered 15% (vol) PuO$_2$ + 85% (vol.) MgO pellets has been determined

- dissolution of sintered noncrushed pellet occurs without residue in the mixture 12N HNO$_3$ + 0,1N HF;

- dissolution temperature is about 110°C;

- total dissolution time is 20 hours.

-

Summary

1 Research and development of new magnesium oxide base fuel material for plutonium utilization in fast reactor has been carried out by using dummy uranium composition.

1.1 Two technology of fuel pellet fabrication for 15% (vol) UO$_2$ + 85% (vol.) MgO composition has been developed
   - mechanical blending of UO$_2$ and MgO powder, pressing operation and pellet sintering;
   - component coprecipitation from nitrate solution with following operations of precipitate heat treatment, pellet pressing and sintering.

1.2. Influence of intermediate product properties on the pellet quality (density, fissuration, side end lamination, porosity and other) has been investigated for both route.

1 3 When studying it was detected total powder specific surface value S$_{BET}$ being preponderant factor for pellet density

1 4. Pellet quality (absence of defects) depends on initial UO$_2$ and MgO powder heat treatment mode (mechanical powder blending, technology 1) and on thermal precipitate decomposition mode (component coprecipitation from solution, technology 2)

1 5 Optimal technological parameters has been selected for fuel pellet fabrication using 15% (vol.) UO$_2$ + 85% (vol.) MgO composition.

1 6 Choice of optimal parameters has been validated by morphological and microstructural evolution of powder which was observed during investigation.

1.7 Main properties of UO$_2$ + MgO pellet has been studied:
   - phase composition;
   - microstructure;
   - dependence of heat conductance versus temperature;
   - dissolution in nitric acid.

1.8 Both technology developed may be recommended for commercial implementation after refinement with plutonium-bearing material and after in-core testing.

180

1.9. UO_2 + MgO fuel pellet fabrication by coprecipitation from solution may be preferred because of improved homogeneity, elevated density and enhanced heat conductance of the pellets. Technology consists in routine operation and equipment implemented at fuel fabrication plant.

2. Fuel pellet fabrication with composition 15% (vol.) PuO_2 + 85% (vol.) MgO has been approved after the technology developed using dummy fuel UO_2.

2.1. Fabricated PuO_2 + MgO composition fuel pellets are qualitative ones and does not have defects their pycnometric density being 4,4 g/cm^3 [90% of theoretical density value for 15% (vol.) PuO_2 + 85% (vol.) MgO].

2.2. PuO_2 + MgO pellets exhibit homogeneous microstructure and homogeneous fuel component distribution.

2.3. Ratio O/Pu in PuO_2 + MgO pellets is 1,997 - 1,998.

2.4. PuO_2 + MgO composition contains two phase only - PuO_2 and MgO.

2.5. Mechanical strength before failure for 15% (vol.) PuO_2 + 85% (vol.) MgO composition fuel pellets is 23 kg/mm^2.

2.6. Activity with plutonium-bearing material shows developed technology of UO_2 + MgO composition fuel pellet fabrication being wholly applicable for PuO_2 + MgO composition fuel pellet fabrication.

SURVEY ON METAL FUEL ON A BASE OF URANIUM ALLOYS

I.I. KONOVALOV
All Russian Institute of Inorganic Materials,
Moscow, Russian Federation

XA9745732

Abstract

The thorough study of metallic fuel on a base of uranium alloys was carried out in VNIINM for different types of reactors. The main characteristics of irradiation behaviour and form change of metallic fuel are summarized. The best results were obtained for alloys containing 1-2 wt.% of γ-stabilizing elements (Zr, Nb, Mo) + several tenths of percentage of compound forming elements (Si, Fe, Al, Sn). It is stated that metallic uranium fuel in a bulk form may be used only for fast reactors, and in dispersed form with Al- and Zr- matrix for commercial LWR and research reactors.

Introduction

The metallic fuel on a base of uranium alloys was developed for different types of nuclear reactors: plutonium production reactors, commercial power reactors, fast reactors, and for other types of reactors.

The initial interest to metallic uranium fuel was caused by its high density and opportunity to produce weapon grade plutonium The first irradiation experience was the severe form changes due to irradiation growth and swelling, fuel rod cracking under thermal stresses. The massive applied and fundamental studies on irradiation behaviour of uranium and its alloys were carried out. This permitted us to understand the bases of radiation damage in uranium, and eliminate negative radiation phenomena in plutonium production fuel elements.

Development of metal fuel

Along with the development of oxide fuel the vast study of metallic fuel was begun, as it has the following obvious advantages:
- high uranium density
- high level of mechanical properties
- absence of gas release under irradiation
- high thermal conductivity; in case of cohesion between fuel rod and cladding it is possible to produce "cold fuel element" for VVER or RBMK-types nuclear reactors with average fuel temperature less than 400°C.

But, the metallic fuel has also serious disadvantages. the first is swelling of fuel, and the second - low compatibility with water coolant.

To investigate behaviour of metallic fuel we use so called "passive" and "active" reactor experiments. "Passive" reactor experiments are usual study, where one irradiates samples of fuel or mock-up fuel elements and then investigates them by common post-irradiation methods. "Active" reactor experiments are carried out with the help of units enabling us to influence upon fuel samples during irradiation

The one unit is the device for in-pile investigation of a fuel under tension. For example the mechanical properties of the low-alloyed uranium under irradiation and after are shown in Fig.1. One may see the significant difference in properties.

The other unit is the dilatometer inserted in channel of research reactor. This unit allows us to measure continuously the change of sample dimensions under irradiation. For example at the bottom in Fig.2 the kinetic of the swelling of low-alloyed uranium is
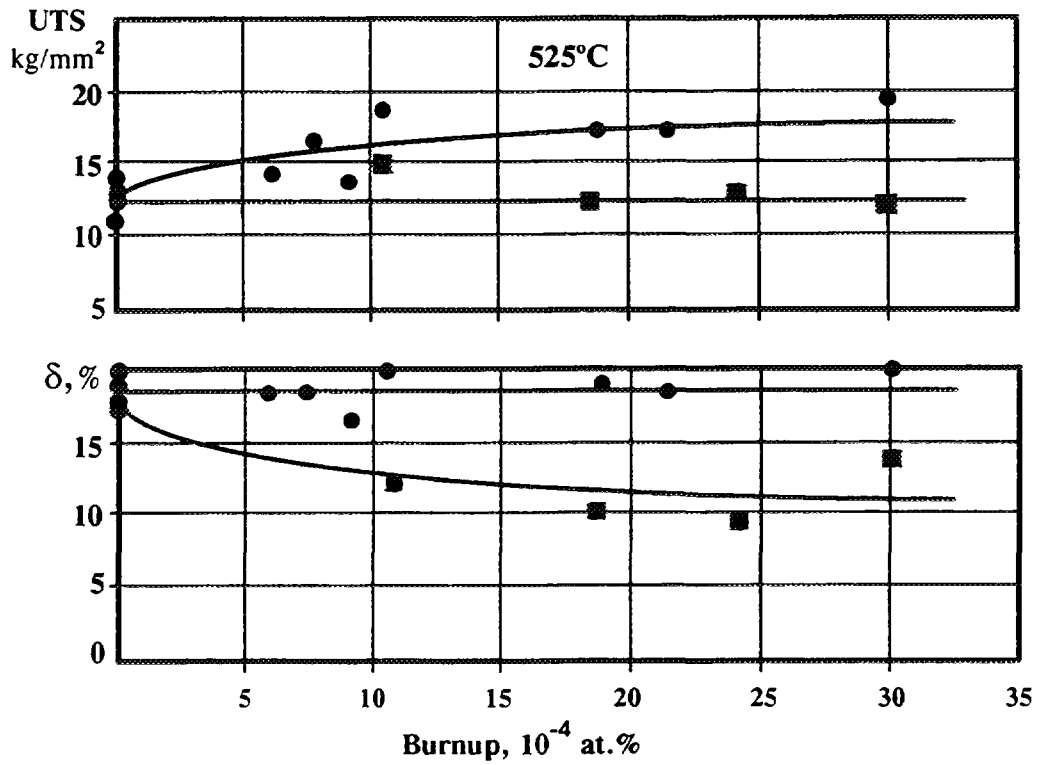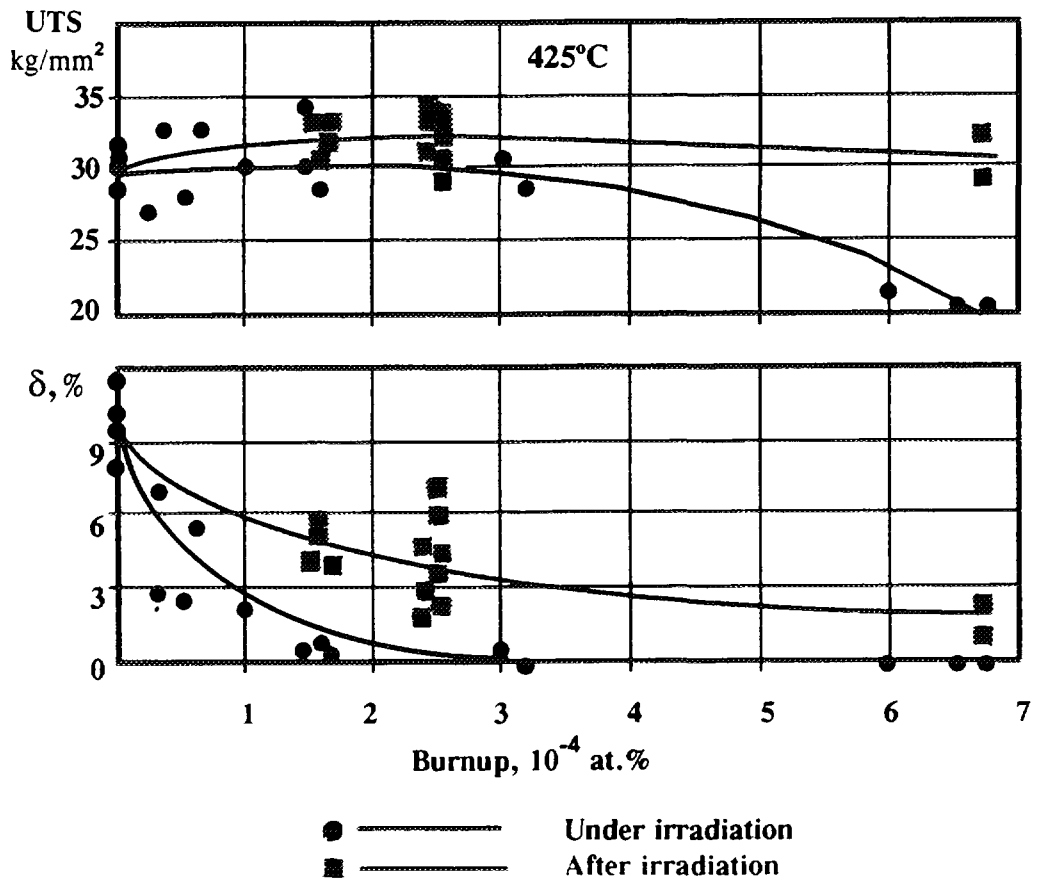
Fig. 1. Mechanical properties of the low-alloyed uranium under and after irradiation.
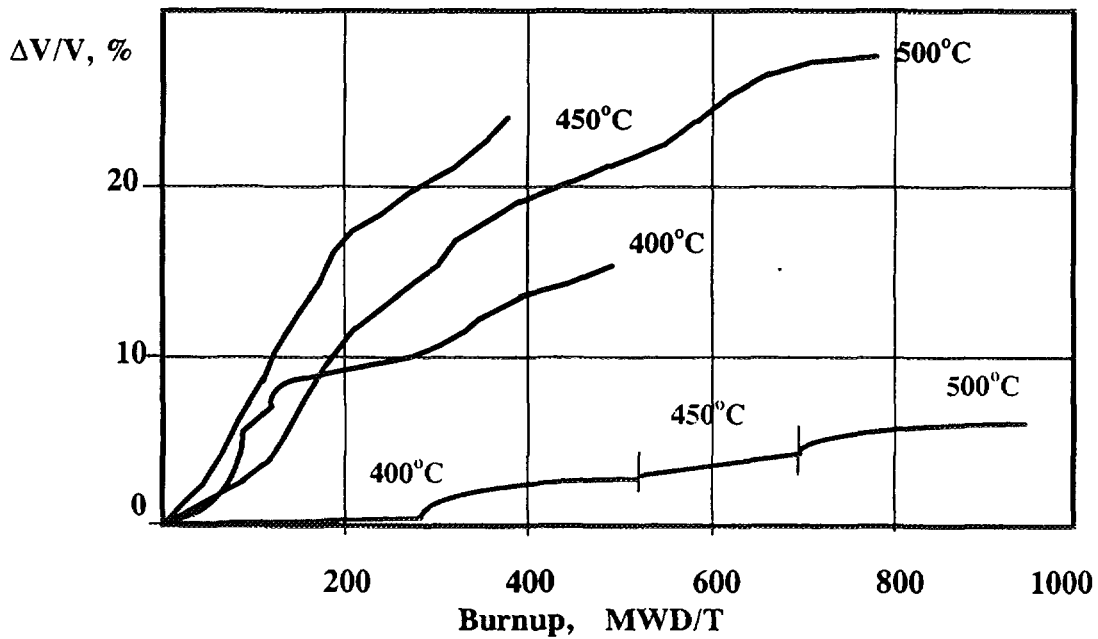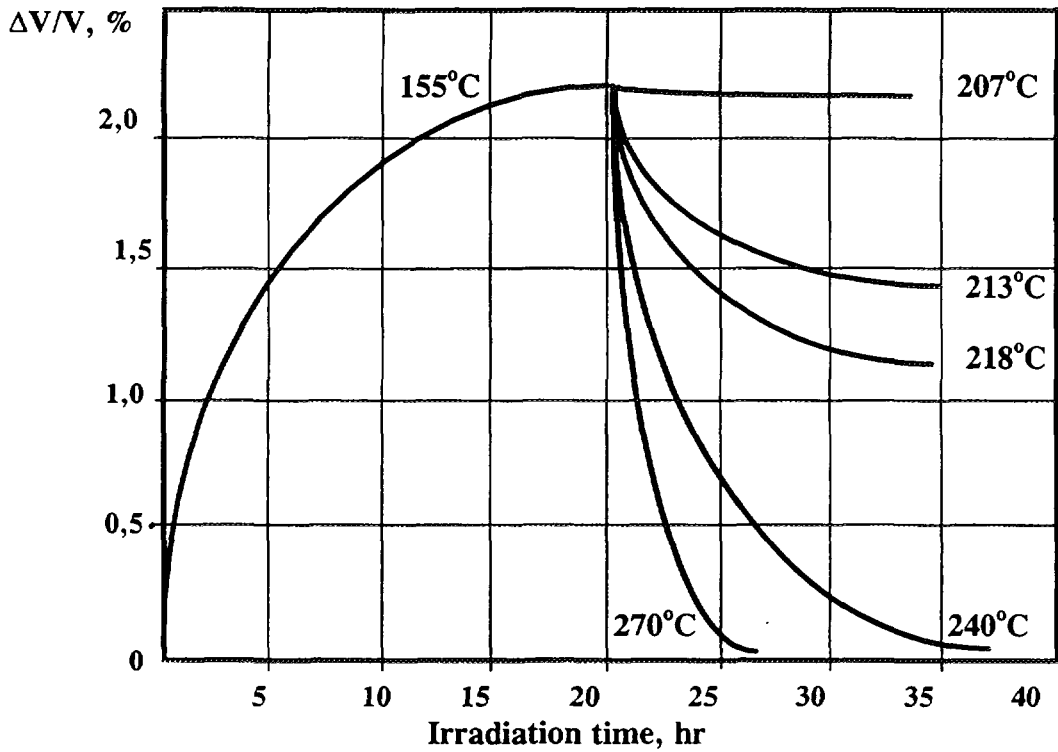
Fig. 2. Volume changes of the low-alloyed uranium (bottom) and uranium silicide (upper).

presented, and on the top - the volume change of uranium silicide U_3Si due to amorphization and further restoring of crystalline structure.

Simultaneously with measuring of sample dimensions we may load a sample and so study irradiation creep. For instance in Fig.3 the irradiation and thermal creep of uranium silicide U_3Si is shown.

On a base of experimental data and computed study we worked out the main characteristics of irradiation behaviour and form changes of metal fuel.
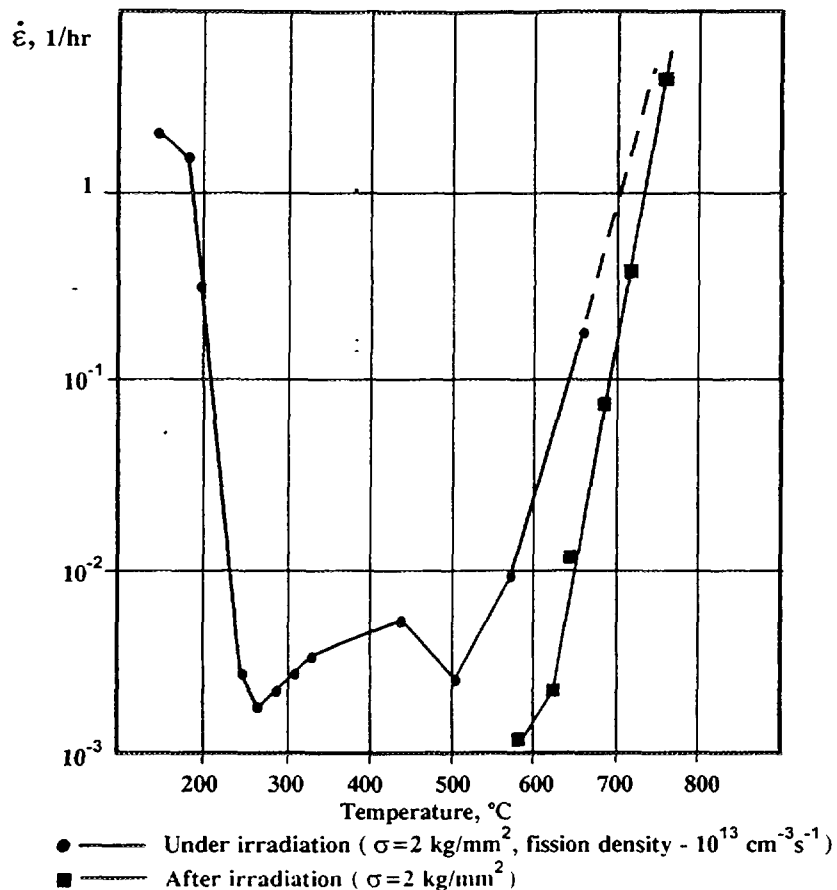
Fig. 3. Temperature dependence of the irradiation and thermal creep of uranium silicide.

The primitive dependence of the swelling from relative temperature and burnup for low-alloyed uranium is given in Fig.4. The darkened areas correspond to working conditions of metallic fuel in research reactors, commercial water cooled reactors and fast reactors.

At temperatures below 0.4 from melting point the swelling is caused by accumulation of fission products (solid swelling). The burnup dependence is linear function with swelling rate about of 6 vol.% per 1.10^{21} fiss./cc (or 15 vol.% per 1g of splitted uranium in 1 cc).

At intermediate temperatures the maximum of swelling is caused by vacancy pores, containing some amount of gas fission products. If we anneal samples after irradiation, they increase the density and their volume decreases.

At high temperatures above of 0.6 from melting point the swelling is due to equilibrium gas bubbles, and so post-irradiation annealing do not reveal any significant volume changes.

At high burnups the maximum of vacancy swelling degenerates and swelling has the gaseous nature. With the increasing of burnups the temperature threshold of the beginning of gas swelling displaces to lower temperatures.

The low-temperature solid swelling and high-temperature gas swelling cannot be suppressed, and the only mean to struggle against these phenomena is to create the free volume in a fuel element which will compensate the swelling, or use such design, which permits deformation of fuel element without rupture.

In opposite, the maximum of vacancy swelling under intermediate temperatures may be effectively suppressed by adjustment of microstructure of uranium fuel. The main approach is creation in fuel structure a great amount of sinks for radiation point defects.

As the sinks, the fine dispersed intermetallic compounds may be considered. For this purpose compound forming elements such as Si, Fe, Sn, Al and others are added to uranium.
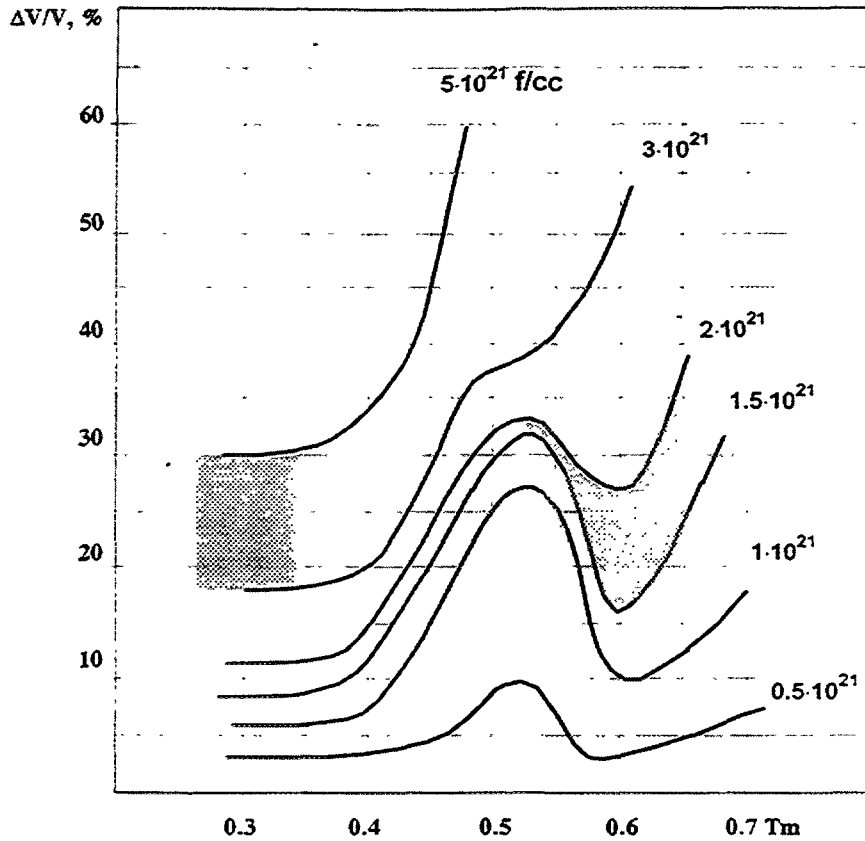
Fig. 4. Schematic dependence of the swelling of low-alloyed U on temperature and burnup.

This method of suppressing the vacancy swelling works when density of intermetallic precipitation's is more than 1.10^{12} particles in cc. At the bottom in Fig.2 the kinetics curves of swelling for uranium with additions of intermetallic forming elements are shown. The composition of samples is the same, but for upper curves we had a coarse network of intermetallic precipitation's and for lower - fine network. This method is effective for relatively low burnup.

For higher burnup typical to commercial reactors, we combine this method with another - creation of the fine two-phase structure. This is the most effective if we use γ-stabilizing elements, such as Zr, Nb, Mo. Using of these elements we may create fine two-phase structure, where boundaries between phases serve as point defects sinks. Example of the influence of the degree of dispersity of two-phase structure (α-Uranium + γ-Uranium) upon irradiation behavior of mock-up fuel elements is given in Fig.5.

Experimentally we established that less than 2 wt.% of γ-stabilizing elements + several tenths of percentage of compound forming elements are enough to suppress the vacancy swelling. We must only do the correct choice of alloying element's combination and heat-deforming treatment. The further alloying has insignificant influence upon irradiation behaviour.

Now we see no difficulties to develop fuel elements with uranium alloy which can work to burnup that of commercial reactors.

The main problem why metallic fuel has limited application in atomic energetic is insufficient corrosion resistance in water coolant.

The distinguishing feature of uranium is absence of solubility of other elements in α-uranium, and so we cannot use common solid-solution methods for improving corrosion

187
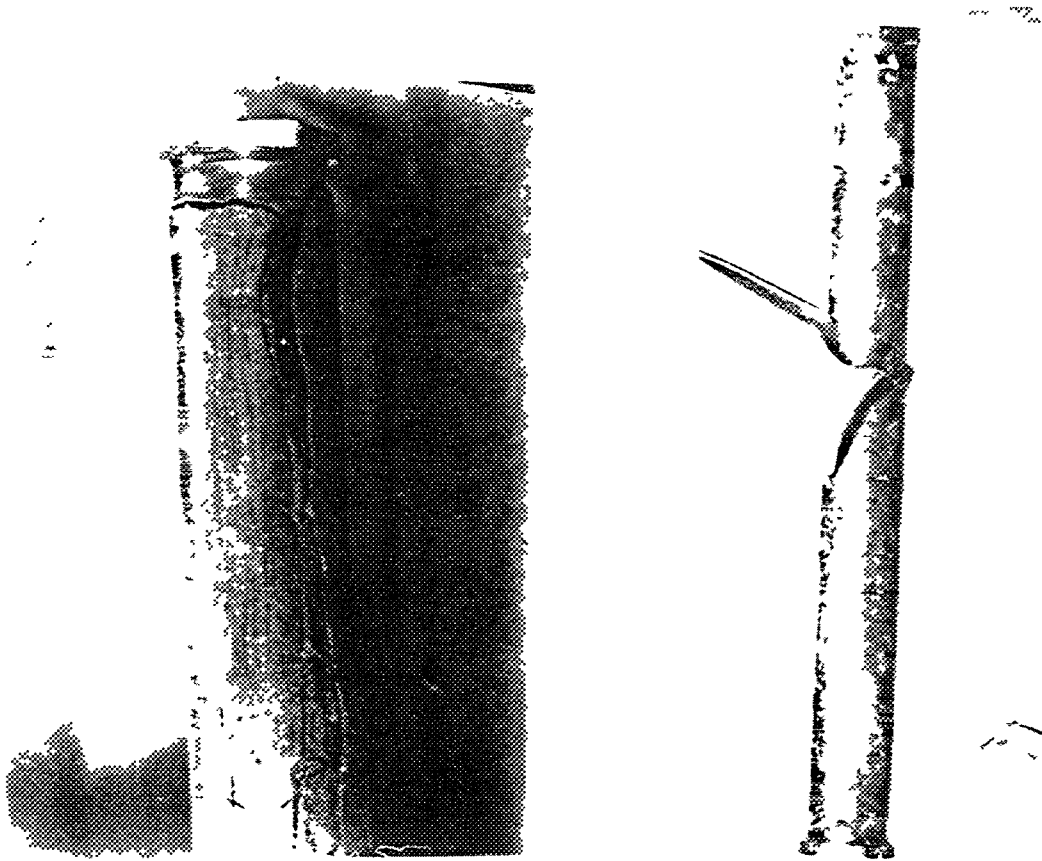
Macrograph (appearance) of fuel elements
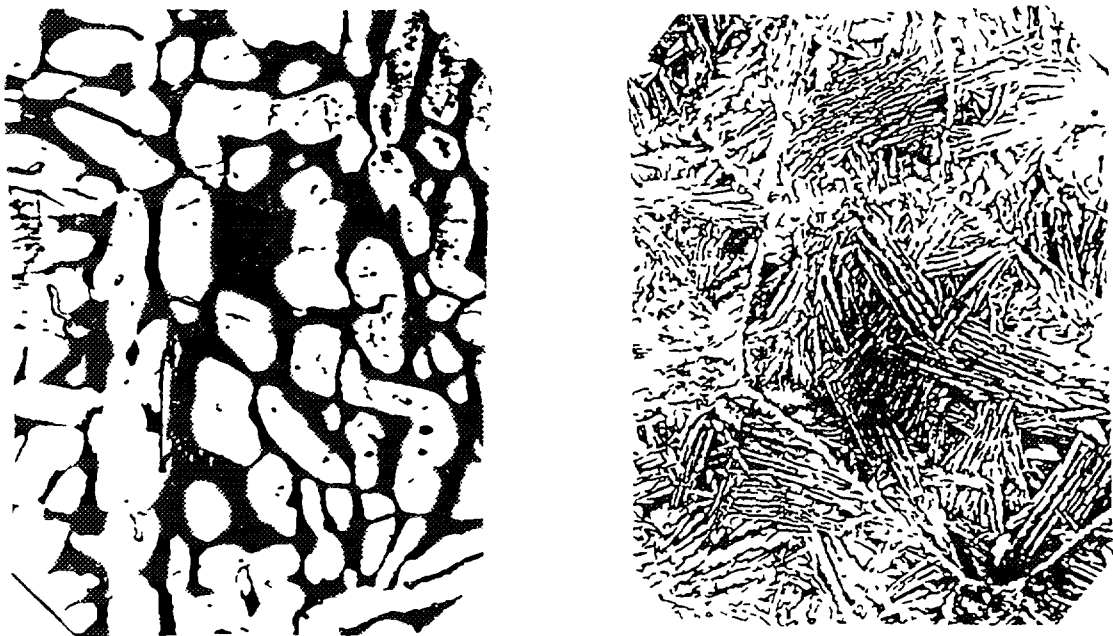
Optical micrograph (x800)

Fig 5 Influence of the degree of dispersity of two-phase structure (α- and γ-uranium) on irradiation behaviour of mock-up fuel elements (dose = $1 \cdot 10^{21}$ f/cc)

resistance. The significant improving of properties may be only archived if we use δ- and γ-phase alloys in U-Mo, U-Nb, U-Ti, U-Zr systems. To receive these structures we must insert in U a significant quantity of alloying elements from 30 to 75 at.%. In ternary alloys we may obtain corrosion resistant metastable γ-phase by minor alloying. But as it metastable there is some problems with stability of γ-phase under irradiation.

A good corrosion resistance has uranium silicide U_3Si. This compound was thoroughly investigated as a fuel for RBMK reactor. The fuel elements with this fuel had satisfactory irradiation behavior, but in case of untight fuel element when the water coolant got into the fuel rod center with the temperature of about 500°C, the whole fuel element was destroyed.

The radical measure to increase the corrosion resistance is to use metallic fuel dispersed in Al- or Zr- matrix. We have preliminary positive results of irradiation to relatively (~1g/cc) high burnup of such dispersion composition.

Conclusion

Summarizing our experience we may say that metallic fuel in a bulk form may be used in fast reactors with sodium coolant, and in dispersion form for atomic energetic and research reactors.

LIST OF PARTICIPANTS

Bibilashvili, Yu.K.	All Russian Scientific and Research Institute of Inorganic Materials,
	Rogova Str. 5, Box 369, 123060 Moscow, Russian Federation
Boero, N.L.	Comisión Nacional de Energía Atómca,
	Av. del Libertator 8250, 1429 Buenos Aires, Argentina
Coquerelle, M.	Institute for Tansuranium Elements, Joint Research Centre,
	P.O. Box 2340, D-76125 Karlsruhe, Germany
Dehaudt, P.	CEA/DTP/SECC,
	17, Rue des Martyrs, F-38054 Grenoble Cedex 09, France
Denis, A.	Comisión Nacional de Energía Atómca,
	Av. del Libertator 8250, 1429 Buenos Aires, Argentina
Golovchenko, Yu.M.	Research Institute of Atomic Reactors,
	433510 Dimitrovgrad-10,
	Ulyanovsk region, Russian Federation
Kim, Ki-Hwan	Korea Atomic Energy Research Institute,
	Dukjin-dong Yusong-gu 150, 305-353 Taejon, Republic of Korea
Konovalov, I.I.	All Russian Scientific and Research Institute of Inorganic Materials,
	Rogova Str. 5, Box 369, 123060 Moscow, Russian Federation
Kurina, I.S.	Institute of Physics and Power Engineering,
	State Scientific Centre of the Russian Federation,
	249020 Bondarenko Square 1, Obninsk, Russian Federation
Moseev, L.I.	Institute of Physics and Power Engineering,
	State Scientific Centre of the Russian Federation,
	249020 Bondarenko Square 1, Obninsk, Russian Federation
Onoufriev, V. *(Scientific Secretary)*	International Atomic Energy Agency,
	Wagramer Strasse 5, P.O.Box 100, A-1400 Vienna, Austria
Panov, A.S.	Scientific and Research Institute LUTCH,
	142100 Podolsk, Russian Federation
Popov, V.V.	Institute of Physics and Power Engineering,
	State Scientific Centre of the Russian Federation,
	249020 Bondarenko Square 1, Obninsk, Russian Federation

Rogozhkin, B.D.	All Russian Scientific and Research Institute of Inorganic Materials, Rogova Str. 5, Box 369, 123060, Moscow, Russian Federation
Ryzkov, A.N.	Institute of Physics and Power Engineering, State Scientific Centre of the Russian Federation, 249020 Bondarenko Square 1, Obninsk, Russian Federation
Sarakhova, G.A.	All Russian Scientific and Research Institute of Inorganic Materials, Rogova Str. 5, Box 369, 123060 Moscow, Russian Federation
Sengupta, A.K.	Radiometallurgy Division, Bhabha Atomic Research Centre, 400085 Trombay, Mumbai, India
Sila-Novitsky, A.G.	Research and Develpment Institute of Power Engineering, P.O. Box 788, 101000 Moscow, Russian Federation
Stetsky, Yu.A.	All Russian Scientific and Research Institute of Inorganic Materials, Rogova Str. 5, Box 369, 123060 Moscow, Russian Federation
Subbotin, A.V.	Research and Development Institute of Power Engineering, P.O. Box 788, 101000 Moscow, Russian Federation
Suzuki, Y.	Department of Chemistry and Fuel Research, Japan Atomic Energy Research Institute, Oarai-machi, Higashi-ibaraki-gun, Ibaraki-ken 311-13, Japan
Trotabas, M.	COGEMA BC, 2, Rue Paul Dautier, B.P. 4, F-78141 Velizy Cedex, France
Vatulin, A.V.	All Russian Scientific and Research Institute of Inorganic Materials, Rogova Str. 5, Box 369, 123060 Moscow, Russian Federation
Weidinger, M.	Danziger Str. 22, D-90491 Nürnberg, Germany

97-01927